UNIVERSITY OF CALIFORNIA SAN DIEGO

Fostering Unsaturated Metal Centers with *m*-Terphenyl Isocyanide Ligands

A dissertation submitted in partial satisfaction of the requirements for the degree Doctor of Philosophy

in

Chemistry

by

Michael Luke Neville

Committee in charge:

Professor Joshua S. Figueroa, Chair
Professor Guy Bertrand
Professor Joseph M. O'Connor
Professor Clifford P. Kubiak
Professor Duncan. Agnew

2022

The dissertation of Michael Luke Neville is approved, and it is acceptable in quality and form for publication on microfilm and electronically.

University of California San Diego

2022

DEDICATION

For my mother.

EPIGRAPH

You don't know until you know.

-An ever-growing number of people

TABLE OF CONTENTS

LIST OF FIGURES

LIST OF SCHEMES

LIST OF TABLES

ACKNOWLEDGEMENTS

First and foremost, I want to thank Professor Joshua S. Figueroa. I came to graduate school with a fairly nebulous idea of what I wanted to do and learn. Josh's understanding of electronic structure theory provided exactly what I didn't know I was looking for. From my time doing research under his supervision to TAing his "undergraduate" inorganic course, he has provided both myself and many others a fundamental and versatile lens with which to understand the world around us. This knowledge has provided my graduate school experience a sense of academic fulfillment. For as much as I have learned about chemistry from Josh, I have learned equally as much about bounds of the human glue that constitute our social structures. As both an advisor and a friend, he has radically shaped the way I view the world.

I owe a debt of gratitude to the incredible researchers that make up the Figueroa Research Group, past, present, and future. The Elders, Brandon, Chuck and Doug (aka B, C, D) kindly conferred to me a wealth of hard-earned wisdom that catalyzed my experimental start the lab. Brandon's suggestion to try to BIM group 9, while proving almost unBIMable, ended up being the basis of this thesis. I will miss his unexpected, Kool-aid man-esque office entrances in random post-graduation visits. After failing to make a previously synthesized compound for the first month of my graduate career, Chuck took the time to teach me how to do it right. Observing Chuck do chemistry is like watching an elegant form of art and without his skilled training this thesis would likely contain half the number of compounds it has. Doug encouraged me to assume I know nothing and ask lots of questions. I have passed that same advice down to future generations of students as I have found it to be key to a successful learning mind set. While the proceeding set of researchers don't have as alliterative of names (aka K, M, J) their impact was just as great. I learned as much about chemistry as I did about life from these three and I look forward to many more life experiences with them. I couldn't have asked for a better person to start in the lab with than Alejandra. Besides saving me hundreds of dollars in registration fees by reminding me to register for classes, she is an incredible researcher and friend. Thank you for always looking out for me. Ritchie, keep making late metal carbynes a thing and keep it classy. Adam, enjoy the single station. Kyle said in

his thesis that we should dump that glove box because of the affability it imparts on those that use it and you certainly fit the mold. As the lone post-doc while I have been in the group, Vincent set a new standard for hard work that I never thought possible. And The Youth - Krista and Sean, your incredible early progress is inspiring as are your memes and youthful culture. Most of all, I look forward to seeing where all of your careers take you and hope for many future opportunities to do science together again.

Outside of the Figueroa Research Group I have had the great fortune of learning from and collaborating with many talented researchers in Department of Chemistry and Biochemistry. Most notably, Prof. Valarie Schmidt has been kind enough to allow me to contribute to some of their amazing azetidine work with Dr. Danimal Flores and attend their weekly group meetings. I am eternally appreciative of the opportunity display boundless naiveté and folly in an effort to learn a new sub-field of chemistry. It has been an honor to learn from such a brilliant chemist and amongst such bright young researchers. Outside the department I have had the great fortune to be a part of a collaboration with the laboratory of Prof. Ulrich Abrams at the Free University of Berlin. Although I was not able to perform any technetium chemistry myself due to a global pandemic, it has been a joy to accomplish so much fundamental group 7 chemistry with such talented chemists as Dr. Federico Salsi and Guilhem Claude.

"Synthesis" may be in the title of this thesis, but the fruits of this labor would remain unknown without characterization. The world class staff and resources at UCSD were instrumental in this effort. Foremost, Prof. Arnie Rheingold, Milan Gembicky and Curtis Moore have built what must be one of the best X-ray facilities in the world. Many of the compounds in this thesis would not have been identified if it weren't for their expertise and the outstanding assets of the X-ray facility. Additionally, I had the opportunity to serve as a TA for the NMR facility where I gained an appreciation for the largely unseen battle our facility mangers, Anthony Mrse and Xuemei Huang, wage to keep the NMR instrumentation running at peak. As a daily user of the facility, I am grateful for that opportunity and their hard work. I would be remiss if I didn't thank our long-time custodian, Aaron. He could always be counted to check in on my nightly productivity and made sure I kept my hair cut to a reasonable length. Aaron was a

constant reminder of the sheer amount of good one person can have in them, and I hope he is enjoying his well-deserved retirement.

If it weren't for Dr. Timothy J. Boyle, I am sure I would not be pursuing the study of chemistry. High schoolers are rarely given a chance to do first-rate chemical research and I am grateful Tim gave me that opportunity. From him I learned that the world is truly what you make of it, and he is a master at transforming it for the better. I hope to be able to have that same effect in my future career. Additionally, I would like to thank Prof. Richard Kemp for introducing me to the magic of molecular orbitals and piquing my interest in their ability to explain chemical structure and reaction. It was this interest that propelled me towards the lab of Prof. Figueroa, and for that I am thankful.

While this thesis is a description of professional accomplishments, it has been fueled by many personal connections. Thus, I wish to thank my friends and family for their love and support throughout this process. While there are too many to list here, I must highlight my mother. There are few more powerful examples of independence and perseverance one can grow up with than a single mother by choice. I am thankful for her endless love and support throughout my life.

Chapters 1 and 2: These chapters are composed of work currently in preparation for publication by M. L. Neville, C. Chan, M. Gembicky, C. Moore, A. L. Rheingold, J. S. Figueroa. The dissertation author is the primary author of this manuscript.

Chapter 3: This chapter discusses work currently unpublished by M. L. Neville, A. M. Grippo, A. L. Rheingold, J. S. Figueroa. The dissertation author is the primary author of work.

VITA

2022 Ph.D. in Chemistry, University of California San Diego

2017 M.S. in Chemistry, University of California San Diego

2015 B.S. in Chemistry with Honors, University of New Mexico

PUBLICATIONS

Flores, D. M., **Neville**, **M. L.**, Schmidt, V. A. "Intermolecular 2+2 Imine-Olefin Photocycloadditions Enabled by Cu(I)-Alkene MLCT." *Accepted. Nature Chem.* **2022**.

Chan, W.C., La Clair, J.J., León, B., Trieger, K.A., Slagt, M.Q., Verhaar, M.T., Bachera, D.U., Rispens, M.T., Hofman, R. M., de Boer, V.L., van der Hulst, R., Bus, R., Hiemstra, P., **Neville**, **M. L.,** Mandla, K.A., Figueroa, J.S., Jamieson, C., Burkart, M.D. "Scalable Synthesis of 17S-FD-895 Expands the Structural Understanding of Splice Modulatory Activity." *Cell Reports Physical Science* **2020**, 1, 100277.

Cluade, G., Salsi, F., Hagenbach, A., Gembicky, M., **Neville, M. L.**, Chan, C., Figueroa, J. S., Abram, U. "Structural and Redox Variations in Technetium Complexes Supported by m-Terphenyl Isocyanides." *Organometallics*, **2020**, 39, 2287-2294.

Salsi, F., **Neville, M. L.**, Drance, M. J., Hagenbach, A., Chan, C., Figueroa, J. S.; Abram, U. "A Closed-Shell Monomeric Rhenium(1–) Anion Provided by m-Terphenyl Isocyanide Ligation." *Chem. Commun.* **2020**, 56, 7009-7012.

Brunner, F. M.; Neville, M. L.; Kubiak, C. P. "Investigation of Immobilization Effects on $Ni(P_2N_2)_2$ Electrocatalysts" *Inorg. Chem*. **2020**, 59, 23, 16872-16881.

Mandla, K.A., **Neville, M. L.,** Moore, C. E., Rheingold, A.L., Figueroa, J.S. "Dianionic Mononuclear Cyclo-P4 Complexes of Zero-Valent Molybdenum: Coordination of the Cyclo-P4 Dianion in the Absence of Intramolecular Charge Transfer." *Angew. Chem. Int. Ed.* **2019**, 58, 15329-1533.

Barnett, B. R., **Neville, M. L**., Moore, C. E. , Rheingold, A. L, Figueroa, J. S. "Oxidative-Insertion Reactivity Across a Constrained-Geometry Metal->Borane Interaction." *Angew. Chem. Int. Ed.* **2017**, 56, 7195-7199.

Boyle, T.J., **Neville, M.L.,** Sears, J.M., Cramer, R. "Alkali Metal Yttrium *neo*-Pentoxide Double Alkoxide Precursors to Alkali Metal Yttrium Oxide Nanomaterials." *Chem.Select*. **2016** 1, *473-481*

Boyle, T.J., **Neville**, **M.L.,** Sears, J. M., Cramer, R., Rodriguez, M.A., Alam, T.M., Bingham, S.P. "Synthesis, X-ray structures, and characterization of hexafluoro-iso-propoxide Group 3 and lanthanide precursors." *Polyhedron* **2016** *118, 52-60.*

Boyle, T.J., **Neville**, **M.L.,** Parkes, M.V. "Synthesis and characterization of a series of Group 4 phenoxy-thiol derivatives." *Polyhedron*. **2015**, *11, 1-13*

Boyle, T.J., Sears, J.M., **Neville, M.L.,** Alam, T.M., Young. V.G. "Structural Properties of the Acidification Products of Scandium Chloride Hydrate." *Inorg. Chem*. **2015**, *54,11831-11841*

Boyle, T.J., Yonemoto**,** D.T., **Neville**, **M.L.,** Bingham, S.P. **"**2-(2-Hydroxy-4-methoxybenzoyl) benzoic acid derivatives of Group 4 metal alkoxides." *Journal of Coord. Chem.* **2014** *67, 747-765.*

Boyle, T.J., Yang, P., Hattar, K., Hernandez-Sanchez, B.A., **Neville**, **M.L.**, Hoppe, S. "Synthesis and Characterization of Solvothermal Processed Calcium Tungstate Nanomaterials from Alkoxide Precursors." *Chemistry of Materials* **2014** *26, 965*

Boyle, T.J. , **Neville**, **M.L.,** Apblett, C.A. , Hoppe, S.M. Gembicky, M. "Synthesis of a Family of Lithium Iron Double Aryloxide Precursors for Nano-$LiFeO_x$ Cathode Materials*." Polyhedron* **2013** 65*, 89.*

IN PREPARATION

Neville, **M. L.**, Chan, C., Gembicky, M., Moore, C. E., Rheingold, A.L., J. S. Figueroa. "Group IX Three-Coordinate Monoanions: Isolable Examples of Coordinatively-Unsaturated Metallate Anions." *In Preparation.*

ABSTRACT OF THE DISSERTATION

Fostering Unsaturated and Low-Valent Metal Centers with *m*-Terphenyl Isocyanide Ligands

by

Michael Luke Neville

Doctor of Philosophy in Chemistry

University of California San Diego, 2022

Professor Joshua S. Figueroa, Chair

This dissertation describes the use of *m*-terphenyl isocyanides as a platform for isolating unsaturated metal centers in molecular and material systems. The first two chapters explore the electronic structure of homoleptic, unsaturated, metalates as well as their redox and reactivity profiles. Metalate complexes – those that possess metal centers in formally negative oxidation states – are typically coordinatively and electronically saturated organometallic species. While the chemistry of such complexes is extensive, there are very few examples were coordinative or electronic unsaturation accompanies highly reduced d-orbital manifolds as means to augment reactivity. Reported here is the isolation of the $16e^-$, d^{10} group 9 metalate anions, $A[M(CNAr^{Dipp2})_3]$, (A = Na, K; M = Co, Rh, Ir), where

coordinative unsaturation is achieved through the use encumbering *m*-terphenyl isocyanide ligands. The cobalt metalate displays a high degree of Lewis-acidity, featuring an agostic interaction in the solid state, and binding N_2 when exposed to an N_2 atmosphere. The heavier rhodium and iridium metalates display an unpredicted distortion to a Y-shaped, roughly C_2v symmetric geometry possible promoting electronic accessibility of the d_{x2-y2} as well as the d_{z2} orbital. Both the Rh and Ir derivatives are shown to support up to two, reverse dative bonding (Z-type) interactions and perform up to four electron swings in oxidation state with substrates like PCl_3, forming complexes of the formulation $MCl(PCl_2)_2(CNAr^{Dipp2})_2$ (M= Rh, Ir). While attempts to achieve similar chemistry with the cobalt metalates were unsuccessful, the electrochemistry of this series of group 9 metalates offer insights as to why. Cyclic voltammetry of the Co metalate reveals two reversible one electron features and one further irreversible oxidation. In contrast, both Rh and Ir congeners display one initial irreversible oxidation, highlighting the stark differences in their oxidative chemistry from formal M(1-) oxidation states. The final portion of this thesis takes lessons learned from molecular work with *m*-terphenyl isocyanides and applies them toward synthesizing MOFs with well-defined, coordinatively unsaturated metal nodes. Balancing the need for structural metal coordination and coordinative unsaturation for inner sphere substrate interactions in a difficult challenge in extended material systems such as metal organic frameworks (MOF). While methods to form unsaturated metal centers like defect engineering can generate some unsaturated sites, the lack of well-defined reactive metal centers makes these systems difficult to study and control. New multi-topic ligands are synthesized using the bulky, $CNAr^{Dipp2}$ and are applied to form a new Cu^{I} based MOF and the first well-defined MOF with coordinatively unsaturated Pd^0 metal nodes. Additionally, the redox properties of these large, conjugated linker ligands are described. The largest of these multitopic linkers show multiple reversible redox features that align well with DFT calculated LUMO energies.

Chapter 1 Synthesis of Unsaturated Group 9 Metalates

1.1 Introduction – Metalates, metals in negative oxidation states

Metal complexes that bear a formal negative oxidation state, referred to as metalates, occur throughout organometallic chemistry but are less visible and well-studied than their higher oxidation state counterparts.[3-4] This is intuitive as metals in the natural world tend to be found in positive oxidation states.[5-6] Additionally, relative to the commonly encountered p-block elements on the periodic table, transition metals hold a more electropositive disposition.[2, 7] Some chemists have gone as far as to ascribe a single, positive charge to each transition metal allowing for no downward mobility.[2, 8] Despite this natural bias towards positively charged metal complexes, for some chemists, metals with negative oxidation states have been a fascination for decades. Ironically, the first verified examples of monatomic metal ions in their negative oxidation states were found in the most electropositive group of the periodic table, the alkali metals. In the 1950's and 1960's, it was found that alkali metals could dissolve in ethereal solutions and other aprotic polar organic solvents, yielding blue, electrically conductive solutions.[11-13] Their conductivity suggested the solutions were electrolytic. This implied charge separation and led to the postulation that the alkali metals were disproportionating into A+ and A- components.[13, 15] In 1974, this idea was confirmed crystallographically by James Dye and co-workers with the isolation of $[Na(cryptand\text{-}2,2,2)]^{+}Na^{-}$.[16]

Since this foundational discovery, monomeric metalates have been synthesized for the full transition metal series (Figure 1.1, A).[4, 17] As more were discovered, so was their utility in bond activations

A

complex	year	complex	year
$[Fe(CO)_4]^{2-}$	1931	$[W(CO)_4]^{4-}$	1978
$[Co(CO)_4]^-$	1932	$[Fe(C_2H_4)_4]^{2-}$	1979
$[Cr(CO)_5]^{2-}$	1955	$[Ti(C_6H_6)_2]^-$	1984[b]
$[V(CO)_6]^-$	1960	$[Nb(mes)_2]^-$	1988
$[Co(PF_3)_4]^-$	1965	$[Co(CNXyl)_4]^-$	1989
$[Os(PF_3)_4]^{2-}$	1969	$[Ru(CNtBu)_4]^{2-}$	1992
$[Co(P(OMe)_3)_4]^-$	1973	$[Mn(1,5\text{-}COD)_2]^{2-}$	1992[b]
$[V(C_6H_6)_2]^-$	1975	$[Co(1,4\text{-}tBu_2C_4H_4)_2]^-$	1993
$[Ni(1,5\text{-}COD)_2]^{2-}$	1975	$[Zr(C_{10}H_8)_3]^{2-}$	1994
$[Mn(CO)_4]^{3-}$	1975	$[Ir(tropp^{Ph})_2]^-$	1998
$[Co(C_2H_4)_4]^-$	1976	$[Co(tmbp)_2]^-$	2000
$[Co(PMe_3)_4]^-$	1977	$[Co(C_{14}H_{10})_2]^-$	2002

B

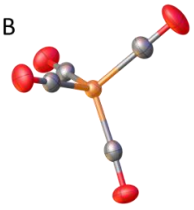

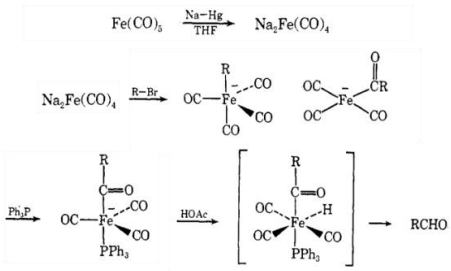

Figure 1.1 A. List of metalates and the year synthesized, modified from Ellis et. al. [4] B. Crystal structure of $[Fe(CO)_4]^{2-}$ and it's synthesis, followed by the step-wise transformation first proposed by Manning and Cooke.[6, 9]

and organic transformations. A classic example is that of disodium tetracarbonyl ferrate, $Na_2Fe(CO)_4$, popularly known as Collman's Reagent.[9] While originally synthesized by Manning and Cooke, Prof. John P. Collman popularized the reagent by exemplifying its ability to transform alkyl halides to their corresponding aldehydes (Figure 1.1 B).[18-19] While a simple and powerful transformation, being stoichiometric in metalate, it suffers from a lack of atom economy. Recently, however, some catalytic examples of metalate-mediated reactions have been described. Lamb, Coates, and co-workers have used $[Co(CO)_4]^-$ as a convenient co-catalyst in the isomerization of epoxides to corresponding ketones. It is proposed that upon O-atom activation of the epoxide by the κ_4-chelated, aluminum-based, Lewis Acid catalyst, the $[Co(CO)_4]^-$ metalate undergoes a regioselective nucleophilic attack generating the ring opened product. The catalyst can then undergo β-hydride elimination from Co to further generate methyl/ethyl ketones, or under an atmosphere of CO do hydroformylation-like CO-insertion to further generate a corresponding lactone.[1, 20-21] Swapping the carbonyl metalate to $[Mn(CO)_5]^-$ results in deoxygenation of disubstituted epoxides while inverting the cis/trans stereochemistry in the product.[2] While investigating Co-catalyzed hydroarylation reactions previously performed by other groups using Co(II) salts and aryl Grignard reagents, Tilley. et al. uncovered the active catalyst to likely be a three coordinate, unsaturated, cobalt metalate. While unable to isolate such a species, in the process of elucidating the active catalyst, they were able to show $Li[Co(N_2)(PPh_3)_3]$ was a competent precatalyst obviating the need for any Grignard reagents and greatly simplifying the reaction conditions.[10] Within the theme of Group 9 metalate catalysis, Lu et al. demonstrated the competence of an indium supported rhodium metalate for the hydrodefluorination

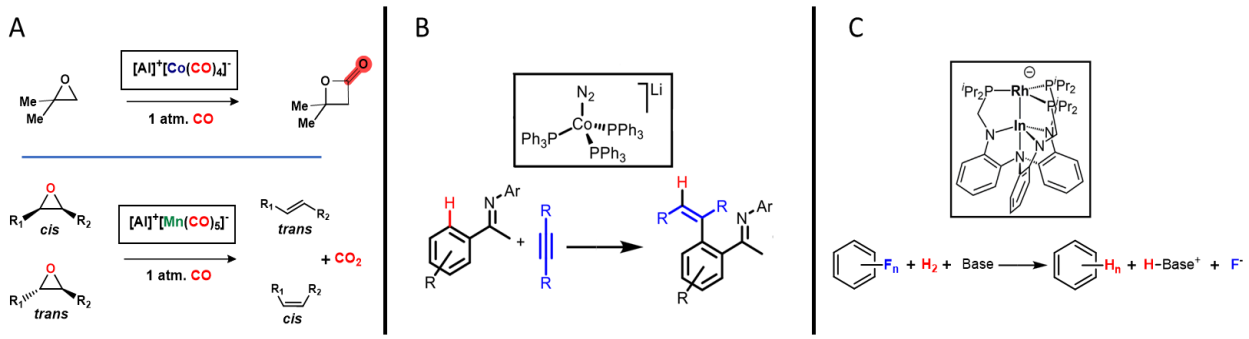

Figure 1.2 Metallates in catalysis – A. Carbonyl metallate mediated epoxide transformations by Coates et al.[1-2] B. Alkyne hydroarylation catalyzed by $Li[N_2Co(PPh_3)_3]$.[10] C. Hydrodefluorination of aryl fluorine bonds by Lu, et al., mediated by an In-supported monoanionic rhodium center.[14]

of notoriously chemically inert Ar-F bonds (~120 kcal/mol).[14, 22] These recent examples illustrate the unique ability of metalates to activate difficult bonds and efficiently achieve unique transformations.

Despite the long synthetic history of metalates and their bourgeoning utility, there is a surprising dearth of unsaturation in the literature. Nearly all examples, to our knowledge, are coordinatively and electronically saturated, with unsaturated examples relegated to low-temperature infrared matrix studies.[4, 23] This is likely due to the characteristics of the commonly used ligands in metalate complexes such as alkenes and arenes (i.e. $[K_2][Zr(\eta^4\text{-}C_{10}H_8)_3)]$[24]), π-acidic phosphines,[25-26] carbon monoxide,[17] and isocyanides.[27-29] To illustrate this point, we can consider three examples of characteristic metalates from across the periodic table; the dipotassium salt of tris(η^4-naphthalene)zirconate, synthesized by Ellis and co-workers in 1994,[24] $[Ni(COD)]^{2-}$ as reported by Klaus in 1975,[30] and finally a mono-anionic cobalt trimethyl phosphite complex, $[Co[P(OMe)_3]_4]^-$.[31] Each of the ligands used in these examples share the ability to accept excess electron density from the metal center via one or more π-symmetric antibonding orbitals. Additionally, they lack a steric profile large enough to prevent ligation of an additional, saturating equivalent of ligand. In each case, the metal used also plays a role in the stability of the metalate. Examples of early transition metalates, like Ellis's zirconium napthlanate, often utilize multi-donor ligands and high coordination numbers to make up for a low initial d-electron count.[32-33] In addition, given the highly reducing nature of these early metals, the ligands used are often described as fully redox non-innocent, complicating the identification of the true oxidation state.[32, 34-35] On the other side of the transition series,

examples of monomeric group 10 metalates like $[Ni(COD)_2]^{2-}$ are rare due to the high initial d-electron count (10 e^-) associated with the corresponding zero-valent metal. With the d-orbitals on the metal filled, reduction of the complex to form a metalate fills the lowest-unoccupied orbitals which are generally ligand based and anti-bonding in character. However, metalate examples from Group 9 like $[Co(P(OMe)_3)_4]^-$ stand out as a possible middle ground. They are electronegative enough and have enough space in the d-orbitals to form a metalate. Unsaturated metalates like $[Co(PhCCPh)(PPh_3)_2]^-$, a 16e^- species, have been implicated as active species in catalytic cycles.

Thus, a reasonable strategy for the preparation of coordinatively unsaturated metalate complexes is the employment of sterically encumbering π-acid ligands on Group 9 metals. The Figueroa research group has previously investigated this approach using the m-terphenyl isocyanide ligand $CNAr^{Mes2}$ (Ar^{Mes2} = 2,6-(2,4,6-$Me_3C_6H_2)_2C_6H_3$),[36] which features two flanking mesityl substituents. While several monomeric isocyanometalates of Mn, Fe, and Co have been prepared with $CNAr^{Mes2}$,[28-29, 37-38] each has featured coordinative saturation and an 18e^- configuration. The initial goal of this thesis was to define a metalate system that was inherently coordinatively unsaturated, such that substrate binding and activation events could be unimpeded. In the first part of this thesis, a route to unsaturation is described by using m-terphenyl isocyanide ligands; a π-acidic ligand with a significant steric profile.

Herein the actualization of this goal, the synthesis of a series of 16e^-, Group 9 metalate monoanions $[Rh(CNAr^{Dipp2})_3]^-$ and $[Ir(CNAr^{Dipp2})_3]^-$, is reported, where the $CNAr^{Dipp2}$ ligand is a more sterically encumbering m-terphenyl isocyanide derivative (Ar^{Dipp2} = 2,6-(2,6-(i-Pr)$_2C_6H_3)_2C_6H_3$).[19-21] Both $[Rh(CNAr^{Dipp2})_3]^-$ and $[Ir(CNAr^{Dipp2})_3]^-$ display unusual electronic structure characteristics on account of their low coordination number, but react as effective metal-based nucleophiles. In addition, this thesis compares and contrasts the reactivity properties of these Rh and Ir metalates with that of the cobalt derivative, $[Co(CNAr^{Dipp2})_3]^-$, and uncover an unusual situation where the heavier Group 9 complexes display weaker Lewis-acidity properties than their lighter congener.

1.2 Synthesis and electronic structure analysis of a series of Group 9 unsaturated metalates

The goal of the initial work described in this thesis was to synthesize examples of coordinatively unsaturated metalates. It is worth noting that at the outset of this project and the time of their synthesis, to our knowledge there were no other published examples of unsaturated metalates. Four years after the synthesis of the Group 9 metalates described herein, two other notable examples were reported, a mixed carbene and alkene complex by Deng and co-workers in 2020 ([(18-crown-6)K(μ-$C_3H_2N_2$Mes-κC^2,κN-)M(η_2:η_2-dvtms)] M=Co, Rh). Unfortunately these complexes were found to be unstable, undergoing C-N bond cleavage of the flanking mesityl of the N-heterocyclic carbene ligand. While these examples stand as a validation of this strategy, to date there has not been a comparison of the electronic structures of the metalates within this group and there has been no reported reactivity of these species.[39]

Synthetic entry to three-coordinate Rh and Ir metalates was provided by the monovalent d^8 complexes, MCl(CNAr^{Dipp2})$_3$ (M =Rh (**1**), Ir (**2**)), which were obtained via the reaction between the dimers,

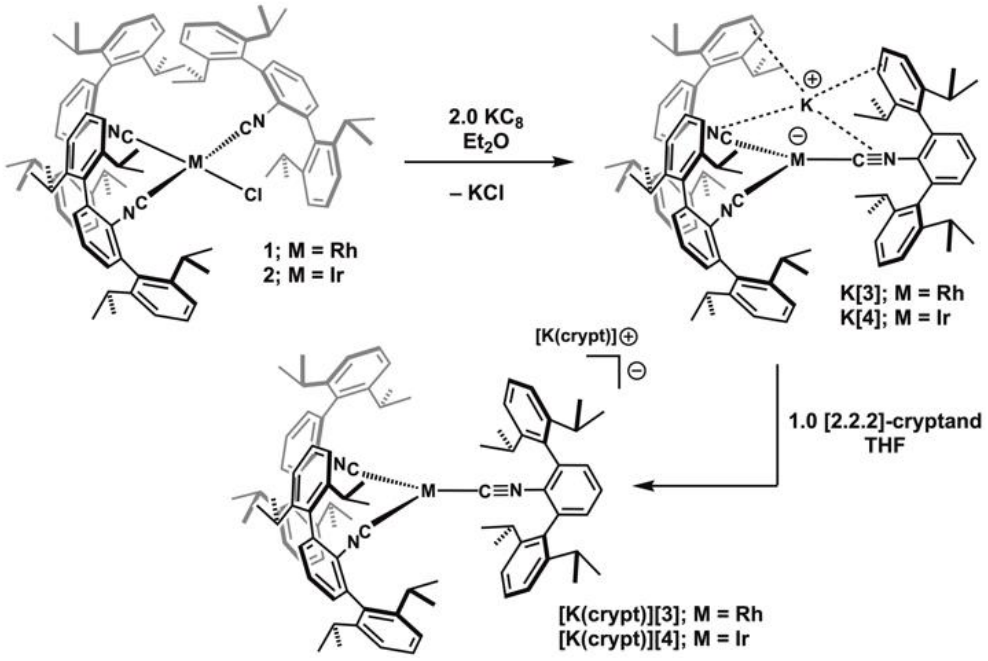

Scheme 1.1 Synthesis of three coordinate Rh and Ir metalate anions.

[MCl(COD)]$_2$ (M = Rh, Ir; COD = 1,5-cyclooctadiene), with 6.0 equiv of CNAr^{Dipp2}. The ^{1}H NMR spectra of complexes **1** and **2** both featured a 2:1 ratio of Ar^{Dipp2} residues, which is diagnostic of a square planar coordination geometry. This was confirmed by crystallographic analysis and it is important to note that the IR spectra of complexes **1** and **2** each possess three ν_{CN} bands in the range of 2156-1967 cm^{-1}, consistent with both a *C*$_2$*v*-symmetric coordination environment and moderate π-backdonation to the CNAr^{Dipp2} ligand π* orbitals.

Reduction of bright yellow complexes **1** or **2** via addition of potassium graphite in a cold Et$_2$O solution forms dark red solutions over the course of an hour (Scheme 1.1). The ^{1}H NMR spectra of these products shows clean conversion to a single CNAr^{Dipp2} environment. Despite the symmetry observed on the NMR timescale, the infrared spectra of the products display a broad series of overlapping peaks in the 2100 cm^{-1} to 1800 cm^{-1} region. Relative to complexes **1** and **2**, these shifts to lower energy indicate the presence of more reduced metal centers, while broadness of the bands are consistent with other isocyanometalates that form tight ion pairing interactions between the isocyanide C≡N units and alkali metal cations.[28-29, 38, 40]

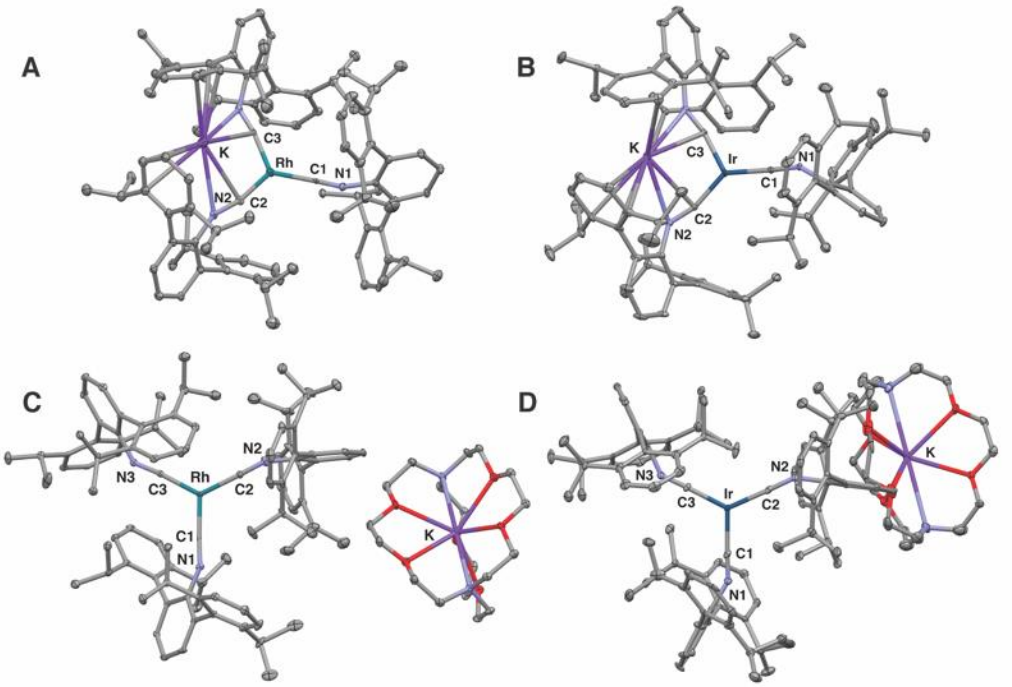

Figure 1.3 Molecular structures of (A) K[Rh(CNAr^{Dipp2})$_3$] (K[3]), (B) K[Ir(CNAr^{Dipp2})$_3$] (K[4]), (C) [K([2.2.2]-cryptand)][Rh(CNAr^{Dipp2})$_3$] ([K(crypt)][3]) and (D) [K([2.2.2]-cryptand)][Ir(CNAr^{Dipp2})$_3$] ([K(crypt)][4]).

Structural determination on crystals grown from Et_2O solution under an N_2 atmosphere identified these products as the three-coordinate metalate salts K[Rh($CNAr^{Dipp2}$)$_3$] (K[**3**]) and K[Ir($CNAr^{Dipp2}$)$_3$] (K[**4**]), which are indeed unsolvated, contact ion-pairs in the solid state. In addition, complexes K[**3**] and K[**4**] give rise to significantly downfield ^{13}C NMR chemical shifts of 212.9 ppm and 225.5 ppm, respectively, for their isocyanide carbon atoms. Such downfield chemical shifts are markers of significant π-backbonding to isocyanide ligands and reflect the presence of highly reduced metal centers, despite the coincidence of a formally 16e$^-$, coordinatively-unsaturated primary coordination sphere.

While the metal centers in K[**3**] and K[**4**] adopt three coordinate environments, inspection of their solid-state structures reveal a significant distortion from an idealized trigonal planar coordination geometry. This is illustrated by the contracted C1-M-C2 angles of 113.0(13)˚ and 112.11(17)˚ for complexes K[**3**] and K[**4**], respectively. The degree to which this is directly caused by the tight ion binding was not clear from these structures and the collected spectroscopic data. To evaluate the structural features of these three-coordinate metalates in the absence of ion pairing, cation encapsulation studies were conducted with [2.2.2]-cryptand. Salts K[**3**] and K[**4**] both reacted readily with [2.2.2]-cryptand in THF solution to form the separated ion pairs [K(crypt)][**3**] and [K(crypt)][**4**] as determined by X-ray crystallography (Scheme 1.1; Figure 1.3). Most remarkably, the [M($CNAr^{Dipp2}$)$_3$]$^-$ anions in [K(crypt)][**3**] and [K(crypt)][**4**] also deviate substantially from an idealized *D*$_3$*h*-symmetric coordination geometry. Instead, they adopt pronounced *C*$_{2v}$ symmetric, Y-shaped structures on account of expanded C2-M-C3 bond angles (125.7(2)˚ and 126.9(8)˚ for [K(crypt)][**3**] and[K(crypt)][**4**], respectively). While predictions for the isolobal and isoelectronic metal carbonyl complexes ([M(CO)$_3$]$^-$) suggest a perfect *D*$_{3h}$, trigonal planar geometry,[23] these structures reveal roughly *C*$_{2v}$ symmetric metal environments. Indeed, the stretching frequencies observed in the infrared spectra of these 2.2.2-cryptand salts are far simplified compared to K[**3**] and K[**4**]. [K(crypt)][**3**] and[K(crypt)][**4**] each show two strong and broad absorbances respectively located at 1782 cm^{-1} and 1738 cm^{-1} for rhodium and 1768 cm^{-1} and 1724 cm^{-1} for iridium. Also observed is a weaker absorbance at 1927 cm^{-1} (Rh), and 1918 cm^{-1} (Ir), consistent with a *C*$_2$*v* symmetric environment at the metal center. This suggests that the distortion towards the lower symmetry coordination environment is retained in solution.

Table 1.1 . Isocyanide-metal-isocyanide bond angles (∠C-M-C) from the solid-state structures of the listed compounds. A. DFT optimized geometry. (B3LYP/ LANL2ZP).

(KCrypt)Co[**4**]	(KCrypt)Rh[**5**]	(KCrypt)Ir[**6**]	$Pd(PPh_3)_3$[41]	$[Rh(CNAr^{Ph2})_3]^{-}$[a]
120°	125.7(2)°	128.7(8)°	126.24(2)°	125.072°
120°	117.4(2)°	117.2(8)°	116.98(3)°	118.267°
120°	116.6(2)°	114.1(7)°	114.82(2)°	116.402°

While a distortion of only a few degrees may seem small, Density Functional Theory (DFT) studies suggest that it has an outsize effect on the frontier orbital landscape. The optimized geometry of truncated models $[Rh(CNAr^{Ph2})_3]$– and $[Ir(CNAr^{Ph2})_3]^{-}$ retain the important parameters of the corresponding structures of [K(crypt)][**3**] and[K(crypt)][**4**]. In an ideal D_3h metal complex in a C_3 symmetric π-acidic ligand field, such as the unstable gas phase molecule $[Rh(CO)_3]^{-}$, the expected HOMO is the metal based a_1' (dz^2 in character) and the HOMO –1 and –2 are the in plane π-back-bonding e′ interaction (d_{x2-y2}, d_{xy}) (Figure 1.4 A). Remarkably, DFT calculations suggest the small distortions observed for [K(crypt)][**3**] and[K(crypt)][**4**] reflect a change in the frontier orbital landscape of the anions, promoting the d_{x2-y2} to be the HOMO above the d_{z2} (HOMO –1) (Figure 1.4 B). Given the higher symmetry observed on the NMR time scale, the energy barrier of the distortion was assessed using a relaxed potential energy scan of an expanding C-Rh-C angle in both carbonyl and phenyl isocyanide (PhNC) model complexes (Figure 1.5). Within the C-M-C angle range of 115° – 133°, encompassing the full upper range of angles experimentally observed, the depth of the potential energy wells show a small barrier of <2 kcal mol^{-1} for the $[Rh(CO)_3]^{-}$ and <1 kcal mol^{-1} for the $[Rh(PhNC)_3]^{-}$. Notably, scanning beyond this range for the small isocyanide suggests rotation of the aryl group in to the plane of the complex and significant bending of the C-N-C bond angles suggesting reduction of the PhNC group. We believe that rotation is unlikely to occur in **3** and **4** due to the drastically increased steric pressures of the *m*-terphenyls, and suggests the flanking terphenyl rings provide stability against potential decomposition pathways with smaller ligands. Given the insights gained from these computational studies, we believe this may impart accessibility to both the d_{x2-y2} and d_{z2} orbitals resulting in diverse reactivity profiles for group 9 unsaturated metalates.

We postulate that the source of this desymmetrization is related to the higher electronegativity of Rh and Ir relative to Co. It has been shown for homoleptic metal carbonyls that as the electronegativity of the metal increases, the importance of the back-bonding interaction lessens while, inversely, the a_1-symmetry, primary M-C sigma bonding interaction increases.[42] Conflated with the greater sigma donor character of the isocyanide compared to carbon monoxide, the net effect imparts a greater resemblance to a phosphine complex rather than a carbonyl complex for [K(crypt)][**3**] and[K(crypt)][**4**].[41] In low temperature IR matrix studies on Group 9 tri-carbonyl monoanions, it was concluded by the authors that the complexes were likely D_3h in symmetry.[23] In contrast, d^{10} phosphine complexes like $Pd(PPh_3)_3$ and $Pt(PPh_3)_3$ are more in line with what is structurally observed for [K(crypt)][**3**] and[K(crypt)][**4**], displaying analogous C_{2v} distortions towards T-shaped geometries (Table 1.1).

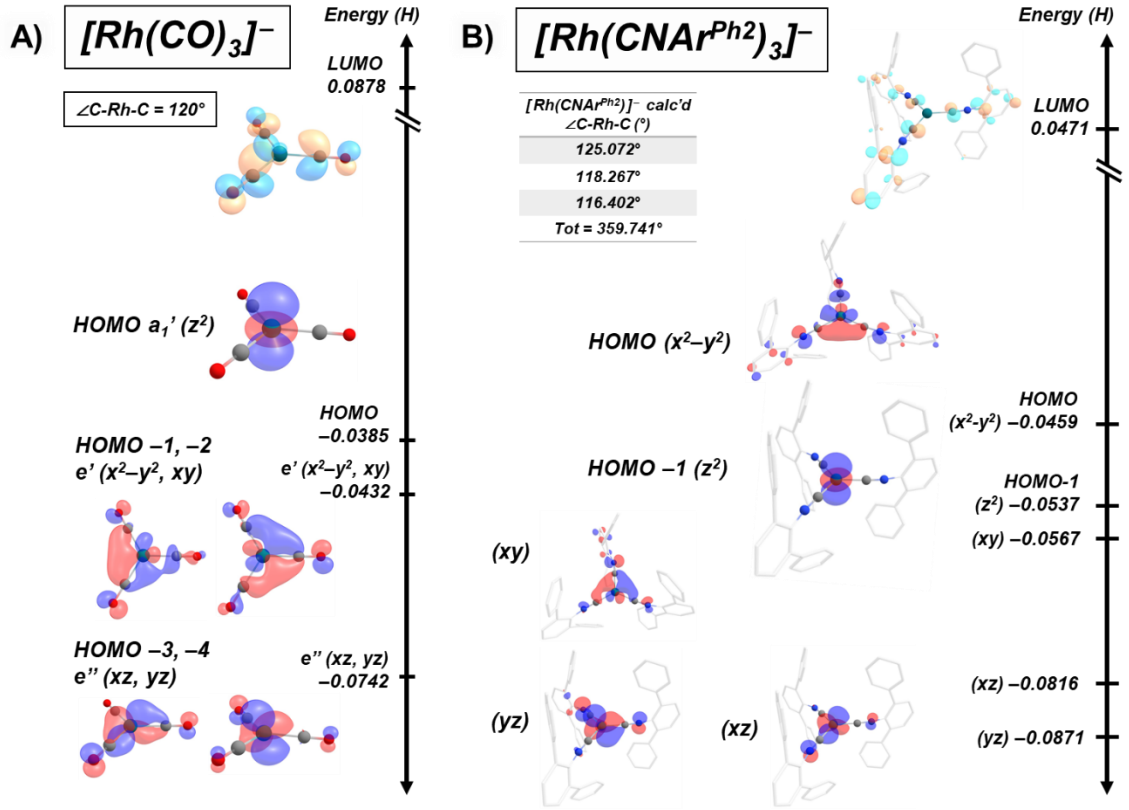

Figure 1.4 DFT-calculated (B3LYP/LANL2ZP) molecular orbitals, associated d-orbital splitting pattern and optimized metrical parameters for the A) D_{3h}-symmetric tricarbonyl metalate $[Rh(CO)_3]^-$ amd B) the C_{2v}-symmetric model complex $[Rh(CNAr^{Ph2})_3]^-$.

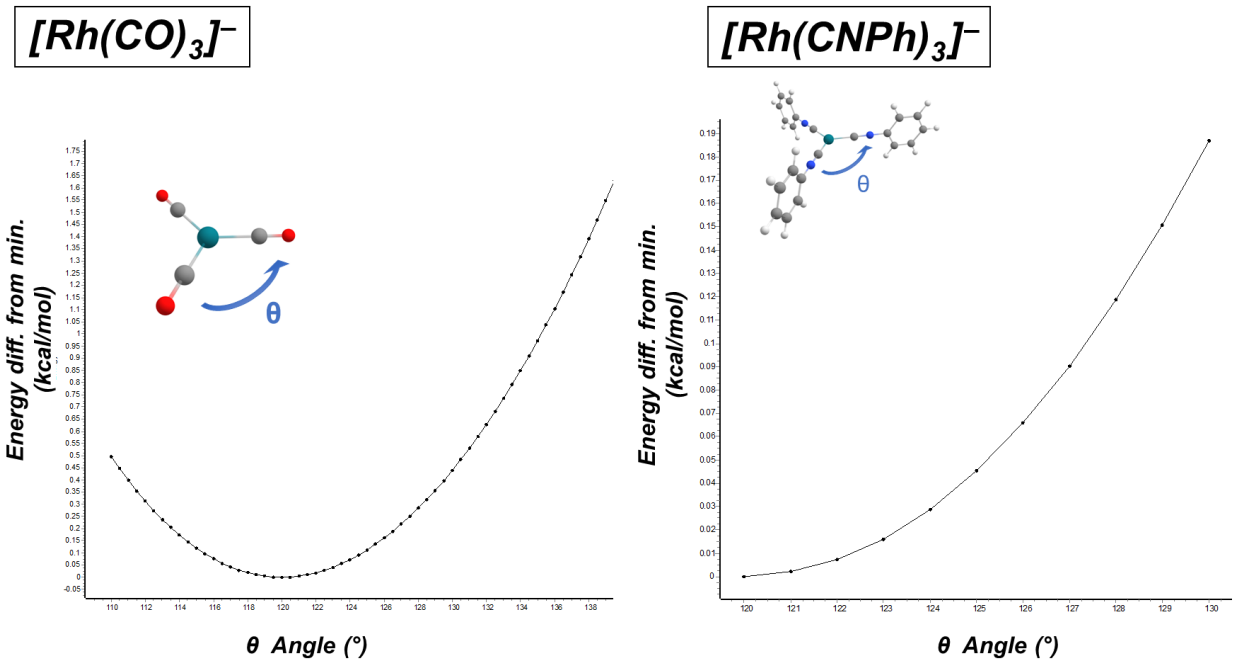

Figure 1.5 DFT-calculated relaxed potential energy scans of in plane C-Rh-C bond angle scans. Left is a graph of the potential energy well for the $[Rh(CO)_3]^-$ from 115°to 140° and on the right is the potential energy well for $[Rh(CNPh)_3]^-$ from 115° to 135°.

Both the K^+ and $[K(crypt)]^+$ salts of metalates **3** and **4** can be prepared and manipulated under an N_2 atmosphere and show no propensity for N_2 binding. However, the cobalt congener, $[Co(CNAr^{Dipp2})_3]^-$, exhibits distinctly different behavior. As shown in Scheme 1.2, treatment of $CoCl_2$ with 3.0 equiv of $CNAr^{Dipp2}$ in THF under N_2, followed by addition of sodium amalgam (Na/Hg), results in the isolation of the four-coordinate dinitrogen complex, $K[Co(N_2)(CNAr^{Dipp2})_3]$ (Na[**5**-N_2]), as determined by X-ray diffraction (Figure 3). Unlike the synthesis of K[**3**] and K[**4**], repeated attempts to prepare the potassium derivative of [**5**-N_2]– using KC_8 often led to overreduction and decomposition. Nevertheless, in the solid state, Na[**5**-N_2] exhibits contact ion-pairing between the isocyanide C≡N units and the Na+ cation, while the terminal N_2 ligand occupies a position distal from the Na center. The solution FTIR spectrum of Na[**5**-N_2] features broad, overlapping ν_{CN} stretches from 2018-1840 cm^{-1}, which are indicative of a significantly reduced Co center and contact ion pairing interaction involving the isocyanide C≡N units (ν_{CN} for free $CNAr^{Dipp2}$ = 2118 cm^{-1}).[43] Most notably, the FTIR spectrum of Na[**5**-N_2] shows a sharp ν_{NN} band centered at 2159 cm^{-1}. This relatively high-energy band reflects only a marginal degree of N≡N bond activation,[44]

which is unusual given the electron-rich nature of the Co center in Na[**5**-N_2]. While isocyanide ligands are expected to function as stronger π-acids than N_2, and therefore more effectively compete for metal based electron density, the magnitude of π-back donation from the Co to the π*(C≡N) orbitals in [**5**-N_2] is similar to that of the Rh and Ir metalates K[**3**] and K[**4**]. However, the fact that the anionic $[Co(CNAr^{Dipp2})_3]^-$ unit binds N_2, while the analogous Rh and Ir do not, suggests that the Co center in these metalates retains a far higher degree of Lewis acidity. Lending further credence to this notion is that the unsolvated metalate salt, $Na[Co(CNAr^{Dipp2})_3]^-$ (Na[**5**]), can be prepared via Na/Hg reduction of $CoCl_2$ under an argon atmosphere (Scheme 1.2). However, rather than adopting a three-coordinate geometry, crystallographic analysis revealed the clear presence of a C-H agostic interaction[45] between the Co center and an isopropyl methyl group of the $CNAr^{Dipp2}$ ligand (Figure 1.6). In addition, this agostic interaction is located in the apical position of a trigonal monopyramid, which is the coordination geometry expected from coordination of fourth ligand to the p_z orbital of a d^{10} metal center.

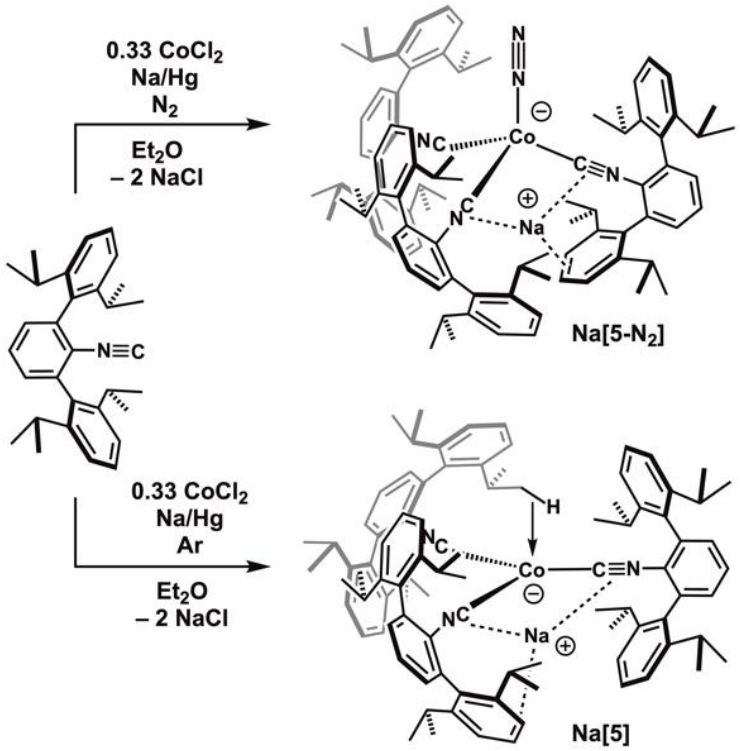

Scheme 1.2 Synthesis of the cobalt metalate complexes $Na[(N_2)Co(CNAr^{Dipp2})_3]$ (Na[5-N2]) and $Na[Co(CNAr^{Dipp2})_3]$ (Na[5]), which possesses a C-H agostic interaction in the solid-state

We contend that the enhanced Lewis acidity displayed by $[Co(CNAr^{Dipp2})_3]^-$ is due to the lower energy of the empty Co $4p_z$ orbital relative to the empty $5p_z$ and $6p_z$ orbitals in K[**3**] and K[**4**], respectively. Importantly, Lu et al. has described a related phenomenon for the rhodium $[ERhL_3]^-$ metalate complexes (E = Al, Ga, In; L = N(*o*-(C_6H_4)$NCH_2P(i\text{-}Pr_2)$)$_3$) featuring Lewis-acid coordination to a formally anionic $[Rh(PR_3)_3]^-$ fragment.[14] In that work, coordination of Al and Ga Lewis acids to the Rh center results in four-coordinate structures. However, upon coordination of the more a Lewis-acidic In center to rhodium, a five-coordinate dinitrogen complex is observed, with the N_2 unit bound trans to the Lewis acid (i.e. Z-type ligand). As has now been established, Lewis-acid coordination to d^{10} metal centers effectively lowers the energy of trans-disposed acceptor orbitals of p-orbital parentage.[46-50] This effect has traditionally been evaluated as a function of the acceptor strength of Lewis acidic ligands.[49, 51] However, a similar effect can be expected for a transition-metal triad when low-coordination numbers, and therefore, empty metal-based p-orbitals are available. To this end, it is important to note that the Na^+ cation in both Na[**5**] and Na[**5**-N_2] occupies a position seemingly within bonding contact to the Co center and could in principle function as a trans-disposed Z-type ligand. However, the zwitterionic complex [η_2-*C*,*C*-PPN][$Co(CNAr^{Mes2})_3$],[37] which possesses the less encumbered $[Co(CNAr^{Mes2})_3]^-$ metalate fragment, binds the traditionally noncoordinating

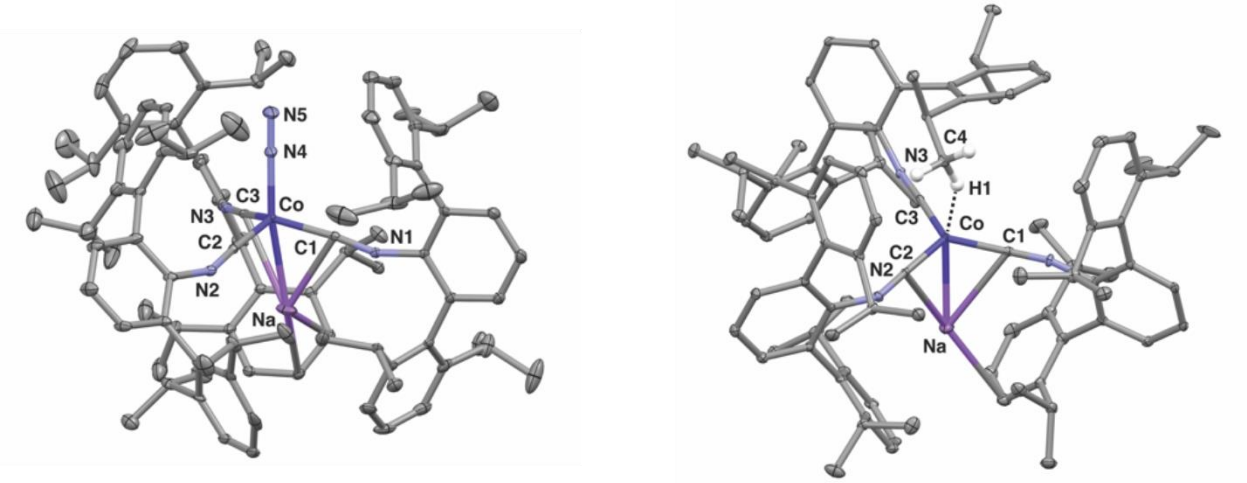

Figure 1.6 Molecular structures of the cobalt metalate complexes Na[(N2)Co($CNAr^{Dipp2}$)$_3$] (Na[5-N_2]; left) and Na[Co($CNAr^{Dipp2}$)$_3$] (Na[5], right). Selected Bond Distances for Na[5] (Å). d(Co-H1) = 2.02(1); d(Co-C4) = 2.899(13).

[PPN]+ cation, which in turn stabilizes the coordinatively-unsaturated Co center. Coupled with the with binding of both N_2 and C-H bonds in Na[**5**] and Na[**5**-N_2], this unusual coordination behavior of [η_2-*C*,*C*-PPN][Co($CNAr^{Mes2}$)$_3$], provides additional evidence that the cobalt congener in three coordinate metalates of the Group 9 triad possess the most significant Lewis acidic properties.

1.3 Concluding remarks and outlook

A full series of homoleptic, unsaturated, metalates have been isolated and described for the first time. The heavier rhodium and iridium metalates display an unpredicted distortion to a Y-shaped, roughly C_2v symmetric geometry possible promoting electronic accessibility of the d_{x2-y2} as well as the d_{z2} orbital. The cobalt metalates surprisingly show a higher degree of Lewis-acidity, displaying an agostic interaction in the solid state, and binding N_2 when exposed to an N_2 atmosphere. The redox behavior and reactivity of these anions are highlighted in the second chapter of this thesis. The electronic and steric diversification of aryl isocyanides used in this chapter as well as other isocyanides are further explored in the third chapter of this thesis.

1.4 Synthetic procedures and characterization data

General Considerations – All manipulations were carried out under an atmosphere of purified dinitrogen using standard Schlenk and glovebox techniques. Unless otherwise stated, reagent-grade starting materials were purchased from commercial sources and either used as received or purified by standard procedures.[52] Solvents were dried and deoxygenated according to standard procedures.[53] Benzene-d_6 (Cambridge Isotope Laboratories) was distilled from NaK alloy/benzophenone ketyl and stored over 4 Å molecular sieves under N_2 for at least 24 h prior to use. Celite 405 (Fisher Scientific) was dried under vacuum (24 h) at a temperature above 250 ˚C and stored in the glovebox prior to use. The m-terphenyl isocyanide $CNAr^{Dipp2}$ was prepared as previously reported.[43, 54]

Solution ^{1}H and $^{13}C\{^{1}H\}$ NMR spectra were recorded on a Bruker Avance 300, a Varian Mercury 400, a Jeol ECA 500, or a Varian X-SENS 500 spectrometer. ^{1}H and $^{13}C\{^{1}H\}$ chemical shifts are reported in ppm relative to $SiMe_4$ (^{1}H and ^{13}C $\delta = 0.0$ ppm) with reference to residual solvent resonances of 7.16 ppm (^{1}H) and 128.06 ppm (^{13}C) for C_6D_6.[55] Solution FTIR spectra were recorded on a Thermo-Nicolet iS10 FTIR spectrometer. Samples were prepared as C_6D_6 solutions injected into a ThermoFisher solution cell equipped with KBr windows. For solution FTIR spectra, solvent peaks were digitally subtracted from all spectra by comparison with an authentic spectrum obtained immediately prior to that of the sample. The following abbreviations were used for the intensities and characteristics of important IR absorption bands: vs = very strong, s = strong, m = medium, w = weak, vw = very weak; b = broad, vb = very broad, sh = shoulder. Combustion analyses were performed by Midwest Microlab LLC, Indianapolis, IN.

Synthesis of $RhCl(CNAr^{Dipp2})_3$ (1): $[RhCl(COD)]_2$ (0.619 g, 1.255 mmol, 0.5 equiv) and $CNAr^{Dipp2}$ (3.124 g, 7.533 mmol, 3 equiv) were combined as solids and dissolved in 40 mL of THF. The yellow/orange reaction was stirred at room temperature for 4 h before being dried *in vacuo*. The resulting yellow solid was slurried 3 times in n-pentane for 10 min and dried to remove excess cyclooctadiene. Recrystallization of the solid from a concentrated THF solution followed by storage at -32 °C for 1 week afforded yellow crystals suitable for X-ray diffraction. Yield: 3.01 g, 2.134 mmol, 85%. ^{1}H NMR (499.8.9 MHz, C_6D_6, 20 ˚C): $\delta = 7.42$ (t, 4H, 8Hz, p-Dipp), 7.29 (d, 8H, 8Hz, m-Dipp), 7.16 (t, 2H, 8Hz, p-Dipp), 7.12 (d, 4H, 8Hz, m-Dipp), 6.93 (d, 4H, 8Hz, m-Ar), 6.89 (d, 2H, 8Hz, m-Ar), 6.83 (dd, 2H, 8Hz, p-Ar), 6.79 (dd, 1H, 8Hz, p-Ar), 2.73 (septet, 8H, 7Hz, $CH(CH_3)_2$), 2.54 (septet, 4H, 7Hz, $CH(CH_3)_2$), 1.27 (d, 24H, 7Hz, $CH(CH_3)_2$), 1.10 (d, 24H, 7Hz, $CH(CH_3)_2$), 1.09 (d, 12H, 7Hz, $CH(CH_3)_2$), 0.96 (d, 12H, 7Hz, $CH(CH_3)_2$) ppm. $^{13}C\{^{1}H\}$ NMR (125.8MHz, C_6D_6, 20 ˚C): $\delta = 163.3$ (d, $J_{CRh} = 70.2$ Hz, CNR), 159.6 (d, $J_{CRh} = 58.8$ Hz, CNR), 147.5, 146.7, 138.1, 137.9, 135.7, 135.4, 131.6, 130.9, 129.6, 129.4, 127.8, 127.5, 127.2, 126.1, 123.6, 31.2, 31.0, 25.4, 24.8, 24.6 ppm. FTIR (KBr windows, C_6D_6, 20 ˚C) $\upsilon(C{\equiv}N) = 2152$ (w), 2094 (vs), 2059 (s), 2036 (s), 2001(s) cm^{-1}; also 3062 (w) 3062 (w), 2962 (s), 2927 (m), 2865 (m), 1577 (w), 1457 (m), 1411 (w), 1384 (w), 1361 (w), 1056 (w), 759 (s) cm^{-1}. Anal. calcd. for $C_{93}H_{111}N_3Rh_1Cl_1$: C, 79.26; H, 7.94; N, 2.98. Found: C, 79.58; H, 8.09; N, 3.02.

Synthesis of IrCl(CNAr^{Dipp2})$_3$ (2): The procedure for RhCl(CNAr^{Dipp2})$_3$ (1) was followed using [IrCl(COD)]$_2$ (0.842 g, 1.253 mmol, 0.5 equiv). Recrystallization of the resulting red solid from n-pentane spiked with 2 drops of Et_2O (5mL total) followed by storage at -32 °C for 1 week afforded red crystals suitable for X-ray diffraction. Yield: 3.21 g, 2.15 mmol, 86%. ^{1}H NMR (499.8.9 MHz, C_6D_6, 20 ˚C): δ = 7.41 (t, 4H, 8Hz, p-Dipp), 7.27 (d, 8H, *J* = 8 Hz, m-Dipp), 7.16 (t, 2H, *J* = 8 Hz, p-Dipp), 7.11 (d, 4H, *J* = 8 Hz, m-Dipp), 7.04 (t, 2H, *J* = 8 Hz, m-Ar), 6.89 (d, 2H, *J* = 8 Hz, m-Ar), 6.81 (t, 2H, *J* = 8 Hz, p-Ar), 6.80 (t, 1H, *J* = 8 Hz, p-Ar), 2.71 (septet, 8H, *J* = 7 Hz, CH(CH$_3$)$_2$), 2.57 (septet, 4H, *J* = 7 Hz, CH(CH$_3$)$_2$), 1.26 (d, 24H, *J* = 7 Hz, CH(CH$_3$)$_2$), 1.10 (d, 24H, *J* = 7 Hz, CH(CH$_3$)$_2$), 1.09 (d, 12H, *J* = 7 Hz, CH(CH$_3$)$_2$), 0.98 (d, 12H, *J* = 7 Hz, CH(CH$_3$)$_2$) ppm. ^{13}C{^{1}H} NMR (125.8MHz, C_6D_6, 20 ˚C): δ = 154.2 (CNR), 151.1 (CNR), 147.0, 146.4, 138.1, 137.0, 135.9, 135.0, 131.2, 130.6, 130.2, 129.2, 128.8, 127.3, 127.2, 126.8, 124.9, 123.2, 123.0, 30.8, 30.6, 29.9, 25.0, 24.6, 24.3, 24.2 ppm. FTIR (KBr windows, C_6D_6, 20 ˚C) υ(C≡N) = 2156 (w), 2082 (vs), 1967 (s) cm^{-1}; also 2962 (s), 2927 (m), 2865 (m), 1577 (w), 1461 (m), 1411 (w), 1384 (w), 1361 (w), 759 (m) cm^{-1}. Anal. calcd. for $C_{93}H_{111}N_3IrCl$: C, 74.54; H, 7.47; N, 2.37. Found: C, 75.68; H, 7.47; N, 2.49.

Synthesis of K[Rh(CNAr^{Dipp2})$_3$] (K[3]): To a thawing 1:2 Et_2O/THF solution (20 mL total) of RhCl(CNAr^{Dipp2})$_3$ (**1**; 0.300 g, 0.213 mmol, 1 equiv) was added KC_8 (0.086 g, 0.639 mmol, 3 equiv.) in two equal portions, letting the reaction stir at −32 °C for 30 minutes between additions. After the second addition, the reaction mixture was allowed stir for an additional 30 minutes at −32 ˚C before filtering over Celite to remove graphite and KCl. The resulting dark brown filtrate was dried *in vacuo* before being subjected to three cycles of slurrying in n-pentane (3 x 5 mL) to remove any remaining THF. The resultant dark solid was dissolved in C_6H_6 and filtered over a plug of Celite packed on fiberglass. The filtrate was frozen and lyophilized to a fluffy powder. Yield: 0.285 g, 0.202 mmol, 95%. Recrystallization of the solid from n-pentane spiked with 3 drops of Et_2O (5 mL total) followed by storage at −32 °C for 3 weeks afforded dark red crystals suitable for X-ray diffraction. ^{1}H NMR (499.8.9 MHz, C_6D_6, 20 ˚C): δ = 7.28 (t, 6H, *J* = 8 Hz, p-Dipp), 7.17 (d, 12H, *J* = 8 Hz, m-Dipp), 6.96 (d, 6H, *J* = 8 Hz, m-Ar), 6.88 (t, 3H, *J* = 8 Hz, p-Ar), 2.86 (septet, 12H, *J* = 7 Hz, CH(CH$_3$)$_2$), 1.18 (d, 36H, *J* = 7 Hz, CH(CH$_3$)$_2$), 1.14 (d, 36H, 7Hz, CH(CH$_3$)$_2$)

ppm. $^{13}C\{^{1}H\}$ NMR (125.8MHz, C_6D_6, 20 ˚C): δ = 212.9 (d, $J_{C\text{-}Rh}$ = 82.3 Hz, CNR), 147.8, 138.3, 135.2, 133.4, 130.2, 128.7, 123.1, 31.0, 25.1, 24.3 ppm. FTIR (KBr windows, C_6D_6, 20 ˚ C) υ(C≡N) = 2067 (w), 2012 (m, sh), 1982 (vs), 1850 (s, br), 1741 (s, br), 1688 (vs), cm^{-1}; also 2962 (s), 2962 (m), 1866 (m), 1461 (m), 1411 (s), 1383 (w), 1362 (w), 1328 (s), 1199 (w), 1177 (w), 1055 (m, br), 757 (s) cm^{-1}. Anal. calcd. for $C_{93}H_{111}N_3RhK$: C, 79.06; H, 7.92; N, 2.97. Found: C, 78.68; H, 7.80; N, 2.87.

Synthesis of K[Ir(CNAr^{Dipp2})$_3$] (K[4]): To a thawing 1:2 Et_2O/THF mixture of IrCl(CNAr^{Dipp2})$_3$ (**2**; 0.126 g, 0.084 mmol, 1 equiv, 15 mL) was added KC_8 (0.034 g, 0.252 mmol, 3 equiv) in two equal portions, letting the reaction stir at −32 ˚C for 30 minutes between additions. After the second addition, the reaction was allowed to stir for an additional 30 minutes at −32 ˚*C* before filtering over Celite packed remove both graphite and KCl. The resulting dark brown filtrate was dried *in vacuo* before being subjected to three cycles of slurrying in n-pentane (3 x 5 mL) and drying *in vacuo* again to remove any remaining THF. The resultant dark solid was dissolved in C_6H_6 and filtered over Celite. The filtrate was frozen and lyophilized to a fluffy powder. Yield: 0.115 g, 0.077 mmol, 91%. Recrystallization of the solid from n-pentane spiked with 2 drops of Et_2O (3 mL total) followed by storage at −32 ˚C for 1 week afforded dark red crystals suitable for X-ray diffraction. ^{1}H NMR (499.8.9 MHz, C_6D_6, 20 ˚C): δ = 7.26 (t, 6H, *J* = 8 Hz, p-Dipp), 7.18 (d, 12H, *J* = 8 Hz, m-Dipp), 7.00 (d, 6H, *J* = 8 Hz, m-Ar), 6.92 (t, 3H, *J* = 8 Hz, p-Ar), 2.9 (septet, 12H, *J* = 7 Hz, $CH(CH_3)_2$), 1.18 (d, 36H, *J* = 7 Hz, $CH(CH_3)_2$), 1.13 (d, 36H, *J* = 7 Hz, $CH(CH_3)_2$) ppm. $^{13}C\{^{1}H\}$ NMR (125.8MHz, C_6D_6, 20 ˚C): δ = 225.5 (CNR), 147.7, 138.4, 137.0, 133.0, 130.3, 128.8, 123.1, 122.7, 31.0, 25.1, 24.2 ppm. FTIR (KBr windows, C_6D_6, 20 ˚C) υ(C≡N) = 2015 (m, sh), 1961 (s), 1804 (vs, sh), 1743 (vs), 1657 (vs), 1660 (vs, sh) cm^{-1}; also 3060 (m), 3038(w, sh), 3022 (w, sh), 2962 (s), 2926 (m), 2866 (m), 1571 (vs), 1461 (s), 1411 (s), 1383 (m), 131 (m), 1331 (s), 1251 (w), 1202 (w), 1177 (w), 1055 (m), 924 (w), 795 (s), 680 (m), 620 (w), 582 (m), 570 (m) cm^{-1}. Anal. calcd. for $C_{93}H_{111}N_3IrK$: C, 74.36; H, 7.45; N, 2.80. Found: C, C, 73.90; H, 7.38; N, 3.23.

Synthesis of [K(cryptand-2.2.2)][Rh(CNAr^{Dipp2})$_3$] ([K(crypt)][3]): To a stirring solution of K[Rh(CNAr^{Dipp2})$_3$] (K[**3**]; 0.027 g, 0.019 mmol, 1 equiv) in 2 mL C_6H_6, cryptand-2.2.2 (0.006 g, 0.015 mmol, 1 equiv) was added as a solid. The reaction was allowed to stir 20 min, during which time a dark

precipitate formed. The precipitate was collected via filtration on a pad of Celite, and washed with *n*-pentane (3 x 2 mL). The precipitate was then dissolved and washed through the Celite with 5 mL of THF. The THF filtrate was the dried *in vacuo* yielding a dark red solid. Yield: 0.032 g, 0.018 mmol, 93%. X-ray quality crystals were grown by dissolving the solid in 2 mL of a THF/benzene (20:1) solution and placing it at *−32* ˚C for 2 weeks. ^{1}H NMR (499.8.9 MHz, C_6D_6, 20 ˚C): δ = 7.28 (t, 6H, 8 *J* = Hz, p-Dipp), 7.17 (d, 12H, *J* = 8 Hz, m-Dipp), 6.96 (d, 6H, *J* = 8 Hz, m-Ar), 6.88 (t, 3H, *J* = 8 Hz, p-Ar), 3.57 (s, 12H, CH_2CH_2O), 3.53 (dd, 12H, OCH_2CH_2N), 2.55 (s, 12H), OCH_2CH_2N), 2.86 (septet, 12H, *J* = 7 Hz, $CH(CH_3)_2$), 1.18 (d, 36H, *J* = 7 Hz, $CH(CH_3)_2$), 1.14 (d, 36H, *J* = 7 Hz, $CH(CH_3)_2$) ppm. ^{13}C{^{1}H} NMR (125.8MHz, C_6D_6, 20 ˚C): δ = 212.9 (d, J_{CRh} = 86.8 Hz, CNR), 147.8, 138.3, 135.2, 133.4, 130.2, 128.7, 123.1, 31.0, 25.1, 24.3 ppm. FTIR (KBr windows, THF, 20 ˚C) υ(C≡N) = 1926 (w), 1781 (vs), 1737 (vs) cm^{-1}; also 1569 (s), 1407 (s), 1380 (w, sh), 1355 (m), 1133 (m), 1108 (s), 755 (s) cm^{-1}. Anal. calcd. for $C_{111}H_{147}N_5O_6RhK$: C, 74.51; H, 8.24; N, 3.91. Found: C, 71.36; H, 8.34; N, 3.90.

Synthesis of [K(cryptand-2.2.2)][Ir(CNAr^{Dipp2})$_3$] ([K(crypt)][4]): This compound was prepared and crystallized analogously to K(crypt)][**3**] using 0.023 g of K[Ir(CNAr^{Dipp2})$_3$] (K[**4**]; 0.017 mmol, 1 equiv) and 0.006 g of cryptand-2.2.2 (0.015 mmol, 1 equiv). Yield (dark red solid): 0.030 g, 0.016 mmol, 92%. ^{1}H NMR (499.8.9 MHz, THF-d^{8}, 20 ˚C): δ = 7.30 (t, 3H, *J* = 8 Hz, p-Ar), 7.03 (t, 6H, *J* = 8 Hz, p-Dipp), 6.90 (d, 12H, *J* = 8 Hz, m-Dipp), 6.74 (d, 6H, *J* = 8 Hz, m-Ar), 3.64 (septet, 12H, *J* = 7 Hz, $CH(CH_3)_2$), 3.60 (s, 12H, CH_2CH_2O), 3.53 (dd, 12H, OCH_2CH_2N), 2.54 (s, 12H), OCH_2CH_2N), 0.87 (d, 36H, *J* = 7 Hz, $CH(CH_3)_2$), 0.84 (d, 36H, *J* = 7 Hz, $CH(CH_3)_2$) ppm. ^{13}C{^{1}H} NMR (125.8MHz, THF-d_8, 20 ˚C): δ = 229.1(CNR), 147.5, 139.2, 132.7, 129.9, 128.8, 127.5, 122.6, 119.4, 71.1, 68.2, 53.5, 31.1, 30.8, 25.2, 24.8, 24.4 ppm. FTIR (KBr windows, THF, 20 ˚C) υ(C≡N) = 1918 (w), 1768 (vs), 1724 (vs), cm^{-1}; also 1569 (s), 1479 (s), 1407 (s), 1355 (m), 752 (m), 680 (s) cm^{-1}. Anal. calcd. for $C_{111}H_{147}N_5O_6IrK$: C, 70.96; H, 7.89; N, 3.73. Found: C, 70.58; H, 7.88; N, 3.48.

Synthesis of Na[(N_2)Co(CNAr^{Dipp2})$_3$] (Na[5-N_2]): This reaction procedure is carried out under $N_{2(g)}$ atmosphere. To a THF (10 mL) suspension of $CoCl_2$ (0.054 g, 0.42 mmol, 1 equiv) was added CNAr^{Dipp2} (0.500 g, 1.26 mmol, 3 equiv). The resulting mixture was allowed to stir for 10 min, after which

0.1 % NaHg (Na: 0.96 g, 4.2 mmol, 10 equivalents; Hg: 9.6 g) was added. The reaction mixture was shaken by hand for *ca.* 7 min, where upon a color change to deep purple was observed. The reaction mixture was allowed to stir for an additional 20 mins upon which time the solution was decanted from the sodium amalgam via filtration over Celite packed on a medium porosity glass sintered frit and evaporated to dryness. The resulting residue was then slurred in *n*-pentane (15 mL) allowed to stir for 5 min and then concentrated to dryness. This step was repeated two additional times to desolvate residual NaCl by-products, whereupon a color change from purple to red was observed. Extraction of the resulting residue with benzene (10 mL), followed by filtration through Celite produced a deep-red solid. Na[(N_2)Co$(CNAr^{Dipp2})$] is isolated as a fluffy red solid, 0.400 g, 0.29 mmol, 69 % yield. ^{1}H NMR (499.9 MHz, C_6D_6, 20℃): δ = 7.31 (t, 6H, *J* = 5 Hz, *p*-Dipp), 7.18 (d, 12H, *J* = 5 Hz, *m*-Dipp), 6.98 (d, 6H, *J* = 5 Hz, *m*-Ph), 6.87 (t, 3H, *J* = 5 Hz, *p*-Ph), 2.91 (sept, *J* = 5 Hz, 12H, C*H*$(CH_3)_2$), 1.27 (d, *J* = 5 Hz, 36H, CH(C*H*$_3)_2$), 1.13 (d, *J* = 5 Hz, 36H, CH(C*H*$_3)_2$) ppm. ^{13}C{^{1}H} NMR (125.7 MHz, C_6D_6, 20℃): δ = 147.5, 138.5, 135.1, 134.0. 130.7, 130.4, 128.6, 127.7, 127.5, 123.1, 34.4, 31.1, 25.4, 24.3, 22.8, 14.3 ppm. FTIR (C_6D_6, KBr windows, 25 ˚C): ν_{NN} = 2159 (m) cm^{-1}, ν_{CN} = 2018 (w), 1946 (m), 1840 (vs) cm^{-1}, also 2961 (s), 2927 (m), 2868 (w), 1463 (m), 1383 (w), 1363 (w) cm^{-1}. Anal. Calcd. for $C_{93}H_{111}N_3CoNa$: C, 80.89; H, 8.10; N, 5.07. Found C, 80.46; H, 8.28; N, 5.06.

1.5 Details of DFT computational studies

General Computational Details: Density Functional Theory (DFT) calculations were performed with ORCA 4.0.0 program suite and/or the Gaussian 16 software package.[56-57] Geometry optimizations, were performed using the B3LYP functional[58-60] in conjunction with the 6-31g(d) basis set[61] for H, C, O and N atoms, and the LANL2DZ basis set[62] plus f-type polarization functions for the rhodium atoms. Atomic coordinates obtained by single-crystal X-ray diffraction analysis on [K(crypt)][**3**] were used as the starting point for optimizations on the truncated model, $[Rh(CNAr^{Ph2})_3]^-$. Optimizations on $[Rh(CO)_3]^-$ used an idealized D_{3h}-symmetric complex as a

starting point. *ChemCraft 1.8* was used for visualization of geometry optimized structures and molecular orbitals (MO).[63]

Input file for model of Rh(CNAr^{Ph2})$_3^-$.

```
%chk=RhL3-.chk
%nprocs=8
%mem=30GB
#P GFINPUT POP(FULL)
# opt freq b3lyp gen pseudo=read geom=connectivity

Rh tris CNArPh2

-1 1
 Rh          -0.02150000   0.01530000   0.29590000
 C           -1.80080000  -0.55920000   0.75720000
 N           -2.90120000  -1.01830000   0.93610000
 C            0.72390000   1.70580000   0.85560000
 N            1.16480000   2.79060000   1.14440000
 C           -4.06180000  -1.72240000   0.98050000
 C            0.92710000  -1.11360000  -0.90680000
 N            1.54040000  -1.79740000  -1.69690000
 C           -4.24540000  -2.73670000   1.96880000
 C            1.50680000   4.05230000   1.49910000
 C            2.94410000   3.14710000   3.41010000
```

C	-1.85370000	-3.37640000	2.50590000
C	1.38750000	6.45770000	1.15570000
H	0.99330000	7.30410000	0.59950000
C	1.01380000	5.16930000	0.75470000
C	-4.98370000	-0.37300000	-0.98460000
C	2.37320000	4.26780000	2.61530000
C	-5.93370000	1.51040000	-2.21040000
H	-6.73850000	2.23040000	-2.34140000
C	-3.17330000	-3.12790000	2.92340000
C	-2.51150000	-3.72820000	5.19380000
H	-2.77410000	-3.85130000	6.24220000
C	2.53370000	-2.23540000	-2.51760000
C	-4.82070000	1.53910000	-3.05380000
H	-4.75650000	2.27600000	-3.85120000
C	4.47470000	-3.64750000	-2.91700000
H	5.23310000	-4.32490000	-2.53300000
C	-3.48180000	-3.30930000	4.28380000
C	-6.53310000	-3.06290000	1.18070000
H	-7.48100000	-3.59020000	1.24890000
C	-6.01190000	0.56510000	-1.18790000
C	3.54270000	-2.37010000	-4.72750000
H	3.56900000	-2.04510000	-5.76430000
C	-3.86840000	-0.32830000	-1.83960000
C	2.21710000	6.67600000	2.25390000
H	2.48730000	7.68720000	2.54640000
C	2.55420000	-1.83920000	-3.88950000

C	-5.48660000	-3.38100000	2.04390000
H	-5.61460000	-4.16900000	2.78140000
C	3.40820000	-2.74560000	0.47370000
C	-1.20640000	-3.97340000	4.76270000
H	-0.44600000	-4.29320000	5.47130000
C	-0.88280000	-3.79380000	3.41600000
H	0.13030000	-3.97250000	3.06550000
C	-0.40100000	5.67850000	-2.72550000
H	-0.15820000	6.26040000	-3.61190000
C	2.70030000	5.58200000	2.96910000
H	3.37080000	5.73870000	3.81000000
C	-1.80410000	4.08570000	-1.57770000
H	-2.66120000	3.41810000	-1.56390000
C	-6.33900000	-2.08560000	0.20670000
H	-7.13510000	-1.85590000	-0.49660000
C	-3.78840000	0.61710000	-2.86210000
H	-2.91180000	0.63090000	-3.50430000
C	3.52890000	-3.62570000	-0.61630000
C	4.49960000	-3.26730000	-4.25710000
H	5.26860000	-3.65010000	-4.92280000
C	0.29300000	1.18400000	-4.42970000
H	0.04280000	2.11150000	-3.92150000
C	-5.12230000	-1.40470000	0.07840000
C	-1.51630000	4.83760000	-2.71930000
H	-2.15320000	4.76440000	-3.59780000
C	3.54050000	2.02820000	2.80200000

C	3.70780000	-4.99420000	-0.34230000
C	0.13790000	5.01610000	-0.43880000
C	3.51140000	-3.15410000	-2.02790000
C	3.76750000	-5.46780000	0.96820000
H	3.89720000	-6.53220000	1.15080000
C	0.41550000	5.76380000	-1.59850000
C	-0.98820000	4.17400000	-0.44930000
C	3.52700000	2.20660000	5.58510000
H	3.50540000	2.27850000	6.67020000
C	4.11930000	1.10450000	4.96620000
H	4.56710000	0.31410000	5.56360000
C	4.12190000	1.02170000	3.57190000
H	4.57780000	0.16800000	3.07660000
C	-0.30120000	0.86630000	-5.65350000
H	-1.01580000	1.54790000	-6.10920000
C	0.02660000	-0.33550000	-6.28540000
H	-0.43770000	-0.60030000	-7.23280000
C	1.21010000	0.31110000	-3.84270000
C	0.94080000	-1.20830000	-5.69630000
C	2.94680000	3.21430000	4.81480000
C	3.64460000	-4.58090000	2.03980000
H	3.68410000	-4.94730000	3.06290000
C	1.55100000	-0.90240000	-4.46580000
C	3.46310000	-3.21960000	1.78470000
H	3.35590000	-2.51660000	2.60680000
H	1.29680000	6.39980000	-1.61900000

H	-1.22890000	3.57820000	0.42340000
H	1.65710000	0.57750000	-2.89190000
H	1.17260000	-2.15360000	-6.18040000
H	-3.05600000	-1.03370000	-1.70700000
H	-6.87020000	0.56210000	-0.52080000
H	3.55040000	1.94720000	1.72100000
H	2.46760000	4.05820000	5.30420000
H	-1.58000000	-3.24220000	1.46560000
H	-4.48990000	-3.09720000	4.63080000
H	3.77710000	-5.69400000	-1.17110000
H	3.26390000	-1.68560000	0.30050000

1 2 1.0 4 1.0 7 1.0

2 3 1.0

3 6 1.0

4 5 1.0

5 10 1.0

6 9 1.0 60 1.0

7 8 1.0

8 23 1.0

9 20 1.0 38 1.0

10 15 1.0 17 1.0

11 17 1.0 63 1.0 83 1.0

12 20 1.0 43 1.0 97 1.0

13 14 1.0 15 1.0 35 1.0

14

15 65 1.0

16 31 1.0 34 1.0 60 1.0

17 47 1.0

18 19 1.0 24 1.0 31 1.0

19

20 28 1.0

21 22 1.0 28 1.0 41 1.0

22

23 37 1.0 66 1.0

24 25 1.0 53 1.0

25

26 27 1.0 56 1.0 66 1.0

27

28 98 1.0

29 30 1.0 38 1.0 51 1.0

30

31 94 1.0

32 33 1.0 37 1.0 56 1.0

33

34 53 1.0 93 1.0

35 36 1.0 47 1.0

36

37 86 1.0

38 39 1.0

39

40 55 1.0 87 1.0 100 1.0

41 42 1.0 43 1.0

42

43 44 1.0

44

45 46 1.0 61 1.0 69 1.0

46

47 48 1.0

48

49 50 1.0 61 1.0 70 1.0

50

51 52 1.0 60 1.0

52

53 54 1.0

54

55 64 1.0 66 1.0

56 57 1.0

57

58 59 1.0 77 1.0 81 1.0

59

60

61 62 1.0

62

63 75 1.0 95 1.0

64 67 1.0 99 1.0

65 69 1.0 70 1.0

66

67 68 1.0 84 1.0

68

69 89 1.0

70 90 1.0

71 72 1.0 73 1.0 83 1.0

72

73 74 1.0 75 1.0

74

75 76 1.0

76

77 78 1.0 79 1.0

78

79 80 1.0 82 1.0

80

81 86 1.0 91 1.0

82 86 1.0 92 1.0

83 96 1.0

84 85 1.0 87 1.0

85

86

87 88 1.0

88

89

90

91

92

93

94

95

96

97

98

99

100

C H N 0

6-31g(d)

****

Rh 0

lanl2dz

****

Rh 0

lanl2dz

Optimized Cartesian Coordinates for Model of [Rh(CNAr^{Ph2})$_3$]$^-$.

Rh	-0.07495523	0.06654014	-0.30681918
C	-1.81422403	-0.35368219	-1.03208863
N	-2.95976414	-0.57243897	-1.33789394
C	1.60538620	-0.52712821	-1.04303259
N	2.66480937	-0.94804092	-1.43787180
C	-4.30873508	-0.68594772	-1.44786075
C	-0.05264925	1.00031661	1.34746157
N	0.02422558	1.56912841	2.41477261
C	-5.06108156	0.33543768	-2.10398411
C	3.75498757	-1.52949859	-1.99352291

C	4.38611102	0.68147911	-3.11164804
C	-3.54519854	2.34749843	-1.83351765
C	5.18384139	-3.46838646	-2.33385578
H	5.39318846	-4.51916046	-2.15151506
C	4.05181617	-2.90378258	-1.73325758
C	-4.23955840	-2.94538196	-0.25387888
C	4.61934052	-0.76149016	-2.83362378
C	-3.86692533	-5.33154169	0.09486275
H	-4.07360318	-6.36121849	-0.18857129
C	-4.43811675	1.58812876	-2.61065189
C	-4.25539433	3.27055009	-4.36832659
H	-4.52857772	3.61703014	-5.36267568
C	0.57603753	2.16138185	3.51035930
C	-2.97018093	-5.05375615	1.12893313
H	-2.48019321	-5.86515699	1.66217454
C	1.33772180	4.15682387	4.67487196
H	1.57017076	5.21842691	4.65697602
C	-4.77982780	2.07130452	-3.88680169
C	-7.08266488	-1.00539206	-1.82871064
H	-8.15491542	-1.12163228	-1.96266240
C	-4.49240816	-4.28842960	-0.58764061
C	1.29498812	2.04994341	5.83160091
H	1.49314981	1.45783524	6.72129948
C	-3.33111092	-2.68247773	0.78670524
C	6.01899009	-2.73130880	-3.17102133
H	6.88824612	-3.19643600	-3.62826996
C	0.80788982	1.39627014	4.69291223
C	-6.43700577	0.14373640	-2.28062848
H	-7.01033853	0.93367351	-2.75854240
C	1.04284213	4.04428376	1.02095802
C	-3.37231864	4.01415373	-3.58309852
H	-2.95609033	4.94588363	-3.95880496
C	-3.01909196	3.54586256	-2.31570195
H	-2.32589631	4.10804040	-1.69550831
C	3.11668664	-5.40499097	0.95743544
H	3.63074627	-6.02028213	1.69261196
C	5.72997528	-1.38907384	-3.40946399
H	6.39115124	-0.79620969	-4.03606653
C	1.07917066	-4.63154852	-0.07830348
H	-0.00457178	-4.63962554	-0.15497182
C	-6.34438679	-1.98773638	-1.17167512
H	-6.84453988	-2.86998207	-0.78088183
C	-2.70438422	-3.72492959	1.46942578
H	-2.00455331	-3.48965614	2.26679610
C	0.61568797	4.41749731	2.30782493
C	1.55948266	3.41806804	5.83494510
H	1.95534803	3.89918237	6.72548448
C	0.75294510	-2.33256607	3.89823083
H	1.10895642	-3.00193156	3.11925974
C	-4.96603275	-1.85756419	-0.96305199
C	1.72365135	-5.44008526	0.86094975

H	1.14463874	-6.08808947	1.51485672
C	4.09880124	1.60192289	-2.08815767
C	-0.02160394	5.66317692	2.45545340
C	3.22086706	-3.75011279	-0.83407500
C	0.84979915	3.56268409	3.50381969
C	-0.22328562	6.50646537	1.36296006
H	-0.72716195	7.46002605	1.50464628
C	3.85382962	-4.56816394	0.12052538
C	1.81796650	-3.79690142	-0.91781595
C	4.35406291	2.52867194	-4.70585503
H	4.44253626	2.87896973	-5.73176697
C	4.07433827	3.43055046	-3.67787471
H	3.94906551	4.48862821	-3.89456541
C	3.94758046	2.95939204	-2.36893194
H	3.72823213	3.65038536	-1.55876643
C	0.06660490	-2.83872357	5.00487323
H	-0.11457123	-3.90724270	5.09573328
C	-0.38877311	-1.96155074	5.99166158
H	-0.93462105	-2.34159808	6.85244172
C	0.98584335	-0.96175920	3.77895808
C	-0.15675042	-0.59169510	5.87050677
C	4.50755529	1.17118678	-4.42429424
C	0.20510039	6.12032166	0.09116093
H	0.04356919	6.77230169	-0.76403335
C	0.53543990	-0.06574599	4.76444004
C	0.83628759	4.88495155	-0.07309620
H	1.16640642	4.56249799	-1.05720706
H	4.93546463	-4.52568425	0.21926799
H	1.29606396	-3.17674315	-1.63702212
H	1.51943860	-0.59024270	2.91163642
H	-0.53382106	0.08833207	6.63016891
H	-3.10865790	-1.65923808	1.06685203
H	-5.17187775	-4.51114828	-1.40636336
H	3.99673121	1.25250342	-1.06693529
H	4.70372544	0.47200979	-5.23301447
H	-3.25544121	2.00268212	-0.84755256
H	-5.44781061	1.48553610	-4.51314891
H	-0.38237032	5.95902452	3.43723867
H	1.53135643	3.08921205	0.86688671

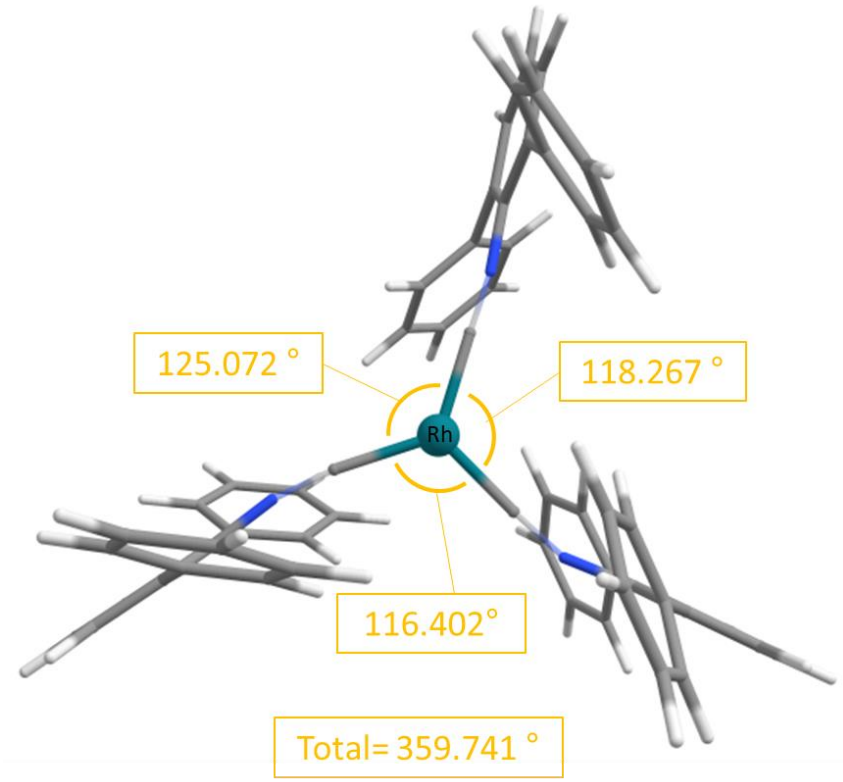

Input file for model of $Rh(CO)_3^-$.

```
%chk=RhCO-.chk
%nprocs=8
%mem=20GB
#P GFINPUT POP(FULL, NBO)
# opt freq b3lyp/Gen Pseudo=Read geom=connectivity

Rh tris CO anion

-1 1
 Rh          -0.00502920   0.00860421  -0.00000012
 C           -1.00494005  -1.72349807  -0.00000027
 C            1.99497079   0.00870717   0.00000000
 C           -1.00511835   1.74060355  -0.00000007
```

Figure 1.7 Optimized structure for $[Rh(CNAr^{Ph2})_3]^-$ with relevant bond angles.

```
 O           -1.56259090  -2.68949118   0.00000026
 O           -1.56286656   2.70654046   0.00000013
 O            3.11037079   0.00875988   0.00000008

 1 2 1.0 3 1.0 4 1.0
 2 5 3.0
 3 7 3.0
```

4 6 3.0
5
6
7

C O 0
6-31g(d)

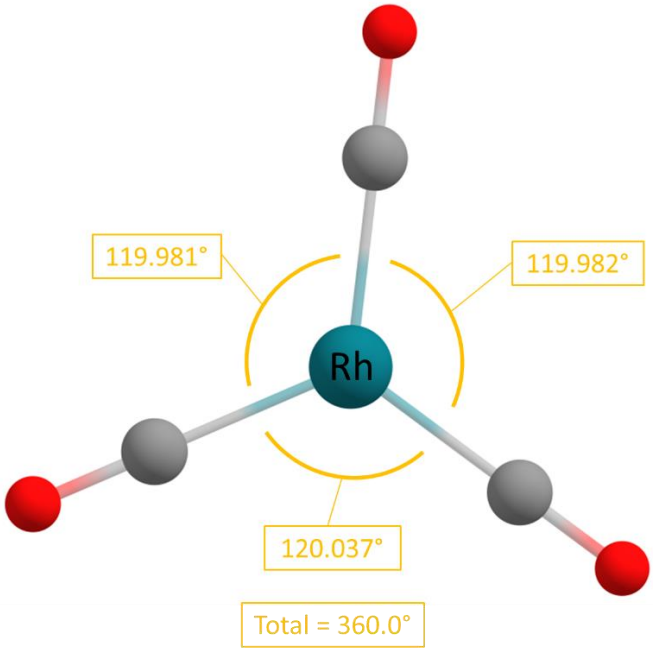

****
Rh 0
lanl2dz
****

Rh 0
lanl2dz

Optimized Cartesian Coordinates for Model of $Rh(CO)_3^-$.

Rh	0.000000000	-0.000235689	0.000000000
C	1.665982158	-0.953385184	0.000000000
C	-1.659060609	-0.965377177	0.000000000
C	-0.006927981	1.919119757	0.000000000
O	2.681133239	-1.534141335	0.000000000
O	-0.011135268	3.088646955	0.000000000
O	-2.669993147	-1.553447917	0.000000000

Figure 1.8 Optimized structure of [Rh(CO)3]- with relevant bond angles.

1.6 Details of crystallographic structure determinations

General Information. Single crystal X-ray structure determinations were carried out at low temperature on a Bruker P4, Platform or Kappa Diffractometer equipped with a Mo or Cu radiation source. Data were acquired with Bruker APEX II, Photon II or Dextris Eiger 1M detectors. All structures were solved via direct methods with SHELXS[64-65] and refined by full-matrix least-squares procedures using SHELXL[64-65] within the Olex2[66] software package. All H-atoms were refined using standard HFIX instruction. Crystallographic data collection and refinement information is listed in Table S3.1. The PLATON crystallographic tool[67] was used to account for overly disordered solvent using SQUEEZE routine,[68] and to identify twin laws in twinned crystalline habits using the TwinRotMat Routine.[69]

Information on Crystallographic Disorder and Twinning: The following molecules contain positionally disordered and/or pseudo-merohedrally twinned components. They are listed along with their respective disordered components.

RhCl(CNAr^{Dipp2})$_3$ (1): Pseudo-meroherdral twinning was observed and a twin law was determined using PLATONs TwinRotMat algorithm (-1 0 0 0 -1 0 0 0 0 1, BASF 0.4397(15)). Two site positional disorder was observed in on flanking isopropyl group (C59A/B) which was modeled using PART/FVAR and EADP commands and subsequently refined anisotropically. **K[Rh(CNAr^{Dipp2})$_3$] (K[3]):** SQUEEZE was used to remove one half of a heavily disordered *n*-pentane or diethyl ether molecule co-crystallized on a special position from the structure (void removed was 189 Å^3 in volume and contained 50 electrons/cell).

K[Ir(CNAr^{Dipp2})$_3$] (K[4]): Two site positional disorder was observed in one diisopropylphenyl group (C52/C52A) and one co-crystalized molecule of *n*-pentane. The diisopropylphenyl disorder

was modeled using PART/FVAR and limited use of EADP commands then refined anisotropically. The *n*-pentane molecule of co-crystallization was modeled using PART/FVAR commands and refined isotropically.

[K(cryptand–2.2.2)][Rh(CNAr^{Dipp2})$_3$] ([K(crypt)][3]): A two-site positional disorder was observed in one methyl group (C62A/B) which was modeled using PART/FVAR and EADP commands and subsequently refined anisotropically.

[K(cryptand–2.2.2)][Ir(CNAr^{Dipp2})$_3$] ([K(crypt)][4]): EADP commands were used to constrain oblate/prolate ellipsoids primarily on the 2,2,2-cryptand moiety. SQUEEZE was used to remove a large solvent void containing partially occupied and disordered *n*-pentane and/or diethyl ether molecules. Void removed was 2304 Å^3 in volume and contained 603.4 electrons.

Na[(N$_2$)Co(CNAr^{Dipp2})$_3$](Na[5-N$_2$]): A two-site positional disorder was observed in one diisopropylphenyl group (C39) and one flanking *i*-Pr group (C14A/C14B). In both cases the disorder was modeled using PART/FVAR and EADP commands then refined anisotropically.

Na[Co(CNAr^{Dipp2})$_3$] (Na[5]): A two-site positional disorder was observed in one flanking *i*-Pr group (C94/C94B). This disorder was modeled using PART/FVAR, SADI, and limited use of EADP commands then refined anisotropically.

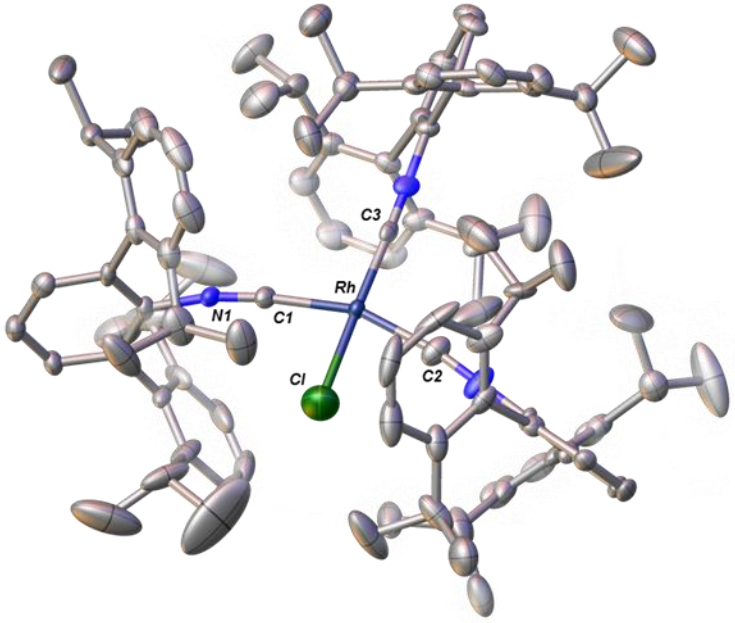

Figure 1.9 Molecular Structure of RhCl(CNAr^{Dipp2})$_3$ (1). Hydrogen atoms and disorder omitted for clarity. Selected bond distances (Å) and angles (°): Rh-C1 = 1.944(5); C1-N1 = 1.156(7); Rh-Cl = 2.369(2); C1-Rh-Cl = 79.97(17); Cl-Rh-C2 = 78.3(2)

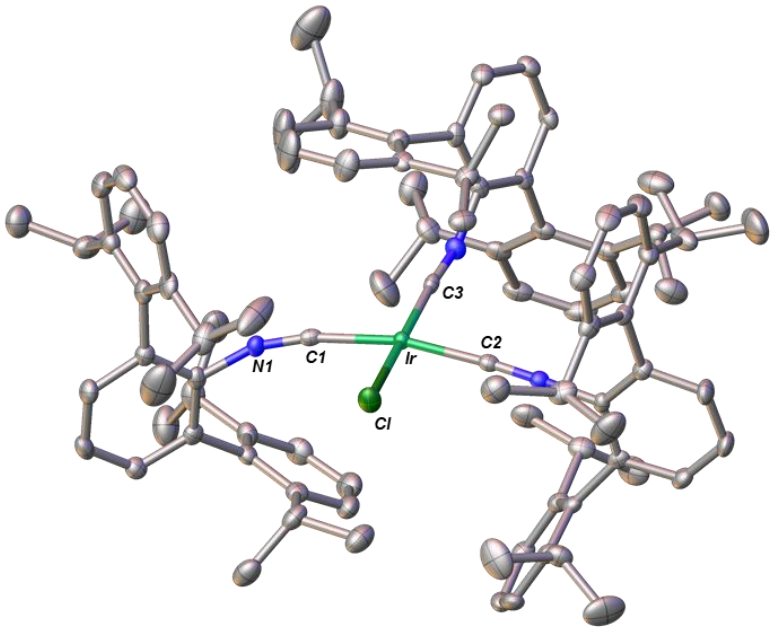

Figure 1.10 Molecular Structure of IrCl(CNAr^{Dipp2})$_3$ (2). Hydrogen atoms omitted for clarity. Selected bond distances (Å) and angles (°): Ir-C1 = 1.959(3); C1-N1 = 1.166(4); Ir-Cl = 2.3605(8); C1-Ir-Cl = 86.42(10); Cl-Ir-C2 = 85.98(11).

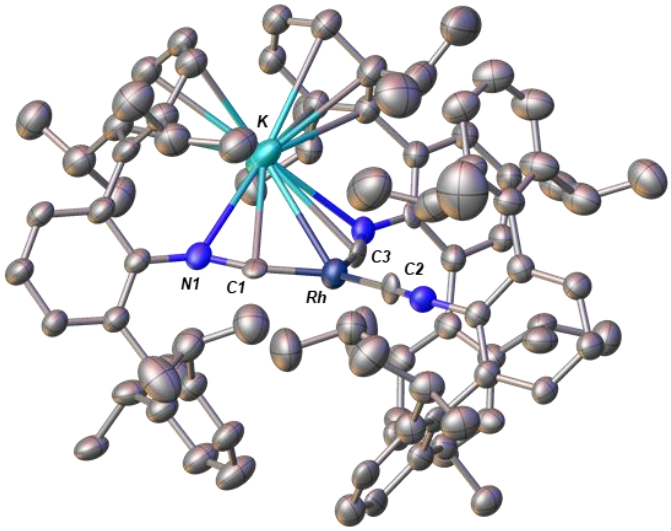

Figure 1.11 Molecular Structure of K[Rh(CNAr^{Dipp2})$_3$] (K[3]). Hydrogen atoms, disorder and one co-crystallized Et_2O molecule omitted for clarity. Selected bond angles and or distances. Selected bond distances (Å) and angles (°): Rh-C1 = 1.77(3); C1-N1 = 1.27(3); Rh-K = 3.374(8); C1-Rh-C2 = 120.5(12); C2-Rh-C3 = 125.9(12); C3-Rh-C1 = 113.0(13).

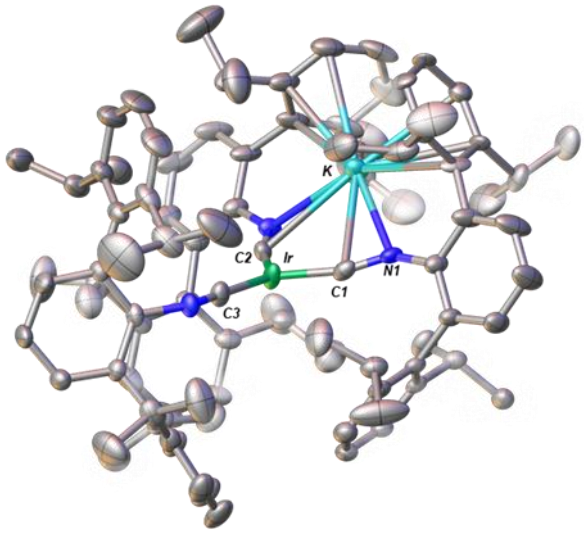

Figure 1.12 Molecular structure of K[Ir(CNAr^{Dipp2})$_3$] (K[4]). Hydrogen atoms and one co-crystallized Et_2O molecule omitted for clarity. Selected bond angles and or distances. Selected bond distances (Å) and angles (°): Ir-C1 = 1.849(4); C1-N1 = 1.211(5); Ir-K = 3.4877(10); C1-Ir-C2 = 112.11(17); C2-IR-C3 = 132.46(17); C3-Ir-C1 = 114.34(17).

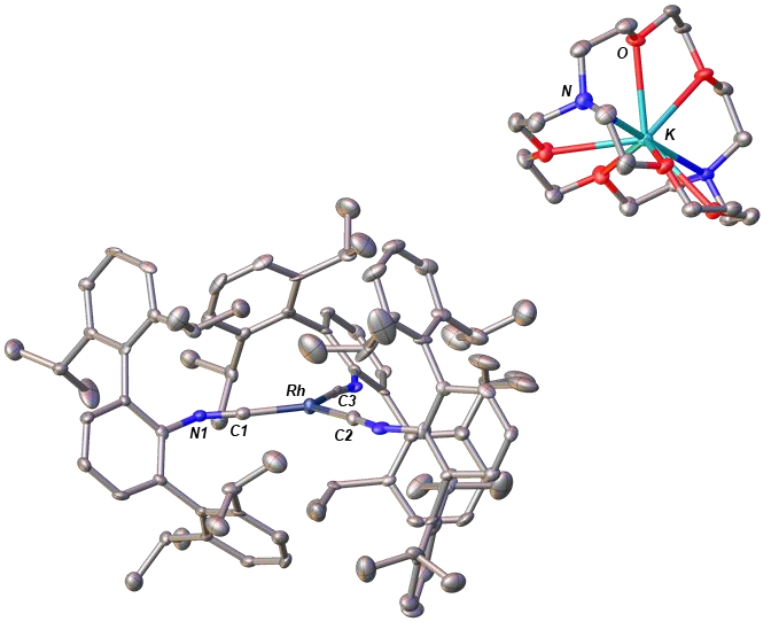

Figure 1.13 Molecular structure of [K(cryptand-2.2.2)][Rh(CNAr^{Dipp2})$_3$] ([K(crypt)][3]). Hydrogen atoms, disorder and one co-crystallized Et_2O molecule omitted for clarity. Selected bond distances (Å) and angles (°): Rh-C1 = 1.887(5); C1-N1 = 1.217(6); C1-Rh-C2 = 125.7(2); C2-Rh-C3 = 116.6(2); C3-Rh-C1 = 117.3(2)

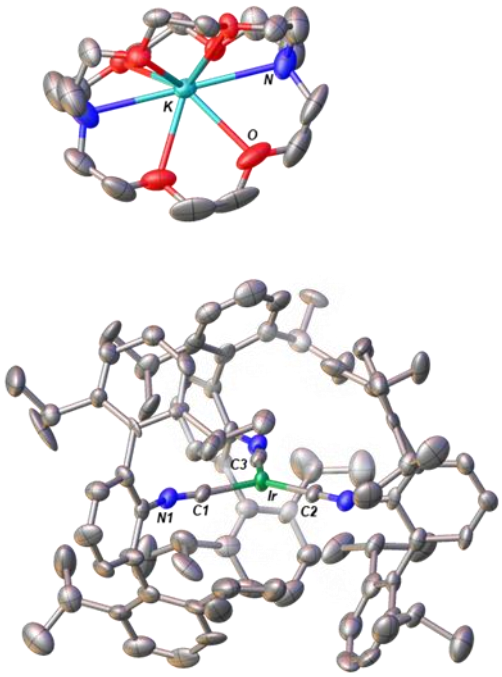

Figure 1.14 Molecular structure of [K(cryptand-2.2.2)][Rh(CNAr^{Dipp2})$_3$] ([K(crypt)][4]). Hydrogen atoms omitted for clarity. bond distances (Å) and angles (°): Ir-C1 = 1.94(2); C1-N1 = 1.12(2); C1-Ir-C2 = 117.2(8); C2-Ir-C3 = 128.6(8); C3-Ir-C1 = 114.2(8).

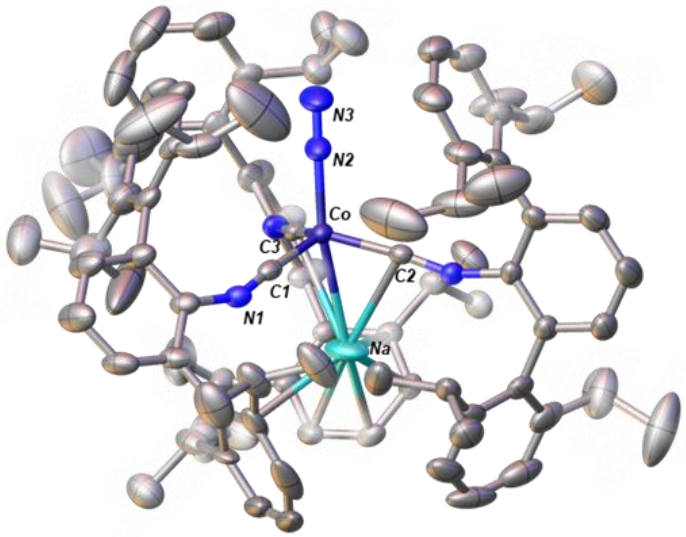

Figure 1.15 Molecular Structure of Na[(N_2)Co($CNAr^{Dipp2}$)$_3$] (Na[5-N_2]). One co-crystalized molecule of C_6H_6, disorder, and hydrogen atoms are omitted for clarity. Selected bond distances (Å) and angles (°): Co-C1 = 1.808(4); C1-N1 = 1.199(4); Co-N2 = 1.875(3); N2-N3 = 1.098(5); Co-Na = 2.7216(16); C1-Co-C2 = 111.76(15); C2-Co-C3 = 118.50(15); C3-Co-C1 = 114.63(15).

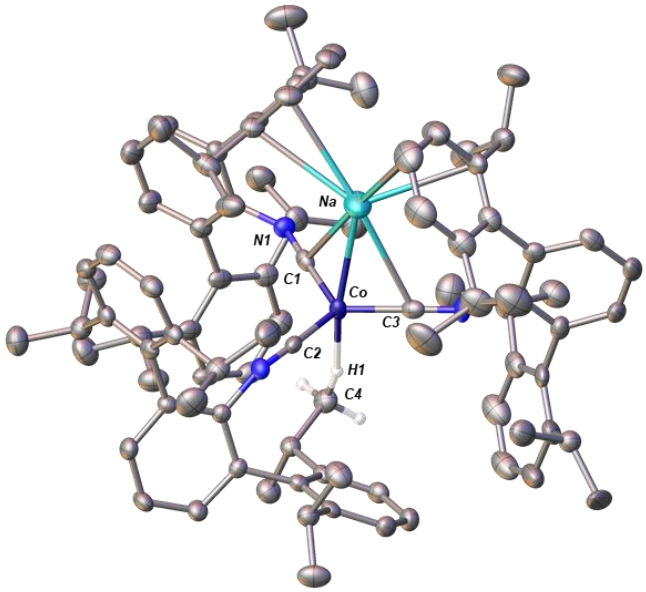

Figure 1.16 Molecular structure of Na[Co($CNAr^{Dipp2}$)$_3$] (Na[5]). Two co-crystalized solvent molecules (one C_6H_6 and one *n*-pentane), disorder, and hydrogen atoms are omitted for clarity excluding H1-H3. Selected bond distances (Å) and angles (°): Co-C1 = 1.765(5); C1-N1 =1.211(6); Co-C4 = 2.895(2); Co-H1 = 2.009(2); Co-Na = 2.724(2); C1-Co-C2 = 116.89(19); C2-Co-C3 = 116.74(19); C3-Co-C1 = 123.6(2).

Table 1.2 Crystallographic Data and Refinement Information.

Name	$RhCl(CNAr^{Dipp2})_3$ (**1**)	$IrCl(CNAr^{Dipp2})_3$ (**2**)	$K[Rh(CNAr^{Dipp2})_3][Et_2O](K[$**3**$])$
Formula	$C_{93}H_{111}ClN_2Rh$	$C_{93}H_{111}ClN_2Ir$	$C_{97}H_{121}KN_3RhO$
Crystal System	Monoclinic	Orthorhombic	Triclinic
Space Group	*$P2_1/n$*	*P 21 21 21*	*P -1*
***a*, Å**	12.1525(11)	13.0746(15)	12.668(3)
***b*, Å**	26.070(3)	21.665(3)	15.428(4)
***c*, Å**	25.366(2)	30.205(3)	26.014(7)
α, deg	90	90	82.208(5)
β, deg	90.135	90	76.170(4)
γ, deg	90	90	67.091(4)
V, Å^3	8036.6(13)	8555.8(17)	4542(2)
Z	4	4	2
Radiation (λ, Å)	Mo-Kα, 0.71073	Mo-Kα, 0.71073	Cu-Kα, 1.54178
ρ (calcd.), g/cm^3	1.165	1.163	1.087
μ (Mo Ka), mm^{-1}	0.292	1.635	2.260
Temp, K	100	100	100
θ max, deg	26.460	26.370	39.877
data/parameters	16503(914)	17460(907)	5090(948)
R_1	0.0715	0.0218	0.1000
wR_2	0.2022	0.0459	0.3151
GOF	1.049	0.992	1.424

Table 1.3 Crystallographic Data and Refinement Information – Continued.

Name	K[Ir(CNAr^{Dipp2})$_3$][C_5H_{14}](K[**3**])	[[2,2,2]-cryptand-K][Rh(CNAr^{Dipp2})$_3$][Et_2O] (K(crypt)[**3**])	[[2,2,2]-cryptand-K][Ir(CNAr^{Dipp2})$_3$](K(crypt)[**4**])
Formula	$C_{98}H_{123}IrKN_3$	$C_{115}H_{115}KN_5O_7Rh$	$C_{111}H_{147}IrKN_5O_6$
Crystal System	Monoclinic	Monoclinic	Monoclinic
Space Group	*P2$_1$/n*	*P2$_1$/c*	*Cc*
***a*, Å**	14.8385(7)	19.1608(18)	14.3476(4)
***b*, Å**	23.6578(11)	23.412(2)	26.3991(7)
***c*, Å**	24.4547(11)	23.752(2)	30.7635(9)
α, deg	90	90	90
β, deg	92.115(1)	91.004(2)	97.567(2)
γ, deg	90	90	90
V, Å^3	8578.9(7)	10653.3(16)	11550.6(6)
Z	4	4	4
Radiation (λ, Å)	Mo-Kα, 0.71073	Mo-Kα, 0.71073	Cu-Kα, 1.54178
ρ (calcd.), g/cm^3	1.219	1.161	1.080
μ (Mo Ka), mm^{-1}	1.651	0.255	2.928
Temp, K	100	100	100
θ max, deg	26.442	23.341	60.171
data/parameters	17647(1035)	15388(1187)	14628(1069)
R$_1$	0.0503	0.0699	0.0894
wR$_2$	0.1079	0.1210	0.2365
GOF	1.117	1.036	1.001

Table 1.4 Crystallographic Data and Refinement Information – Continued.

Name	$Na[Co(CNAr^{Dipp2})_3][C_6H_6]$ (Na[**5**-N_2])	$Na[Co(CNAr^{Dipp2})_3][C_6H_6][C_5H_{14}]$ (Na[**5**])
Formula	$C_{99}H_{117}CoN_5Na$	$C_{104}H_{129}CoN_3Na$
Crystal System	Monoclinic	Orthorhombic
Space Group	$P2_1/c$	$Pna2_1$
***a*, Å**	12.5833(5)	26.175(2)
***b*, Å**	25.3208(10)	22.4836(18)
***c*, Å**	28.7835(10)	16.1776(13)
α, deg	90	90
β, deg	94.443(1)	90
γ, deg	90	90
V, Å^3	9143.4(6)	9520.7(13)
Z	4	4
Radiation (λ, Å)	Mo-Kα, 0.71073	Mo-Kα, 0.71073
ρ (calcd.), g/cm^3	1.060	1.049
μ (Mo Ka), mm^{-1}	0.238	0.229
Temp, K	100	100
θ max, deg	24.196	24.180
data/parameters	14646(1035)	15236(1026)
R_1	0.0718	0.0455
wR_2	0.2110	0.1135
GOF	1.015	1.033

1.7 Acknowledgements

Complexes discussed in chapter 1 are currently in preparation for publication by M. L. Neville, C. Chan, M. Gembicky, C. Moore, A. L. Rheingold, J. S. Figueroa. The dissertation author is the primary author of this manuscript.

1.8 References

1. Hubbell, A. K.; Lamb, J. R.; Klimovica, K.; Mulzer, M.; Shaffer, T. D.; MacMillan, S. N.; Coates, G. W., *ACS Catalysis* **2020,** *10* (21), 12537-12543.

2. Lamb, J. R.; Hubbell, A. K.; MacMillan, S. N.; Coates, G. W., *Journal of the American Chemical Society* **2020,** *142* (17), 8029-8035.

3. Gómez-Suárez, A.; Nelson, D. J.; Nolan, S. P., Chapter Five - Metallate Complexes of the Late Transition Metals: Organometallic Chemistry and Catalysis. In *Advances in Organometallic Chemistry*, Pérez, P. J., Ed. Academic Press: 2018; Vol. 69, pp 283-327.

4. Ellis, J. E., *Inorganic Chemistry* **2006,** *45* (8), 3167-3186.

5. Moore, E. K.; Hao, J.; Prabhu, A.; Zhong, H.; Jelen, B. I.; Meyer, M.; Hazen, R. M.; Falkowski, P. G., *Journal of Geophysical Research: Biogeosciences* **2018,** *123* (3), 743-759.

6. Huskic, I.; Friscic, T., *Acta Crystallographica Section B Structural Science, Crystal Engineering and Materials* **2018,** *74*, 539-559.

7. Little Jr, E. J.; Jones, M. M., *Journal of chemical education* **1960,** *37* (5), 231.

8. Wolczanski, P. T., *Organomet. Chem.* **2017,** *36* (3), 622-631.

9. Cooke, M. P., *Journal of the American Chemical Society* **1970,** *92* (20), 6080-6082.

10. Suslick, B. A.; Tilley, T. D., *Journal of the American Chemical Society* **2020,** *142* (25), 11203-11218.

11. Matalon, S.; Golden, S.; Ottolenghi, M., *The Journal of Physical Chemistry* **1969,** *73* (9), 3098-3101.

12. Down, J. L.; Lewis, J.; Moore, B.; Wilkinson, G., *Journal of the Chemical Society (Resumed)* **1959,** (0), 3767-3773.

13. Dye, J. L.; Dewald, R. R., *The Journal of Physical Chemistry* **1964,** *68* (1), 135-142.

14. Moore, J. T.; Lu, C. C., *Journal of the American Chemical Society* **2020,** *142* (27), 11641-11646.

15. Dye, J. L., *The Journal of Physical Chemistry* **1984,** *88* (17), 3842-3846.

16. Tehan, F. J.; Barnett, B. L.; Dye, J. L., *Journal of the American Chemical Society* **1974,** *96* (23), 7203-7208.

17. Ellis, J. E., *Organomet. Chem.* **2003,** *22* (17), 3322-3338.

18. Collman, J. P., *Accounts of Chemical Research* **1975,** *8* (10), 342-347.

19. Collman, J. P.; Winter, S. R., *Journal of the American Chemical Society* **1973,** *95* (12), 4089-4090.

20. Lamb, J. R.; Jung, Y.; Coates, G. W., *Organic Chemistry Frontiers* **2015,** *2* (4), 346-349.

21. Lamb, J. R.; Mulzer, M.; LaPointe, A. M.; Coates, G. W., *Journal of the American Chemical Society* **2015,** *137* (47), 15049-15054.

22. Luo, Y.-R. L. Y.-R., *Comprehensive handbook of chemical bond energies*. CRC Press: Boca Raton, 2007.

23. Zhou, M.; Andrews, L., *The Journal of Physical Chemistry A* **1999,** *103* (39), 7773-7784.

24. Jang, M.; Ellis, J. E., *Angewandte Chemie International Edition in English* **1994,** *33* (19), 1973-1975.

25. Kruck, T.; Lang, W.; Engelmann, A., *Angewandte Chemie International Edition in English* **1965,** *4* (2), 148-149.

26. Nixon, J. F., Trifluorophosphine Complexes of Transition Metals. In *Advances in Inorganic Chemistry*, Emeléus, H. J.; Sharpe, A. G., Eds. Academic Press: 1985; Vol. 29, pp 41-141.

27. Warnock, G. F.; Cooper, N. J., *Organomet. Chem.* **1989,** *8* (7), 1826-1827.

28. Margulieux, G. W.; Weidemann, N.; Lacy, D. C.; Moore, C. E.; Rheingold, A. L.; Figueroa, J. S., *J. Am. Chem. Soc* **2010,** *132* (14), 5033-5035.

29. Stewart, M. A.; Moore, C. E.; Ditri, T. B.; Labios, L. A.; Rheingold, A. L.; Figueroa, J. S., *Chem Commun* **2011,** *47* (1), 406-408.

30. Jonas, K., *Angewandte Chemie International Edition in English* **1975,** *14* (11), 752-753.

31. Muetterties, E. L.; Hirsekorn, F. J., *Journal of the Chemical Society, Chemical Communications* **1973,** (18), 683b-684.

32. Jilek, R. E.; Jang, M.; Smolensky, E. D.; Britton, J. D.; Ellis, J. E., *Angew. Chem. Int. Ed.* **2008,** *47* (45), 8692-8695.

33. Elschenbroich, C.; Gerson, F., *Journal of the American Chemical Society* **1975,** *97* (12), 3556-3557.

34. Gore-Randall, E.; Irwin, M.; Denning, M. S.; Goicoechea, J. M., *Inorganic Chemistry* **2009,** *48* (17), 8304-8316.

35. Green, M. L. H., *Journal of Organometallic Chemistry* **1995,** *500* (1), 127-148.

36. Fox, B. J.; Sun, Q. Y.; Dipasquale, A. G.; Fox, A. R.; Rheingold, A. L.; Figueroa, J. S., *Inorganic Chemistry* **2008,** *47* (19), 9010-9020.

37. Carpenter, A. E.; Margulieux, G. W.; Millard, M. D.; Moore, C. E.; Weidemann, N.; Rheingold, A. L.; Figueroa, J. S., *Angew. Chem. Int. Ed.* **2012,** *51* (37), 9412-9416.

38. Mokhtarzadeh, C. C.; Margulieux, G. W.; Carpenter, A. E.; Weidemann, N.; Moore, C. E.; Rheingold, A. L.; Figueroa, J. S., *Inorganic Chemistry* **2015,** *54* (11), 5579-5587.

39. Wang, P.; Cheng, J.; Wang, D.; Yang, C.; Leng, X.; Deng, L., *Organomet. Chem.* **2020,** *39* (15), 2871-2877.

40. Mokhtarzadeh, C. C.; Moore, C. E.; Rheingold, A. L.; Figueroa, J. S., *Angew. Chem. Int. Ed.* **2017,** *56* (36), 10894-10899.

41. Tejel, C.; Asensio, L.; del Río, M. P.; de Bruin, B.; López, J. A.; Ciriano, M. A., *Angew. Chem. Int. Ed.* **2011,** *50* (38), 8839-8843.

42. Diefenbach, A.; Bickelhaupt, F. M.; Frenking, G., *Journal of the American Chemical Society* **2000,** *122* (27), 6449-6458.

43. Ditri, T.; Fox, B.; Moore, C.; Rheingold, A.; Figueroa, J., *Inorganic Chemistry* **2009,** *48* (17), 8362-8375.

44. Kim, S.; Loose, F.; Chirik, P. J., *Chemical Reviews* **2020,** *120* (12), 5637-5681.

45. Brookhart, M.; Green, M. L. H.; Parkin, G., *Proceedings of the National Academy of Sciences* **2007,** *104* (17), 6908-6914.

46. Lin, T.-P.; Wade, C. R.; Pérez, L. M.; Gabbaï, F. P., *Angew. Chem. Int. Ed.* **2010,** *49* (36), 6357-6360.

47. Barnett, B. R.; Labios, L. A.; Moore, C. E.; England, J.; Rheingold, A. L.; Wieghardt, K.; Figueroa, J. S., *Inorg Chem* **2015,** *54* (14), 7110-21.

48. Vollmer, M. V.; Xie, J.; Lu, C. C., *Journal of the American Chemical Society* **2017,** *139* (19), 6570-6573.

49. Cammarota, R. C.; Xie, J.; Burgess, S. A.; Vollmer, M. V.; Vogiatzis, K. D.; Ye, J.; Linehan, J. C.; Appel, A. M.; Hoffmann, C.; Wang, X.; Young, V. G.; Lu, C. C., *Chemical Science* **2019,** *10* (29), 7029-7042.

50. You, D.; Gabbaï, F. P., *Trends in Chemistry* **2019,** *1* (5), 485-496.

51. Cammarota, R. C.; Lu, C. C., *Journal of the American Chemical Society* **2015,** *137* (39), 12486-12489.

52. Arnarego, W. L. F.; Chai, C. L. L., *Purification of Laboratory Chemicals*. 5th ed. ed.; Elsevier: 2003.

53. Pangborn, A. B.; Giardello, M. A.; Grubbs, R. H.; Rosen, R. K.; Timmers, F. J., *Organomet. Chem.* **1996,** *15* (5), 1518-1520.

54. Ditri, T. B.; Barnett, B. R.; Carpenter, A. E.; Mokhtarzadeh, C. C.; Agnew, D. W.; Figueroa, J. S., *Inorg. Synth.* **2018,** *37*, 109-115.

55. Fulmer, G. R.; Miller, A. J. M.; Sherden, N. H.; Gottlieb, H. E.; Nudelman, A.; Stoltz, B. M.; Bercaw, J. E.; Goldberg, K. I., *Organometallics* **2010,** *29* (9), 2176-2179.

56. Neese, F., *Wiley Interdisciplinary Reviews: Computational Molecular Science* **2011,** *2* (1), 73-78.

57. Frisch, M. J.; Trucks, G. W.; Schlegel, H. B.; Scuseria, G. E.; Robb, M. A.; Cheeseman, J. R.; Scalmani, G.; Barone, V.; Petersson, G. A.; Nakatsuji, H.; Li, X.; Caricato, M.; Marenich, A. V.; Bloino, J.; Janesko, B. G.; Gomperts, R.; Mennucci, B.; Hratchian, H. P.; Ortiz, J. V.; Izmaylov, A. F.; Sonnenberg, J. L.; Williams; Ding, F.; Lipparini, F.; Egidi, F.; Goings, J.; Peng, B.; Petrone, A.; Henderson, T.; Ranasinghe, D.; Zakrzewski, V. G.; Gao, J.; Rega, N.; Zheng, G.; Liang, W.; Hada, M.; Ehara, M.; Toyota, K.; Fukuda, R.; Hasegawa, J.; Ishida, M.; Nakajima, T.; Honda, Y.; Kitao, O.; Nakai, H.; Vreven, T.; Throssell, K.; Montgomery Jr., J. A.; Peralta, J. E.; Ogliaro, F.; Bearpark, M. J.; Heyd, J. J.; Brothers, E. N.; Kudin, K. N.; Staroverov, V. N.; Keith, T. A.; Kobayashi, R.; Normand, J.; Raghavachari, K.; Rendell, A. P.; Burant, J. C.; Iyengar, S. S.; Tomasi, J.; Cossi, M.; Millam, J. M.; Klene, M.; Adamo, C.; Cammi, R.; Ochterski, J. W.; Martin, R. L.; Morokuma, K.; Farkas, O.; Foresman, J. B.; Fox, D. J. *Gaussian 16 Rev. C.01*, Wallingford, CT, 2016.

58. Becke, A. D., *The Journal of Chemical Physics* **1986,** *84* (8), 4524-4529.

59. Becke, A. D., *The Journal of Chemical Physics* **1993,** *98* (7), 5648-5652.

60. Lee, C.; Yang, W.; Parr, R. G., *Physical Review B* **1988,** *37* (2), 785-789.

61. Petersson, G. A.; Bennett, A.; Tensfeldt, T. G.; Al-Laham, M. A.; Shirley, W. A.; Mantzaris, J., *The Journal of Chemical Physics* **1988,** *89* (4), 2193-2218.

62. Hay, P. J.; Wadt, W. R., *The Journal of Chemical Physics* **1985,** *82* (1), 299-310.

63. D. A. Zhurko, G. A.; Zhurko, “ChemCraft 2014,” can be found under

www.chemcraftprog.com, 2014.

64. Sheldrick, G. M., *Acta Crystallographica Section A Foundations of Crystallography* **2008,** *64* (Pt 1), 112-122.

65. Sheldrick, G., *Acta Crystallographica Section C* **2015,** *71* (1), 3-8.

66. Dolomanov, O. V.; Bourhis, L. J.; Gildea, R. J.; Howard, J. A. K.; Puschmann, H., *Journal of Applied Crystallography* **2009,** *42* (2), 339-341.

67. Spek, A., *Journal of Applied Crystallography* **2003,** *36* (1), 7-13.

68. Spek, A., *Acta Crystallographica Section C* **2015,** *71* (1), 9-18.

69. Ivlev, S. I.; Conrad, M.; Kraus, F., *Zeitschrift für Kristallographie - Crystalline Materials* **2019,** *234* (6), 415-418.

Chapter 2 Reactivity and Redox Profile of Group 9 Metallates

2.1 Stoichiometric reactivity studies

Reactivity of metalates has historically been dominated by simple salt-elimination type reactions.[1-2] Generally these reactions were derivatizations, taking advantage of the pseudo-halide like nature of metalates to help support the structural identification of the parent metalate.[3-7] Indeed, this type of simple transformation can be quite powerful. The strong thermodynamic driving force provided by the precipitation of a simple inorganic salt can be used to break strong covalent bonds or install otherwise unstable and difficult to access chemical functionalities at the metal center.[8-9] For instance, as mentioned in Chapter 1, alkylation of Collman's reagent and the hydrodefluorination of Ar-F bonds by Lu's Rh(-1) metallate proceed with concomitant loss of sodium halide salts.[10-11] More exotic reactions include Drance, Figueroa and co-workers example of the first isolation of a terminal boron monofluoride ligand (BF); a diatomic otherwise rarely observed outside the gas-phase. Addition of 2.8 equivalents of boron trifluoride etherate to the Collman's reagent analog, $K_2[Fe(CO)_2(CNAr^{Tripp2})_2]$ proceeds to make the $Fe(BF)(CO)_2(CNAr^{Tripp2})$. The process is believed to proceed through installation of BF_2 and concomitant loss of KF, with the second fluoride abstraction coinciding with the loss of KBF_4.[12] As the chemistry of Collman's reagent suggests, metallates act as potent, metal-based nucleophiles. Next to Collman's reagent, few have exemplified this more than $[Co(CO)_4]^-$. The work done by Prof. Coates group using well-defined, $[Co(CO)_4]^-$ containing catalysts to perform various transformations on epoxides was discussed in Chapter 1.[13] However, they are just one stand out example of a few groups who have used this carbonyl cobaltate for its ability to perform nucleophilic attack at carbon. As far back as 1960, Eisenmann et al. noted that propylene oxide could be hydroesterified in moderate yields (<40%) using

catalytic amounts of $Co_2(CO)_8$ in methanol under 3000 psi of CO.[14] While no mechanism was proposed, later studies by others using $Co_2(CO)_8$ in similar reactions found that the likely active species was $[Co(CO)_4]^-$.[15-17] Since then, more research has utilized well-defined $[Co(CO)_4]^-$ salts to act as nucleophiles in various catalytic applications such as actylation[18] and ring-opening of epoxides[19] and aziridines[15]. As detailed in this chapter, the reactivity profiles of K[**3**] and K[**4**] display a rich reactivity profile in the context of these notable examples.

Seeing as the coordinatively unsaturated Rh and Ir metalates K[**3**] and K[**4**] do not bind N_2 or coordinating solvents such as THF or Et_2O, we sought to assess whether the coordination of a Z-type ligand could induce such behavior.[20] Previously we demonstrated that binding of Tl(I) ions to the d^{10} nickel tris-isocyanide complex $Ni(CNAr^{Mes2})_3$ results in the p-coordination of a $CNAr^{Mes2}$ ligand mesityl group to the Ni center.[21] This interaction is absent in $16e^-$ $Ni(CNAr^{Mes2})_3$, which adopts a near perfect trigonal planar coordination geometry.[22] As shown in **Scheme 2.1**, treatment of the Ir metalate K[**4**] with 1.0 equivalent of thallium triflate (TlOTf; [OTf]– = $[O_3SCF_3]^-$) under N_2 readily generates the neutral,

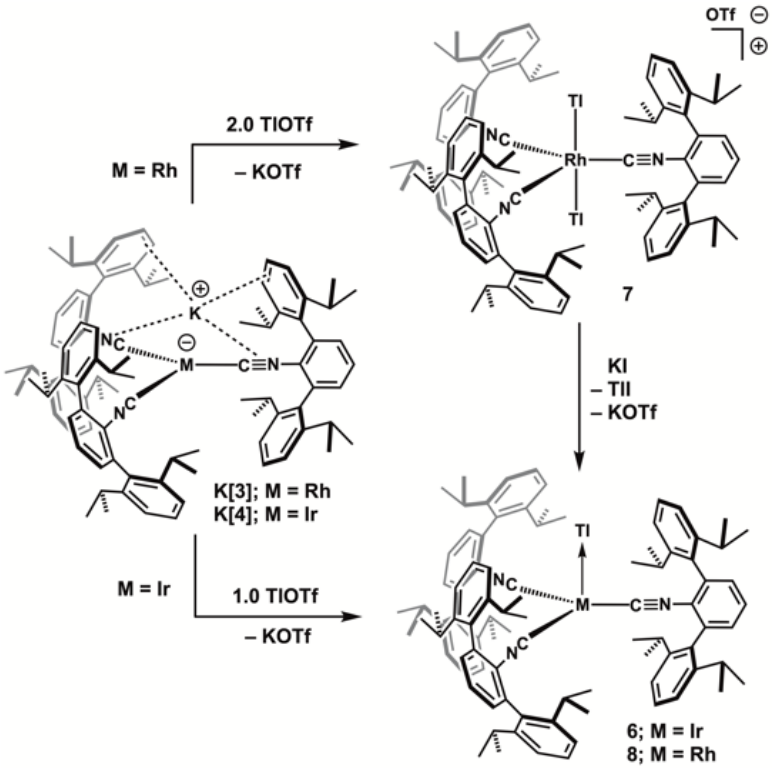

Scheme 2.1 Tl(I) coordination to Rh and Ir metalate anions.

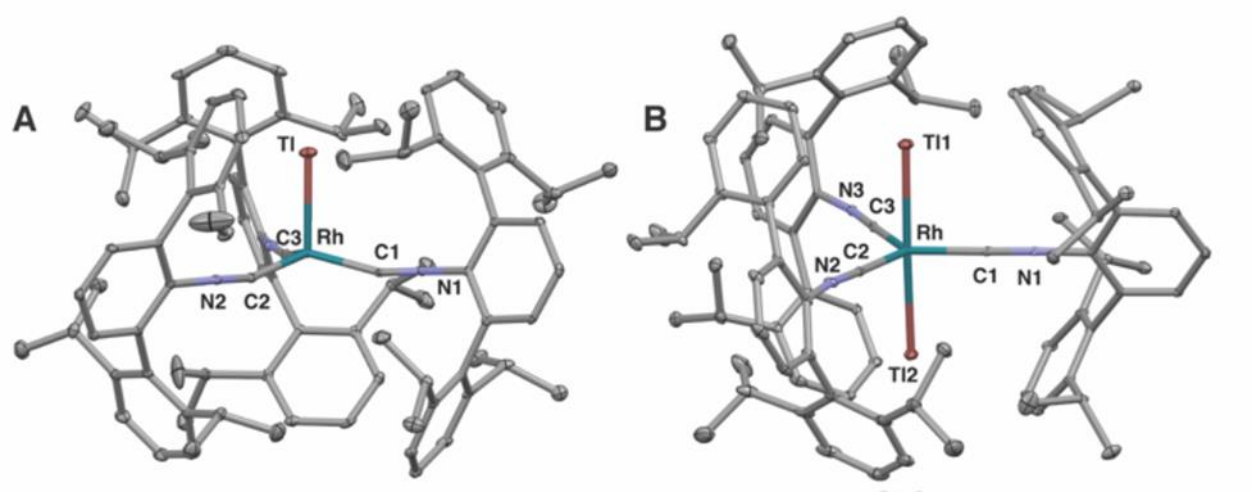

Figure 2.1 Molecular structures of (A) $Tl_2Rh(CNAr^{Dipp2})_3$] (8) and (B) [$Tl_2Rh(CNAr^{Dipp2})_3$]OTf (7).

four coordinate complex $TlIr(CNAr^{Dipp2})_3$ (**6**) as determined by X-ray diffraction (**Figure 2.1**). In contrast, the Rh derivative K[**3**] reacts with equimolar TlOTf to afford 0.5 equiv of the bis-thallium salt [$Tl_2Rh(CNAr^{Dipp2})_3$]OTf (**7**), leaving 0.5 equivalent of starting material remaining (**Scheme 2.1**; **Figure 2.1**). However, treatment of K[**3**] with 2.0 equivalents of TlOTf furnishes salt **7**, which can then be readily converted to the neutral mono-thallium adduct, $TlRh(CNAr^{Dipp2})_3$ (**8**), by simple addition of potassium iodide (KI) under an N_2 atmosphere. Notably, mono-thallium adducts **6** and **8** can be viewed as neutral analogues of Lu's anionic Rh/Group 13 element $[ERhL_3]^-$ metalate complexes with respect to the EML_3 unit.[11] Most importantly however, the Ir and Rh centers in complexes **6** and **8**, respectively, adopt trigonal monopyramidal coordination geometries that are free of N_2, bound solvent or secondary interactions from the $CNAr^{Dipp2}$ ligands. As formally Tl(I) centers are reasonably assumed to be less effective Lewis acids than trivalent Group 13 EX_3 species, we interpret that these observations are a result of the inability of Tl(I)-coordination to low enough p-orbital energies to enable Lewis base binding. Consequently, these findings suggest that $16e^-$ d^{10} Rh and Ir metalates are not as inherently Lewis acidic as their coordinatively-unsaturated nature would indicate.

To further explore the nucleophilic character of the anions, we chose to test their reactivity with protons, a smaller and more electronegative monocation. The Rh and Ir metalates react smoothly and stoichiometrically with benzoic acid to form the mono-hydrides $HM(CNAr^{Dipp2})_3$ (M= Rh [**10**], Ir [**11**])

(**Scheme 2.2; Figure 2.2 A**). Structures of **10** and **11** adopt C_{2v} symmetric, pseudo square planar geometries in line with other Group 9 metal hydrides of the formulation HML_3.[23-25] Solution infrared spectra reveal two broad N≡C stretching absorbances from 2000 to 2040 cm^{-1}, indicative of a relatively oxidized Rh(I) or Ir(I) metal center and a C_{2v} geometry around the metal center. The structural differences between the products of the two monoatomic monocations , H^+ and Tl^+, highlight and reflect the differences in metal-ligand bonding character. The relatively electronegative, X-type, hydride ligand leads the complex to adopt a classic d_8 square planar geometry, comparable to the $MCl(CNAr^{Dipp2})_3$ complexes discussed in Chapter 1. In contrast, the mono-thallium adducts **6** and **8** exhibit trigonal monopyramidal geometries similar to other complexes bearing Z-type interactions, such as boratrane ligands, but without requiring the chelating/buttressing supports.[20, 26-27] Notably, the Rh congener, **10**, is an isolobal mimic of the proposed active species in Rh based hydroformylation, $HRh(CO)_3$.[28] While there are many examples of complexes of the formulation $HRhL_3$ known, there are relatively few complexes of the like $HIrL_3$

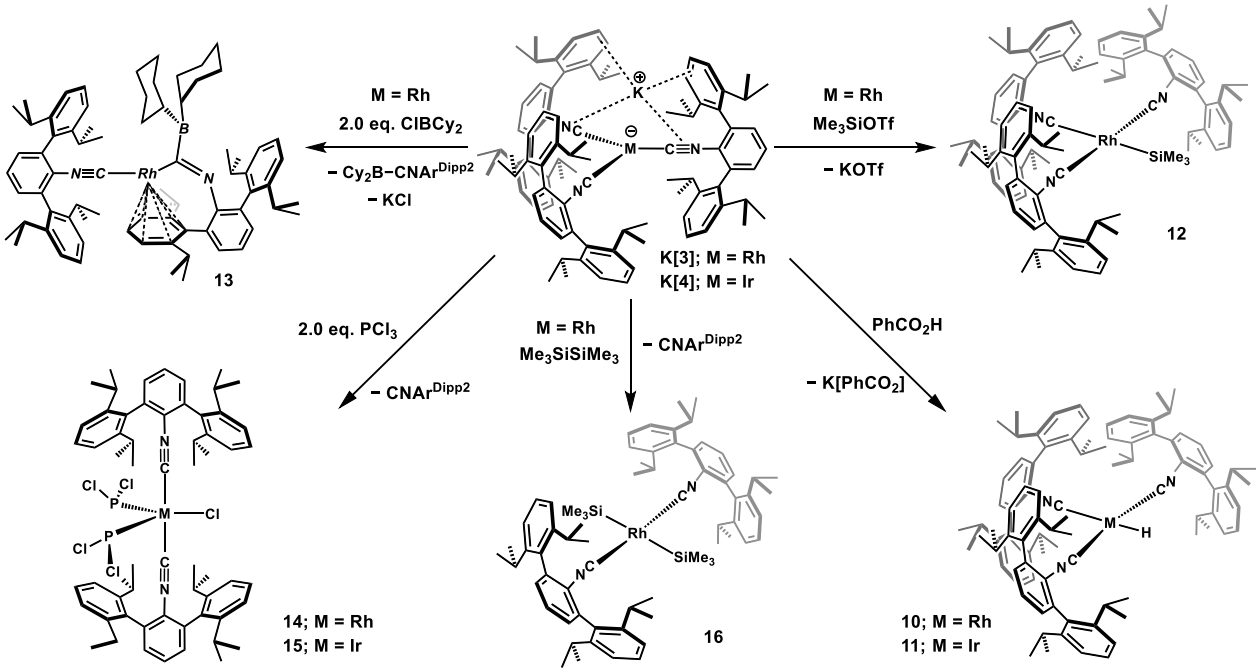

Scheme 2.2 Nucleophilic and oxidative chemistry of $[M(CNAr^{Dipp2})_3]^-$ metalate anions (M = Rh, Ir).

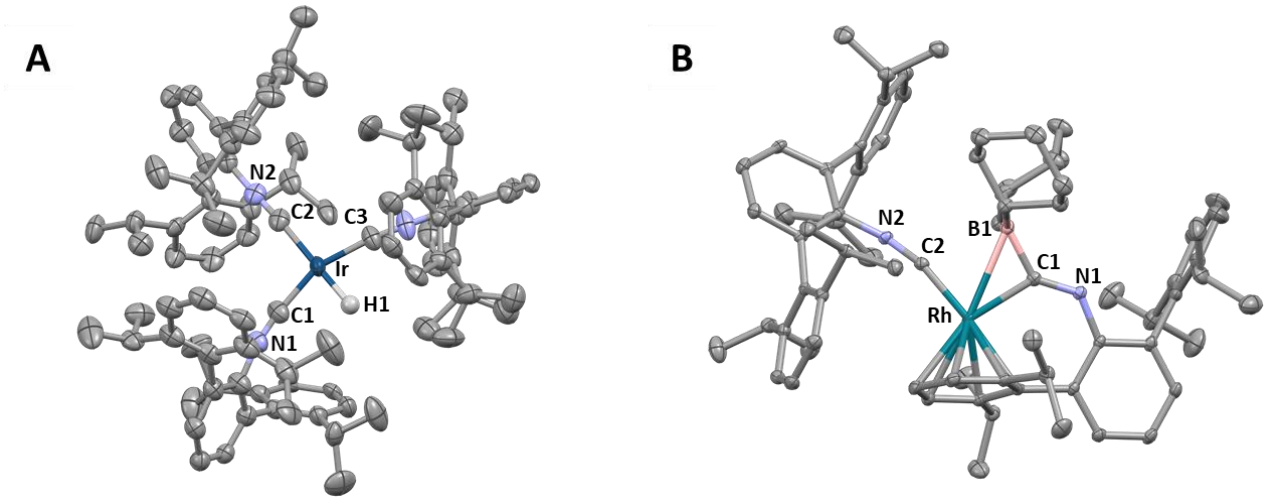

Figure 2.2 Molecular structures of (A) IrH ($CNAr^{Dipp2}$)$_3$ (11) and (B) Rh($CNAr^{Dipp2}$)(η_6-κ-C,Ar-Cy_2BIM) (13)

despite being implicated in number of important chemical processes. Additionally, to our knowledge, its synthesis from K[**4**] and benzoic acid represents a unique protonation-based preparation of such a species. The three existing examples include two pincer complexes, a pyridinde-di-carbene ((CNHC−N−CNHC)IrH) reported by Danopoulos et al.[29] and a pyridine-di-phosphine ((PNP)IrH reported by Milstein et al.[30], and the final example [IrH(N_2)(PmAd(iPr)$_2$)$_2$] (mAd = methylene-1-adamantyl) reported by our group.[23] Notably, only the rigid di-carbene pincer is completely retained in solution, whereas the other two examples form an immediate equilibrium with C-H bond activation products when dissolved. By contrast, we report an efficient synthesis of a four-coordinate iridium mono-hydride which is isolable as a pure substance in in both solution and solid state. This makes it an ideal substrate for bond activation studies. If left at room temperature in solution for extended periods (>1hr), **10** and **11** are both observed to decompose via ligand loss and alpha-hydride migration to the isocyanide, forming an iminoformyl complex M(η^6-(Dipp)-κ^1*C*-C(H)NAr^{Dipp2})($CNAr^{Dipp2}$), (M = Rh, Ir). This decomposition pattern is similar to the icocyano-cobalt-hydride complex HCo($CNAr^{DMP2}$)$_4$, but lower coordinate.[31]

K[**3**] and K[**4**] react cleanly with a range of electrophiles in a manner consistent with metalate-type nucleophilic behavior. For example, the Rh metalate K[**3**] reacts readily with trimethylsilyl triflate (Me_3SiOTf) to generate the neutral, monovalent silyl complex Rh($SiMe_3$)($CNAr^{Dipp2}$)$_3$ (**12**) with the elimination of KOTf (**Scheme 2.2**). Addition of two equivalents of choro(dicyclohexyl)borane to the Rh

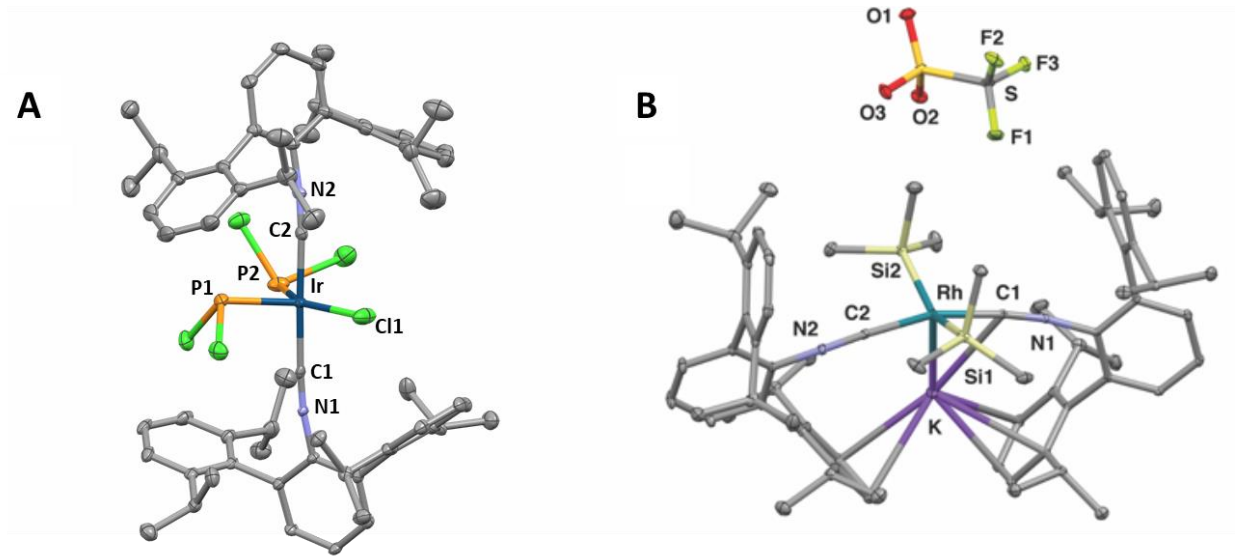

Figure 2.3 Molecular structures of (A) $IrCl(PCl_2)_2(CNAr^{Dipp2})_2$ (15) and (B) $[Rh(SiMe_3)_2(CNAr^{Dipp2})_3]OTf$ (16).

metalate K[**3**] cleanly forms $Rh(CNAr^{Dipp2})(\eta_6\text{-}\kappa\text{-}C,Ar\text{-}^{Cy2}BIM)$ [**13**], where a boryliminomethyl fragment is generated and bound to the metal center through the N,B-bridging methyl (**Scheme 2.2**). The reaction proceeds with concomitant loss of KCl and one equivalent of $CNAr^{Dipp2}$ which forms a Lewis acid-base adduct with the second equivalent of borane (**Figure 2.2 B**). This complex shares a similar ligand fragment as $Pt(k_2\text{-}2\text{-}N,B\text{-}^{Cy2}BIM)(CNAr^{Dipp2})$ which features a L,Z-chelate with a unique, singly buttressed short metal borane bond (2.3 Å).[32] The same fragment is reversed in **12**, however it still features a Z-type interaction between the metal center and the borane at a longer length of 2.6 Å. Given the nucleophilic nature of Rh metalate K[**3**], we favor a proposed mechanism of formation that starts with a metal-borane Z-type interaction producing an intermediate similar to $TlM(CNAr^{Dipp2})_3$ (**8**). Loss of KCl and formal oxidation of the metal center would lead to a d^8, likely square planar, $Rh(BCy_2)(CNAr^{Dipp2})_3$ intermediate which could be followed by migration of the rhodium-boryl bond to an adjacent isocyanide carbon. This would lend enough flexibility to the flanking 2,6,-diisopropylphenyl group to bind the unsaturated metal center offering a 3L, $6e^-$ donor group, encouraging the concomitant release of an equivalent of the sterically encumbering $CNAr^{Dipp2}$. In the line of halogenated main group fragments, metalates K[**3**] and K[**4**] react with two equivalents of PCl_3 to form $MCl(PCl_2)_2(CNAr^{Dipp2})_2$ (M= Rh

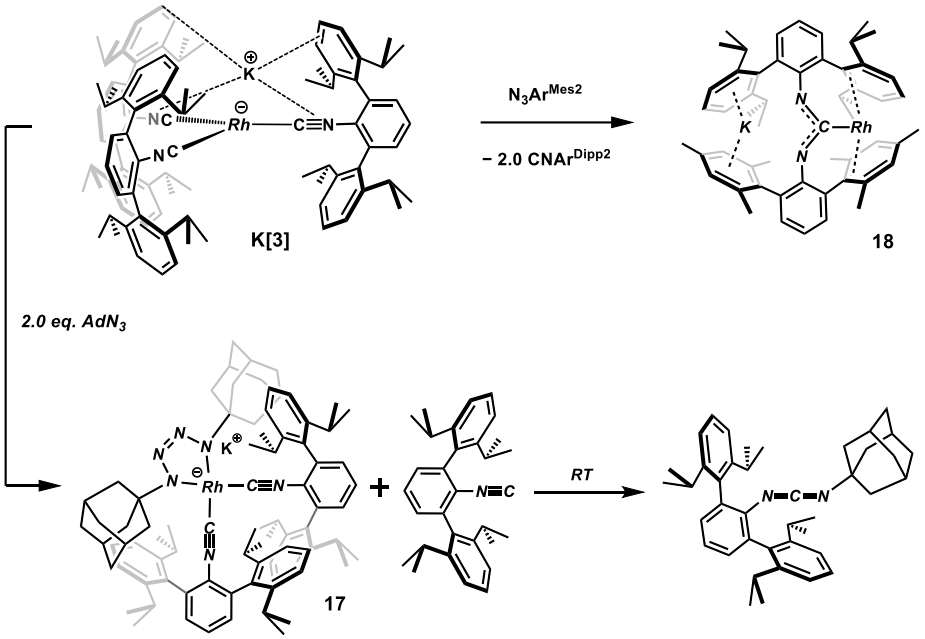

Scheme 2.3 Reactivity of Rh metalate with small and large organic azides.

[**14]**, Ir, [**15**]) (**Scheme 2.2**; **Figure 2.3 A**) with single ^{31}P signals at 365.5 (d) ppm and 335.6 (s) ppm, respectively. This represents a full, four electron swing in oxidation state at the metal center, combining the well-known M(I)/M(III) oxidative couple with the M(1-)/M(I) oxidative couple explored extensively herein. Repeated attempts to form complexes with fewer equivalencies of PCl_3, including sub-stoichiometric amounts at low temperatures, resulted in deep-purple-colored solutions. However, upon warming to room temperature, the reactions returned to an orange color and the only isolable products were **14** and **15**. More remarkably however, the nucleophilic reactivity of these three coordinate Group 9 metalates can also be extended to weakly electrophilic substrates. As shown in Scheme 4, the rhodium derivative K[**3**] reacts with hexamethyldisilane ($Me_3SiSiMe_3$) in THF solution to afford the bis-silyl salt, K[trans-Rh($SiMe_3$)$_2$($CNAr^{Dipp2}$)$_2$] (**16**; **Scheme 2.2**; **Figure 2.3 B**), concomitant with the release of one $CNAr^{Dipp2}$ ligand. Oxidative cleavage of Si-Si bonds is well established for zero-valent Pd and Pt complexes but is rare for other metals.[33-37] Notably, this nucleophilic behavior of metalates K[**3**] and K[**4**] demonstrate that they can engage with substrates along the formal M(1-)/M(I) redox couple.

Complimentarily, organic azides represent an attractive two-electron oxidant with recently increasing interest in their reactivity with late transition metals.[38-40] Addition of two equivalents of

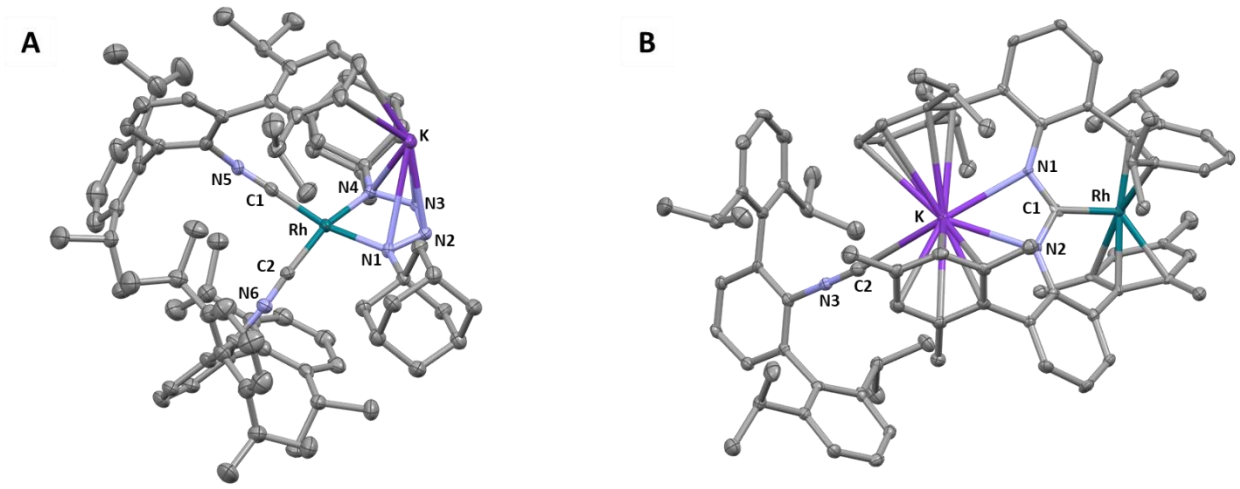

Figure 2.4 Molecular structures of (A) K[(κ$_2$-N,N-Ad$_2$N$_4$)Rh(CNAr^{Dipp2})$_2$] (17) and (B) K[Rh(κ$_3$-C,C,C-^{Mes2}ArNCNAr^{Dipp2})][CNAr^{Dipp2}] (18).

adamantal azide results in loss of an equivalent of CNAr^{Dipp2} and formation of a tetrazene complex K[(κ$_2$-N,N-Ad$_2$N$_4$)Rh(CNAr^{Dipp2})$_2$] (**17**) (**Scheme 2.3; Figure 2.4A**). In the solid state the potassium-tetrazene interactions bridge to form a trimeric species. Allowing the reaction mixture sit at room temperature over the course of an hour results in formation of the asymmetric carbodiimide AdN=C=NAr^{Dipp2}.[41] Formation of this complex is thought to occur through the transfer of a fleeting metal-imido.[39, 42] Studies on earlier transition metals lend support for this pathway. In studying high-valent niobium tetrazene complexes, Arnold et al., found that they were in equilibrium at room temperature with the uncyclized, terminal azido-imido; observable *via* variable temperature, solution, ^{1}H NMR studies.[43] Similar cyclized/uncyclized combinations were observable in disordered crystal structures of a Mn(IV)(N$_4$Ad$_2$)$_2$ system by Zdilla et al.[44] Given the information in these studies, the inability of low-valent rhodium to form secondary π-bonds from exogenous donors, and the electrophilic nature of the low-lying π* orbitals on the isocyanide we favor a mechanism involving the formation and transfer of a metal-imido, followed by reductive elimination of the carbodiimide.

Further evidence of this can be found from the reaction of a bulkier azide like the *m*-terphenyl azide, N$_3$Ar^{Mes2}. Addition of just one equivalent of N$_3$Ar^{Mes2} yields K[Rh(κ$_3$-*C,C,C*-^{Mes2}ArNCNAr^{Dipp2})][CNAr^{Dipp2}] (**18**) (**Scheme 2.3; Figure 2.4B**), which in the context of the AdN$_3$ chemistry represents a pre-reductive elimination, doubly reduced carbodiimide. In a broader chemical

context, this complex represents a unique, acyclic carbodiiminate pincer ligand. Notably, the equivalent of ^{Dipp2}ArNC observed in the solid-state structure (**Figure 2.4B**) is observable in the ^{1}H NMR at exactly 1.0 equivalent, even after repeated washing with *n*-pentane. The electronic structure of the ligand appears similar to that of the acyclic carbodicarbene, or a bent-allene.[45] DFT calculations of the theoretical, truncated ligand fragment ([PhNCNPh]$^{2-}$) reflect a roughly C_2-symmetric ligand, where the bent carbodiimidate displays orthogonal a- and b-symmetric frontier molecular orbitals. Similar to carbodicarbenes like Bertrand et al.'s seminal bis-NHC supported example ("$(NHC)_2C$"; **Figure 2.5B**)[45], these a- and b-symmetric orbitals are capable of acting as both σ and π donors, respectively (**Figure 2.5A**).[45-48] The flanking NAr groups twist from the plane of the carbodiimide, similar to other carbodicarbenes, which give the π-symmetric molecular orbitals a similar split, helical shape as a bent

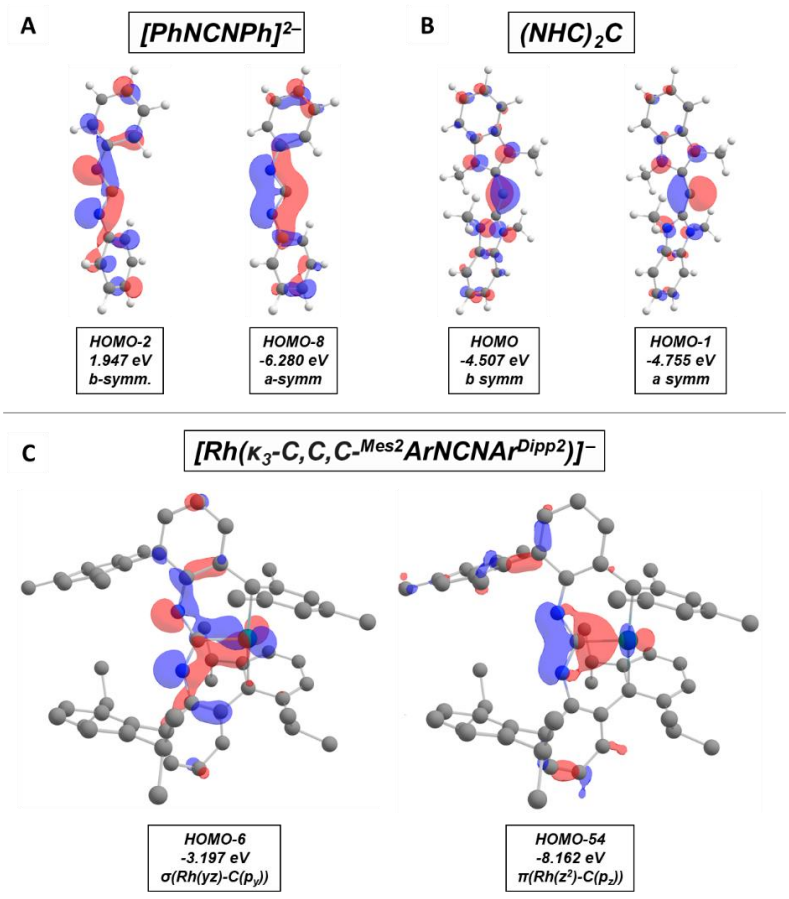

Figure 2.5 DFT-calculated (B3LYP/DEF2-TDVPP) molecular orbitals of π- and σ-bonding symmetries for the A) hypothetical ligand fragment [PhNCNPh]$^{2-}$, B) Betrand, et al.'s $(NHC)_2C$ free carbodicarbene, and C) [Rh(κ$_3$-C,C,C-^{Mes2}ArNCNAr^{Dipp2})]$^{-}$.

allene.[49] Further DFT studies of **18** show the σ- and π-ligand-metal bonding interactions through the respective d_{z2} and d_{yz} orbitals on rhodium (**Figure 2.5C**).

In contrast to the two electron, -1/+1 oxidation chemistry displayed in the two previously described reactions, we sought to probe one-electron chemistry of the metallates. Nitrosoarenes are well known to be redox non-innocent ligands that are often used as spin traps for organic- and transition-metal-based radicals, making them ideal targets for this application.[50] Combination of nitrosobenzene (PhNO) and K[Ir($CNAr^{Dipp2}$)$_3$] K[**4**] forms the diamagnetic complex K[Ir($PhNOCNAr^{Dipp2}$)($CNAr^{Dipp2}$)$_2$] (**19**) as determined by X-ray crystallography (**Scheme 2.4**). This compound features a unique four-membered metal-NCO metallocycle incorporating an ostensibly Ir(I) metal center. From this we can rationalize two different routes of formation: a nucleophilic attack from PhNO to the isocyanide carbon or a radical mechanism first involving a reduction of the nitrosoarene. Previous studies with isocyano-platinum group metal complexes have shown that nitrosoarenes can be effective $1e^-$ oxidants in the solid state, harboring a majority of the spin on the N-O fragment but exhibit instability in solution.[51] In addition, La Monica and Otsuka observed O-atom transfer reactivity from PhNO to form isocyanates and phosphenoxides from Re and Ni nitrosoarene coordination complexes.[52-54] The most conclusive evidence for initial coordination of the nitrosoarene comes from the electrochemistry of the m-terphenyl, ^{Mes2}ArNO, measured by Deng and co-workers where they found the $E_{1/2}$ of the (0/1-) couple to be ~1.4V (v. Fc/Fc^+).[55-56] As shown in section 2.2, this is likely not sufficient to oxidize K[**4**] via outer sphere electron transfer. With these examples in mind, we favor the latter route of formation where **19** represents a stabilized intermediate in the formation

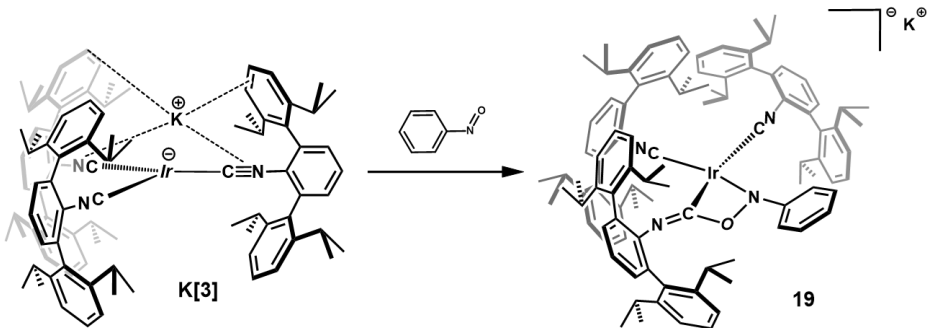

Scheme 2.4 Formation of N-O-C-Ir metallocycle containing K[Ir($PhNOCNAr^{Dipp2}$)($CNAr^{Dipp2}$)$_2$] (19).

of isocyanate from a reduced nitrosoarene, likely formed post-coordination of PhNO to the metal center.

Most importantly, the nucleophilic behavior of metalates K[**3**] and K[**4**] demonstrates that they can engage with a wide variety of substrates along the formal M(1-)/M(I) redox couple. As reactivity utilizing the M(I)/M(III) redox couple is well established for Rh(I) and Ir(I) complexes, access to the formally M(1-) state offers a path forward for the development of four-electron redox processes using these heavier, Group 9 metals.

2.2 Electrochemical investigations of metalate redox profiles

There is a general dearth of electrochemical data on metallates in the literature, likely due to their highly reducing nature and propensity to decompose in high polarity solutions,.[1, 57] Nonetheless, we set out to use cyclic voltammetry to better understand the redox profiles of Group 9 metallates.

$Na[Co(N_2)(CNAr^{Dipp2})_3]$ Na[**5**-N_2] shows two reversible redox features at -1.088 V (Co(-1)/Co(0)) and -0.816 V (Co(0)/Co(+1)) versus Fc/Fc^+, in addition to one irreversible oxidation around -0.652 V (**Figure 2.6**). Note that irreversible features are reported with both the peak current ($\boldsymbol{E^{(p)}}$) and the inflection point ($\boldsymbol{E^{(i)}}$) of the peak current. While peak currents are often reported for irreversible features, it has been suggested that the inflection point is a more accurate measure of the $E°_{redox}$ as it is less affected by scan rate and solution resistance.[58] Because the anions readily reacted with common electrolytes such as $[PF_6]^-$ and quickly decomposed in higher polarity solvents such as acetonitrile, these experiments were performed in 0.1M $[NBu_4][BArF_{24}]$ tetrahydrofuran (THF) solutions ($BArF_{24}$ = Tetrakis[3,5-bis(trifluoromethyl)phenyl]borate) where solution resistance is relatively high. As a note, even under these relatively low-polarity conditions, decomposition of the analytes was observed at timescales greater than 30 min. To add context to the redox behavior of [**5**-N_2], cyclic voltammograms of $NaCo(CNAr^{Mes2})_4$ and $NaCo(CO)_4$ were also collected (**Figure 2.7**). Like [**5**-N_2], $NaCo(CNAr^{Mes2})_4$ features reversible (-1/0) and (0/+1) redox couples in addition to a irreversible oxidation. However, the separation and absolute value of these potentials are greater. The (-1/0) couple is at -1.984 V, almost a whole -1 V more reducing

than [**5**-N_2]. The (0/+1) redox pair has a wider than normal peak separation at 290 mV. Stoichiometric studies previously conducted on $NaCo(CNAr^{Mes2})_4$ have shown that oxidation from the anion to the cation $[Co(THF)(CNAr^{Mes2})_4][OTf]$ involves binding of a solvent molecule and a change in geometry from tetrahedral to square pyramidal. These changes introduce a kinetic barrier to the (0/+1) couple and are believed to be the source of the larger peak separation. The small peaks in the returning anodic sweep of the voltammogram without corresponding oxidations are not visible when just scanning the first two reversible redox features (scan window of ~2.3 V to 0 V), suggesting that they are fragmented products of

the irreversible oxidation. The cyclic voltammogram of $NaCo(CO)_4$ reveals a slightly different redox profile with no fully reversible features at generally lower potentials (**Figure 2.7D**). The first oxidation at -0.487 V is likely a one electron oxidation which would form the exceedingly well studied dimeric, dicobaltoctacarbonyl, $Co_2(CO)_8$. This conclusion is further supported by the irreversible oxidation at +0.687 V, which is observed in voltammograms of similar, lightly substituted dicobalt carbonyl complexes.[59-60] Like $NaCo(CNAr^{Mes2})_4$, the smaller reductions on the reverse sweep (~ -1.6 V) is no longer observed with a smaller scan window, excluding the final irreversible oxidation. Instead, just the

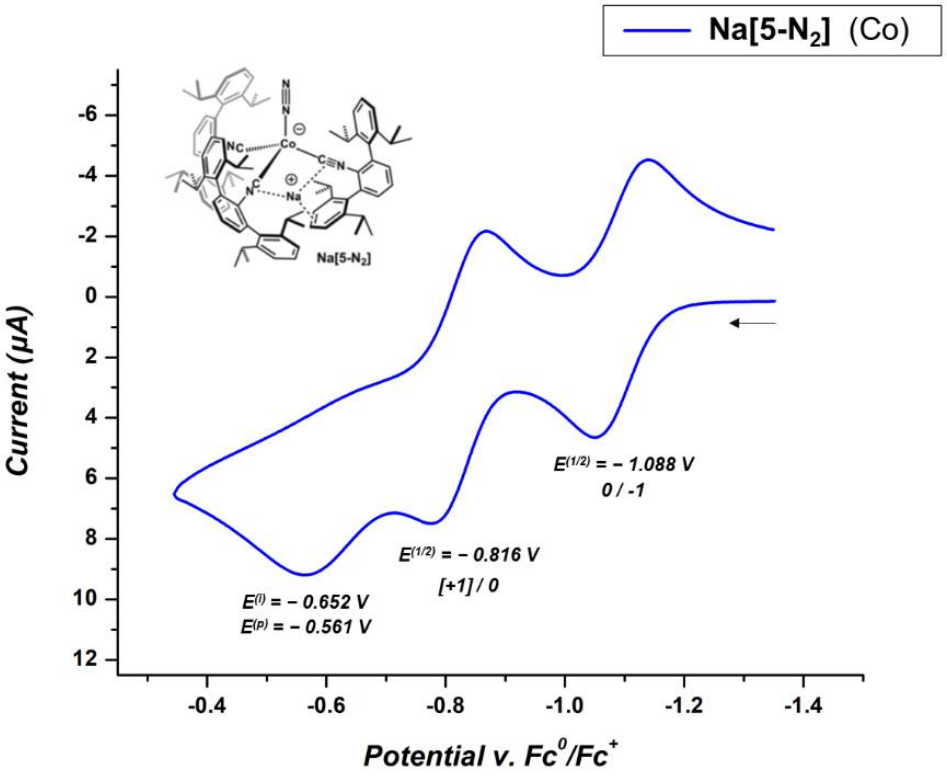

Figure 2.6 Cyclic voltammogram of $Na[Co(N_2)(CNAr^{Dipp2})_3]$ Na[5-N_2] sweeping from -1.4 V to -0.3 V at a scan rate of 100mV/s.

putative Co(0)/Co(-1) features are observed with a $E^{(p)}$ separation of 313 mV, but a small $E^{(i)}$ separation of just 86 mV.

The heavier Group 9 congeners display distinctly different redox behavior than their 3d metal counterparts. Each species shows one initial irreversible oxidative event. For the rhodium metalate, K[**3**], this feature has an $E^{(i)}$ of -1.459 V and a $E^{(p)}$ of -1.386 V (**Figure 2.7 A-B**). The corresponding first oxidative event for iridium is at has an $E^{(i)}$ of -1.207 V and a $E^{(p)}$ of -1.126 V suggesting K[**4**] is less reducing than K[**3**] (**Figure 2.7 C-D**). This difference also reflects the TlOTf reactivity of the anions.

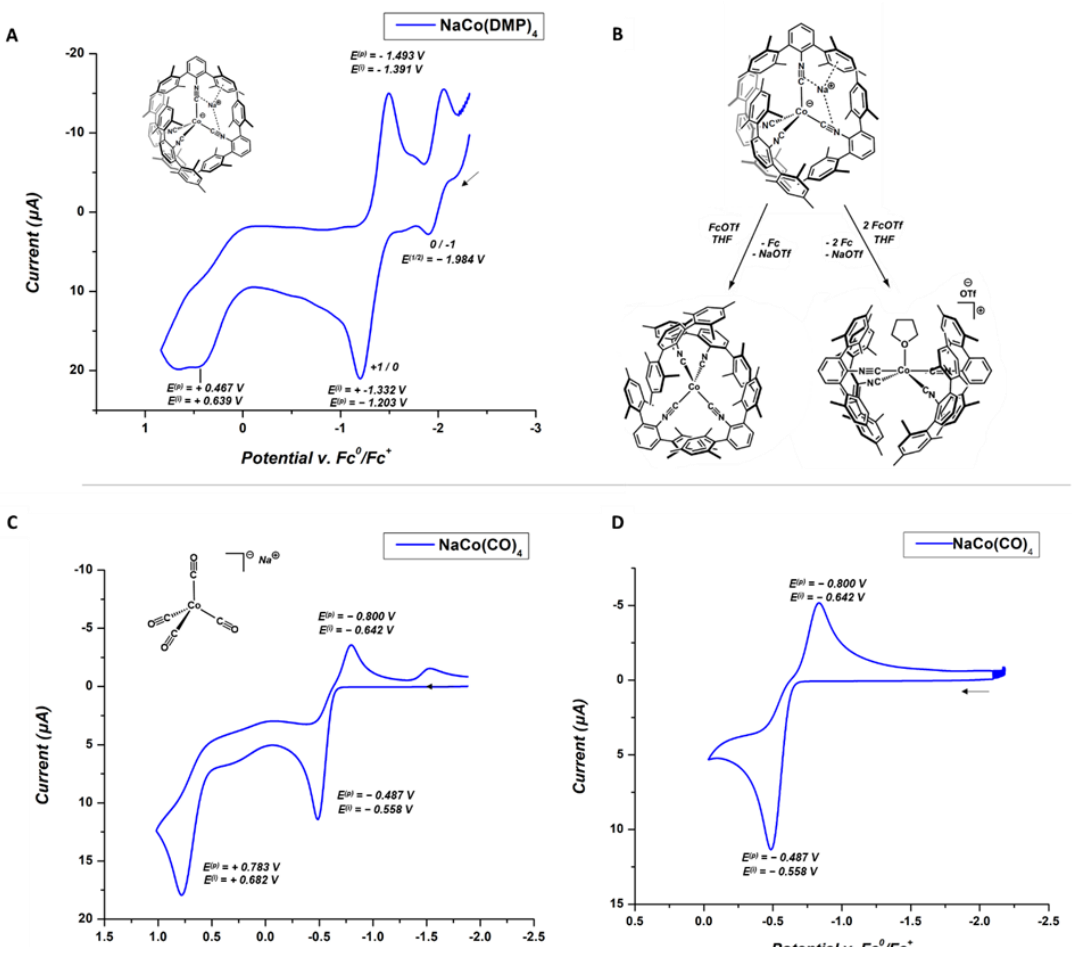

Figure 2.7 Cyclic voltammograms of A) Na[Co(CNAr^{DMP2})$_4$], C) NaCo(CO)$_4$ and, D) NaCo(CO)$_4$ scanning short of the second oxidation to highlight the cleaner return reduction. B) Scheme of the oxidative chemistry of Na[Co(CNAr^{DMP2})$_4$].

While the reactions in the iridium system to form Tl adducts **6** and **9** react cleanly, the corresponding reactivity of K[**3**] frequently formed easily separable Rh(I) byproducts, likely oxidized by Tl(I). The only other metallates we could find with electrochemical data to compare were Prof. Connie Lu's series of Group 13 supported rhodium metalates, Na[RhM[N(*o*-(NCH_2P*i*-Pr_2)C_6H_4)$_3$] (M = Al, Ga, In). The cyclic voltammograms of these species are considerably different than those observed in K[**3**] and K[**4**], containing two, reversible one-electron events corresponding to the Rh(-1/0) and Rh(0/+1) redox couples. The potentials of the Rh(-1/0) vary from 1.61 V (v Fc/Fc^+) for the Al supported complex, -1.51 V for the Ga supported, and -1.35 V for the In supported complex. The difference in redox behavior is likely due to

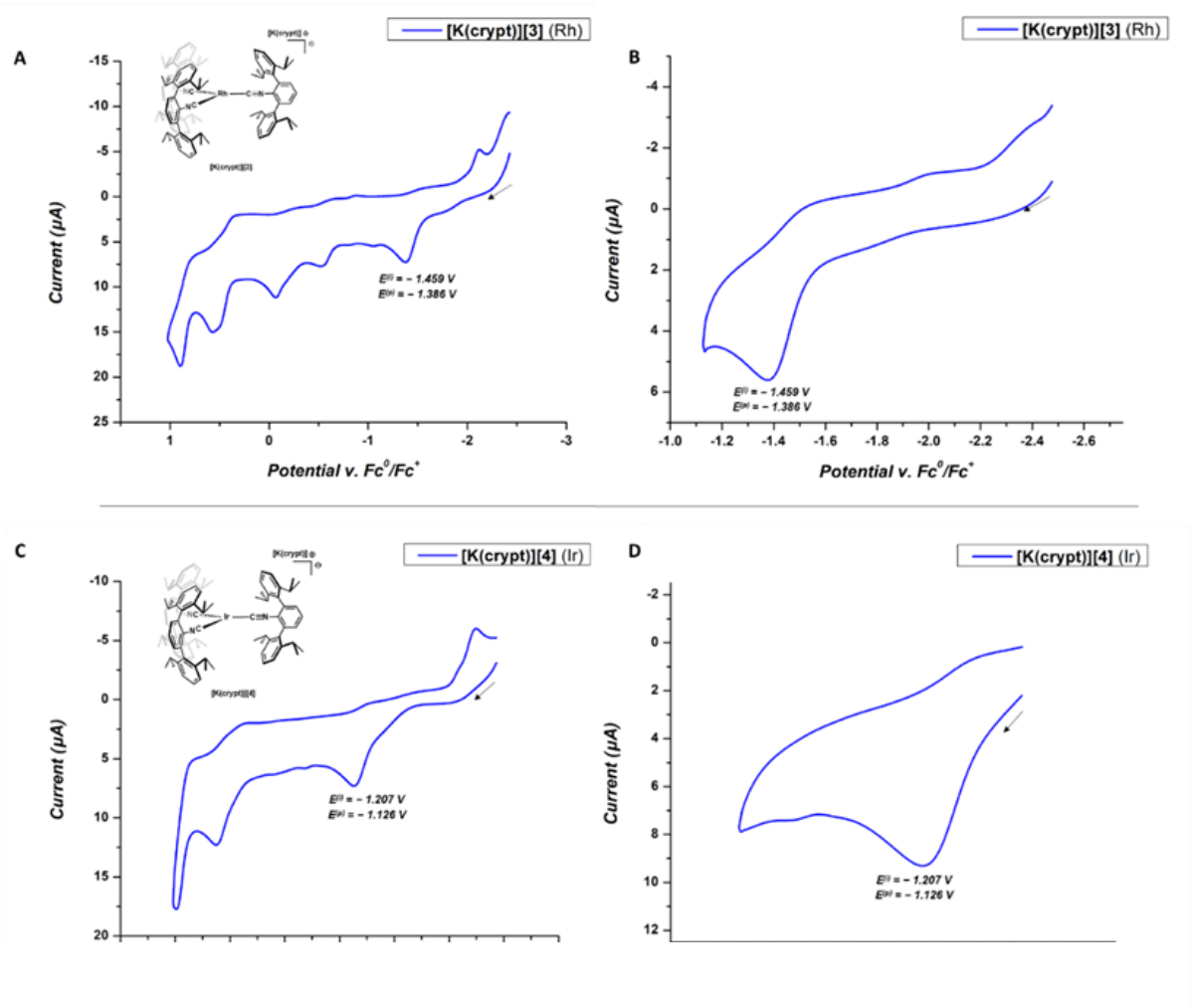

Figure 2.8 Cyclic voltammograms of A) K[Rh($CNAr^{Dipp2}$)$_3$] K[3] – full scan window, B) K[3] with a scan window that only includes the first oxidation. C) K[Ir($CNAr^{Dipp2}$)$_3$] K[4], and D) K[4] with a similarly reduced scan window.

the chelating and supporting metallo-ligand, which provides rigid coordination geometry and stabilization of the partially filled metal d_{z2} orbital upon oxidation. This is distinct from the monodentate terphenyl ligands used in K[**3**] and K[**4**] which allow for greater flexibility in the metal's coordination geometry.

2.3 Concluding remarks

The group 9 metalates, K[**3**] and K[**4**] can make good use of their unsaturation, exhibiting a variety of nucleophilic and oxidative chemistry. Both K[**3**] and K[**4**] are shown to support up to two reverse dative bonding (Z-type) interactions and perform up to four electron swings in oxidation state with substrates like PCl_3, forming complexes of the formulation $MCl(PCl_2)_2(CNAr^{Dipp2})_2$ (M= Rh [**14]**, Ir, [**15**]). While attempts to achieve similar chemistry with the cobalt metalates were unsuccessful, the electrochemistry of this series of Group 9 metalates offer insights as to why. Cyclic voltammetry of Na[**5-**N_2] reveals two reversible one electron features and one further irreversible oxidation. In contrast, both heavier Rh and Ir congeners display one initial irreversible oxidation, highlighting the stark differences in their oxidative chemistry from formal M(1-) oxidation states.

2.4 Synthetic procedures and characterization data

General Considerations – All manipulations were carried out under an atmosphere of purified dinitrogen using standard Schlenk and glovebox techniques. Unless otherwise stated, reagent-grade starting materials were purchased from commercial sources and either used as received or purified by standard procedures.[61] Solvents were dried and deoxygenated according to standard procedures.[62] Benzene-d_6 (Cambridge Isotope Laboratories) was distilled from NaK alloy/benzophenone ketyl and stored over 4 Å molecular sieves under N_2 for at least 24 h prior to use. Celite 405 (Fisher Scientific) was dried under vacuum (24 h) at a temperature above 250 ˚C and stored in the glovebox prior to use. The m-terphenyl isocyanide $CNAr^{Dipp2}$ was prepared as previously reported.[63-64]

Solution ^{1}H and $^{13}C\{^{1}H\}$ NMR spectra were recorded on a Bruker Avance 300, a Varian Mercury 400, a Jeol ECA 500, or a Varian X-SENS 500 spectrometer. ^{1}H and $^{13}C\{^{1}H\}$ chemical shifts are reported in ppm relative to $SiMe_4$ (^{1}H and ^{13}C $\delta = 0.0$ ppm) with reference to residual solvent resonances of 7.16 ppm (^{1}H) and 128.06 ppm (^{13}C) for C_6D_6.[65] Solution FTIR spectra were recorded on a Thermo-Nicolet iS10 FTIR spectrometer. Samples were prepared as C_6D_6 solutions injected into a ThermoFisher solution cell equipped with KBr windows. For solution FTIR spectra, solvent peaks were digitally subtracted from all spectra by comparison with an authentic spectrum obtained immediately prior to that of the sample. The following abbreviations were used for the intensities and characteristics of important IR absorption bands: vs = very strong, s = strong, m = medium, w = weak, vw = very weak; b = broad, vb = very broad, sh = shoulder. Combustion analyses were performed by Midwest Microlab LLC, Indianapolis, IN.

All cyclic voltammetry (CV) experiments were performed at room temperature under an dinitrogen atmosphere with a Gamry Interface 1010E potentiostat. A single-compartment cell was used for all experiments. Voltammograms were recorded in 0.1M $[NBu_4][BArF_{24}]$ THF solution at $\upsilon = 100$ mV/s with a 3mm glassy carbon working electrode, a Pt wire counter electrode and a silver wire pseudoreference electrode (separated from the bulk solution by a Vycor tip). Potentials were calibrated against the Fc/Fc^{+} redox couple (internal standard). Analyte complex concentrations ranged from 1-1.5 mM.

Synthesis of $TlIr(CNAr^{Dipp2})_3$ (6): An Et_2O solution of $K[Ir(CNAr^{Dipp2})_3]$ (K[**3**]; 0.049 g, 0.032 mmol, 1 equiv, 2 mL) was added to a thawing slurry of TlOTf in Et_2O (0.011 g, 0.032 mmol, 1 equiv, 2 mL). The reaction was left to stir and warm to room temperature for 1 hr before being filtered through Celite. The resulting filtrate was then evaporated to dryness *in vacuo*, leaving $TlIr(CNAr^{Dipp2})_3$ (**6**) as a green powder. Yield*:* 0.050 g, 0.030 mmol, 94%. Recrystallization of the solid from a 3 mL Et_2O solution at −32 °C for 2 days afforded green crystals suitable for X-ray diffraction. ^{1}H NMR (499.8.9 MHz, C_6D_6, 20 ˚C): $\delta = 7.28$ (t, 6H, J = 8 Hz, p-Dipp), 7.17 (d, 12H, J = 8 Hz, m-Dipp), 7.03 (d, 6H, J = 8 Hz, m-Ar), 6.90 (t, 3H, J = 8 Hz, p-Ar), 2.84 (septet, 12H, 7Hz, $CH(CH_3)_2$), 1.15 (d, 36H, J = 7 Hz, $CH(CH_3)_2$), 1.14 (d, 36H, J = 7 Hz, $CH(CH_3)_2$) ppm. $^{13}C\{^{1}H\}$ NMR (125.8MHz, C_6D_6, 20 ˚C): $\delta = 180.4$

(CNR), 147.6, 137.3, 134.1, 133.4, 130.5, 128.4, 123.5, 123.0, 31.1, 25.2, 25.1 ppm. FTIR (KBr windows, C_6D_6, 20 ˚C) υ(C≡N) = 2027 (m, sh), 1996 (m, sh), 1896 (vs) cm^{-1}; also 2962 (s), 2926 (m), 2866, (m), 1615 (w), 1576 (m), 1459 (m), 1410 (m), 1383 (w), 1362, (w), 759 (m), 680 (w) cm^{-1}. Anal. calcd. for $C_{93}H_{111}N_3IrTl$: C, 66.99; H, 6.71; N, 2.52. Found: C, 66.64; H, 6.95; N, 2.45.

Synthesis of $[Tl_2Rh(CNAr^{Dipp2})_3]OTf$ (7): An Et_2O solution of $K[Rh(CNAr^{Dipp2})_3]$ (K[**3**]; 0.096 g, 0.068 mmol, 1 equiv) was added to a stirring slurry of TlOTf in THF (0.053 g, 0.150 mmol, 2.2 equiv). The reaction was left to stir for 24hr before being dried *in vacuo*. The reaction was then subjected to three cycles of slurrying in n-pentane (3 x 5 mL) to remove any remaining THF. The resultant solid was slurried in 30 mL of *n*-pentane and filtered over Celite. The remaining solid and Celite was extracted with 30 mL of Et_2O then dried *in vacuo*. The resultant powder was dissolved in 2 mL of toluene, and 2 mL of *n*-pentane was layered on top. The solution was allowed to sit for 24 h at −32 ˚C to give forest green, X-ray quality crystals, which were rinsed with minimal amounts of *n*-pentane. Yield: 0.027 g, 0.014 mmol, 21%. ^{1}H NMR (499.8.9 MHz, C_6D_6, 20 ˚C): δ = 7.79 (t, 6H, J = 8 Hz, p-Dipp), 7.41 (d, 12H, J = 8 Hz, m-Dipp), 6.92 (d, 6H, J = 8 Hz, m-Ar), 6.86 (t, 3H, J = 8 Hz, p-Ar), 2.69 (septet, 12H, J = 7 Hz, $CH(CH_3)_2$), 1.19 (d, 36H, J = 7 Hz, $CH(CH_3)_2$), 1.07 (d, 36H, J = 7 Hz, $CH(CH_3)_2$) ppm. $^{13}C\{^1H\}$ NMR (125.8 MHz, C_6D_6, 20 ˚C): δ = 147.5, 136.2, 135.7, 131.4, 130.4, 125.4, 124.2, 31.2, 24.8, 24.7 ppm. Note, repeated scanning failed to locate the isocyanide ^{13}C resonances. Presumably this is a manifestation of higher order coupling between ^{103}Rh and ^{203}Tl/^{205}Tl. FTIR (KBr windows, C_6D_6, 20 ˚C) υ(C≡N) = 2034, (m, sh), 2004 (s, sh), 1967 (vs) cm^{-1}; also 1577 (w), 1462 (m), 1409 (m), 1384 (w), 1363 (w), 1328 (s), 1291 (m), 1240 (s), 1157 (m), 1056 (w), 1026 (s), 761 (m), 680 (w), 637 (m) cm^{-1}. Anal. calcd. for $C_{94}H_{111}N_3SO_3F_3RhTl_2$: C, 70.78; H, 7.09; N, 2.66. Found: C, 51.34; H, 5.22; N, 1.80.

Synthesis of $TlRh(CNAr^{Dipp2})_3$ (8): To a stirring Et_2O/THF (1:5) solution of $[Tl_2Rh(CNAr^{Dipp2})_3]OTf$ (**7**; 0.145 g, 0.075 mmol, 1 equiv), KI was added as a solid (0.062 g, 0.375 mmol, 5 equiv) and was left to stir for 4 days. The volatiles were then removed *in vacuo*. The dark residue was then eluted through a 5cm thick plug of Celite with *n*-pentane, collecting only the dark fraction. Drying the *n*-pentane solution *in vacuo* yields **8** as a dark green solid. 1566.9Yield: 0.012 g, 0.007 mmol,

10%. Recrystallization of the solid from a 2 mL *n*-pentane solution spiked with 1 drop of Et_2O at −32 °C for 5 days afforded dark green crystals suitable for X-ray diffraction. ^{1}H NMR (499.8.9 MHz, C_6D_6, 20 ˚C): δ = 7.45 (t, 6H, 8Hz, p-Dipp), 7.35 (d, 12H, 8Hz, m-Dipp), 6.99 (t, 3H, 8Hz, p-Ar), 6.90 (d, 6H, 8Hz, m-Ar), 2.95 (septet, 12H, 7Hz, $CH(CH_3)_2$), 1.52 (d, 36H, 7Hz, $CH(CH_3)_2$), 1.23 (d, 36H, 7Hz, $CH(CH_3)_2$) ppm. ^{13}C{^{1}H} NMR (125.8MHz, C_6D_6, 20 ˚C): δ = 147.6, 137.3, 134.1, 133.4, 130.5, 128.4, 123.5, 123.0, 31.1, 25.2, 25.1 ppm. 8 MHz, C_6D_6, 20 ˚C): δ = 147.5, 136.2, 135.7, 131.4, 130.4, 125.4, 124.2, 31.2, 24.8, 24.7 ppm. Note, repeated scanning failed to locate the isocyanide ^{13}C resonances. Presumably this is a manifestation of higher order coupling between ^{103}Rh and ^{203}Tl/^{205}Tl. FTIR (KBr windows, Et_2O, 20 ˚C) υ(C≡N) = 2033 (w), 1964 (vs) cm^{-1}; also 2960 (m), 2924 (w), 2867 (w), 1578 (w), 1462 (w), 1413 (m), 1361 (w), 1328 (s), 1178 (m), 1045 (m, br), (758 (m), 680 (m) cm^{-1}. Anal. calcd. for $C_{93}H_{111}N_3RhTl$: C, 70.78; H, 7.09; N, 2.66. Found: C, 40.13; H, 4.38; N, 0.99.

Synthesis of [Tl$_2$Ir(CNAr^{Dipp2})$_3$]OTf [9]: To a stirring Et_2O/THF (3:1) solution of K[Ir(CNAr^{Dipp2})$_3$] (**2**; 0.049 g, 0.033 mmol, 1 equiv), TlOTf (was added as a solid. Reaction was stirred for 3 hr before being filtered through Celite and drying *in vacuo*. The reaction was then subjected to three cycles of slurrying in n-pentane (3 x 5 mL) to remove any remaining THF. That solid was extracted with Et_2O and recrystallized from a concentrated 1mL solution of toluene with 1mL of *n*-pentane layered on top. The solution was allowed to sit for 24 hr at *−32 °C* to give green crystals which were rinsed with minimal amounts of *n*-pentane. Yield: 0.046 g, 0.023 mmol, 69%. ^{1}H NMR (499.8.9 MHz, C_6D_6, 20 °C): δ = 7.75 (t, 6H, 8Hz, p-Dipp), 7.40 (d, 12H, 8Hz, m-Dipp), 6.93 (d, 6H, 8Hz, m-Ar), 6.86 (t, 3H, 8Hz, p-Ar), 2.72 (septet, 12H, 7Hz, $CH(CH_3)_2$), 1.20 (d, 36H, 7Hz, $CH(CH_3)_2$), 1.09 (d, 36H, 7Hz, $CH(CH_3)_2$) ppm. ^{13}C{^{1}H} NMR (125.8MHz, C_6D_6, 20 °C): δ = 162.0 (CNR), 147.7, 136.6, 134.7, 131.3, 130.5, 124.9, 124.3, 31.2, 24.8 ppm. FTIR (KBr windows, C_6D_6, 20 °C) υ(C≡N) = 2016 (m, sh), 1957 (vs) cm^{-1}; also 2963 (s), 2927 (m), 2868 (m), 1576 (w), 1462 (w), 1409 (m), 1384 (w), 1362 (w), 1328 (s), 1291

(m), 1239 (s) 1221 (w, sh), 1156 (m), 1055 (w), 1026 (s), 792 (m), 637 (s) cm^{-1}. Anal. calcd. for $C_{94}H_{111}N_3SO_3F_3IrTl_2$: C, 55.87; H, 5.54; N, 2.08. Found: C, 57.65; H, 5.81; N, 1.97.

Synthesis of $HRh(CNAr^{Dipp2})_3$ (10): To a solution of $K[Rh(CNAr^{Dipp2})_3]$ (K[**3**]; 0.019 g, 0.014 mmol, 1 equiv) in 3 mL of C_6H_6, benzoic acid (0.0017 g, 0.014 mmol, 1 equiv) in an additional 1 mL of C_6H_6 was added dropwise. The reaction was let stir for 15 min before being filtered through a fiberglass syringe filter and dried *in vacuo* to yield an orange solid. Yield*:* 0.015 g, 0.011 mmol, 80%. X-ray quality crystals were grown by dissolving the solid in 2 mL of a n-pentane/benzene (20:1) solution and placing it at *−32* ˚C for 3 days. ^1H NMR (499.8.9 MHz, C_6D_6, 20 ˚C): δ = 7.35 (t, 4H, J = 8 Hz, p-Dipp), 7.30 (t, 2H, J = 8Hz, p-Dipp), 7.22 (d, 8H, J = 8 Hz, m-Dipp), 7.17 (d, 4H, J = 8 Hz, m-Dipp), 6.94 (d, 2H, J = 8 Hz, m-Ar), 6.93 (dd, 2H, J = 8 Hz, p-Ar), 6.88 (d, 4H, J = 8 Hz, m-Ar), 6.80 (t, 1H, J = 8 Hz, p-Ar), 2.72 (septet, 8H, J = 7 Hz, $CH(CH_3)_2$), 2.60 (septet, 4H, J = 7 Hz, $CHf(CH_3)_2$), 1.19 (d, 24H, J = 7 Hz, $CH(CH_3)_2$), 1.18 (d, 24H, 7Hz, $CH(CH_3)_2$), 1.15 (d, 12H, 7Hz, $CH(CH_3)_2$), 0.93 (d, 12H, 7Hz, $CH(CH_3)_2$), -7.61 (d, 1H, J = 15.4 Hz, RhH) ppm. $^{13}C\{^1H\}$ NMR (125.8MHz, C_6D_6, 20 ˚C): δ = 169.5 (CNR), 168.9 (CNR), 147.0, 146.9, 137.7, 135.9, 135.9, 130.6, 130.4, 130.1,129.7, 129.1, 128.6 127.3, 127.6, 126.2, 123.5, 123.3, 31.5, 31.1, 25.0, 24.8, 24.6, 24.5, 24.2 ppm. FTIR (KBr windows, C_6D_6, 20 ˚C) υ(C≡N) = 2075 (m, sh), 2036 (vs), 2001 (s) cm^{-1}; also 3062 (w), 3023 (w), 2962 (s), 2927 (m), 2865 (m), 1577 (w), 1508 (w), 1457 (m), 1415 (m), 1384 (w), 1361 (w), 1334 (w), 1329 (w), 1253 (w), 1176 (w), 1056 (w), 813 (vs), 794 (w), 759 (s) cm^{-1}. Anal. Calcd. for $C_{93}H_{112}N_3Rh$: C, 81.25; H, 8.21; N, 3.06. Found: C, 81.30; H, 8.31; N, 3.13.

Synthesis of $HIr(CNAr^{Dipp2})_3$ (11): To a solution of $K[Ir(CNAr^{Dipp2})_3]$ (K[**4**]; 0.020 g, 0.013 mmol, 1 equiv) in 3 mL of C_6H_6, benzoic acid (0.0015 g, 0.013 mmol, 1 equiv) in an additional 1 mL of C_6H_6 was added dropwise. The reaction was let stir for 20 min before being filtered through a fiberglass syringe filter and dried *in vacuo* yielding a dark red solid. Yield: 0.015 g, 0.010 mmol, 77%. X-ray quality crystals were grown by dissolving the solid in 2 mL of a n-pentane/benzene (20:1) solution and placing it at *−32* ˚C for 3 days. ^1H NMR (499.8.9 MHz, C_6D_6, 20 °C): δ = 7.33 (t, 4H, J = 8 Hz, p-Dipp),

7.29 (t, 2H, J = 8 Hz, p-Dipp), 7.20 (d, 8H, J = 8 Hz, m-Dipp), 7.17 (d, 4H, J =8 Hz, m-Dipp), 6.89 (dd, 2H, J = 8 Hz, m-Ar), 6.89 (dd, 2H, J = 8 Hz, p-Ar), 6.93 (d, 4H, J = 8 Hz, m-Ar), 6.81 (t, 1H, J = 8 Hz, p-Ar), 2.72 (septet, 8H, J = 7 Hz, $CH(CH_3)_2$), 2.60 (septet, 4H, J = 7 Hz, $CH(CH_3)_2$), 1.18 (d, 24H, J = 7 Hz, $CH(CH_3)_2$), 1.16 (d, 24H, J = 7 Hz, $CH(CH_3)_2$), 1.13 (d, 12H, J = 7 Hz, $CH(CH_3)_2$), 0.90 (d, 12H, J = 7 Hz, $CH(CH_3)_2$), –2.45 (s, 1H, IrH) ppm. $^{13}C\{^1H\}$ NMR (125.8MHz, C_6D_6, 20 ˚C): δ = 168.1 (CNR), 163.5 (CNR), 147.0, 146.9, 137.8, 137.2, 136.0, 135.9, 131.2, 130.6, 130.1, 130.8, 130.5 129.2, 129.0, 128.6 127.3, 127.6, 126.2, 124.9, 123.5, 123.4, 123.0, 31.2, 31.1, 25.1, 24.8, 24.7, 24.7, 24.6 ppm. FTIR (KBr windows, C_6D_6, 20 ˚C) υ(C≡N) = 2082 (m, sh), 2032 (vs), 2005 (vs) cm^{-1}; also 2962 (s), 2927 (m), 2862 (m), 1735 (w), 1693 (w), 1577 (w), 1457 (m), 1446 (m), 1415 (m), 1384 (w), 1361 (w), 1334 (w), 1056 (w), 809 (m), 759 (s), 713 (w) cm^{-1}. Anal. Calcd. for $C_{93}H_{112}N_3Ir$: C, 76.29; H, 7.71; N, 2.87. Found: C, 75.23; H, 7.91; N, 2.10.

Synthesis of Rh(TMS)(CNAr^{Dipp2})$_3$ (12): To a stirring solution of K[Rh(CNAr^{Dipp2})$_3$] (K[**3**]; 0.035 g, 0.025 mmol, 1 equiv) in 3 mL of C_6H_6, trimethylsilyl triflate (Me_3SiOTf; 4.5 µL, 0.025 mmol, 1 equiv) was added dropwise with a 10 µL syringe. The reaction mixture was allowed to stir for 20 min, gradually changing in color from red to dark green. The reaction mixture was then filtered through Celite, and the resulting filtrate dried *in vacuo*. X-ray quality crystals were grown by dissolving the resulting solid in 3 mL of a n-pentane/benzene (20:1) solution and placing it at −32 ˚*C* for 3 d. Yield: 0.013 g, 0.010 mmol, 42%. ^1H NMR (499.8.9 MHz, C_6D_6, 20 ˚C): δ = 7.32 (t, 2H, J = 8 Hz, p-Dipp), 7.22 (d, 8H, J = 8 Hz, m-Dipp), 7.15 (d, 4H, J = 8 Hz, m-Dipp), 7.09 (t, 4H, 8Hz, p-Dipp), 6.98 (dd, 4H, J = 8 Hz, m-Ar), 6.97 (dd, 2H, J = 8 Hz, p-Ar), 6.95 (d, 2H, J = 8 Hz, m-Ar), 6.93 (t, 1H, J = 8 Hz, p-Ar), 2.76 (septet, 8H, J = 7 Hz, $CH(CH_3)_2$), 2.70 (septet, 4H, J = 7 Hz, $CH(CH_3)_2$), 1.39 (d, 24H, J = 7 Hz, $CH(CH_3)_2$), 1.29 (d, 12H, J = 7 Hz, $CH(CH_3)_2$), 1.12 (d, 24H, J = 7 Hz, $CH(CH_3)_2$), 1.09 (d, 12H, J = 7 Hz, $CH(CH_3)_2$), 0.04 (s, 9H, $(CH_3)_3Si$) ppm. $^{13}C\{^1H\}$ NMR (125.8MHz, C_6D_6, 20 ˚C): δ = 147.0 (CNR), 146.7 (CNR), 139.5, 138.5, 135.3, 134.9, 130.1, 129.7, 129.5, 127.6, 126.9, 126.6, 123.4, 122.6, 35.5, 31.5, 31.4, 30.3, 24.9, 24.5, 24.3, 24.2, 22.8, 14.3, 9.2 ppm. FTIR (KBr windows, C_6D_6, 20 ˚C) υ(C≡N) = 2073 (s), 2023

(s), 1988 (s), 1923 (vs) cm^{-1}; also 2960 (vs), 2929 (m), 2862 (m), 1329 (s), 1255 (vs), 1031 (m), 811 (s), 487 (s) cm^{-1}.

Synthesis of Rh(CNAr^{Dipp2})(η$_6$-κ-C,Ar-^{Cy2}BIM) (13): To a thawing, stirring solution of K[Rh(CNAr^{Dipp2})$_3$] (K[**3**]; 0.040 g, 0.029 mmol, 1 equiv) in 5 mL of *n*-pentane, chlorodicylcohexylborane ($ClBCy_2$; 60 µL, 0.060 mmol, 2 equiv) was added dropwise with a 10 µL syringe. The reaction mixture was allowed to stir for 30 min, gradually changing lightening in color from dark red to cherry red. The reaction mixture was then filtered through Celite, and the resulting filtrate dried *in vacuo*. X-ray quality crystals were grown by dissolving the resulting solid in 3 mL of a n-pentane/Et_2O (3:1) solution and placing it at −32 ˚*C* for 2 d. ^{1}H NMR (499.8.9 MHz, C_6D_6, 20 ˚C): Spectra for this species suggest a highly desymmeterized ligand environment with complex cyclohexyl resonances, consistent with the solid-state structure. The full spectrum is provided below.

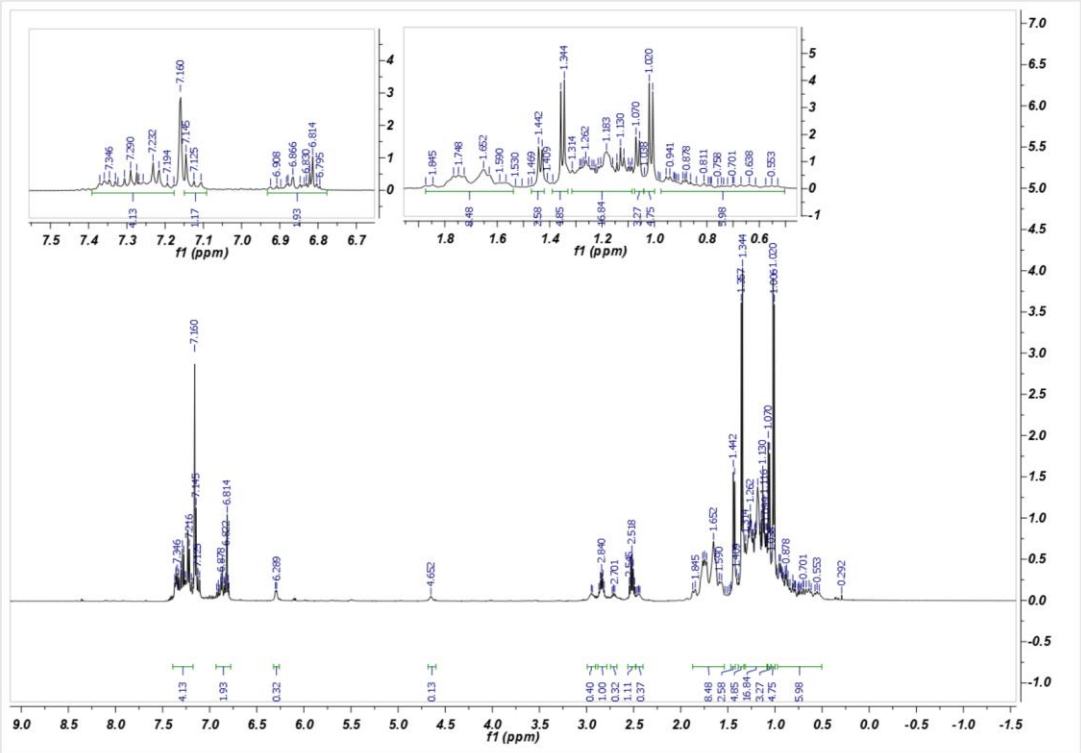

^{11}B{^{1}H} NMR (160.462 MHz, C_6D_6, 20 ˚C): δ = 75.4 ppm. FTIR (KBr windows, C_6D_6, 20 ˚C) υ(C≡N) = 2063 (s), 2018 (s), 1984 (s) cm^{-1}; also 3062 (w), 2962 (vs), 2924 (s), 2866 (m), 2849 (m), 1629 (w), 1615 (w), 1568 (w), 1458 (m), 1447 (m), 806 (m), 794 (m), 759(m) cm^{-1}.

Synthesis of $RhCl(PCl_2)_2(CNAr^{Dipp2})_2$ (14): To a stirring, thawing solution of $K[Rh(CNAr^{Dipp2})_3]$ (K[**3**]; 0.125 g, 0.089 mmol, 1 equiv) in 8 mL of Et_2O, phosphorus trichloride (PCl_3; 15.4 µL, 0.177 mmol, 2 equiv) was added dropwise as a solution in 4mL of Et_2O. The reaction mixture was allowed to stir for 1 hr, quickly changing in color from dark red to a lighter cherry red. The reaction mixture was then filtered through Celite, and the resulting filtrate dried *in vacuo*. The solid was rinsed with C5 (3 x 2mL yielding a light red product. X-ray quality crystals were grown by dissolving the resulting solid in 3 mL of a n-pentane/benzene (20:1) solution and placing it at −32 ˚*C* for 3 d. Yield: 0.090 g, 0.075 mmol, 8590%. ^{1}H NMR (499.8.9 MHz, C_6D_6, 20 ˚C): δ = 7.37 (t, 4H, J = 8 Hz, p-Dipp), 7.22 (d, 8H, J = 8 Hz, m-Dipp), 6.95 (dd, 2H, J = 8 Hz, m-Ar), 6.85 (dd, 2H, J = 8 Hz, p-Ar). 2.64 (septet, 4H, J = 7 Hz, $CH(CH_3)_2$), 1.45 (d, 24H, J = 7 Hz, $CH(CH_3)_2$), 0.98 (d, 12H, J = 7 Hz, $CH(CH_3)_2$), ppm. $^{31}P\{^1H\}$ NMR (202.4MHz, C_6D_6, 20 ˚C): 365.5 (d, J = 22.7 Hz, Rh) ppm.

Synthesis of $IrCl(PCl_2)_2(CNAr^{Dipp2})_2$ (15): To a stirring solution of $K[Ir(CNAr^{Dipp2})_3]$ (K[**3**]; 0.027 g, 0.018 mmol, 1 equiv) in 8 mL of Et_2O, phosphorus trichloride (PCl_3; 1.56 µL, 0.018 mmol, 1 equiv) was added dropwise as a solution in 4mL of Et_2O. The reaction mixture was allowed to stir for 1 hr, quickly changing in color from dark red to a lighter cherry red. The reaction mixture was then filtered through Celite, and the resulting filtrate dried *in vacuo*. X-ray quality crystals were grown by dissolving the resulting solid in 3 mL of a n-pentane/Et_2O (1:5) solution and placing it at −32 ˚*C* for 5 d. Yield: 0.005 g, 0.004 mmol, 22%. ^{1}H NMR (499.8.9 MHz, C_6D_6, 20 ˚C): δ = 7.38 (t, 4H, J = 8 Hz, p-Dipp), 7.28 (d, 8H, J = 8 Hz, m-Dipp), 6.95 (dd, 2H, J = 8 Hz, m-Ar), 6.86 (dd, 2H, J = 8 Hz, p-Ar). 2.65 (septet, 4H, J = 7 Hz, $CH(CH_3)_2$), 1.44 (d, 24H, J = 7 Hz, $CH(CH_3)_2$), 0.98 (d, 12H, J = 7 Hz, $CH(CH_3)_2$), ppm. $^{31}P\{^1H\}$ NMR (202.4MHz, C_6D_6, 20 ˚C): 335.6 (s) ppm.

Synthesis of K[*trans*-$Rh(SiMe_3)_2(CNAr^{Dipp2})_2$] (16): To a stirring solution of $K[Rh(CNAr^{Dipp2})_3]$ (K[**3**]; 0.045 g, 0.032 mmol, 1 equiv) in 4 mL of an Et_2O/*n*-pentane (3:1) solution, hexamethyldisilane (65µL, 0.319 mmol, 10 equiv) was added via micro-syringe. The reaction was let stir for 3 hours after which X-ray quality crystals had formed at the edge of the meniscus which were used for single crystal X-ray diffraction analysis. The remaining solid and solution was cooled in a liquid-nitrogen cold well until a

dark precipitate formed. It was then filtered over celite and washed with chilled n-pentane (3 x 2mL), before being washed through with 10 mL of benzene. The benzene solution was lyophilized to yield a brown solid. Yield: 0.035 g, 0.031mmol, 95%. ^{1}H NMR (499.8.9 MHz, C_6D_6, 20 ˚C): δ = 7.17 (t, 4H, 8Hz, p-Dipp), 7.13 (d, 8H, 8Hz, m-Dipp), 7.04 (d, 4H, 8Hz, m-Ar), 6.88 (t, 2H, 8Hz, p-Ar), 2.96 (septet, 12H, 7Hz, $CH(CH_3)_2$), 1.37 (d, 24H, 7Hz, $CH(CH_3)_2$), 1.04 (d, 24H, 7Hz, $CH(CH_3)_2$), 0.21 (s, 18H, $Si(CH_3)_3$) ppm. $^{13}C\{^{1}H\}$ NMR (125.8MHz, THF-d_8, 20 ˚C): δ = 197.7 (d, 63Hz, CNR), 148.5, 138.4, 131.7, 131.3, 128.6, 127.5, 123.1, 122.7, 31.1, 30.9, 30.3, 25.9, 24.0, 8.6 ppm. FTIR (KBr windows, C_6D_6, 20 ˚C) υ(C≡N) = 1974 (sh), 1901 (vs) cm^{-1}; also 2962 (s), 2927 (m), 2870 (m), 1574 (m), 1458 (m), 1408 (s), 1385 (w), 1361 (w), 1331 (w), 1223 (w), 810 (s) , 707 (w) cm^{-1}. Anal. Calcd. for $C_{93}H_{111}N_3RhTl$: C, 71.92; H, 8.17; N, 2.47. Found: C, 71.14; H, 7.89; N, 2.35.

Synthesis of K[(κ_2-N,N-Ad_2N_4)Rh($CNAr^{Dipp2}$)$_2$] (17): To a stirring, thawing solution of K[Rh($CNAr^{Dipp2}$)$_3$] (K[**3**]; 0.105 g, 0.074 mmol, 1 equiv) in 9 mL of a *n*-pentane/Et_2O mixture (9:1), adamantyl azide (AdN_3; 39.6 mg, 0.223 mmol, 3 equiv) was added dropwise as an Et_2O solution (3 mL). The reaction mixture was allowed to stir for 25 min, gradually warming to room temperature. The reaction mixture was then slurried in *n*-pentane (5mL) and filtered over celite, and the insoluble light red powder dried was *in vacuo*. X-ray quality crystals were grown by dissolving the resulting solid in 4 mL of a *n*-pentane/Et_2O (1:4) solution and placing it at −32 ˚*C* for 3 d. Yield: 0.040 g, 0.041 mmol, 42%. ^{1}H NMR (499.8.9 MHz, C_6D_6, 20 ˚C): Spectra for this species suggest a highly desymmeterized ligand environment, consistent with the solid-state structure. The full spectrum is provided below.

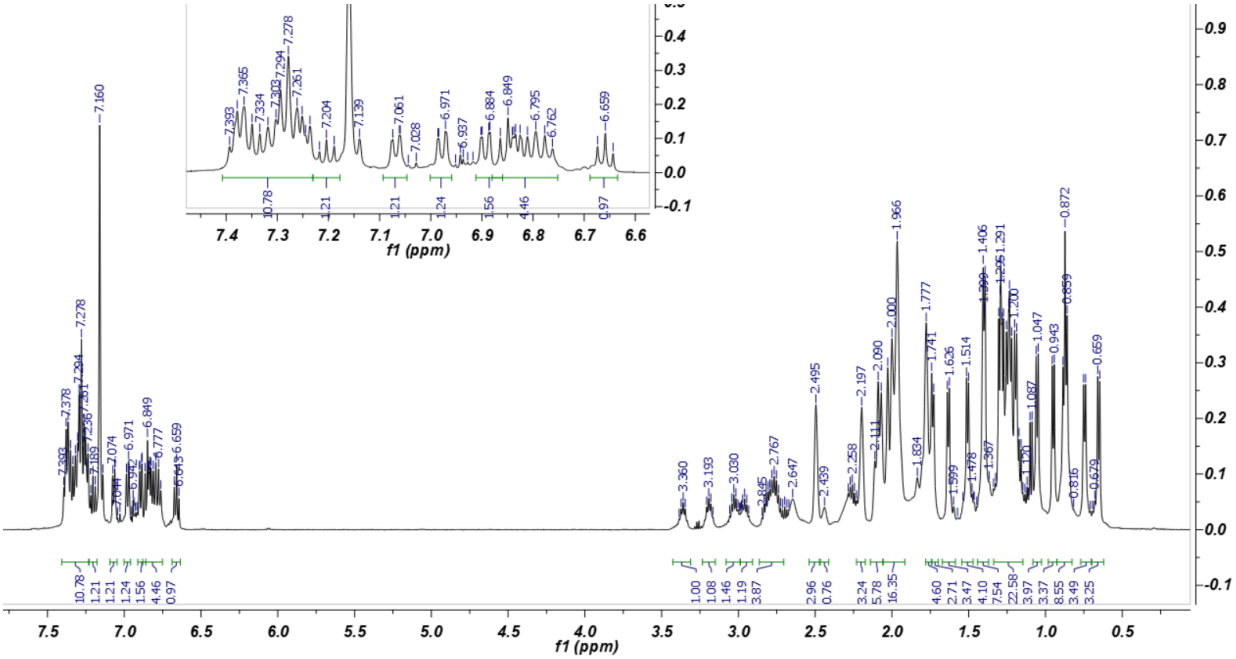

Synthesis of K[Rh(κ$_3$-*C,C,C*-^{Mes2}ArNCNAr^{Dipp2})][CNAr^{Dipp2}] (18): To a stirring solution of K[Rh(CNAr^{Dipp2})$_3$] (K[**3**]; 0.065 g, 0.046 mmol, 1 equiv) in 4 mL of a *n*-pentane, ^{Mes2}ArN$_3$ (^{DMP}ArN$_3$; 16.4 mg, 0.046 mmol, 1 equiv) was added dropwise as an Et$_2$O solution (3 mL). The reaction mixture was allowed to stir for 35 min. The reaction mixture was then washed 2x with cold *n*-pentane (1.5mL) and filtered over celite, and the less soluble brown-red powder was dried *in vacuo*. X-ray quality crystals were grown by dissolving the resulting solid in 4 mL of a *n*-pentane/Et$_2$O (1:4) solution and placing it at −32 ˚*C* for 3 d. Yield: 0.020 g, 0.015 mmol, 33%. ^{1}H NMR (400 MHz, C$_6$D$_6$, 20 ˚C):

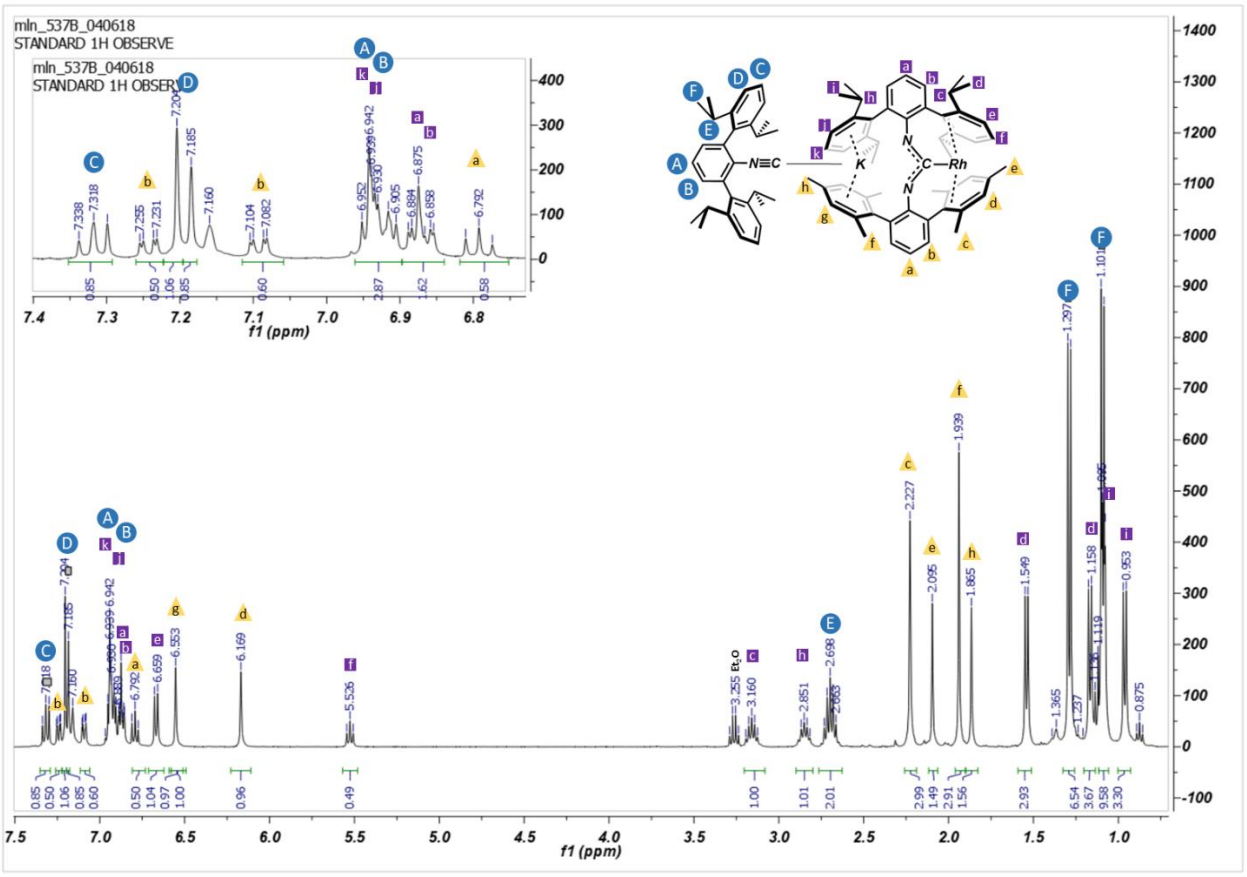

Synthesis of K[Ir(PhNOCNAr^{Dipp2})(CNAr^{Dipp2})$_2$] (19): To a stirring solution of K[Ir(CNAr^{Dipp2})$_3$] (K[**3**]; 0.47 g, 0.031 mmol, 1 equiv) in 7 mL of Et_2O, nitrosobenzene (PhNO; 3.4 mg, 0.031 mmol, 1 equiv) was added dropwise with as a Et_2O solution (3 mL). The reaction mixture was allowed to stir for 15 min before being dried *in vacuo*. Reaction was then dissolved in 2 mL of toluene before being filtered through celite and dried *in vacuo* to yield a red solid. X-ray quality crystals were grown by dissolving the resulting solid in 2 mL of a toluene/Et_2O (20:1) solution and placing it at −32 ˚*C* for 15 d. Yield: 0.014 g, 0.012 mmol, 39%. ^{1}H NMR (499.8.9 MHz, C_6D_6, 20 ˚C): Spectra for this species suggest a highly desymmeterized ligand environment, consistent with the solid-state structure. The full spectrum is provided below.

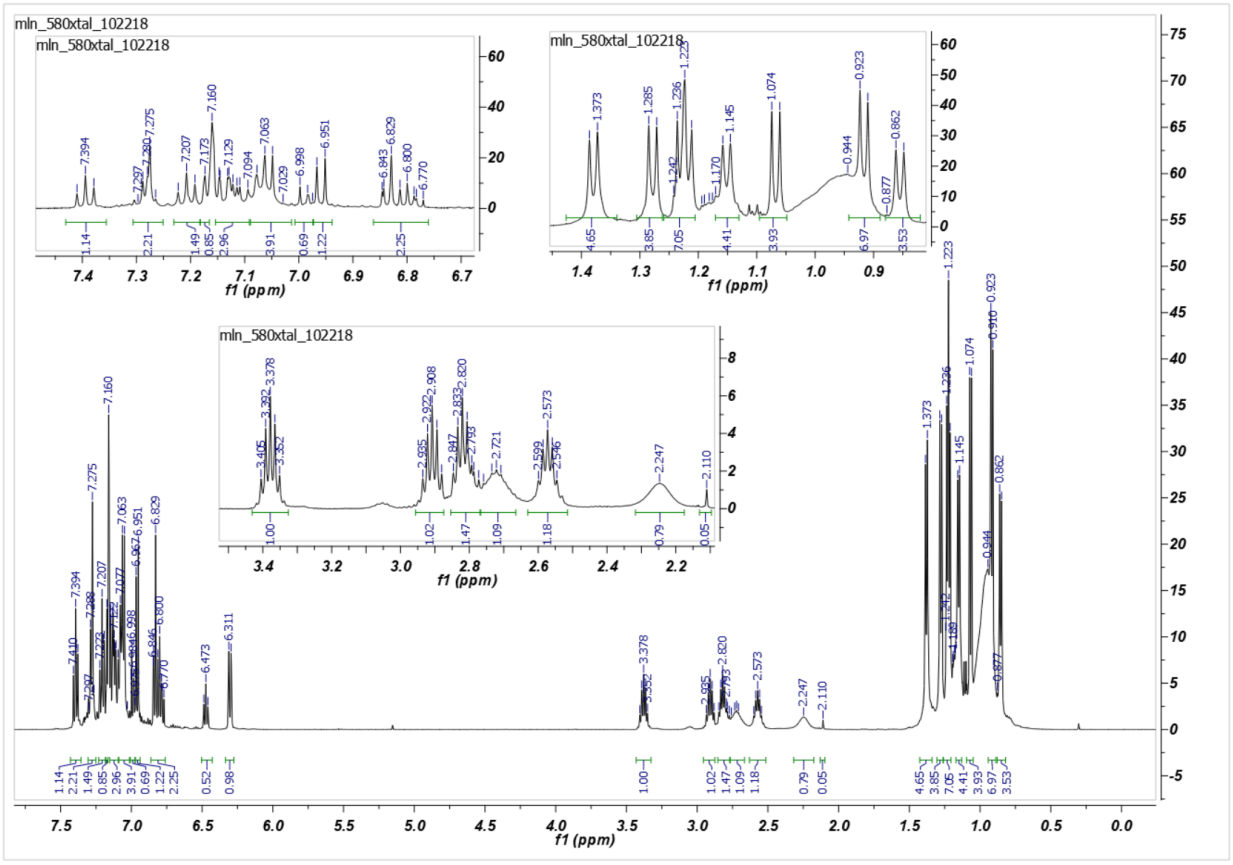

$^{13}C\{^{1}H\}$ NMR (125.8MHz, C_6D_6, 20 ˚C): δ = (CNR), 179.7 (CNR), 165.8, 163.646, 158.2, 149.5, 148.0, 147.2, 146.9, 146.8, 141.1, 137.5, 137.0, 133.7, 132.0, 132.0, 131.3, 130.5, 129.8, 129.7, 125.7, 124.5, 124.2, 124.1, 123.5, 123.2, 122.148, 122.1, 121.7, 112.3, 109.2, 31.7, 31.2, 30.9, 30.6, 30.3, 26.6, 26.5, 25.5, 24.8, 24.7, 23.9, 23.8, 23.7 ppm. FTIR (KBr windows, C_6D_6, 20 ˚C) υ(C≡N) = 2044 (vs), 2013 (s), 1952 (s), 1909 (vs) cm^{-1}; also 3059 (m), 2962 (vs), 2927 (s), 2865 (m), 1581.2 (m), 1546.7 (s), 1485.0 (m), 1457 (m), 1411.7 (m), 1384.7 (m), 1361.5 (w), 1311.4 (w), 1280.5 (w), 1172.5 (w), 1126.3 (m), 1083.8 (m), 1056.8 (m), 983.6 (w), 890.9 (w), 759.9 (m), 582.4 (w) cm^{-1}.

2.5 Details of DFT computational studies

General Computational Details: Density Functional Theory (DFT) calculations were performed with ORCA 4.0.0 program suite and/or the Gaussian 16 software package.[66-67] Geometry optimizations, were performed using the B3LYP functional[68-70] in conjunction with the Def2TZVP/Def2TZVPP basis sets[71-72]. Atomic coordinates obtained by single-crystal X-ray diffraction analysis on K[Rh(κ_3-*C,C,C*-^{Mes2}ArNCNAr^{Dipp2})][CNAr^{Dipp2}] **(18)** were used as the starting point for optimizations on the truncated model, [Rh(κ_3-*C,C,C*-^{Mes2}ArNCNAr^{Dipp2})]$^-$ and the [PhNCNPh]$^{2-}$ fragment. Optimizations on $(NHC)_2C$ used atomic coordinates obtained from single-crystal X-ray diffraction analysis as a starting point.[45] *ChemCraft 1.8* was used for visualization of geometry optimized structures and molecular orbitals (MO).[73]

Input file for model of [Rh(κ_3-*C,C,C*-^{Mes2}ArNCNAr^{Dipp2})]$^-$.

%chk=RhNCN-.chk

%nprocs=8

%mem=21GB

opt pop=full b3lyp/def2tzvp int=ultrafinegrid

Rh-carbodiimide-

-1 1

Rh	9.11770000	10.23780000	12.12050000
N	8.69540000	10.22400000	15.04360000
N	10.10780000	8.63030000	14.37120000
C	9.36250000	9.68750000	14.00470000

C	7.39320000	10.77320000	17.41500000
C	8.14110000	11.48270000	15.10800000
C	8.17030000	12.48440000	14.11770000
C	9.95350000	8.34780000	11.37070000
C	11.35880000	5.97310000	16.49230000
C	7.15910000	8.73670000	19.31100000
H	7.08950000	8.03190000	19.94550000
C	7.15920000	13.12400000	16.63700000
H	6.77300000	13.33040000	17.47900000
C	11.95190000	7.14140000	14.35100000
C	11.88350000	7.11600000	15.85180000
C	5.38840000	9.82720000	16.13250000
H	5.51910000	10.68910000	15.64300000
C	7.32090000	14.13360000	15.68630000
H	7.10380000	15.03520000	15.89270000
C	10.27170000	9.29060000	10.34470000
C	9.33470000	11.80180000	18.71370000
H	8.94400000	12.67800000	18.43240000
C	7.55140000	11.82880000	16.36880000
C	10.84740000	4.79370000	15.70240000
H	10.33540000	4.20170000	16.29300000
H	11.60410000	4.30010000	15.32450000
H	10.26860000	5.11120000	14.97800000
C	10.99420000	7.88590000	13.61060000
C	7.79710000	13.79070000	14.45220000
H	7.88050000	14.46850000	13.79200000

C	6.29850000	8.78270000	18.23460000
H	5.63380000	8.11130000	18.13970000
C	11.99480000	6.96040000	11.59320000
H	11.99720000	6.87790000	10.64750000
C	10.45980000	12.68750000	11.11930000
H	11.38800000	12.75100000	10.93380000
C	7.89370000	9.46210000	9.75060000
C	6.38670000	9.80180000	17.27750000
C	8.25300000	10.75100000	18.54220000
C	8.62760000	12.25260000	12.71850000
C	7.68030000	12.61130000	11.64660000
C	12.36870000	11.58750000	13.21870000
H	12.18410000	10.64300000	13.03230000
H	12.97130000	11.65580000	13.99000000
H	12.79370000	11.99860000	12.43610000
C	8.12060000	9.71760000	19.46530000
H	8.70250000	9.68430000	20.21450000
C	6.19400000	12.64940000	11.95370000
H	6.08160000	13.25260000	12.74390000
C	11.06120000	12.31290000	13.52790000
H	10.66460000	11.88430000	14.33870000
C	10.03260000	12.22240000	12.40830000
C	12.92520000	6.40650000	13.71390000
H	13.57690000	5.94610000	14.23110000
C	11.71140000	7.02230000	18.66120000
C	8.57910000	7.99220000	11.57860000

C	11.28660000	5.95570000	17.88510000
H	10.93080000	5.18580000	18.31620000
C	7.57990000	8.55090000	10.76240000
H	6.67520000	8.30490000	10.90150000
C	5.65600000	8.69220000	15.14020000
H	6.55400000	8.79700000	14.76060000
H	4.99240000	8.72400000	14.42050000
H	5.59690000	7.83190000	15.60430000
C	12.97690000	6.32230000	12.32540000
H	13.66860000	5.83820000	11.89150000
C	12.31850000	8.20170000	16.62380000
C	6.81840000	10.04140000	8.86670000
H	6.90440000	9.67000000	7.96360000
H	6.91540000	11.01450000	8.83090000
H	5.93770000	9.81450000	9.23130000
C	12.24060000	8.13030000	18.00650000
H	12.55810000	8.86210000	18.52280000
C	8.17560000	6.91600000	12.54300000
H	8.50390000	7.13980000	13.43910000
H	8.56140000	6.06040000	12.25740000
H	7.19770000	6.84460000	12.56310000
C	11.00490000	7.71920000	12.20340000
C	10.52630000	11.51610000	17.77810000
H	10.97670000	10.69380000	18.06440000
H	11.15790000	12.26370000	17.81470000
H	10.20240000	11.40810000	16.85910000

C	9.22100000	9.82080000	9.57310000
H	9.43130000	10.45420000	8.89770000
C	11.65510000	6.95250000	20.16290000
H	10.83610000	6.48740000	20.43840000
H	11.65470000	7.86050000	20.53090000
H	12.43680000	6.46520000	20.49650000
C	9.57190000	13.03520000	10.16470000
H	9.88220000	13.33520000	9.31740000
C	5.64090000	11.27640000	12.36940000
H	5.63270000	10.67800000	11.59450000
H	4.72610000	11.38270000	12.70940000
H	6.20650000	10.89540000	13.07320000
C	11.33740000	13.78120000	13.86950000
H	11.98720000	13.83040000	14.60130000
H	10.50400000	14.21610000	14.14500000
H	11.69960000	14.23840000	13.07960000
C	8.18300000	12.95580000	10.41760000
H	7.57730000	13.14630000	9.71120000
C	9.84480000	11.97320000	20.14240000
H	9.08320000	12.06850000	20.75050000
H	10.40500000	12.77480000	20.19520000
H	10.37160000	11.18750000	20.39750000
C	12.81820000	9.45890000	15.95680000
H	13.37470000	9.22240000	15.18460000
H	13.35030000	9.97950000	16.59440000
H	12.05440000	9.99380000	15.65590000

C 11.69330000 9.65260000 9.99410000

H 11.72380000 10.57640000 9.66820000

H 12.01950000 9.04940000 9.29580000

H 12.25800000 9.56680000 10.78960000

C 5.32320000 13.23040000 10.83690000

H 5.62900000 14.13680000 10.62170000

H 4.38900000 13.26530000 11.13390000

H 5.39100000 12.66370000 10.04060000

C 3.94110000 9.80810000 16.63740000

H 3.77230000 8.96840000 17.11090000

H 3.33000000 9.88270000 15.87550000

H 3.79860000 10.56210000 17.24650000

1 4 1.0 8 1.0 40 1.0 83 1.0

2 4 2.0 6 1.0

3 4 1.0 28 2.0

4

5 23 2.0 38 1.0 39 1.0

6 7 2.0 23 1.0

7 29 1.0 40 1.0

8 20 1.0 56 1.0 78 1.0

9 15 1.0 24 1.0 57 2.0

10 11 1.0 31 1.0 46 2.0

11

12 13 1.0 18 2.0 23 1.0

13

14 15 2.0 28 1.0 53 1.0

15 67 1.0

16 17 1.0 38 1.0 61 1.0 117 1.0

17

18 19 1.0 29 1.0

19

20 83 1.0 109 1.0

21 22 1.0 39 1.0 79 1.0 101 1.0

22

23

24 25 1.0 26 1.0 27 1.0

25

26

27

28 78 1.0

29 30 1.0

30

31 32 1.0 38 2.0

32

33 34 1.0 65 1.0 78 2.0

34

35 36 1.0 52 2.0 89 1.0

36

37 59 2.0 68 1.0 83 1.0

38

39 46 1.0

40 41 1.0 52 1.0

41 48 1.0 99 2.0

42 43 1.0 44 1.0 45 1.0 50 1.0

43

44

45

46 47 1.0

47

48 49 1.0 91 1.0 113 1.0

49

50 51 1.0 52 1.0 95 1.0

51

52

53 54 1.0 65 2.0

54

55 57 1.0 72 2.0 85 1.0

56 59 1.0 74 1.0

57 58 1.0

58

59 60 1.0

60

61 62 1.0 63 1.0 64 1.0

62

63

64

65 66 1.0

66

67 72 1.0 105 1.0

68 69 1.0 70 1.0 71 1.0

69

70

71

72 73 1.0

73

74 75 1.0 76 1.0 77 1.0

75

76

77

78

79 80 1.0 81 1.0 82 1.0

80

81

82

83 84 1.0

84

85 86 1.0 87 1.0 88 1.0

86

87

88

89 90 1.0 99 1.0

90

91 92 1.0 93 1.0 94 1.0

92

93

94

95 96 1.0 97 1.0 98 1.0

96

97

98

99 100 1.0

100

101 102 1.0 103 1.0 104 1.0

102

103

104

105 106 1.0 107 1.0 108 1.0

106

107

108

109 110 1.0 111 1.0 112 1.0

110

111

112

113 114 1.0 115 1.0 116 1.0

114

115

116

117 118 1.0 119 1.0 120 1.0

118

119

120

Optimized Cartesian Coordinates for Model of [Rh(κ$_3$-*C,C,C*-^{Mes2}ArNCNAr^{Dipp2})]$^-$.

Rh	1.885712173	-0.724532889	0.225647994
N	-0.388635114	0.963451067	-0.070302027
N	-0.941331992	-1.223378132	-0.321039045
C	-0.029164995	-0.307211000	-0.070999027
C	-1.872847387	3.267026123	-0.515123059
C	0.137804842	2.076559186	0.499175014
C	1.320969921	2.178118280	1.290845072
C	1.692500283	-2.417345027	-1.235616113
C	-4.100023166	-1.947487415	-1.031847094
C	-4.214793567	3.403057961	-2.042435170
H	-5.121854638	3.454966900	-2.633844213
C	-0.272795361	4.452812324	0.960013045
H	-0.891865472	5.331027335	0.813361037
C	-2.000247916	-3.311405361	-0.736968073
C	-3.308845048	-2.790197416	-0.230952039
C	-0.476384332	3.853969265	-2.578921208
H	0.312262737	3.684417313	-1.846371157
C	0.838088712	4.516530413	1.797017108
H	1.093785667	5.432816483	2.314458142
C	2.682436385	-2.817311982	-0.277411042
C	-3.239431440	2.611731976	1.548471089
H	-2.237141372	2.641974053	1.974177120
C	-0.630563302	3.273555212	0.324559001
C	-3.592425167	-1.438646342	-2.353551190
H	-4.366209265	-0.877305361	-2.878884231
H	-3.257556083	-2.255567376	-2.996780239
H	-2.735905153	-0.780829231	-2.190045179

C	-0.814474892	-2.510736217	-0.733719073
C	1.613046854	3.377582384	1.945577117
H	2.490812916	3.411673454	2.582257163
C	-2.984134496	3.653851067	-2.628168211
H	-2.938893513	3.900559089	-3.682672288
C	0.345823332	-4.408258266	-1.749014148
H	1.267406431	-4.827418232	-2.139981174
C	3.052908260	-0.799485809	2.920783189
H	2.828490301	-1.571224880	3.646146241
C	4.449858440	-1.886592787	-1.710657143
C	-1.805275405	3.586359150	-1.885074160
C	-3.121438460	3.000711010	0.081282984
C	2.290158074	1.051568265	1.469742083
C	3.683170154	1.281521387	1.108887057
C	0.094919100	-1.490584078	3.352291220
H	-0.038444871	-2.012369123	2.406143149
H	-0.877541972	-1.434312142	3.847231257
H	0.750105189	-2.090369071	3.989772266
C	-4.276037547	3.074720931	-0.697079073
H	-5.238365604	2.863640847	-0.245769040
C	4.058856102	2.407665496	0.144042988
H	3.502383996	3.292668518	0.453171011
C	0.643864035	-0.078996934	3.122953204
H	-0.094147056	0.455204050	2.528156161
C	1.971244129	-0.049240835	2.358098146
C	-1.975720820	-4.605202454	-1.242261113
H	-2.897139846	-5.177637562	-1.240858111
C	-5.871542312	-1.985914547	0.640361024
C	2.119719263	-1.696392942	-2.399645196
C	-5.364325284	-1.568399481	-0.586445065
H	-5.964783396	-0.919406480	-1.216134108
C	3.468295340	-1.466845827	-2.623372208
H	3.768634322	-0.943543768	-3.524922275
C	-0.229889243	2.881706217	-3.741356293

H	-0.293826172	1.848865138	-3.398669267
H	0.764972815	3.039951297	-4.166678321
H	-0.959276303	3.017925172	-4.544169351
C	-0.814435696	-5.168276406	-1.762037147
H	-0.816267623	-6.173127464	-2.165980176
C	-3.802762053	-3.214648487	1.013391053
C	5.903489536	-1.597517660	-1.971515163
H	6.550079628	-2.202081654	-1.333616120
H	6.137890451	-0.545959566	-1.775130151
H	6.168837583	-1.796628654	-3.012899237
C	-5.071227177	-2.805920547	1.427112082
H	-5.438498154	-3.137279598	2.393662149
C	1.108057159	-1.295598989	-3.441228268
H	0.232542062	-0.830267017	-2.989557240
H	0.754346195	-2.170300078	-3.994503312
H	1.544836139	-0.595234905	-4.154118321
C	0.371614239	-3.112114172	-1.237882113
C	-3.757841371	1.176138834	1.709446099
H	-4.777517436	1.074065755	1.330201074
H	-3.766665354	0.891107811	2.765393174
H	-3.126663276	0.471452830	1.167740060
C	4.044506461	-2.525066861	-0.554166062
H	4.791383536	-2.851938833	0.161164989
C	-7.225389439	-1.526546614	1.118405056
H	-7.159182486	-0.558343541	1.625172093
H	-7.659577414	-2.235128699	1.826748111
H	-7.923361477	-1.408870654	0.286592998
C	4.351807336	-0.538717696	2.589954162
H	5.154399436	-1.124127679	3.024123198
C	3.623714089	2.107828439	-1.299653116
H	4.152999195	1.238566419	-1.693981143
H	3.839364042	2.964877519	-1.945070165
H	2.557381027	1.895406345	-1.356185122
C	0.780950994	0.666820130	4.462390299

H	-0.182422080	0.702555062	4.978432337
H	1.119450943	1.692718230	4.312090287
H	1.496654080	0.166482146	5.120601346
C	4.660640285	0.481141400	1.662861097
H	5.697504329	0.636042488	1.399157077
C	-4.096290572	3.608636983	2.343451144
H	-3.699199621	4.623147087	2.264908143
H	-4.117120555	3.333889965	3.401662224
H	-5.129329648	3.626182908	1.986166123
C	-2.983421932	-4.099203491	1.920742114
H	-2.860433847	-5.103863554	1.509078087
H	-3.459223956	-4.191528533	2.898579187
H	-1.980218890	-3.695425386	2.065103128
C	2.392054439	-3.837987075	0.800541036
H	3.061077476	-3.688218018	1.648837095
H	2.552607526	-4.853658136	0.421044008
H	1.366480360	-3.782014146	1.154794062
C	5.541520180	2.794683632	0.170396990
H	5.882199201	3.036878672	1.179127060
H	5.699227118	3.674217708	-0.458345055
H	6.182445270	2.000019618	-0.220374038
C	-0.357607430	5.313272380	-3.044409240
H	-1.122151504	5.558698332	-3.786444296
H	0.620211627	5.494256449	-3.499716276
H	-0.473358489	6.002899398	-2.206026183

Visualized Metal Ligand Bonding Molecular Orbitals

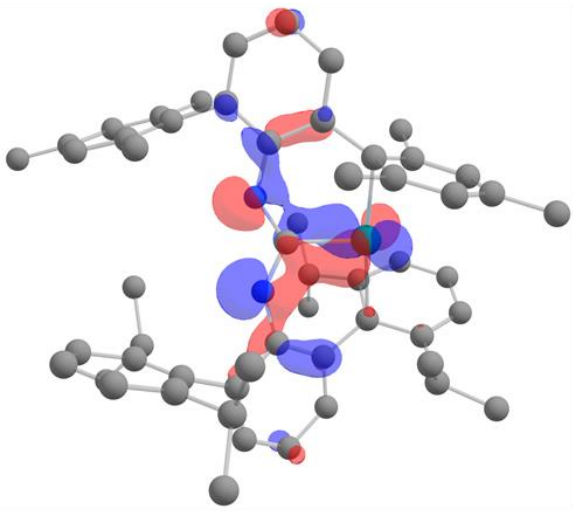

HOMO-6
-3.197 eV
σ(Rh(yz)-C(p_y))

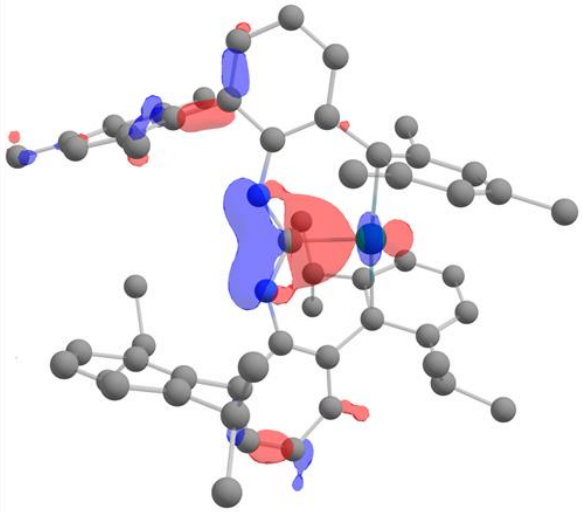

HOMO-54
-8.162 eV
π(Rh(z^2)-C(p_z))

Input file for model of [PhNCNPh]$^-$.

%chk=ArNCNAr2-_opt.chk

%nprocs=8

%mem=21GB

opt pop=full b3lyp/def2tzvpp int=superfinegrid

ArNCNr2- opt

-2 1

N	8.69540000	10.22400000	15.04360000
N	10.10780000	8.63030000	14.37120000
C	9.36250000	9.68750000	14.00470000
C	8.14110000	11.48270000	15.10800000

C	8.17030000	12.48440000	14.11770000
C	7.15920000	13.12400000	16.63700000
H	6.77300000	13.33040000	17.47900000
C	11.95190000	7.14140000	14.35100000
C	7.32090000	14.13360000	15.68630000
H	7.10380000	15.03520000	15.89270000
C	7.55140000	11.82880000	16.36880000
C	10.99420000	7.88590000	13.61060000
C	7.79710000	13.79070000	14.45220000
H	7.88050000	14.46850000	13.79200000
C	11.99480000	6.96040000	11.59320000
H	11.99720000	6.87790000	10.64750000
C	12.92520000	6.40650000	13.71390000
H	13.57690000	5.94610000	14.23110000
C	12.97690000	6.32230000	12.32540000
H	13.66860000	5.83820000	11.89150000
C	11.00490000	7.71920000	12.20340000
H	10.23850000	8.18520000	11.60190000
H	11.91520000	7.15260000	15.43030000
H	8.47780000	12.24620000	13.11020000
H	7.41240000	11.06450000	17.11900000

1 3 2.0 4 1.0

2 3 2.0 12 1.0

3

4 5 2.0 11 1.0

5 13 1.0 24 1.0

6 7 1.0 9 2.0 11 1.0

7

8 12 2.0 17 1.0 23 1.0

9 10 1.0 13 1.0

10

11 25 1.0

12 21 1.0

13 14 1.0

14

15 16 1.0 19 1.0 21 2.0

16

17 18 1.0 19 2.0

18

19 20 1.0

20

21 22 1.0

22

23

24

25

Optimized Cartesian Coordinates for Model of [PhNCNPh]$^{-}$.

N	1.106764051	-0.878801959	0.244791018
N	-1.106748107	-0.878434069	-0.244377018
C	0.000308938	-0.139079961	-0.001152000
C	2.332705115	-0.348749864	0.105934007
C	2.665865083	0.786292234	-0.712776052

C	4.746515296	-0.495057758	0.616544042
H	5.552573370	-1.004901754	1.141430082
C	-3.450045271	-0.955137184	-0.764863054
C	5.040891265	0.614227336	-0.192054014
H	6.060660312	0.959943410	-0.327469023
C	3.449956226	-0.954981855	0.764867054
C	-2.332832218	-0.349181088	-0.105572007
C	3.965956157	1.238568329	-0.842659063
H	4.161475128	2.103306402	-1.476323105
C	-3.965979415	1.238354949	0.842997059
H	-4.161565469	2.103213002	1.476492109
C	-4.746529388	-0.494958215	-0.616708045
H	-5.552568395	-1.004364290	-1.142109080
C	-5.040760463	0.614975852	0.191154014
H	-6.060814567	0.958916828	0.328944024
C	-2.665963299	0.785825976	0.713423051
H	-1.842315262	1.281390051	1.210990087
H	-3.235434215	-1.813027238	-1.394479102
H	1.842169003	1.282306231	-1.209831089
H	3.235180252	-1.812722924	1.394647100

Visualized Frontier Molecular Orbitals of [PhNCNPh]$^{-}$.

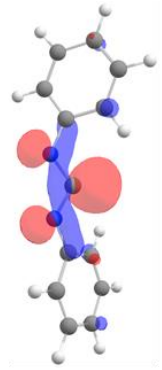

HOMO
4.238 eV
a, symm

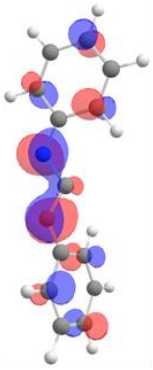

HOMO-1
2.751 eV
a, symm

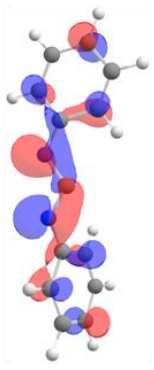

HOMO-2
1.947 eV
b-symm.

HOMO-3
2.751 eV
b symm

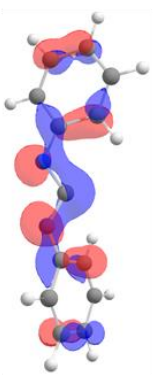

HOMO-4
0.1055 eV
a symm

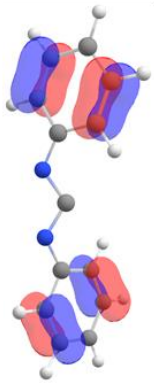

HOMO-5
-0.0238 eV

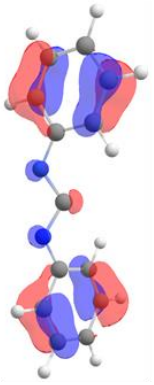

HOMO-6
-0.0505 eV

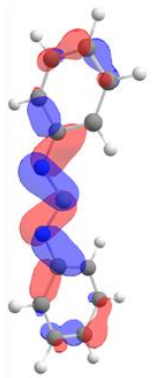

HOMO-7
-1.0723 eV
b symm

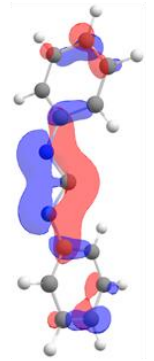

HOMO-8
-6.280 eV
a-symm

Input file for model of $(NHC)_2C$.

%chk=Carbodicarbene_bp86.chk

%nprocs=8

%mem=21GB

opt freq=noraman pop=full bp86/def2tzvpp int=superfinegrid

Bertrand bent allene - carbodicarbene

0 1

N	8.08990000	2.00930000	11.75370000
N	8.35510000	0.31840000	10.35110000
C	9.91410000	0.38390000	12.22920000
C	8.91510000	0.90010000	11.49460000
C	7.20140000	0.97530000	9.97350000
C	6.28860000	0.72920000	8.96350000
H	6.41650000	0.02290000	8.34190000
C	5.16800000	1.56670000	8.89650000
H	4.51680000	1.41750000	8.22130000
C	4.98820000	2.60570000	9.79120000
H	4.21280000	3.14900000	9.72140000
C	5.92250000	2.87410000	10.79460000
H	5.80610000	3.59790000	11.39920000
C	7.02640000	2.04140000	10.87080000
C	8.22720000	2.87770000	12.90640000
H	8.56160000	3.75310000	12.61730000
H	8.85920000	2.48000000	13.54180000

H	7.35510000	2.98720000	13.33800000
C	8.89260000	-0.85490000	9.70430000
H	8.20000000	-1.54620000	9.65450000
H	9.65350000	-1.19310000	10.22030000
H	9.18920000	-0.62270000	8.80010000
N	11.73820000	2.00930000	12.70470000
N	11.47300000	0.31840000	14.10730000
C	10.91300000	0.90010000	12.96380000
C	12.62670000	0.97530000	14.48490000
C	13.53960000	0.72920000	15.49490000
H	13.41160000	0.02290000	16.11640000
C	14.66010000	1.56670000	15.56190000
H	15.31130000	1.41750000	16.23710000
C	14.83990000	2.60570000	14.66720000
H	15.61540000	3.14900000	14.73700000
C	13.90570000	2.87410000	13.66380000
H	14.02210000	3.59790000	13.05920000
C	12.80180000	2.04140000	13.58760000
C	11.60100000	2.87770000	11.55200000
H	11.26660000	3.75310000	11.84110000
H	10.96900000	2.48000000	10.91660000
H	12.47310000	2.98720000	11.12040000
C	10.93560000	-0.85490000	14.75410000
H	11.62810000	-1.54620000	14.80380000
H	10.17470000	-1.19310000	14.23800000
H	10.63890000	-0.62270000	15.65830000

1 4 1.0 14 1.0 15 1.0

2 4 1.0 5 1.0 19 1.0

3 4 1.0 25 1.0

4

5 6 1.0 14 1.0

6 7 1.0 8 1.0

7

8 9 1.0 10 1.0

9

10 11 1.0 12 1.0

11

12 13 1.0 14 1.0

13

14

15 16 1.0 17 1.0 18 1.0

16

17

18

19 20 1.0 21 1.0 22 1.0

20

21

22

23 25 1.0 35 1.0 36 1.0

24 25 1.0 26 1.0 40 1.0

25

26 27 1.0 35 1.0

27 28 1.0 29 1.0

28

29 30 1.0 31 1.0

30

31 32 1.0 33 1.0

32

33 34 1.0 35 1.0

34

35

36 37 1.0 38 1.0 39 1.0

37

38

39

40 41 1.0 42 1.0 43 1.0

41

42

43

Optimized Cartesian Coordinates for Model of $(NHC)_2C$.

N	-1.866679572	-0.586603516	-0.723156864
N	-2.338938754	1.071287733	0.677174314
C	0.000000490	0.872812111	-0.000005231
C	-1.269600669	0.458704803	0.006230767
C	-3.530634526	0.443824448	0.375631408
C	-4.829154975	0.683423929	0.789947018
H	-5.061594981	1.483273293	1.479085950
C	-5.838203352	-0.147536746	0.286740338
H	-6.861363329	0.019049689	0.595004909

C	-5.545641783	-1.179937538	-0.595132123
H	-6.342891918	-1.809349266	-0.966341285
C	-4.230490086	-1.426084653	-1.010591007
H	-4.007278482	-2.236142343	-1.690928462
C	-3.234031070	-0.603865183	-0.515690629
C	-1.159997091	-1.447460593	-1.635808815
H	-1.015580233	-2.450134579	-1.224324576
H	-0.185953212	-1.010103132	-1.841091640
H	-1.711371505	-1.534359430	-2.573753443
C	-2.188948946	2.215968514	1.538316056
H	-2.917990541	2.985432102	1.277366393
H	-1.183892878	2.608129787	1.396347040
H	-2.320957497	1.950791264	2.590777483
N	1.866676598	-0.586606850	0.723149355
N	2.338941422	1.071287008	-0.677176653
C	1.269600045	0.458700824	-0.006242011
C	3.530635912	0.443822307	-0.375631133
C	4.829157965	0.683423601	-0.789939954
H	5.061600845	1.483274955	-1.479075478
C	5.838204463	-0.147538528	-0.286731314
H	6.861365657	0.019049216	-0.594991172
C	5.545639348	-1.179940919	0.595137701
H	6.342887949	-1.809353219	0.966349582
C	4.230485895	-1.426088685	1.010591288
H	4.007272084	-2.236147354	1.690926864
C	3.234028641	-0.603869162	0.515687718
C	1.159991895	-1.447457651	1.635805539
H	1.015572105	-2.450132801	1.224325296
H	0.185949225	-1.010096602	1.841086597
H	1.711366092	-1.534354355	2.573750512
C	2.188956873	2.215973911	-1.538311209
H	2.917990912	2.985439891	-1.277346978
H	1.183897069	2.608129088	-1.396352358
H	2.320980400	1.950804441	-2.590772704

Visualized Frontier Molecular Orbitals of $(NHC)_2C$.

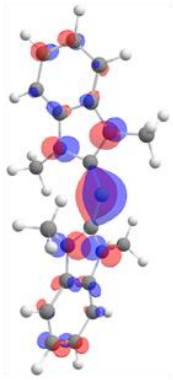

HOMO
-4.507 eV
b symm

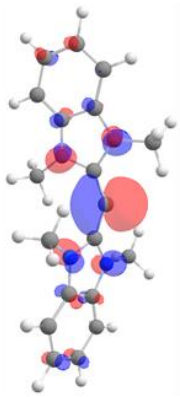

HOMO-1
-4.755 eV
a symm

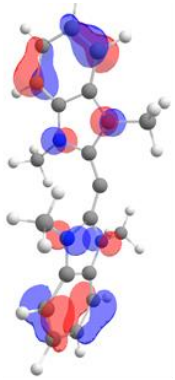

HOMO-2
-6.272 eV

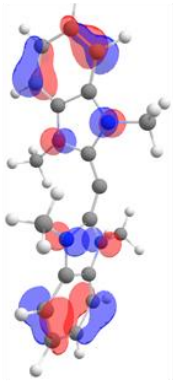

HOMO-3
-6.280 eV

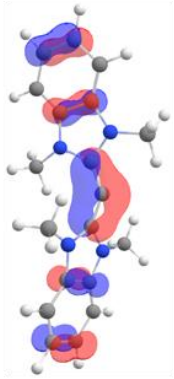

HOMO-4
-6.793 eV

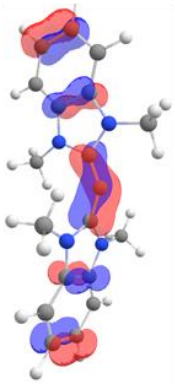

HOMO-5
-7.139 eV

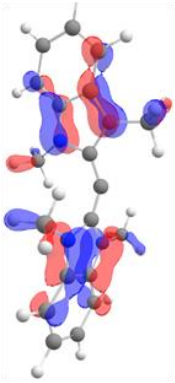

HOMO-6
-8.186 eV

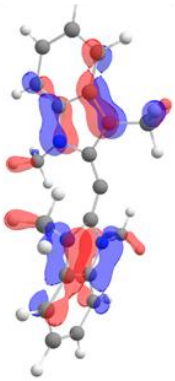

HOMO-7
-8.190 eV

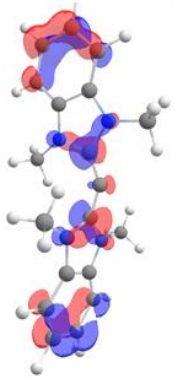

HOMO-8
-9.301 eV

2.6 Details of crystallographic structure determinations

General Information. Single crystal X-ray structure determinations were carried out at low temperature on a Bruker P4, Platform or Kappa Diffractometer equipped with a Mo or Cu radiation source. Data were acquired with Bruker APEX II, Photon II or Dextris Eiger 1M detectors. All structures were solved via direct methods with SHELXS[74-75] and refined by full-matrix least-squares procedures using SHELXL[74-75] within the Olex2[76] software package. All H-atoms were refined using standard HFIX instruction. Crystallographic data collection and refinement information is listed in Table S3.1. The PLATON crystallographic tool[77] was used to account for overly disordered solvent using SQUEEZE routine,[78] and to identify twin laws in twinned crystalline habits using the TwinRotMat Routine.[79]

Information on Crystallographic Disorder and Twinning: The following molecules contain positionally disordered and/or pseudo-merohedrally twinned components. They are listed along with their respective disordered components.

$TlIr(CNAr^{Dipp2})_3$ (6): This structure is refined as an inversion twin (BASF 0.454(9)) in a Pn space group. Attempts to solve or transform the solution into a centrosymmetric space group failed to give a suitable solution. AFIX 66 restraints were used to secure unstable aryl groups and EADP commands were used to constrain oblate/prolate ellipsoids. Similar to (**8**) a minor amount of inverted whole molecule disorder was observed in the difference map. However, in this case modeling the disorder did not improve the solution.

$[Tl_2Rh(CNAr^{Dipp2})_3]OTf$ (7): The triflate anion lies along a special position splitting the moiety. To correctly model its structure, PART -1 was used. SQUEEZE was used to remove one

heavily disordered *n*-pentane or diethyl ether molecule of co-crystallization from the structure (void removed was 465 $Å^3$ in volume and contained 235 electrons/cell). A second molecule of diethyl ether was modeled and refined isotropically.

$TlRh(CNAr^{Dipp2})_3$ (8): Pseudo-meroherdral twinning was observed and a twin law was determined using PLATONs TwinRotMat algorithm (-1 0 0 0 -1 0 0 0 1) BASF 0.2899(6)). Two-site positional disorder was observed in a methyl group (C61A/B) and the Rh-Tl moiety. Both were modeled using PART/FVAR commands and refined anisotropically. In the case of the Rh-Tl moiety, the disordered components were found to have occupancies of 95% and 5% which may indicate a minor amount of inverted whole molecule disorder only visible in the heavy atoms.

$HRh(CNAr^{Dipp2})_3$ (10): Two-site positional disorder was observed in two flanking isopropyl groups (C34A/B and C12), which was modeled using PART/FVAR commands then refined anisotropically.

$HIr(CNAr^{Dipp2})_3$ (11): Pseudo-meroherdral twinning was observed and a twin law was determined using PLATONs TwinRotMat algorithm (-1 0 0 0 -1 0 0 0 1 2) BASF 0.49. The hydride atom's electron density was observable in the difference map but did not refine well without restraints so it's position was fixed.

$HIr(CNAr^{Dipp2})_3$ (11): Pseudo-meroherdral twinning was observed and a twin law was determined using PLATONs TwinRotMat algorithm (-1 0 0 0 -1 0 0 0 1 2) BASF 0.49. The hydride atom's electron density was observable in the difference map but did not refine well without restraints so it's position was fixed.

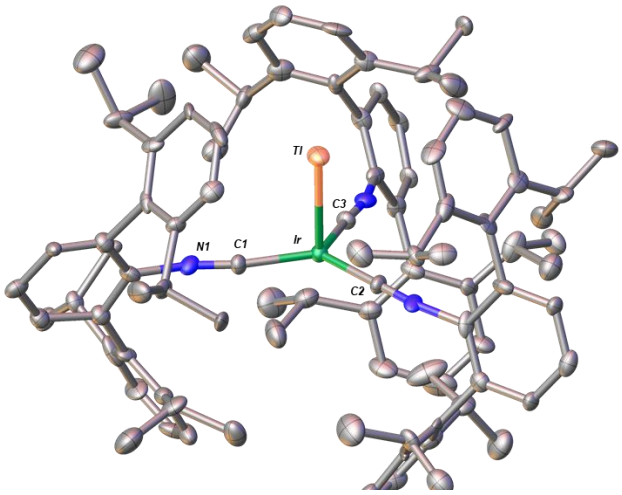

Figure 2.9 Molecular structure of TlIr(CNAr^{Dipp2})$_3$ (6). Hydrogen atoms and the second molecule in the asymmetric unit omitted for clarity. Selected bond distances (Å) and angles (°): Ir-C1 = 1.94(3); C1-N1 = 1.16(4); Ir-Tl= 2.6365(18); C1-Ir-C2 = 127.1(13); C2-Ir-C3 = 114. 2(12); C3-Ir-C1 = 117.5(12).

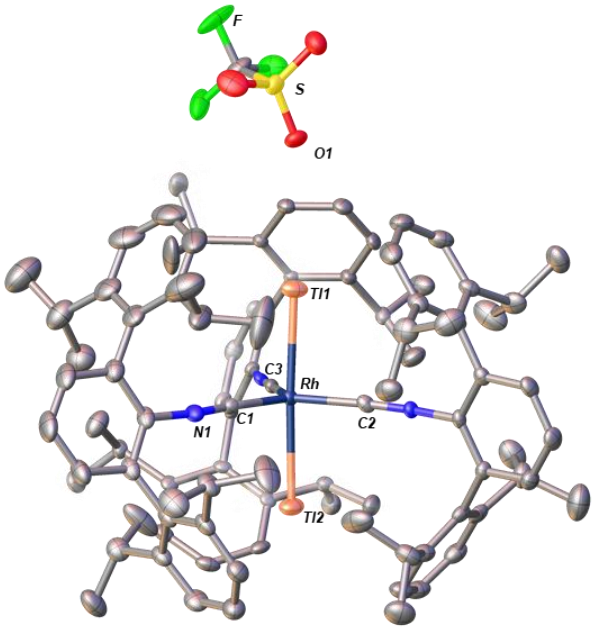

Figure 2.10 Molecular structure of [Tl$_2$Rh(CNAr^{Dipp2})$_3$]OTf (7). Hydrogen atoms, disorder and one co-crystalized molecule of Et$_2$O were omitted for clarity. Selected bond distances (Å) and angles (°): Rh-C1 = 1.976(5); C1-N1 = 1.176(6); Rh-Tl1= 2.6994(4); Rh-Tl2= 2.7109(4); O1-Tl1= 3.688(4); Tl1-Rh-Tl2 = 176.848(17); C1-Rh-C2 = 119.18(18); C2-Rh-C3 = 122.05(18); C3-Rh-C1 = 118.73(18).

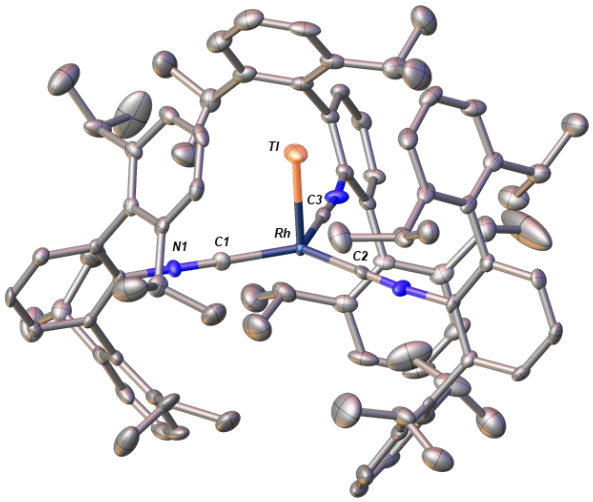

Figure 2.12 Molecular structure of $TlRh(CNAr^{Dipp2})_3$ (8). Hydrogen atoms and disorder omitted for clarity. Selected bond distances (Å) and angles (°): Rh-C1 = 1.936(4); C1-N1 = 1.175(5); (95%)Rh-Tl= 2.5896(4); C1-Rh-C2 = 128.13(17); C2-Rh-C3 = 113.42(17); C3-Rh-C1 = 117.82(17).

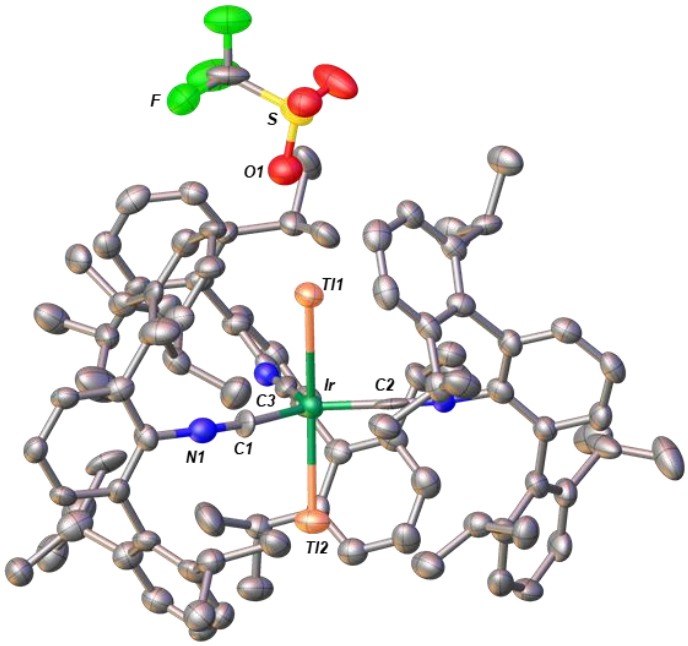

Figure 2.11 Molecular structure of $[Tl_2Ir(CNAr^{Dipp2})_3]OTf$ (9). Hydrogen atoms, disorder and one co-crystalized molecule of THF were omitted for clarity. Selected bond distances (Å) and angles (°): Ir-C1 = 1.950(11); C1-N1 = 1.172(14); Ir-Tl1= 2.8298(8); Ir-Tl2= 2.7120(8); O1-Tl1= 3.002(8); Tl1-Ir-Tl2 = 168.84(3); C1-Ir-C2 = 128.36(6); C2-Ir-C3 = 120.15(2); C3-Ir-C1 = 111.5(6).

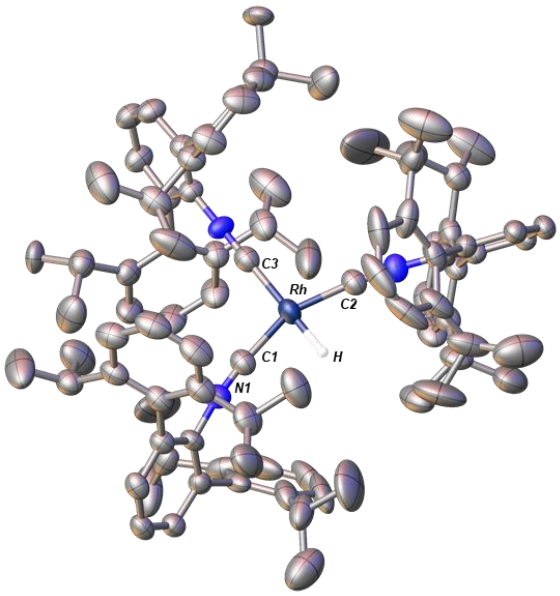

Figure 2.13 Molecular structure of $HRh(CNAr^{Dipp2})_3$ (10). Hydrogen atoms and disorder, excluding the rhodium hydride (H) were omitted for clarity. Selected bond distances (Å) and angles (°): Rh-C1 = 1.896(6); Rh-C2 = 1.896(6); Rh-C3 = 1.960(10); C1-Rh-H = 77.75(18); C1-Rh-C3 = 102.68(18).

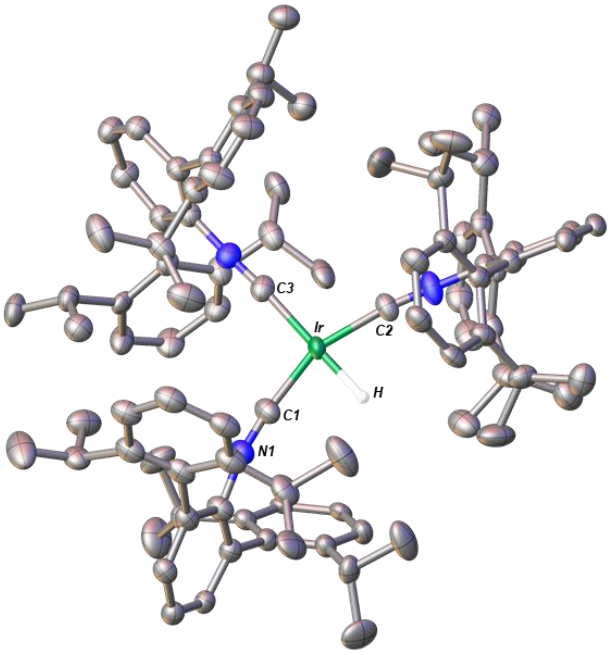

Figure 2.14 Molecular structure of $HIr(CNAr^{Dipp2})_3$ (11). Hydrogen atoms and disorder, excluding the iridium hydride (H) were omitted for clarity. Selected bond distances (Å) and angles (°): Ir-C1 = 1.908(11); Ir-C2 = 1.907(11); Ir-C3 = 1.970(7); C1-Ir-H = 78.4(4); C1-Ir-C3 = 101.76(6).

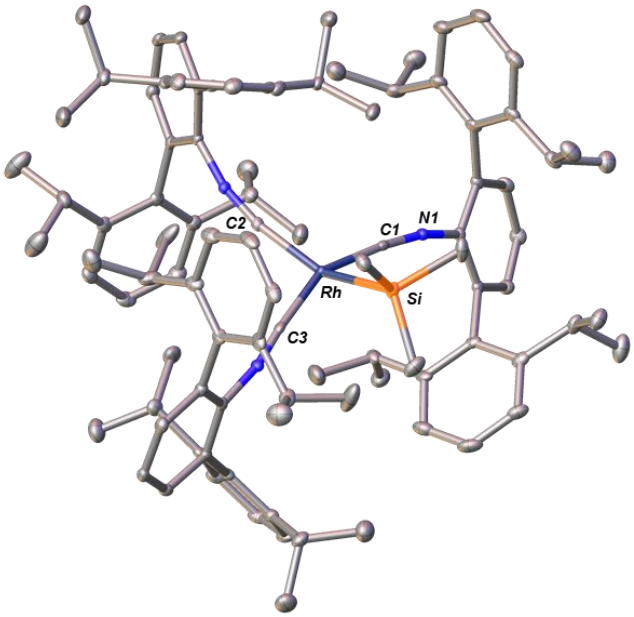

Figure 2.16 Molecular Structure of K[trans-Rh(SiMe$_3$)$_2$(CNAr^{Dipp2})$_2$] (12). Hydrogen atoms omitted for clarity. Selected bond distances (Å) and angles (°): Rh-C1 = 1.8997(19); C1-N1 = 1.186(2); Rh-Si = 2.3891(7); Rh-K = 3.0525(5).

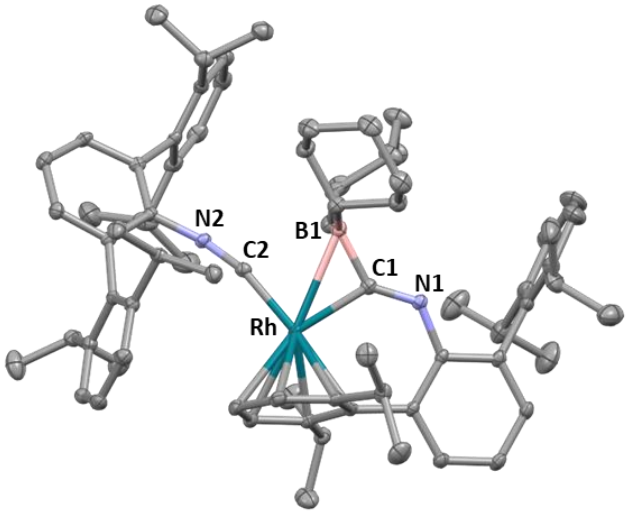

Figure 2.15 Molecular Structure of Rh(CNAr^{Dipp2})(η$_6$-κ-C,Ar-^{Cy2}BIM) (13) Hydrogen atoms omitted for clarity. Selected bond distances (Å) and angles (°): Rh-C1 = 2.0219(19); C1-N1 = 1.268(2); Rh-B= 2.602(2); Rh-C2 = 1.9143(2), Rh-C1-N1 = 131.497(18).

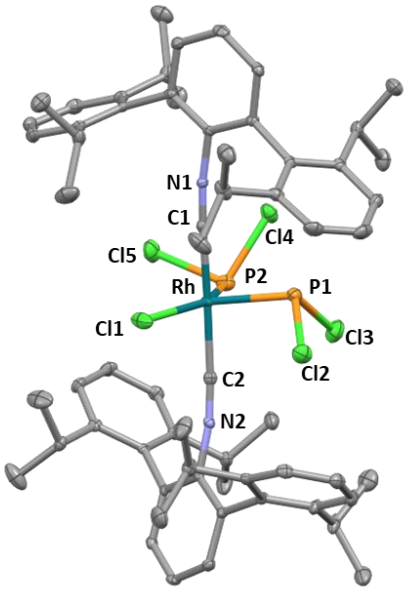

Figure 2.17 Molecular Structure of $RhCl(PCl_2)_2(CNAr^{Dipp2})_2$ (14) Hydrogen atoms omitted for clarity. Selected bond distances (Å) and angles (°): Rh-C1 = 1.988(3); C1-N1 = 1.151(3); Rh-P1= 2.2700(9); Rh-P2= 2.2827(9); Rh-Cl1= 2.3708(9); P1-Rh-P2 = 88.03(3); P1-Rh-Cl1 = 125.41(4); P2-Rh-Cl1 = 146.56(4).

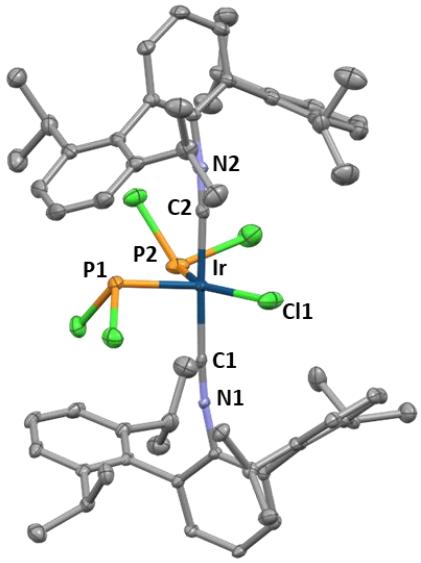

Figure 2.18 Molecular Structure of $IrCl(PCl_2)_2(CNAr^{Dipp2})_2$ (15) Hydrogen atoms omitted for clarity. Selected bond distances (Å) and angles (°): Ir-C1 = 1.978(4); C1-N1 = 1.146(5); Ir-P1= 2.266(1); Ir-P2= 2.2840(11); Ir-Cl1= 2.3522(11); P1-Ir-P2 = 86.56(4); P1-Ir-Cl1 = 128.17(5); P2-Ir-Cl1 = 145.24(5).

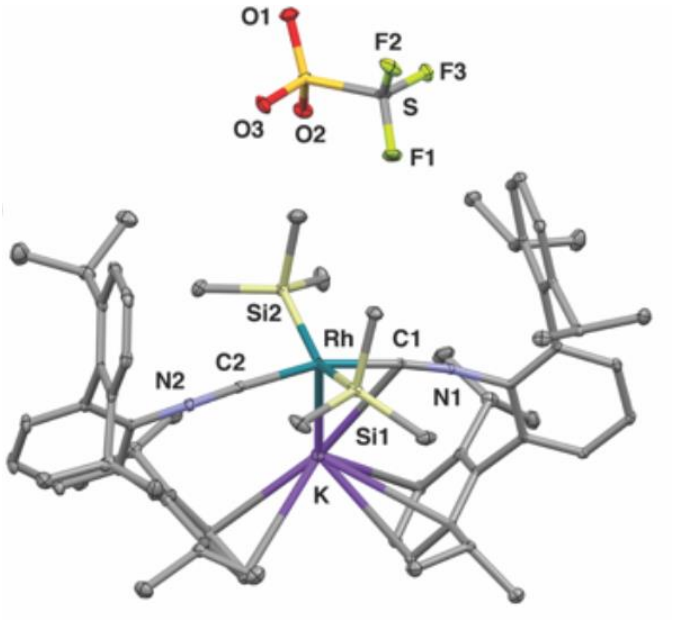

Figure 2.20 Molecular Structure of K[trans-Rh(SiMe$_3$)$_2$(CNAr^{Dipp2})$_2$] (16). Hydrogen atoms omitted for clarity. Selected bond distances (Å) and angles (°): Rh-C1 = 1.8997(19); C1-N1 = 1.186(2); Rh-Si = 2.3891(7); Rh-K = 3.0525(5).

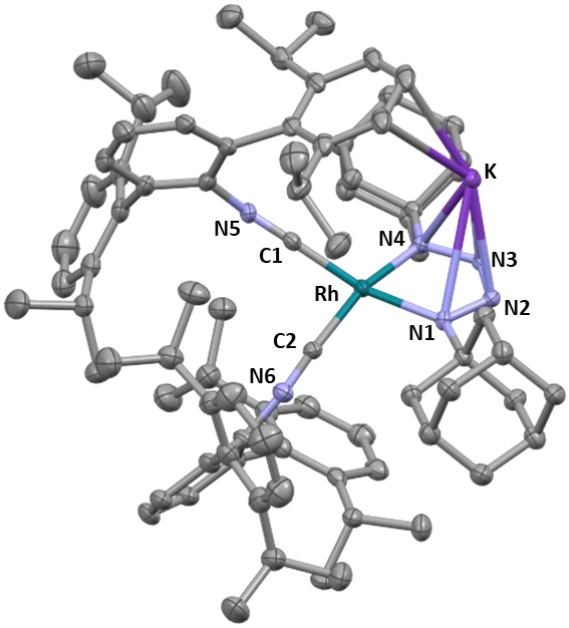

Figure 2.19 Molecular Structure of K[(κ$_2$-N,N-Ad$_2$N$_4$)Rh(CNAr^{Dipp2})$_2$] (17). Hydrogen atoms omitted for clarity. Selected bond distances (Å) and angles (°): Rh-C1 = 1.869(7); C1-N1 = 1.202 (8); Rh-N1 = 2.045(5); N1-N2 = 1.360(7); N2-N3 = 1.294(8); N3-N4 = 1.378(7); N1-Rh-N4 = 75.1(2); C1-Rh-C2 = 85.2(3);

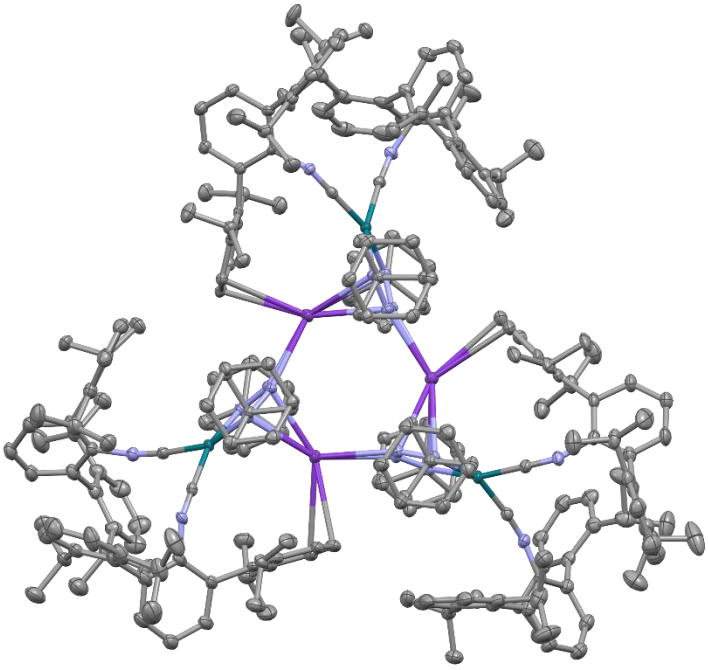

Figure 2.22 Molecular Structure of [K[(κ_2-N,N-Ad$_2$N$_4$)Rh(CNAr^{Dipp2})$_2$]]$_3$ (17) showing the full trimerized form of the molecules solid state structure. Hydrogen atoms omitted for clarity.

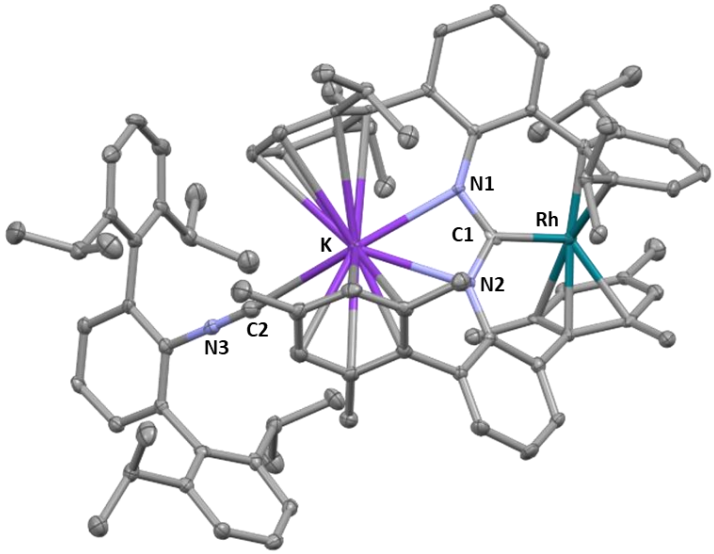

Figure 2.21 Molecular Structure of K[Rh(κ_3-C,C,C-^{Mes2}ArNCNAr^{Dipp2})][CNAr^{Dipp2}] (18). Hydrogen atoms omitted for clarity. Selected bond distances (Å) and angles (°): Rh-C1 = 1.978(4); C1-N1 = 1.347(5); C1-N2 = 1.344(5); C2-K = 3.152(5); C2-N3 = 1.159(5); N3-N4 = 1.378(7); N1-C1-N2 = 112.2(3).

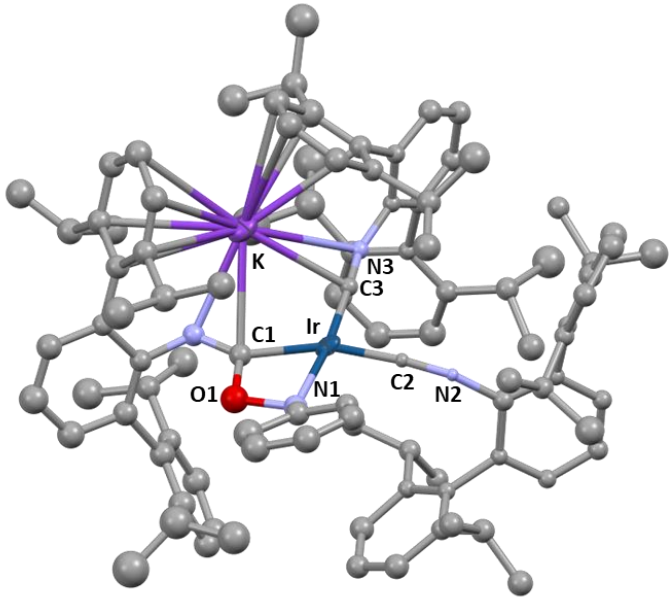

Figure 2.23 Molecular Structure of K[Ir(PhNOCNAr^{Dipp2})(CNAr^{Dipp2})$_2$] (19). Hydrogen atoms omitted for clarity. Selected bond distances (Å) and angles (°): Rh-C1 = 2.08(3); C1-O1 = 1.45(3); O1-N1 = 1.51(3); N1-Ir = 2.05(2); Ir-C2 = 1.80(2); C2-N2 = 1.24(2); C1-O1-N1 = 101.4(17).

Table 2.1 Crystallographic Data and Refinement Information

	$TlIr(CNAr^{Dipp2})_3$ (**6**)	$[Tl_2Rh(CNAr^{Dipp2})_3]$ OTf $[Et_2O]$ (**7**)	$TlRh(CNAr^{Dipp2})_3$ (**8**)
Formula	$C_{186}H_{221}Ir_2N_6Tl_2$	$C_{98}H_{121}F_3N_3O_4RhSTl_2$	$C_{90}H_{110}N_3RhTl$
Crystal System	Monoclinic	Monoclinic	Monoclinic
Space Group	*Pn*	*P2/c*	$P2_1/n$
a, Å	12.180(4)	20.3961(9)	12.1262(6)
b, Å	25.668(8)	20.2270(9)	25.7018(14)
c, Å	26.051(8)	22.7811(9)	26.0938(14)
α, deg	90	90	90
β, deg	90.078(7)	104.209(1)	90.063(2)
γ, deg	90	90	90
V, $Å^3$	8145(4)	9259.5(7)	8132.5(7)
Z	2	4	4
Radiation (λ, Å)	Mo-Kα, 0.71073	Mo-Kα, 0.71073	Mo-Kα, 0.71073
ρ (calcd.), g/cm^3	1.359	1.439	1.288
μ (Mo Ka), mm^{-1}	3.654	3.727	2.227
Temp, K	100	100	100
θ max, deg	26.391	28.282	25.740
data/parameters	33243(1658)	22998(1065)	15512(926)
R_1	0.0447	0.0452	0.0371
wR_2	0.1239	0.1071	0.0870
GOF	1.082	1.151	1.051

Table 2.2 Crystallographic Data and Refinement Information – Continued

	$[Tl_2Ir(CNAr^{Dipp2})_3]$ OTf $[Et_2O]$ (**9**)	$HRh(CNAr^{Dipp2})_3$ (**10**)	$HIr(CNAr^{Dipp2})_3$ (**11**)
Formula	$C_{94}H_{111}F_3IrN_3O_3STl_2$ $[C_4H_8O]$	$C_{93}H_{112}RhN_3$	$C_{93}H_{112}IrN_3$
Crystal System	Monoclinic	Orthorhombic	Monoclinic
Space Group	*P2₁/n*	*Pbcn*	*P2₁/n*
a, Å	13.5878(10)	12.067(3)	12.1467(8)
b, Å	25.3847(18)	25.762(6)	25.9061(16)
c, Å	25.661(2)	25.795(6)	25.3543(17)
α, deg	90	90	90
β, deg	93.500(2)	90	90.009(2)
γ, deg	90	90	90
V, Å^3	8834.5(11)	8019(3)	7978.3(9)
Z	4	4	4
Radiation (λ, Å)	Mo-Kα, 0.71073	Mo-Kα, 0.71073	Mo-Kα, 0.71073
ρ (calcd.), g/cm^3	1.574	1.139	1.219
μ (Mo Ka), mm^{-1}	5.224	0.259	1.720
Temp, K	100	100	100
θ max, deg	25.429	22.056	26.427
data/parameters	8949 (1048)	4930(472)	9459 (973)
R_1	0.0734	0.1183	0.0593
wR_2	0.1744	0.2475	0.1584
GOF	1.046	1.126	1.063

Table 2.3 Crystallographic Data and Refinement Information – Continued

	$Rh((SiMe_3)(CNAr^{Dipp2})_3$ $[C_5H_{14}]$ (**12**)	$Rh(CNAr^{Dipp2})(\eta_6$-κ-C,Ar-^{Cy2}BIM) (**13**)	$RhCl(PCl_2)_2(CNAr^{Dipp2})_2$ (**14**)
Formula	$C_{101}H_{132}N_3RhSi$	$C_{74}H_{96}BN_2Rh$ 2$[C_4H_{10}O]$	$C_{62}H_{74}Cl_5N_2P_2Rh$
Crystal System	Monoclinic	Primitive	Primitive
Space Group	*P2₁/c*	*P-1*	*P-1*
a, Å	22.7838(15)	12.9941(10)	10.6085(12)
b, Å	12.1769(9)	14.6272(12)	14.1071(16)
c, Å	32.978(3)	19.7112(17)	20.931(2)
α, deg	90	92.739(2)	80.248(3)
β, deg	101.115(2)	100.053(2)	89.919(3)
γ, deg	90	96.751(2)	82.063(3)
V, Å^3	8976.2(12)	3654.4(5)	3056.8(6)
Z	4	2	1
Radiation (λ, Å)	Mo-Kα, 0.71073	Mo-Kα, 0.71073	Mo-Kα, 0.71073
ρ (calcd.), g/cm^3	1.124	1.159	1.292
μ (Mo Ka), mm^{-1}	0.250	0.280	0.589
Temp, K	100	100	100
θ max, deg	25.409	28.366	26.419
data/parameters	16531(984)	15483(813)	9962 (665)
R_1	0.0437	0.0418	0.0420
wR_2	0.1126	0.1095	0.1074
GOF	1.045	1.083	1.035

Table 2.4 Crystallographic Data and Refinement Information – Continued

	$IrCl(PCl_2)_2(CNAr^{Dipp2})_2$ (**15**)	K[*trans*-$Rh(SiMe_3)_2(CNAr^{Dipp2})_2$] (**16**)	$[K[(\kappa_2\text{-}N,N\text{-}Ad_2N_4)Rh(CNAr^{Dipp2})_2]]_3$ (**17**)
Formula	$C_{62}H_{74}Cl_5IrN_2P_2$	$C_{68}H_{92}KN_2RhSi_2$	$HC_{251}K_3N_{18}Rh_3$
Crystal System	Monoclinic	Monoclinic	Primitive
Space Group	*P2₁/c*	*P2₁/c*	*P-1*
a, Å	19.4207(13)	16.3162(6)	25.3376(10)
b, Å	19.4207(13)	19.0266(7)	29.6266(12)
c, Å	20.3333(14)	22.2326(9)	33.7210(13)
α, deg	90	90	72.582(2)
β, deg	114.341(1)	111.373(1)	79.544(2)
γ, deg	90	90	81.170(2)
V, $Å^3$	6263.8(7)	6427.3(4)	23618.4(16)
Z	4	4	4
Radiation (λ, Å)	Mo-Kα, 0.71073	Mo-Kα, 0.71073	Mo-Kα, 0.71073
ρ (calcd.), g/cm^3	1.356	1.174	1.038
μ (Mo Ka), mm^{-1}	2.434	0.407	0.311
Temp, K	100	100	100
θ max, deg	26.423	28.461	25.789
data/parameters	11246(665)	13226(689)	61751 (4861)
R_1	0.0326	0.351	0.0909
wR_2	0.0916	0.853	0.2936
GOF	1.086	1.039	1.090

Table 2.5 Crystallographic Data and Refinement Information – Continued

	K[Rh(κ$_3$-C,C,C ^{Mes2}ArNCNAr^{Dipp2})][CNAr^{Dipp2}] (**18**)	K[Ir(PhNOCNAr^{Dipp2})(CNAr^{Dipp2})$_2$] (**19**)
Formula	$C_{86}H_{99}KN_3Rh$	$C_{99}H_{116}IrKN_4O$
Crystal System	Monoclinic	Monoclinic
Space Group	*P2$_1$/c*	*P2$_1$/n*
a, Å	20.6542(15)	12.113(3)
b, Å	15.8733(11)	28.562(7)
c, Å	23.7017(16)	26.721(6)
α, deg	90	90
β, deg	114.758(2)	93.914(5)
γ, deg	90	90
V, Å^3	7056.4(9)	9223(4)
Z	4	4
Radiation (λ, Å)	Mo-Kα, 0.71073	Mo-Kα, 0.71073
ρ (calcd.), g/cm^3	1.239	1.159
μ (Mo Ka), mm^{-1}	0.349	1.538
Temp, K	100	100
θ max, deg	25.399	20.489
data/parameters	8080 (842)	5560 (459)
R_1	0.0549	0.1370
wR_2	0.1157	0.3260
GOF	1.018	1.123

2.7 Acknowledgments

Complexes discussed in chapter 2 are currently in preparation for publication by M. L. Neville, C. Chan, M. Gembicky, C. Moore, A. L. Rheingold, J. S. Figueroa. The dissertation author is the primary author of this manuscript.

2.8 References

1. Ellis, J. E., *Inorganic Chemistry* **2006,** *45* (8), 3167-3186.

2. Ellis, J. E.; Barger, P. T.; Winzenburg, M. L., *Journal of the Chemical Society, Chemical Communications* **1977,** (19), 686-687.

3. Lin, J. T.; Hagen, G. P.; Ellis, J. E., *Organomet. Chem.* **1983,** *2* (9), 1145-1150.

4. Linn, J. T.; Hagen, G. P.; Ellis, J. E., *Organomet. Chem.* **1984,** *3* (8), 1288-1292.

5. Ellis, J. E.; Fjare, K. L.; Hay, T. G., *Journal of the American Chemical Society* **1981,** *103* (20), 6100-6106.

6. Breimair, J.; Robl, C.; Beck, W., *Journal of Organometallic Chemistry* **1991,** *411* (3), 395-404.

7. Allen, J. M.; Brennessel, W. W.; Buss, C. E.; Ellis, J. E.; Minyaev, M. E.; Pink, M.; Warnock, G. F.; Winzenburg, M. L.; Young, V. G., *Inorganic Chemistry* **2001,** *40* (20), 5279-5284.

8. Davies, J. A., *Synthetic coordination chemistry: principles and practice*. World Scientific: 1996.

9. Linke, W. F.; Seidell, A., **1958**.

10. Collman, J. P., *Accounts of Chemical Research* **1975,** *8* (10), 342-347.

11. Moore, J. T.; Lu, C. C., *Journal of the American Chemical Society* **2020,** *142* (27), 11641-11646.

12. Drance, M. J.; Sears, J. D.; Mrse, A. M.; Moore, C. E.; Rheingold, A. L.; Neidig, M. L.; Figueroa, J. S., *Science* **2019,** *363* (6432), 1203-1205.

13. Hubbell, A. K.; Coates, G. W., *The Journal of Organic Chemistry* **2020,** *85* (21), 13391-13414.

14. Eisenmann, J.; Yamartino, R.; Howard, J. J., *The Journal of Organic Chemistry* **1961,** *26* (6), 2102-2104.

15. Piotti, M. E.; Alper, H., *Journal of the American Chemical Society* **1996,** *118* (1), 111-116.

16. Hinterding, K.; Jacobsen, E. N., *The Journal of Organic Chemistry* **1999,** *64* (7), 2164-2165.

17. Denmark, S. E.; Ahmad, M., *The Journal of Organic Chemistry* **2007,** *72* (25), 9630-9634.

18. Wack, H.; Drury, W. J.; Taggi, A. E.; Ferraris, D.; Lectka, T., *Organic Letters* **1999,** *1* (12), 1985-1988.

19. Kramer, J. W.; Rowley, J. M.; Coates, G. W., Ring-Expanding Carbonylation of Epoxides. In *Organic Reactions*, pp 1-104.

20. Green, M. L. H., *Journal of Organometallic Chemistry* **1995,** *500* (1), 127-148.

21. Barnett, B. R.; Figueroa, J. S., *Chem Commun* **2016,** *52* (96), 13829-13839.

22. Fox, B. J.; Millard, M. D.; DiPasquale, A. G.; Rheingold, A. L.; Figueroa, J. S., *Angew. Chem. Int. Ed.* **2009,** *48* (19), 3473-3477.

23. Millard, M. D.; Moore, C. E.; Rheingold, A. L.; Figueroa, J. S., *Journal of the American Chemical Society* **2010,** *132* (26), 8921-8923.

24. Strauss, S. H.; Diamond, S. E.; Mares, F.; Shriver, D. F., *Inorganic Chemistry* **1978,** *17* (11), 3064-3068.

25. Yoshida, T.; Thorn, D. L.; Okano, T.; Otsuka, S.; Ibers, J. A., *Journal of the American Chemical Society* **1980,** *102* (21), 6451-6457.

26. Hill, A. F.; Owen, G. R.; White, A. J. P.; Williams, D. J., *Angew. Chem. Int. Ed.* **1999,** *38* (18), 2759-2761.

27. Trofimenko, S., *Chemical Reviews* **1993,** *93* (3), 943-980.

28. Zhang, J.; Poliakoff, M.; George, M. W., *Organomet. Chem.* **2003,** *22* (8), 1612-1618.

29. Danopoulos, A. A.; Pugh, D.; Wright, J. A., *Angew. Chem. Int. Ed.* **2008,** *47* (50), 9765-9767.

30. Feller, M.; Gellrich, U.; Anaby, A.; Diskin-Posner, Y.; Milstein, D., *Journal of the American Chemical Society* **2016,** *138* (20), 6445-6454.

31. Carpenter, A. E.; Rheingold, A. L.; Figueroa, J. S., *Organomet. Chem.* **2016,** *35* (14), 2309-2318.

32. Barnett, B. R.; Moore, C. E.; Rheingold, A. L.; Figueroa, J. S., *Journal of the American Chemical Society* **2014,** *136* (29), 10262-10265.

33. Pan, Y.; Mague, J. T.; Fink, M. J., *Organomet. Chem.* **1992,** *11* (11), 3495-3497.

34. Suginome, M.; Oike, H.; Shuff, P. H.; Ito, Y., *Journal of Organometallic Chemistry* **1996,** *521* (1), 405-408.

35. Suginome, M.; Ito, Y., *Journal of the Chemical Society, Dalton Transactions* **1998,** (12), 1925-1934.

36. Roscher, A.; Bockholt, A.; Braun, T., *Dalton Transactions* **2009,** (8), 1378-1382.

37. Ansell, M. B.; Roberts, D. E.; Cloke, F. G. N.; Navarro, O.; Spencer, J., *Angew. Chem. Int. Ed.* **2015,** *54* (19), 5578-5582.

38. Dong, Y.; Clarke, R. M.; Porter, G. J.; Betley, T. A., *Journal of the American Chemical Society* **2020,** *142* (25), 10996-11005.

39. Baek, Y.; Das, A.; Zheng, S.-L.; Reibenspies, J. H.; Powers, D. C.; Betley, T. A., *Journal of the American Chemical Society* **2020,** *142* (25), 11232-11243.

40. Dong, Y.; Lukens, J. T.; Clarke, R. M.; Zheng, S.-L.; Lancaster, K. M.; Betley, T. A., *Chemical Science* **2020,** *11* (5), 1260-1268.

41. Barnett, B. R.; Neville, M. L.; Moore, C. E.; Rheingold, A. L.; Figueroa, J. S., *Angew. Chem. Int. Ed.* **2017,** *56* (25), 7195-7199.

42. Carsch, K. M.; DiMucci, I. M.; Iovan, D. A.; Li, A.; Zheng, S.-L.; Titus, C. J.; Lee, S. J.; Irwin, K. D.; Nordlund, D.; Lancaster, K. M.; Betley, T. A., *Science* **2019,** *365* (6458), 1138-1143.

43. Obenhuber, A. H.; Gianetti, T. L.; Berrebi, X.; Bergman, R. G.; Arnold, J., *Journal of the American Chemical Society* **2014,** *136* (8), 2994-2997.

44. Vaddypally, S.; McKendry, I. G.; Tomlinson, W.; Hooper, J. P.; Zdilla, M. J., *Chemistry – A European Journal* **2016,** *22* (30), 10548-10557.

45. Dyker, C. A.; Lavallo, V.; Donnadieu, B.; Bertrand, G., *Angew. Chem. Int. Ed.* **2008,** *47* (17), 3206-3209.

46. Tonner, R.; Frenking, G., *Angew. Chem. Int. Ed.* **2007,** *46* (45), 8695-8698.

47. Chen, W.-C.; Shih, W.-C.; Jurca, T.; Zhao, L.; Andrada, D. M.; Peng, C.-J.; Chang, C.-C.; Liu, S.-k.; Wang, Y.-P.; Wen, Y.-S.; Yap, G. P. A.; Hsu, C.-P.; Frenking, G.; Ong, T.-G., *Journal of the American Chemical Society* **2017,** *139* (36), 12830-12836.

48. Munz, D., *Organomet. Chem.* **2018,** *37* (3), 275-289.

49. Hendon, C. H.; Tiana, D.; Murray, A. T.; Carbery, D. R.; Walsh, A., *Chemical Science* **2013,** *4* (11), 4278-4284.

50. Rehorek, D., *Chemical Society Reviews* **1991,** *20* (3), 341-353.

51. Barnett, B. R.; Labios, L. A.; Moore, C. E.; England, J.; Rheingold, A. L.; Wieghardt, K.; Figueroa, J. S., *Inorg Chem* **2015,** *54* (14), 7110-21.

52. Otsuka, S.; Aotani, Y.; Tatsuno, Y.; Yoshida, T., *Inorganic Chemistry* **1976,** *15* (3), 656-660.

53. La Monica, G.; Cenini, S., *Journal of the Chemical Society, Dalton Transactions* **1980,** (7), 1145-1149.

54. Lee, J.; Chen, L.; West, A. H.; Richter-Addo, G. B., *Chemical Reviews* **2002,** *102* (4), 1019-1066.

55. Namazian, M.; Lin, C. Y.; Coote, M. L., *Journal of Chemical Theory and Computation* **2010,** *6* (9), 2721-2725.

56. Wang, D.; Tamizmani, M.; Leng, X.; Deng, L., *Chinese Journal of Chemistry* **2020,** *38* (2), 158-162.

57. Ellis, J. E., *Organomet. Chem.* **2003,** *22* (17), 3322-3338.

58. Espinoza, E. M.; Clark, J. A.; Soliman, J.; Derr, J. B.; Morales, M.; Vullev, V. I., *Journal of The Electrochemical Society* **2019,** *166* (5), H3175-H3187.

59. Coleman, A.; Pryce, M. T., *Inorganic Chemistry* **2008,** *47* (23), 10980-10990.

60. Duffy, N. W.; Robinson, B. H.; Simpson, J., *Journal of Organometallic Chemistry* **1999,** *573* (1), 36-46.

61. Arnarego, W. L. F.; Chai, C. L. L., *Purification of Laboratory Chemicals*. 5th ed. ed.; Elsevier: 2003.

62. Pangborn, A. B.; Giardello, M. A.; Grubbs, R. H.; Rosen, R. K.; Timmers, F. J., *Organomet. Chem.* **1996,** *15* (5), 1518-1520.

63. Ditri, T.; Fox, B.; Moore, C.; Rheingold, A.; Figueroa, J., *Inorganic Chemistry* **2009,** *48* (17), 8362-8375.

64. Ditri, T. B.; Barnett, B. R.; Carpenter, A. E.; Mokhtarzadeh, C. C.; Agnew, D. W.; Figueroa, J. S., *Inorg. Synth.* **2018,** *37*, 109-115.

65. Fulmer, G. R.; Miller, A. J. M.; Sherden, N. H.; Gottlieb, H. E.; Nudelman, A.; Stoltz, B. M.; Bercaw, J. E.; Goldberg, K. I., *Organometallics* **2010,** *29* (9), 2176-2179.

66. Neese, F., *Wiley Interdisciplinary Reviews: Computational Molecular Science* **2011,** *2* (1), 73-78.

67. Frisch, M. J.; Trucks, G. W.; Schlegel, H. B.; Scuseria, G. E.; Robb, M. A.; Cheeseman, J. R.; Scalmani, G.; Barone, V.; Petersson, G. A.; Nakatsuji, H.; Li, X.; Caricato, M.; Marenich, A. V.; Bloino, J.; Janesko, B. G.; Gomperts, R.; Mennucci, B.; Hratchian, H. P.; Ortiz, J. V.; Izmaylov, A. F.; Sonnenberg, J. L.; Williams; Ding, F.; Lipparini, F.; Egidi, F.; Goings, J.; Peng, B.; Petrone, A.;

Henderson, T.; Ranasinghe, D.; Zakrzewski, V. G.; Gao, J.; Rega, N.; Zheng, G.; Liang, W.; Hada, M.; Ehara, M.; Toyota, K.; Fukuda, R.; Hasegawa, J.; Ishida, M.; Nakajima, T.; Honda, Y.; Kitao, O.; Nakai, H.; Vreven, T.; Throssell, K.; Montgomery Jr., J. A.; Peralta, J. E.; Ogliaro, F.; Bearpark, M. J.; Heyd, J. J.; Brothers, E. N.; Kudin, K. N.; Staroverov, V. N.; Keith, T. A.; Kobayashi, R.; Normand, J.; Raghavachari, K.; Rendell, A. P.; Burant, J. C.; Iyengar, S. S.; Tomasi, J.; Cossi, M.; Millam, J. M.; Klene, M.; Adamo, C.; Cammi, R.; Ochterski, J. W.; Martin, R. L.; Morokuma, K.; Farkas, O.; Foresman, J. B.; Fox, D. J. *Gaussian 16 Rev. C.01*, Wallingford, CT, 2016.

68. Becke, A. D., *The Journal of Chemical Physics* **1986,** *84* (8), 4524-4529.

69. Becke, A. D., *The Journal of Chemical Physics* **1993,** *98* (7), 5648-5652.

70. Lee, C.; Yang, W.; Parr, R. G., *Physical Review B* **1988,** *37* (2), 785-789.

71. Weigend, F., *Physical Chemistry Chemical Physics* **2006,** *8* (9), 1057-1065.

72. Weigend, F.; Ahlrichs, R., *Physical Chemistry Chemical Physics* **2005,** *7* (18), 3297-3305.

73. D. A. Zhurko, G. A.; Zhurko, "ChemCraft 2014," can be found under

www.chemcraftprog.com, 2014.

74. Sheldrick, G. M., *Acta Crystallographica Section A Foundations of Crystallography* **2008,** *64* (Pt 1), 112-122.

75. Sheldrick, G., *Acta Crystallographica Section C* **2015,** *71* (1), 3-8.

76. Dolomanov, O. V.; Bourhis, L. J.; Gildea, R. J.; Howard, J. A. K.; Puschmann, H., *Journal of Applied Crystallography* **2009,** *42* (2), 339-341.

77. Spek, A., *Journal of Applied Crystallography* **2003,** *36* (1), 7-13.

78. Spek, A., *Acta Crystallographica Section C* **2015,** *71* (1), 9-18.

79. Ivlev, S. I.; Conrad, M.; Kraus, F., *Zeitschrift für Kristallographie - Crystalline Materials* **2019,** *234* (6), 415-418.

Chapter 3 Design and Synthesis of Varied Aryl-Isocyanide Ligand Topologies

3.1 Introduction – Ligands for low-valent metal-organic frameworks

In the past few decades, the study of Metal-organic Frameworks (MOFs) has flourished and there now seems to be no limit to the amount of these multi-dimensional structures.[1-2] MOF's typically pair hard, Lewis acidic metal centers and similarly hard, anionic ligands. These hard-hard interactions make strong, ionic bonds at coordinatively saturated metal notes, ideal for making robust crystalline latices.[4] However, the types of chemical transformations these MOFs have been shown to facilitate are typically limited by the chemistry available to the metal nodes. For example, one the most well studied MOFs, UiO-66 with it's Zr-oxo cluster nodes, has been proven in many times to be a competent Lewis-acid catalyst, similar to the metal node itself.[5-8] However, these d^0, high valent metals lack the capacity to do multi-electron reductive chemistry and poorly engage with "soft" Lewis bases. In contrast, organometallic complexes, particularly with low-valent metal centers, are well known to perform muti-electron, multi-bond transformations. Additionally, the variety of neutral and anionic ligands used in organometallics allow for a high degree of control over the manner with which metal interacts with substrates.[9-14]

Building low-valent, organometallic metal nodes into MOFs has generally followed two different routes: adding low-valent metals as nonstructural units to a well-known MOF lattice, or directly building them into the structural components.[5] The former has been well explored, especially in the realm of Post-Synthetic Modification (PSM) and has provided functionality in some existing MOF platforms.[15-17] However, the mixing of hard/soft ligand platforms and the fact that they aren't part of the structural lattice itself can lead to leaching, degradation, and struggle to achieve high metal loadings.[17-19] These short-comings are overcome by instead building the molecule of interest directly into the lattice of the MOF.

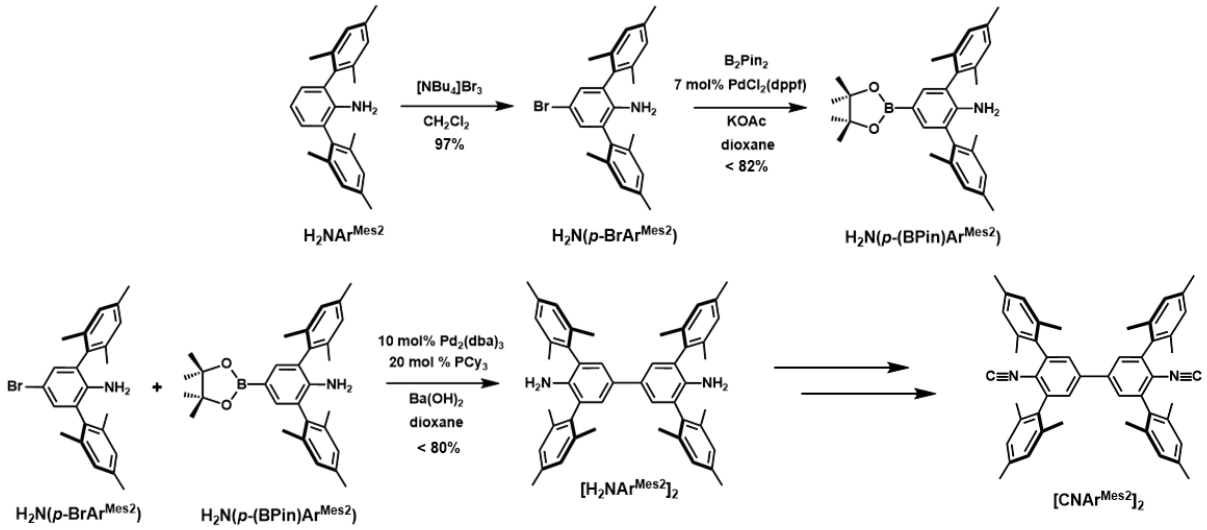

Scheme 3.1 Original synthesis of [CNAr^{Mes2}]$_2$ developed by Dr. Douglas Agnew and co-workers.[3]

However, integrating the functionality of a metal center while it acts as a structural component has many challenges. Often, the initial step in a catalytic cycle is loss of a ligand from the metal center, to provide a room for a substrate to bind.[20] In the context of a structural node in a MOF, this represents degradation of the material. Defect engineering provides a controlled route to coordinative unsaturation but suffers from many of the same pitfalls as post-synthetic modification.[21-23] Ideally, the metal nodes would both be structural and contain some degree of coordinative unsaturation. Like the strategy used in Chapter 1, *m*-terphenyl isocyanide ligands provide a potentially attractive strategy to achieve this goal.

Initial forays into framework synthesis by our group utilized a novel, ditopic m-terphenyl isocyanide ligand, [CNAr^{Mes2}]$_2$, prepared via Suzuki-Miyaura coupling of monotopic linkers (**Scheme 3.1**).[3] This ligand was used by Dr. Douglas Agnew and co-workers to successfully synthesize diamonded lattices with four-coordinate, tetrahedral Cu(I) and Ni(0) nodes (**Scheme 3.2**).[3, 24] Notably, Ni-^{ISO}CN-2 · ([CNAr^{Mes2}]$_2$)$_{0.5}$, an analogue of the molecular species Ni(CNAr^{Mes2})$_4$, was the first porous metal-organic material constructed from zero-valent metal nodes. However, these initial MOFs contained very little porosity/accessible surface area due to a combination of interpenetrating lattices and small pores. In an effort to improve these properties, Dr. Alejandra Arroyave developed a longer, phenylene spaced ditopic

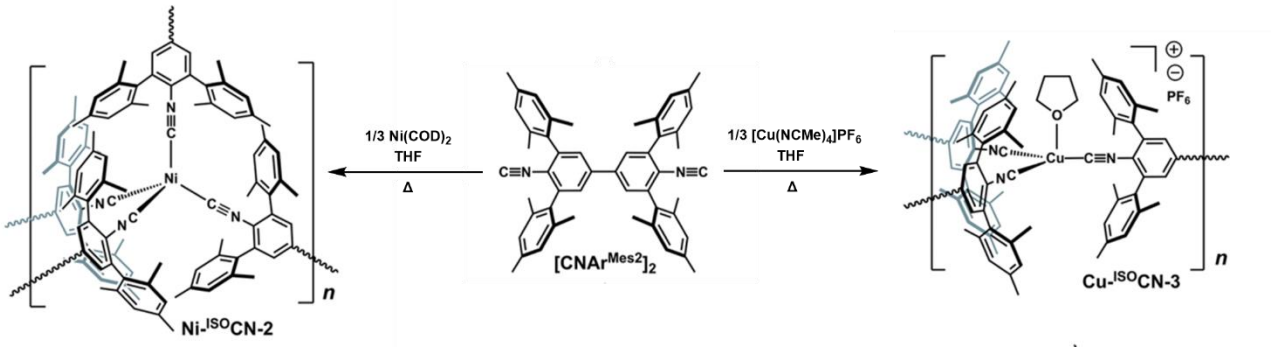

Scheme 3.2 Previously synthesized ^{ISO}CN metal organic frameworks with [CNAr^{Mes2}]$_2$ with Cu and Ni nodes.

ligand, 1,4-(CNAr^{Mes2})$_2$C$_6$H$_4$, designed to space out metal-nodes. Despite continued interpenetration, 1,4-(CNAr^{Mes2})$_2$C$_6$H$_4$ yielded a MOF (Cu-^{ISO}CN-4) with solvent accessible pores 28 Å x 19 Å, and trigonal pyramidal, THF-solvated Cu(I) nodes of the formulation, [Cu(THF)(CNR)$_3$]$^+$.[25] Importantly, the solvent accessible pores, combined with the solvent protected coordination site at the structural copper nodes proved amenable to ligand exchange. Soaking (Cu-^{ISO}CN-4) in pyridine solutions allowed for complete exchange of the coordinated THF. However, from these initial works, it became apparent that maximum ligand coordination is generally energetically preferred, and to maintain an open coordination site at a metal center, a more reliable strategy for precluding coordinative saturation at structural metal nodes was needed. In the molecular chemistry of late metal *m*-terphenyl-isocyanide complexes, the larger CNAr^{Dipp2} and CNAr^{Tripp2} derivatives were used to achieve this. These larger ligands showed a maximum coordination number of 3 at a single metal center even in instances where CNAr^{Mes2} realized a coordination number of 4.[26-27] However, initial attempts at synthesizing a ditopic CNAr^{Dipp2} linker via the same synthetic conditions as [CNAr^{Mes2}]$_2$, and 1,4-(CNAr^{Mes2})$_2$C$_6$H$_4$ resulted in abject failure. This chapter explores the process of synthesizing larger and electronically varied, muti-topic *m*-terphenyl isocyanide linkers and their application in the synthesis of low-valent, coordinatively unsaturated MOFs.

3.1.1 Synthesis of multi-topic CNAr^{Dipp}, CNAr^{Tripp} and CNAr^{DArF} linkers

The original syntheses of the ditopic ^{Mes2}ArNC linkers start at the corresponding, monotopic aniline, ^{Mes2}ArNH$_2$.[28, 57] Taking advantage of the strongly directing nature of the aniline, [NBu$_4$][Br$_3$] is used to para-brominate the central aryl setting the *m*-terphenyl up for Suzuki-Miyaura type couplings. To prepare the coupling partner, borylation of the brominated cite is achieved using B_2Pin_2, and $PdCl_2$(dppf) (dppf = 1,1–Bis(diphenylphosphino)ferrocene) as the pre-catalyst.[3] The yield for this borylation is reported at 84%, but in practice yields this high were rarely seen. This preparation was used as a starting point for attempts at synthesizing a ditopic ^{Dipp2}ArNC derivative. However, these conditions yielded none of the desired borylated product, p-Bpin-^{Dipp2}ArNC (**Figure 3.1**). As assayed by ^{1}H NMR and mass-spectrometry, only a small amount of the p-Br-^{Dipp2}ArNH$_2$ was consumed via protodebromination to form the progenitor of the brominated starting material, ^{Dipp2}ArNH$_2$. Given the strongly electron releasing nature of the aniline, it was hypothesized that oxidative addition of the aryl-bromide bond was likely the largest energetic hurdle in this catalytic cycle. To alleviate this barrier, both the substrate and the catalyst were improved. First, the aniline was converted to the formamide, p-Br-^{Dipp2}ArNHCHO, to decrease the electron releasing nature of the functional group. Second, the ligand on the Pd catalyst used was reconsidered. Dppf is a di-chelating aryl-phosphine ligand that enforces a cis-geometry of the coupling partners on Pd. This is useful for electron poor aryl coupling partners that may be slow to reductively eliminate, however, this is not the case in this reaction. In fact, electron rich aryl group bound to Pd are known to readily scramble with aryl-phosphine

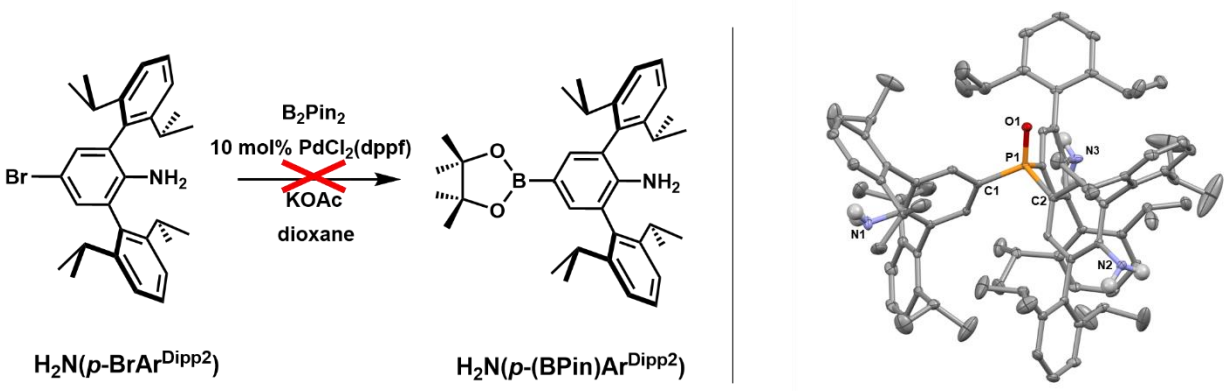

Figure 3.1 (Left) Initial failed conditions based on [CNar^{Mes2}]$_2$] synthesis. (Right) the solid-state structure of an isolated product of the failed borylation, OP(Ar^{Dipp2}NH$_2$)$_3$.

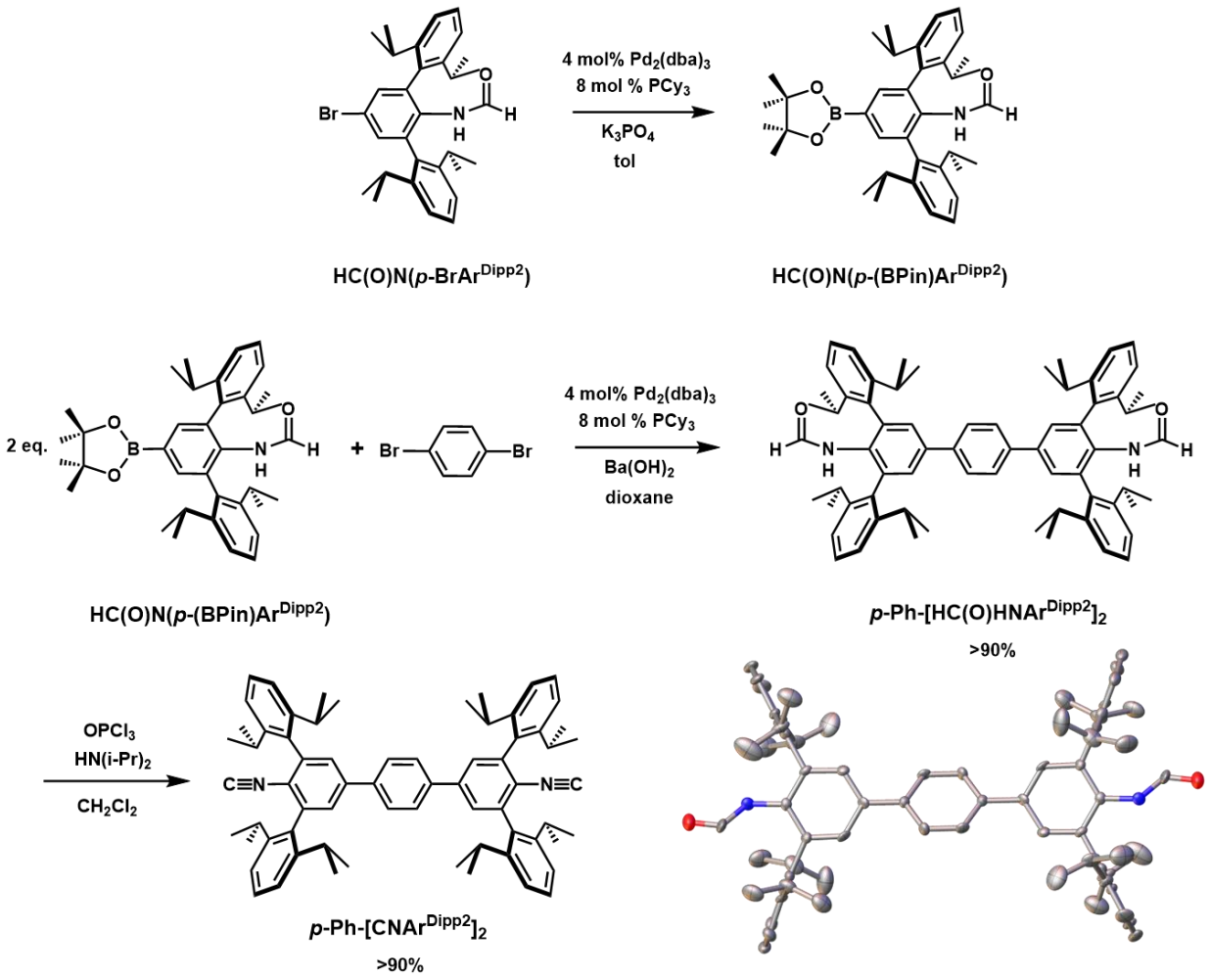

Figure 3.2 Final conditions for the synthesis of p-Ph-[CNAr^{Dipp2}]$_2$ (1,4-(CNAr^{Dipp2})$_2$C$_6$H$_4$) as well as the solid-state structure of the formamide, p-Ph-[NHCHOAr^{Dipp2}]$_2$ (1,4-(NHCHOAr^{Dipp2})$_2$C$_6$H$_4$).

bonds.[29-30] This reaction, even with ^{Mes2}ArNH$_2$, was observed to release a significant amount of a red byproduct, likely ferrocene, and may be a primary contributing factor in the low observed yields. In one reaction, OP(^{Dipp2}ArNH$_2$)$_3$ was isolated after workup in near quantitative yield relative to dppf (**Figure 3.1**). Instead, a series of sterically hindering, strongly donating, modern, monotopic phosphine ligands were screened with p-Br-^{Dipp2}ArNHCHO. Of the phosphines screened, PCy$_3$, Sphos, Xphos, all performed similarly well achieving <12hr conversions and high yields (>85%) under test conditions. PCy$_3$ was selected for final conditions given its relatively low cost and availability (**Figure 3.2**).

For the aryl-aryl Suzuki cross-coupling reaction, once again, the conditions used for the ditopic ^{Mes2}ArNC linkers were used as the entry point for the ^{Dipp2}ArNC synthesis (Figure). Surprisingly, a similar

result was observed to the first attempts at the borylation; the aryl-aryl cross-coupling reaction yielded no detectable amount of the desired product and minor amounts of the protodeborylated product. From the successful synthesis of the *p*-Bpin-^{Dipp2}ArNHCHO, we know that oxidative addition of the Br-Ar bond is unlikely to be the issue. Previous studies have shown that the electronic differences between ^{Dipp2}ArNC and ^{Mes2}ArNC are negligible, which suggested the issue may be the increased steric profile of the 2,6-diisopropylphenyl groups. That would imply that the issue may be the transmetalation from *p*-Bpin-^{Dipp2}ArNHCHO to form a putative Pd(^{Dipp2}ArNHCHO)$_2$(PCy3)$_n$ intermediate. Reductive elimination can be a heavily sterically driven process, so if this species were to form, it would likely quickly reductively eliminate the coupled product. To confirm the viability of *p*-Bpin-^{Dipp2}ArNHCHO as a coupling partner with a less sterically hindered substrate, a test reaction was run with phenyl bromide (BrC_6H_5) which quickly and quantitatively formed the expected product *p*-Ph-^{Dipp2}ArNHCHO (**Figure 3.2**). In the absence of observed, directly coupled [^{Dipp2}ArNHCHO]$_2$, a phenylene spaced derivative emerged as a possible strategy to circumvent the issue caused by the steric hinderance. Indeed, like the synthesis of 1,4-(NH_2Ar^{Mes2})$_2C_6H_4$, reaction of 1,4-dibormobenzene ($Br_2C_6H_4$) and *p*-Bpin-^{Dipp2}ArNHCHO formed 1,4-(NHCHOAr^{Dipp2})$_2C_6H_4$ in high yield. The ditopic formamide ligand can be readily dehydrated to form the ditopic isocyanide ligand, 1,4-($CNAr^{Dipp2}$)$_2C_6H_4$ (**Figure 3.2**).

Given the preference of $CNAr^{Dipp2}$ to form low-coordinate metal centers, access to higher dimensional solids can be facilitated by a higher dimensional linker ligands. Hence, we sought to develop a tritopic ligand using the planar, 1,3,5-Tris(4-bromophenyl)benzene as template. When added to *p*-Bpin-^{Dipp2}ArNC under similar conditions as the 1,4-($CNAr^{Dipp2}$)$_2C_6H_4$ coupling, the tritopic ligand 1,3,5-Tris(4-PhNHCHOAr^{Dipp2})C_6H_3 is synthesized in moderate to high yields and is readily dehydrated to form the isocyanide, 1,3,5-Tris(4-PhNCAr^{Dipp2})C_6H_3 (**Figure 3.3**). This chemistry was also extended to the bulkier ^{Dipp2}ArNC derivatives (1,4-($CNAr^{Tripp2}$)$_2C_6H_4$ and 1,3,5-Tris(4-PhCNAr^{Tripp2})C_6H_3), with the caveat that coupling reaction times were frequently 2x to 4x longer than observed with the $CNAr^{Dipp2}$ chemistry. These conditions were also found to be amenable to the synthesis of the electronically distinct, $CNAr^{DArF}$, ligand,

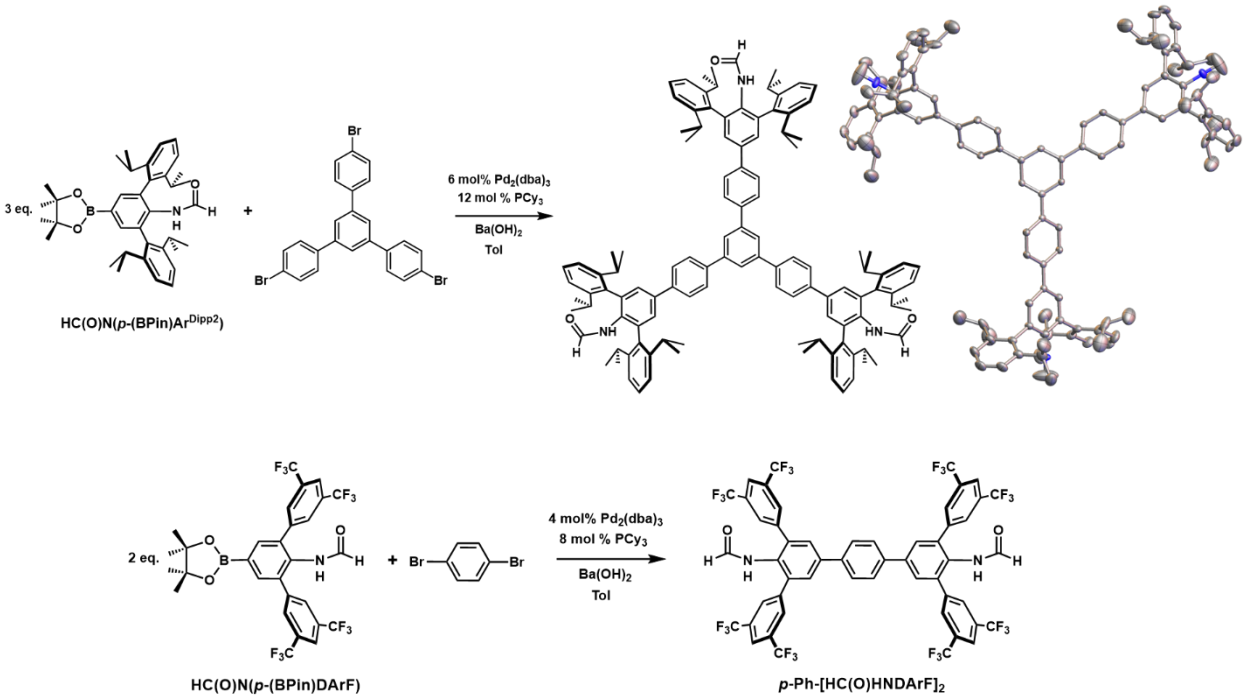

Figure 3.3 (Top) Coupling conditions of the tritopic linker 1,3,5-Tris(4-PhNHCHOAr^{Dipp2})C$_6$H$_3$ and the solid-state structure of the corresponding isocyanide. (Bottom) Coupling conditions for the synthesis of *p*-Ph-[HC(O)HNDArF]$_2$, (1,4-(NHCHOAr^{DArF})$_2$C$_6$H$_4$).

successfully synthesizing a ditopic variant 1,4-(NHCHOAr^{DArF})$_2$C$_6$H$_4$ (**Figure 3.3**). Relative to more electron rich aryl-isocyanide ligands like CNAr^{Dipp2}, *p*-F-CNAr^{DArF} has been observed to be capable of faster and further substitution of carbon monoxide on low- and zero-valent metal carbonyl complexes. For instance, ligand substitution of CNAr^{Dipp2} on both ReBr(CO)$_5$ and Re$_2$(CO)$_{10}$ is limited to two substitutions per metal.[31] However, in the same realm *p*-F-CNAr^{DArF} can achieve four, forming complexes ReBr(CO)(*p*-F-CNAr^{DArF})$_4$(CO) and Re(CO)(*p*-F-CNAr^{DArF})$_4$.[32] Given the variety and importance of zero-valent metal carbonyls, 1,4-(CNAr^{DArF})$_2$C$_6$H$_4$ opens up an exciting possibility of using these as potential precursors for use as metal nodes in higher dimensional solids.

3.1.2 Applications of ^{Dipp2}ArNC based multi-topic linkers in frameworks

Given the robust nature of previously synthesized Cu(I) isocyanide networks, initial studies of network (^{ISO}CN) formation with the tritopic linker 1,3,5-Tris(4-PhCNAr^{Dipp2})C$_6$H$_3$ were assessed with

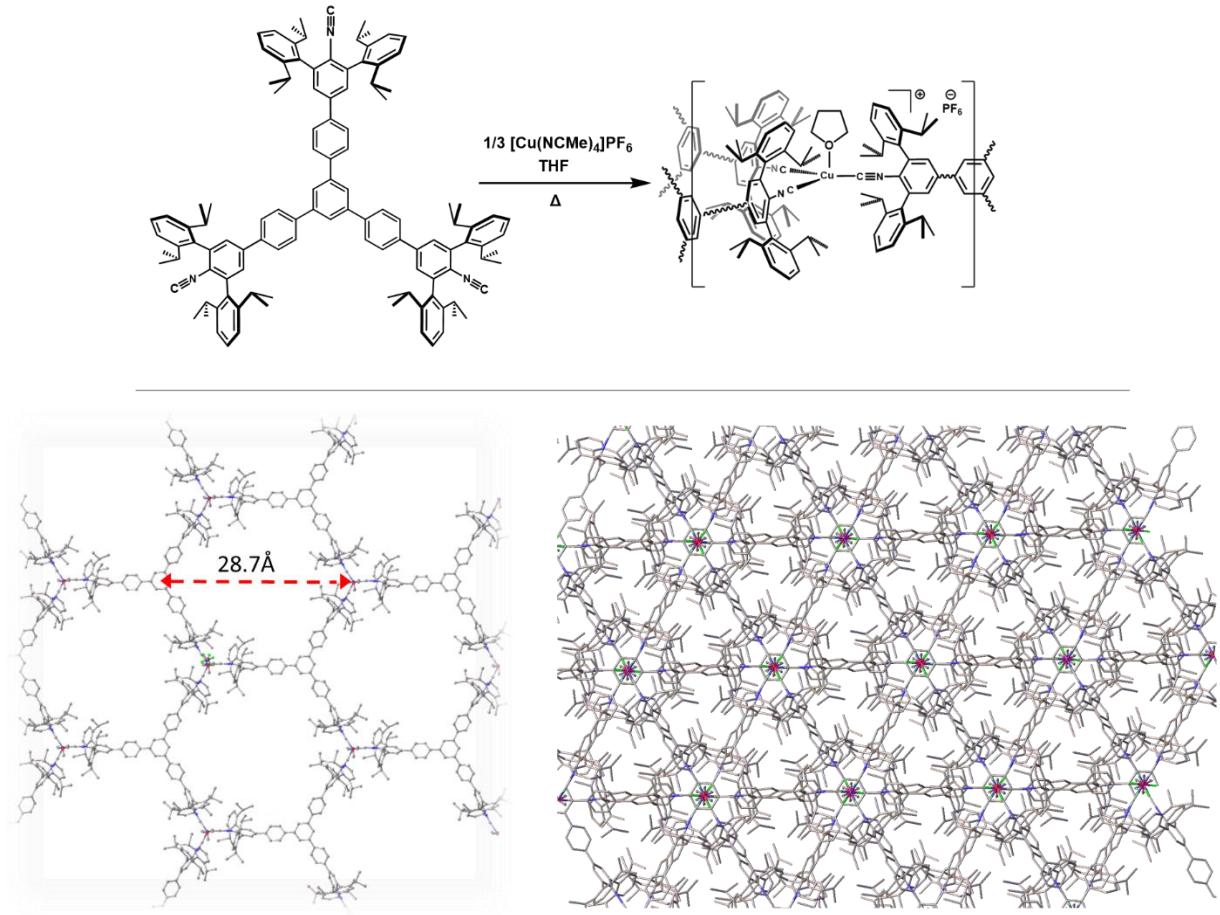

Figure 3.4 (Top) Scheme depicting the synthesis of Cu-^{ISO}CN-5 with tritopic isocyanide linker 1,3,5-Tris(4-PhNCAr^{Dipp2})C$_6$H$_3$. (Bottom; left) One sheet of the material depicting the length of the pore at the longest points. (Bottom; right) View of stacked sheets illustrating the lack of porosity due to overlap of staggered-sequential nodes and pores.

Cu(I). Similar to the syntheses of previous Cu-^{ISO}CNs with CNAr^{Mes2}-based, ditopic ligands, addition of a THF solution of 1,3,5-Tris(4-PhCNAr^{Dipp2})C$_6$H$_3$ to [Cu(NCMe)$_4$]PF$_6$ produces an amorphous, polymeric material after stirring for a short time.[3, 25] Heating this material in THF under solvothermal conditions for 24-48 h produces large, colorless crystals of Cu-^{ISO}CN-5 (**Figure 3.4**). Spectroscopic analysis of these crystals by ATR-IR show a strong, sharp absorption at 2140 cm^{-1}, slightly redshifted relative to Cu-^{ISO}CN-3 and -4 (2142 and 2146 cm^{-1} respectively) suggesting a non-pyramidalized Cu metal center.[25] Further structural characterization reveals the solid-state structure to be comprised of [Cu(THF)(CNR)$_3$]$^+$ nodes with outer sphere [PF$_6$]$^-$ counterions, analogous to Cu-^{ISO}CN-3 and -4. The metal nodes in Cu-^{ISO}CN-5 arrange into well-ordered 2D honeycomb sheets where the largest distance across the hexagonal pore's

measures 28.7 Å. While Cu-^{ISO}CN-4 displays a similar 2D honeycomb network with sizable hexagonal pores, it is beset by four-fold interpenetration. In contrast, Cu-^{ISO}CN-5 features densely stacked, staggered sheets where the node of one sheet overlaps with the central point of a 1,3,5-Tris(4-PhCNAr^{Dipp2})C_6H_3 linker in the sheet on top, which then overlaps with the pore of the following sheet, repeating forward and backward. This staggered arrangement appears to prevent accessibility to the $[Cu(THF)(CNR)_3]^+$. While solvent exchange of the Cu bound THF to pyridine was observed for Cu-^{ISO}CN-4, similar reactivity was not observed with Cu-^{ISO}CN-5 despite the similar coordination environment around the Cu center. At the same time, this lack of realized porosity may enhance the chemical stability and robustness of Cu-^{ISO}CN-4.

Pd is well recognized as a synthetically useful catalyst for a wide variety of organic transformations.[33-36] Recently, Sikma and Cohen published the first example of a MOF with Pd^0 metal nodes using a tetratopic phosphine linker.[37] The Pd^0 nodes are four coordinate forming $Pd(PPh_2R)_4$ coordination environments comparable to $Pd(PPh_3)_4$, a well-known and commonly used catalyst. However, $Pd(PPh_3)_4$ is coordinatively and electronically saturated. Mechanistically, $Pd(PPh_3)_4$ catalyzed reactions depends on ligand substitution to facilitate binding of a substrate.[38] In the context of the $Pd(PPh_2R)_4$ nodes this type of chemistry would represent degradation of the extended framework. To access the rich, synthetic chemistry of Pd^0, the metal nodes would ideally be synthesized with unsaturation incorporated into the structure. Having proven 1,3,5-Tris(4-PhCNAr^{Dipp2})C_6H_3, can facilitate the formation of coordinatively unsaturated metal nodes in isocyanide-based MOFs with Cu-^{ISO}CN-5, we set out to apply this ligand to form a coordinatively unsaturated Pd^0 MOF. The Pd^0 isocyanide complex $Pd(CNAr^{Dipp2})_2$ was selected as an ideal Pd source due it its coordinative and electrically unsaturated predisposition, in addition to the rapid ligand exchange kinetics.[39] Variable temperature studies on $Pd(CNAr^{Dipp2})_2$ showed that degenerate isocyanide

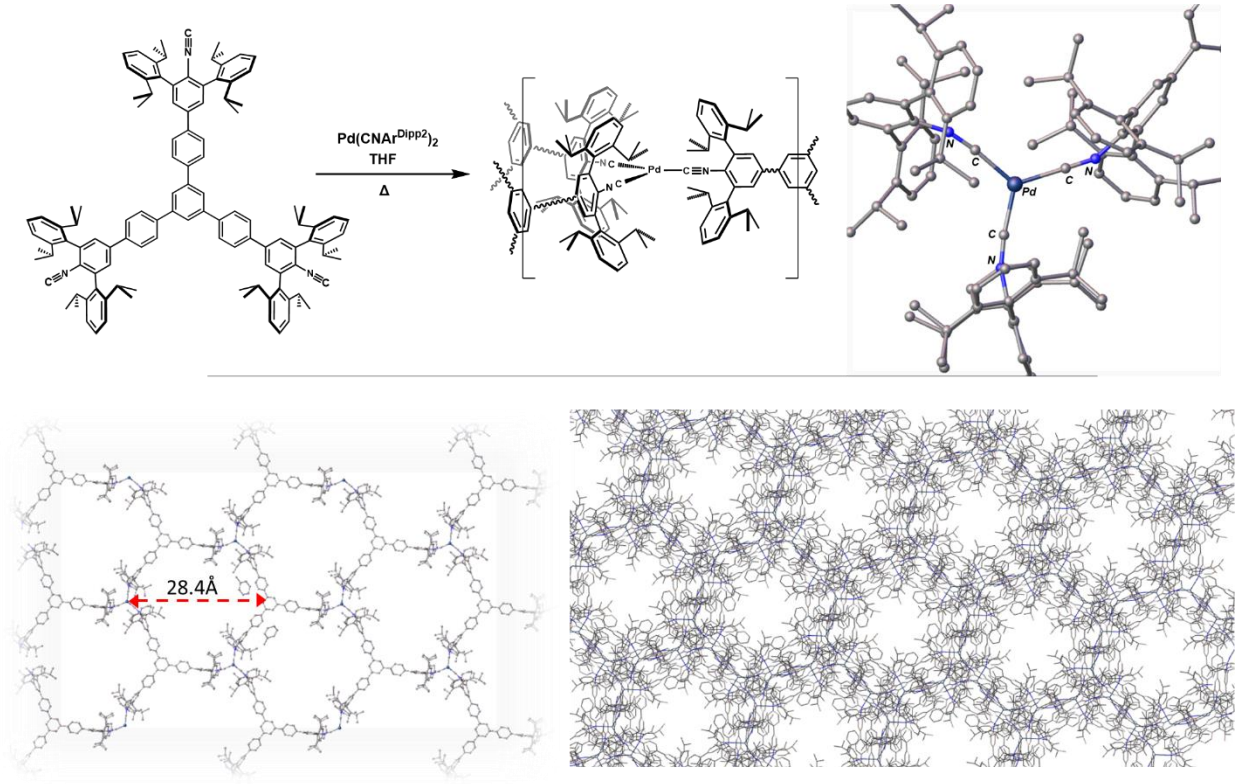

Figure 3.5 (Top) Scheme depicting the synthesis of Pd-^{ISO}CN-1 with tritopic isocyanide linker 1,3,5-Tris(4-PhNCAr^{Dipp2})C$_6$H$_3$. (Bottom; left) One sheet of the material depicting the length of the pore at the longest points. (Bottom; right) View of stacked sheets illustrating the porosity retained in the bulk material.

exchange remained fast down to -80 °C on the ^{1}H NMR time scale, suggesting that substitution of the tritopic linker would be viable and the monotopic CNAr^{Dipp2} could possibly act as an integrated modulator.

Deviating slightly from the synthesis of Cu-^{ISO}CN frameworks, addition of a THF solution of 1,3,5-Tris(4-PhCNAr^{Dipp2})C$_6$H$_3$ to a Pd(CNAr^{Dipp2})$_2$ dissolved in toluene, gently heated at 40 °C in a vial yields large orange crystals of Pd-^{ISO}CN-1. Single crystal X-ray diffraction studies reveal the framework to be comprised of trigonal planar, coordinatively unsaturated [Pd(CNR)$_3$] nodes (**Figure 3.5**). Like Cu-^{ISO}CN-5, these Pd nodes form 2D-honeycomb sheets with hexagonal pores measuring 28.4 Å across. Importantly though, unlike Cu-^{ISO}CN-5, the pores of the sheets align to form hexagonal channels containing toluene molecules resolved in the difference map. This could allow for significant realized surface area and allow for exogenous substrates to interact with the metal center. Studies to further understand the physical and chemical characteristics Pd-^{ISO}CN-1, as well as other network formations with 1,3,5-Tris(4-PhCNAr^{Dipp2})C$_6$H$_3$ are underway.

3.1.3 Electrochemical investigation of multitopic *m*-terphenyl isocyanide reductions

Through the synthesis of these multi-aryl, multi-topic linkers we grew curious about the ability of these conjugated systems to be reduced. As a reference point, cyclic voltammograms of the monotopic isocyanides were first collected (**Figure 3.6**). The bulkiest derivative, $CNAr^{Tripp2}$, showed a near irreversible reduction with a $E^{1/2}$ of -3.162 V (referenced to Fc^0/Fc^+) where as $CNAr^{Dipp2}$ and $CNAr^{Mes2}$ both showed pseudo-reversible reductions at about -3.114V. All told, the reductive chemistry of these three species are roughly equivalent. Attempts by numerous students to isolate a reduced version of these isocyanides via alkali metal reduction resulted in a color change at low temperature but eventual decomposition of the aryl-

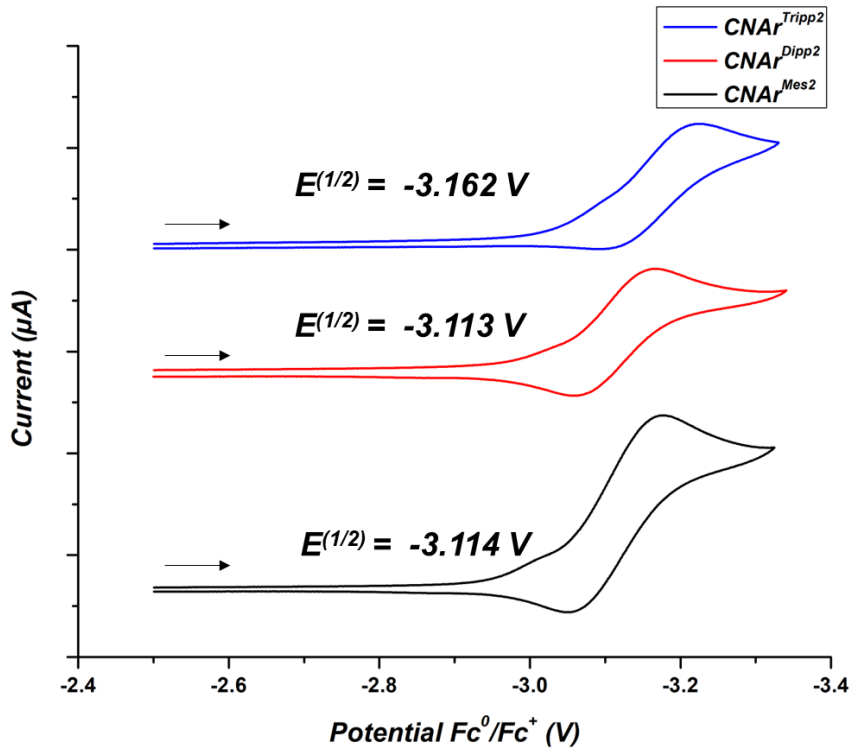

Figure 3.6 Cyclic voltammograms of monotopic isocyanide ligands (top to bottom) $CNAr^{Tripp2}$, $CNAr^{Dipp2}$, and $CNAr^{Mes2}$. All potentials reported to the reversible Ferrocene/Ferrocenium redox couple.

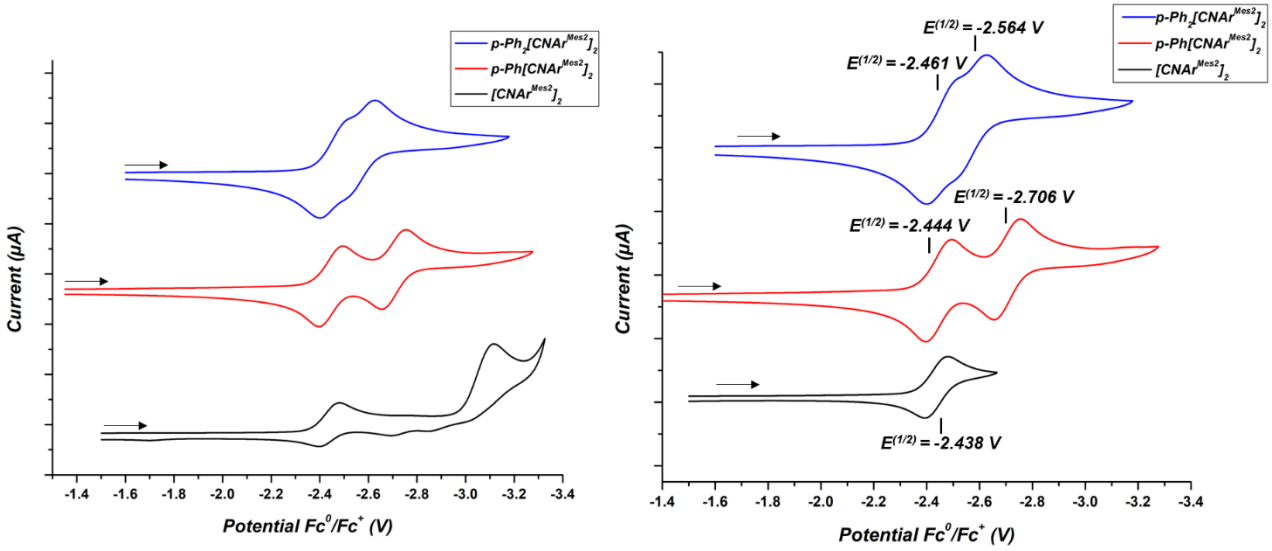

Figure 3.7 Cyclic voltammograms of ditopic isocyanide linker ligands (top to bottom), p-Ph$_2$[CNAr^{Mes2}]$_2$, p-Ph[CNAr^{Mes2}]$_2$, and [CNAr^{Mes2}]$_2$. (Left) Full potential window including irreversible second reduction of [CNAr^{Mes2}]$_2$. (Right) Trimmed potential including only the reversible first reduction of [CNAr^{Mes2}]$_2$.

isocyanides up warming to room temperature. Decomposition products including the H-substituted parent *m*-terphenyl (i.e. HAr^{Tripp2}) suggest loss of CN- might be a possible route.

Cyclic voltammograms of [CNAr^{Mes2}]$_2$, p-Ph[CNAr^{Mes2}]$_2$, and p-Ph$_2$[CNAr^{Mes2}]$_2$, on the other hand, reveal two reductions within the same window (**Figure 3.7**). Each ligand reports a reversible reduction are around -2.4V v Fc^0/Fc^+. The exact $E^{1/2}$ of this reduction shifts to a slightly less negative potential with decreasing length, from -2.461 V for [CNAr^{Mes2}]$_2$ to -2.461 V for p-Ph$_2$[CNAr^{Mes2}]$_2$. The second reduction is considerably more affected by linker length. The second reduction for [CNAr^{Mes2}]$_2$ is in the range of the monotopic ligand reduction at ~-3.1 V and proves to be irreversible at a 100mV/s scan rate. Notably, not scanning out to the second reduction improves reversibility of the first reduction for [CNAr^{Mes2}]$_2$ (**Figure 3.7**). Adding a phenylene spacer considerably reduces the reduction potential and adds reversibility to the second feature. For p-Ph$_2$[CNAr^{Mes2}]$_2$, the second, fully reversible feature is observed at -2.706 V v Fc^0/Fc^+. A second phenylene spacer continues this trend. For p-Ph$_2$[CNAr^{Mes2}]$_2$ the second reduction nearly meets the first with an $E^{1/2}$ of -2.564 V. In contrast to the monotopic ligands, stoichiometric reduction of 1,4-

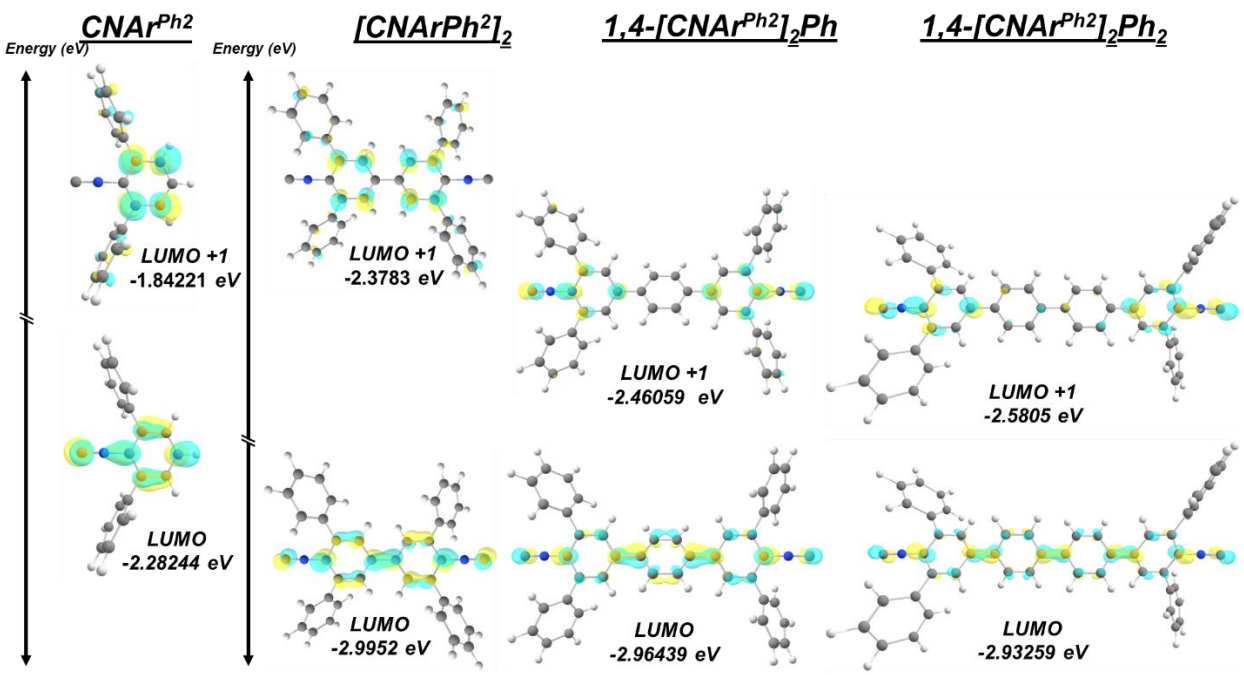

Figure 3.8 Frontier Lowest Unoccupied Molecular Orbitals (LUMOs) for the $CNAr^{Ph2}$, $[CNAr^{Ph2}]_2$, 1,4-$[CNAr^{Ph2}]_2Ph$ and 1,4-$[CNAr^{Ph2}]_2Ph_2$ model ligands. Energies are displayed in labels with the corresponding ligands and loosely represented specially via the axis to the left.

$(CNAr^{Dipp2})_2C_6H_4$ results in a persistent color change to a dark green. Unfortunately, the product was found to be exceedingly air and moisture sensitive, precluding further characterization.

To better understand the reductive chemistry of these *m*-terphenyl isocyanides density functional theory (DFT) calculations were performed on model compounds $CNAr^{Ph2}$, $[CNAr^{Ph2}]_2$, 1,4-$[CNAr^{Ph2}]_2Ph$ and 1,4-$[CNAr^{Ph2}]_2Ph_2$. The relative energies of the LUMOs of these ligands offer a possible explanation for the relative relationship between the reduction potentials of these different ligands. The LUMO of the monotopic $CNAr^{Ph2}$ has CN π* character, in conjugation with the aryl backbone (**Figure 3.8**). The LUMO of the ditopic ligands is similar but is significantly larger, spread-out across the longer backbone of the ligand. The relative energies of these orbitals reflect this difference, dropping from -2.282 eV for $CNAr^{Ph2}$ to -2.995 eV for $[CNAr^{Ph2}]_2$ as the MO more than doubles in length. The differences in LUMO energies for the series of lengthening ditopic ligands is relatively minor decreasing around 0.03 eV for each addition of a Ph spacer. The behavior of the first reductive feature in the CVs for these ligands closely follows the

Table 3.1 Changes in LUMO and LUMO +1 energies compared the changes in reduction potential of the redox features, as a function of increasing ligand length.

ΔE	$CNAr^{Ph2}$ – $[CNArPh^2]_2$	$[CNArPh^2]_2$ – $1,4\text{-}[CNAr^{Ph2}]_2Ph$	$1,4\text{-}[CNAr^{Ph2}]_2Ph$ – $1,4\text{-}[CNAr^{Ph2}]_2Ph_2$
LUMO (eV) / 1^{st} $E^{1/2}$ (V)	-7.127 eV / 0.67 V	-0.031 eV / 0.006 V	-0.031 eV / 0.017 V
LUMO +1 (eV)/ 1^{st} $E^{1/2}$ (V)	---	-0.536 eV / -0.344 V	-0.119 eV / -0.142 V

differences in energy of the LUMOs (**Table 3.1**). From the monotopic, $CNAr^{Ph2}$, to the ditopic, $[CNAr^{Ph2}]_2$, the LUMO energy has a large drop of 0.7127 eV, and the corresponding first reduction potential drops around 0.67 V. The small changes in energies of around ~0.03 eV for the ditopic ligands are matched with small changes in reduction potential of 0.006-0.017 V. The second reduction feature in the ditopic ligands follows a similar pattern, matching the relative changes in energies of the corresponding LUMO +1 orbitals. This data combined with the peak-to-peak separation of the reversible redox features being ~30 mV smaller than the Fc/Fc^+ reference suggests that each of the redox features in the ditopic ligands are $2e^-$ redox processes.

3.2 Concluding remarks and outlook

A new series of multi-topic *m*-terphenyl isocyanide ligands have been synthesized with the intention of synthesizing MOFs containing low-valent and coordinatively unsaturated nodes. Both di- and tritopic linkers based on $CNAr^{Dipp2}$ and $CNAr^{Tripp2}$ have been synthesized to enforce maximum coordination numbers of three at the structure metal nodes. Additionally, a ditopic linker based on $CNAr^{DArF}$ has been successfully synthesized to enable the use of metal carbonyls as metal nodes, a potentially plentiful source of zero and low valent metal centers. Initial studies of 1,3,5-Tris(4-$PhCNAr^{Dipp2}$)C_6H_3 based networks have yielded Cu-^{ISO}CN-5 and Pd-^{ISO}CN-1. Both form 2D, honeycomb sheets with pores around 28 A in diameter. In Cu-^{ISO}CN-5 these sheets stack in a staggered fashion preventing access to the internal structure whereas the sheets in Pd-^{ISO}CN-1 align to form hexagonal channels running through the solid. Studies to discern the chemistry available to the unique, coordinatively unsaturated Pd^0 metal nodes in Pd-^{ISO}CN-1 are underway.

Cyclic voltammograms of these large, conjugated terphenyl isocyanide ligands reveal quasi-reversible reductions for the monotopic ligands at very reducing potentials (<-3.1 V v. Fc/Fc^+). The longer ditopic ligands however, show fully reversible reductions around -2.4 V and a subsequent second reduction that becomes easier to reduce as a function of increasing length. The frontier molecular orbitals offer a potential explanation for the differences re reduction potential between the monotopic, and lengthening ditopic ligands.

3.3 Synthetic procedures and characterization data

General Considerations – All manipulations were carried out under an atmosphere of purified dinitrogen using standard Schlenk and glovebox techniques. Unless otherwise stated, reagent-grade starting materials were purchased from commercial sources and either used as received or purified by standard procedures.[40] Solvents were dried and deoxygenated according to standard procedures.[41] Benzene-d_6 (Cambridge Isotope Laboratories) was distilled from NaK alloy/benzophenone ketyl and stored over 4 Å molecular sieves under N_2 for at least 24 h prior to use. Celite 405 (Fisher Scientific) was dried under vacuum (24 h) at a temperature above 250 ˚C and stored in the glovebox prior to use. The *m*-terphenyl isocyanides $CNAr^{Mes2,}$ $CNAr^{Dipp2}$ and $CNAr^{Tripp2}$ were prepared as previously reported.[26, 42]

Solution ^1H and $^{13}C\{^1H\}$ NMR spectra were recorded on a Bruker Avance 300, a Varian Mercury 400, a Jeol ECA 500, or a Varian X-SENS 500 spectrometer. ^1H and $^{13}C\{^1H\}$ chemical shifts are reported in ppm relative to $SiMe_4$ (^1H and ^{13}C $\delta = 0.0$ ppm) with reference to residual solvent resonances of 7.16 ppm (^1H) and 128.06 ppm (^{13}C) for C_6D_6.[43] Solution FTIR spectra were recorded on a Thermo-Nicolet iS10 FTIR spectrometer. Samples were prepared as C_6D_6 solutions injected into a ThermoFisher solution cell equipped with KBr windows. For solution FTIR spectra, solvent peaks were digitally subtracted from all spectra by comparison with an authentic spectrum obtained immediately prior to that of the sample. The following abbreviations were used for the intensities and characteristics of important IR absorption bands:

vs = very strong, s = strong, m = medium, w = weak, vw = very weak; b = broad, vb = very broad, sh = shoulder. Combustion analyses were performed by Midwest Microlab LLC, Indianapolis, IN.

All cyclic voltammetry (CV) experiments were performed at room temperature under an dinitrogen atmosphere with a Gamry Interface 1010E potentiostat. A single-compartment cell was used for all experiments. Voltammograms were recorded in 0.3M $[NBu_4][PF_6]$ THF solution at υ = 100 mV/s with a 3mm glassy carbon working electrode, a Pt wire counter electrode and a silver wire pseudoreference electrode (Ag/AgCl). Potentials were calibrated against the Fc/Fc^+ redox couple (internal standard). Analyte complex concentrations ranged from 1-1.5 mM.

Synthesis of $H_2N(p\text{-}BrAr^{Dipp2})$. A CH_2Cl_2 solution of $[N(n\text{-}Bu)_4][Br_3]$ (5.8 g, 250 ml, 56 mM) was added quickly to a stirring solution of H_2NAr^{Dipp2} in CH2Cl2 (7.1g, 250 ml, 59 mM, 1.05 eq) under air. The solution changed from orange to light yellow over 10 minute, and the solution was allowed to stir for an additional 5 hours. The mixture was then stripped of volatiles v rotiaary evaporator, and the resultant solid was dissolved in 250 ml Et2O. This solution was washed and extracted with 1 M NaOH (100 ml), deionized water (2 X 100 ml),then dried over $MgSO_4$ and filtered. All volatiles were removed in vacuo, providing a cream-colored solid. Yield, 6.1 g, 88%. ^{1}H NMR (300.1 MHz, $CDCl_3$, 20 ˚C) d = 7.38 (t, 2H, *J* = 8 Hz, *p*-Dipp), 7.25 (d, 4H, *J* = 8 Hz, m-Dipp), 7.11 (s, 2H, *m*-Ar), 3.16 (s, 1H, m-Dipp), 2.74 (sep, 4H, *J* = 7 Hz, *o*-Dipp-C*H*), 1.15 (d, 12H, *J* = 7 Hz, *o*-Dipp-CH_3), 1.11 (d, 12H, *J* = 7 Hz, *o*-Dipp-C*H3*). ^{13}C{^{1}H} NMR (125.7 MHz, CDCl3, 20˚C) δ= 147.8, 141.5, 134.0, 131.3, 128.7 126.8, 123.3, 109.0, 77.3, 77.1, 76.8, 30.5, 24.5 (*o*-Dipp-*C*H), 24.0 (*o*-Dipp-*C*H_3) ppm. FTIR (diamond ATR crystal, 20 ˚C): 3471 (w), 3374 (m), 2960 (s), 2925 (w), 2866 (w), 1592 (s), 1565 (w), 1437 (s), 1362 (m), 807 (s) cm^{-1}. HR-MS (ESI-TOFMS): predicted for [M+H]+ = $C_{30}H_{38}NBr$, 492.2260 , found m/z = 492.2255

Synthesis of $HC(O)HN(p\text{-}BrAr^{Dipp2})$. Formic Acid (2.25 g, 48.9 mmol, 6 eq.) was added dropwise via syringe to stirring acetic anhydride (4.15 g, 49.7 mmol, 5 eq.). The mixture was warmed at 50 ºC for 2 h to generate formyl acetic anhydride, cooled to RT, and transferred to a stirring THF solution of $H_2N(p\text{-}BrAr^{Dipp2})$ (6.1 g, 250 ml, 50 mM) via syringe. Solution was stirred at RT for 48 hours, whereupon all volatiles were removed *in vacuo*. Resulting solid was placed under high-vacuum at 80 ºC for 16 hours to

remove all remaining anhydride and acid. Resulting white solid was triturated with hexanes (1 X 20ml) and dried *in vacuo*. Yield: 94%. ^{1}H NMR (400.1 MHz, $CDCl_3$, 20 ˚C) d = 7.59 (d, 1H, *J* = 8 Hz, *m*-Dipp), 7.41 (t, 2H, *J* = 8 Hz, *p*-Dipp), 7.35 (s, 2H, *m*-Ar) 7.24 (s, 2 H, *m*-Dipp), 6.53 (d, 1H, *m*-Dipp), 2.59 (sep, 4H, *o*-Dipp-C*H*), 1.15 (d, 12H, *o*-Dipp-C*H3*), 1.11 (d, 12H, *o*-Dipp-C*H3*). ^{13}C{^{1}H} NMR (125.7 MHz, CDCl3, 20˚C) δ= 162.1, 146.5, 133.5, 133.4, 133.1, 129.8, 123.9, 77.3, 77.1, 76.8, 30.8, 24.8 (*o*-Dipp-*C*H), 23.2 (*o*-Dipp-*C*H_3) ppm. FTIR (diamond ATR crystal, 20 ˚C): υ(C=O) = 1677; also 3345 (w), 3056 (w), 2957 (m), 2925 (w), 2866 (m), 1568 (w), 1467 (m), 1252 (s), 1219 (m), 810 (s), 752 (s) cm^{-1}. HR-MS (ESI-TOFMS): predicted for [M+H]+ = $C_{31}H_{38}BrNO$, 520.2210, found m/z = 520.2206

Synthesis of HC(O)HN(*p*-(BPin)Ar^{Dipp2}) (Pin = 1,1,2,2-Me$_4$C$_2$O$_2$). In a glovebox atmosphere, a toluene solution of PCy_3 (0.2 g, 10 ml, 70.2 mM, 6 mol %) was added to stirring toluene solution of Pd_2DBA_3 (0.108 g, 10ml, 11.7 mM, 1 mol %, dba = dibenzylideneacetone) and stirred at 50 ºC for 20 minutes. The solution changed from deep maroon to medallion yellow over the course of heating. Solution was cooled to RT, filtered through 0.45 micron ptfe syringe filter, and added to a baffled Morton flask containing a rapidly stirring solution of HC(O)HN(*p*-BrAr^{Dipp2}) (6.1g, 12 mmol) and B_2Pin_2 (3.3g, 13 mmol, 1.1 eq) in toluene (35ml). The solution was heated at 85 ºC for 10 minutes and K_3PO_4 (1.02 g, 4.8 mmol, 5 eq) was added slowly in 0.1 g aliquots, allowing complete dispersion of solid between additions. Solution was stirred at 85 ºC for 48 hrs, periodically monitoring via ^{1}H NMR until SM was consumed. The resulting solution was cooled to RT and, under ambient atmosphere, vacuum filtered through a medium porosity fritted funnel packed with 0.5 cm of basic alumina, and the cake further extracted with THF (2 X 5 ml). Volatiles were removed *in vacuo*, resulting in free-flowing light-yellow solid. Solid was triturated with hexanes (2 X 5 ml) giving an off-white solid. Yield: 6.2 grams, 93%.^{1}H NMR (400.1 MHz, $CDCl_3$, 20 ˚C) d = 8.11 (s, 2H, *m*-Dipp), 7.27 (t, 2H, *J* = 7 Hz, *p*-Dipp), 7.13 (d, 4H, J = 8 Hz, *m*-Dipp) 2.90 (sep, 4 H, *o*-Dipp-C*H*), 6.53 (d, 1H, m-Dipp), 2.59 (sep, 4H, *J* = 7 Hz *o*-Dipp-C*H*), 1.12 (d, 12H, *J* = 7 Hz *o*-Dipp-C*H3*), 1.03 (m, 12H, *o*-Dipp-CH_3)

Synthesis of 1,4-(HC(O)HNAr^{Dipp2})$_2$C$_6$H$_4$. In a glovebox atmosphere, SPhos (17.3 mg, 10 ml, 6 mol %) was added as solid to stirring toluene solution of Pd_2DBA_3 (10.8 mg, 1.5 mol %, DBA =

dibenzylideneacetone) and stirred at 50 ºC for 30 minutes. The solution changed from deep maroon to medallion yellow over the course of heating. Solution was cooled to RT, filtered through 0.45 micron PTFE syringe filter. Pd solution was added to a three-neck Morton flask containing a rapidly stirring solution of HC(O)HN(*p*-BPinAr^{Dipp2}) (0.456 g, 0.786 mmol, 2 eq) and 1,4-dibromobenzene (0.996 g, 0.228 mmol, 1 eq) in 250ml toluene. The pale-yellow solution was warmed to 80 ºC over 30 minutes, then BaOH (986. g, 29.2 mmol, 8 eq) was added slowly in 0.1 g aliquots, allowing complete dispersion of solid between additions. Solution was stirred for 16 hrs, whereupon BaOH (0.672 g, 3.84 mmol, 10 eq) was added slowly in 3 portions. Reaction was monitored twice daily for conversion until starting material was consumed. Upon completion, reaction mixture was transferred to ambient atmosphere and vacuum filtered through a medium porosity fritted funnel packed with 0.5 cm of basic alumina. Solution was dried *in vacuo* and resulting pale-yellow solid was triturated with heptane (2 X 20 ml). Solids were dried under high-vacuum for 24 hours at RT, resulting in a free-flowing off white powder. Yield: 0.410 g, 0.463 mmol, 59%. ^{1}H NMR (400.1 MHz, C_6D_6, 20 ˚C): δ = 8.12 (s, 4H, C_6H_4), 7.27 (t, 4H, J = 8 Hz, *p*-Dipp), 7.14 (d, 8H, J = 8 Hz, *m*-Dipp), 6.79 (s, 4H, *m*-Ar), 2.90 (septet, 8H, J = 7 Hz, $CH(CH_3)_2$), 1.03 (d, 24H, J = 7 Hz, $CH(CH_3)_2$), 1.02 (d, 24H, J = 7 Hz, $CH(CH_3)_2$) ppm.

Synthesis of 1,4-(CNAr^{Dipp2})$_2$C$_6$H$_4$. . Under an air-free atmosphere, to a stirring CH_2Cl_2 solution of 4-(HC(O)HNAr^{Dipp2})$_2$C$_6$H$_4$ (0.300 g, 0.305 mmol, 1 equiv) diisopropylamine (0.30 mL, 2.13 mmol, 7 equiv) was added via syringe. After stirring for 5 min, $OPCl_3$ (0.14 mL, 1.52 mmol, 5 equiv) was added dropwise via syringe and the solution was stirred for 24 h. Water (100 mL) was added and the resulting mixture and stirred for 2 h. The organic and aqueous layers were then separated, and the organic layer was washed with 50 mL H_2O. The aqueous layers were combined and extracted with CH_2Cl_2 (3 × 150 mL). The organic extracts were combined and dried over $MgSO_4$, filtered, and volatiles were removed by rotary evaporation. The resultant solid was washed with cold acetonitrile, collected by filtration, and dried under reduced pressure. Yield: 0.24 g, 0.26 mmol, 85% ^{1}H NMR (499.8 MHz, $CDCl_3$, 20 ˚C): δ = 7.71 (s, 4H, C_6H_4), 7.56 (s, 4H, *m*-Ar), 7.44 (t, 4H, J = 8 Hz, *p*-Dipp), 7.29 (d, 8H, J = 8 Hz, *m*-Dipp), 2.60 (septet, 8H, J = 7 Hz, $CH(CH_3)_2$), 1.20 (d, 24H, J = 7 Hz, $CH(CH_3)_2$), 1.17 (d, 24H, J = 7 Hz, $CH(CH_3)_2$) ppm. ^{13}C{^{1}H}

NMR (125.8MHz, $CDCl_3$, 20 ˚C): δ = 169.3 (CNR), 146.6, 140.2, 139.8, 139.0, 134.3, 129.3, 127.9, 127.7, 123.3, 31.3, 24.7, 24.1 ppm. FTIR (C_6D_6, KBr windows, 20 ˚C, 20 ˚C): υ(CN) = 2116; also 2962 (s), 2927 (m), 2870 (w), 1697 (s), 1594.9(w), 1465 (s), 1431 (s), 1385 (m), 1363 (m), 1261 (w), 1234(w), 1055 (w) cm^{-1}.

Synthesis of 1,3,5-(HC(O)HN(Ar^{Dipp2})C_6H_4)$_3C_6H_3$. In a glovebox atmosphere, a toluene solution of PCy_3 (184 mg, 50 ml, 13.1 mM, 6 mol %) was added to stirring toluene solution of Pd_2DBA_3 (100 mg, 50 ml, 2.2 mM, 1 mol %, dba = dibenzylideneacetone) and stirred at 50 ºC for 30 minutes. The solution changed from deep maroon to medallion yellow over the course of heating. Solution was cooled to RT, filtered through 0.45 micron ptfe syringe filter. Pd solution was added to a baffled Morton flask containing a rapidly stirring solution of HC(O)HN(*p*-BPinAr^{Dipp2}) (6.2g, 10.9mmol, 3 eq) and 1,3,5-Tris(4-bromophenyl)benzene (1.98g, 3.65 mmol, 1 eq) in 250ml toluene. The pale-yellow solution was warmed to 80 ºC over 30 minutes, then K_3PO_4 (6.2 g, 29.2 mmol, 8 eq) was added slowly in 0.1 g aliquots, allowing complete dispersion of solid between additions. Solution was stirred for 16 hrs, whereupon BaOH (5 g, 29.2 mmol, 8 eq) was added slowly in 0.1g aliquots. Addition of BaOH was repeated every 24 hours for 5 days (total 25 g, 146 mmol, 40 eq). Added KO*t*Bu (0.5 g, 4.5 mmol, 1.2 eq) slowly in 0.1 gram aliquots. Addition of KO*t*Bu was repeated every 24 hours for 5 days (total 2.5 g, 22.5 mmol, 6 eq). Reaction was monitored twice daily for conversion until starting material was consumed. Upon completion, reaction mixture was transferred to ambient atmosphere and vacuum filtered through a medium porosity fritted funnel packed with 0.5 cm of basic alumina. Solution was dried *in vacuo* and resulting pale-yellow solid was triturated with heptane (2 X 20 ml), followed by trituration with acetonitrile (3 x 20 ml). Decanted solvent was collected concentrated and recrystallized from 1:1 THF:acetonitrile. Solids were dried under high-vacuum for 24 hours at RT, resulting in a free-flowing white powder. Yield: 4.4 g, 3.78 mmol, 72%. ^{1}H NMR (499.9 MHz, $CDCl_3$, 20 ˚C): δ = 8.46 (s, 3H, (O)CH), 7.77 (s, 3H, C_6H_3), 7.71 (d, 6H, J = 8 Hz, (C_6H_4)), 7.65 (d, 6H, J = 8 Hz, (C_6H_4)), 7.59 (s, 6H, m-Ar), 7.37 (t, 6H, J = 8 Hz, p-Dipp), 7.23 (d, 12H, J = 8 Hz, m-Dipp), 6.62 (d, 3H, J = 11 Hz NHC(O)), 2.65 (septet, 12H, J = 7 Hz, $CH(CH_3)_2$), 1.11 (d, 36H, J = 7 Hz, $CH(CH_3)_2$), 1.09 (d, 36H, J = 7 Hz, $CH(CH_3)_2$) ppm. $^{13}C\{^1H\}$ NMR (125.8MHz, $CDCl_3$, 20 ˚C):

δ = 162.5,146.7, 141.9, 140.3, 138.9, 136.2, 134.8, 132.9, 132.1, 129.6, 128.9, 128.0, 127.3, 124.0, 31.0, 25.7, 25.1, 23.3 ppm. FTIR ($CDCl_3$, KBr windows, 20 ˚C, 20 ˚C): υ(C=O) = 1679; also 2966 (s), 2931 (m), 2869 (w), 1679 (s), 1465 (w), 1272 (w) cm^{-1}.

S1.5 Synthesis of 1,3,5-(CN(Ar^{Dipp2})C_6H_4)$_3C_6H_3$. Under an air-free atmosphere, to a stirring CH_2Cl_2 solution of 1,3,5-(HC(O)HN(Ar^{Dipp2})C_6H_4)$_3C_6H_3$ (3.40 g, 3.42 mmol, 1 equiv) diisopropylamine (10.1 mL, 71.8 mmol, 21 equiv) was added via syringe. After stirring for 5 min, $OPCl_3$ (4.85 mL, 51.3 mmol, 15 equiv) was added dropwise via syringe and the solution was stirred for 24 h. Water (100 mL) was added and the resulting mixture was stirred for 2 h. The organic and aqueous layers were then separated, and the organic layer was washed with 50 mL H_2O. The aqueous layers were combined and extracted with CH_2Cl_2 (3 × 150 mL). The organic extracts were combined and dried over $MgSO_4$, filtered, and volatiles were removed by rotary evaporation. The resultant solid was washed with cold acetonitrile, collected by filtration, and dried under reduced pressure. Yield: 3.6 g, 2.3 mmol, 66% ^{1}H NMR (499.9 MHz, $CDCl_3$, 20 ˚C): δ = 7.85 (s, 3H, C_6H_3), 7.80 (d, 6H, J = 8 Hz, (C_6H_4)), 7.74 (d, 6H, J = 8 Hz, (C_6H_4)), 7.59 (s, 6H, m-Ar), 7.43 (t, 6H, J = 8 Hz, p-Dipp), 7.29 (d, 12H, J = 8 Hz, m-Dipp), 2.62 (septet, 12H, J = 7 Hz, $CH(CH_3)_2$), 1.20 (d, 36H, J = 7 Hz, $CH(CH_3)_2$), 1.18 (d, 36H, J = 7 Hz, $CH(CH_3)_2$) ppm. $^{13}C\{^1H\}$ NMR (125.8MHz, C_6D_6, 20 ˚C): δ = 169.0 (s, CNR), 146.5, 141.8, 140.8, 140.4, 139.6, 138.4, 134.3, 129.2, 128.0, 127.9, 127.7, 127.6, 127.3, 125.9, 125.3, 123.9, 123.2, 123.1, 31.2, 30.8, 24.5, 24.0 ppm. FTIR (diamond ATR crystal, 20 ˚C) υ(C≡N) = 2113; also 3053 (w), 2959 (vs) cm^{-1} 2926 (m), 2866 (m), 1774 (w), 1699 (w), 1594 (m), 1463 (s), 1057 (m) cm^{-1}.

Synthesis of OP(Ar^{Dipp2}NH$_2$)$_3$. A resealable ampoule was charged with p-Br-Ar^{Dipp2}NH$_2$ (0.500 g, 1.02 mmol), $PdCl_2$(dppf) (0.113 g, 0.113 mmol, 15 mol %), B_2Pin_2 (0.613 g, 1.02 mmol, 1 eq.), KOAc (0.646 g, 6.59 mmol, 3 eq.), and dioxane (7 ml). The ampoule was then sealed under an N_2 atmosphere and stirred at 80 ˚C for 14 h. The resultant red mixture was cooled and all volatiles were removed under reduced pressure. The residue was then purified by column chromatography (silica gel, with Celite packing on top using a 2% EtOAc/hexanes solution). The fractions were collected and concentrated to a solid by rotatory evaporation to afford a colorless solid. X-ray quality crystals were formed via slow evaporation of the

column fraction. Yield: 0.20 g, 0.156 mmol, 69%. ^{1}H NMR (499.9 MHz, $CDCl_3$, 20 ˚C): δ = 7.85 (d, 3H, J = 11 Hz, *m*-Ar), 7.31 (t, 6H, J = 8 Hz, *p*-Dipp), 7.15 (d, 12H, J = 8 Hz, *m*-Dipp), 2.52 (septet, 12H, J = 7 Hz, $CH(CH_3)_2$), 1.02 (d, 36H, J = 7 Hz, $CH(CH_3)_2$), 0.076 (d, 36H, J = 7 Hz, $CH(CH_3)_2$) ppm. $^{13}C\{^{1}H\}$ NMR (125.8MHz, C_6D_6, 20 ˚C): δ = 147.9, 134.4, 132.6 (d, J = 11.5 Hz), 128.7 (t, J = 12.3Hz), 124.4 (d, J = 18.6 Hz), 30.6, 24.1, 23.99.

Synthesis of Cu^{Iso}CN-5. Under an air-free atmosphere, a THF solution of 1,3,5-$(CN(Ar^{Dipp2})C_6H_4)_3C_6H_3$ (20mg, 2ml, 6.4 mM) was added dropwise over 2 minutes to a rapidly stirring THF solution of $[Cu(MeCN)_4]PF_6$ (4.7 mg, 6.4 mM). A white precipitant began to persist after half of the isocyanide was added. The combined reagents were allowed to stir for 40 min, and an amorphous suspension was deposited on the tube wall. The supernatant was removed, and the solid was gently washed with THF (3 X 5 ml). Upon removal of the final wash, with residual solvent remaining, the tube was sealed with a Teflon screw cap equipped with a Viton O-ring. The tube was placed in an oven at 100 ºC for 24 h. tube was removed from oven and allowed to cool to room temperature. In place of the amorphous polymer was a colorless crystalline solid, with single crystals that could be selected for X-ray crystallographic analysis. Bulk collection of the material is performed via the addition of 5 ml THF, followed by 30 min sonication in a room temperature bath, the supernatant was decanted. Wash was repeated 3 times, then all volatiles are removed in vacuo to afford microcrystalline Cu^{ISO}CN-5. Yield: 0.007 g. ATR-IR spectrum and Powder X-ray diffraction pattern are displayed below.

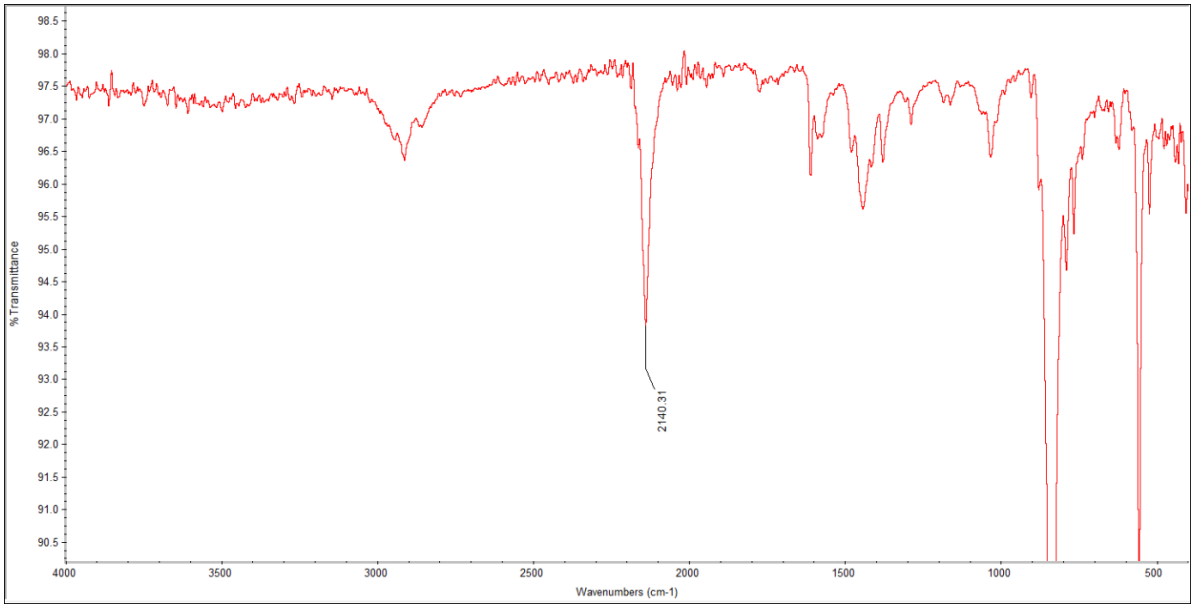

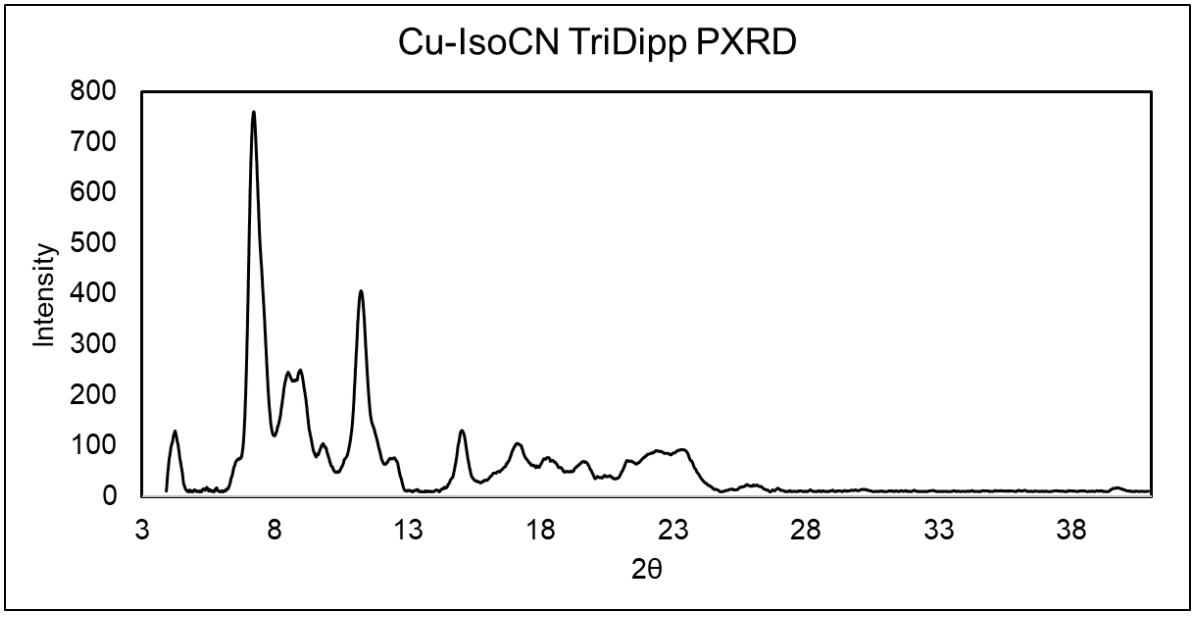

Synthesis of Pd^{Iso}CN-1. Under an air-free atmosphere, 1,3,5-(CN(Ar^{Dipp2})C$_6$H$_4$)$_3$C$_6$H$_3$ (20 mg, 12.7 µmol) was dissolved in a mixture of toluene (2 ml) and THF (0.8 ml) in an 11 dram vial. The solution was heated to 40 ºC and, upon full dissolution of solid, a preheated toluene solution of Pd(CNAr^{Dipp2})$_2$ (13.4 mg, 2ml, 7 mM) was added dropwise over 2 minutes with rapid stirring. The solution changed in color from lemon-yellow to cinnabar over the course of 5 minutes. The solution was stirred at 40 ºC for 20 minutes as a translucent colorless polymer slowly deposited on

the sides of the vial. The stir bar was removed, and the solution was maintained at 40 ºC for 48 hours, then cooled to room temperature. Single crystals had formed along the wall of the vial that could be selected for X-ray crystallographic analysis. Yield: 0.003 g. ATR-IR spectrum displayed below.

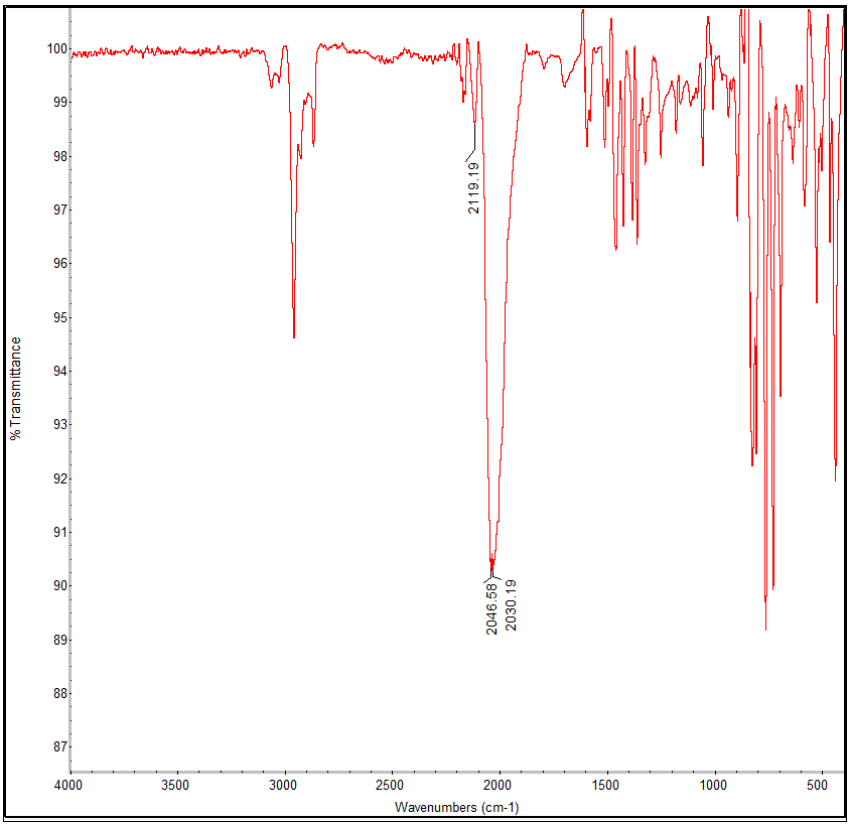

3.4 Details of DFT computational studies

General Computational Details: Density Functional Theory (DFT) calculations were performed with ORCA 4.0.0 program suite and/or the Gaussian 16 software package.[44-45] Geometry optimizations, were performed using the BP86 functional[46-47] in conjunction with the Def2TZVP/Def2TZVPP basis sets[48-49]. Atomic coordinates obtained by single-crystal X-ray diffraction analysis on $CNAr^{Dipp2}$ were used as the starting point for optimizations on the truncated model, $CNAr^{Ph2}$. *ChemCraft 1.8* was used for visualization of geometry optimized structures and molecular orbitals (MO).[50]

Input file for model of $CNAr^{Ph2}$.

```
%chk=Ph_0.chk
%nprocs=8
%mem=22GB
# opt freq=noraman pop=full bp86/def2tzvp int=superfinegrid geom=connectivity

Ph_0 opt freq

0 1
 N          0.00000000   -0.00010000   -1.35760000
 C          0.00010000    0.00000000   -2.52650000
 C          0.00000000    0.00000000    0.02710000
 C         -4.40450000    1.19800000   -0.97470000
 H         -4.89430000    2.12990000   -1.22750000
```

C	-5.02520000	-0.00030000	-1.28700000
H	-5.99070000	-0.00040000	-1.77760000
C	-4.40430000	-1.19850000	-0.97470000
H	-4.89390000	-2.13050000	-1.22760000
C	-3.16090000	-1.22420000	-0.34400000
C	-1.23160000	0.00000000	0.70520000
C	1.23170000	0.00010000	0.70520000
C	1.20290000	0.00010000	2.09840000
H	2.14110000	0.00020000	2.63790000
C	0.00000000	0.00010000	2.79110000
H	0.00000000	0.00020000	3.87380000
C	-1.20290000	0.00000000	2.09830000
H	-2.14110000	0.00000000	2.63790000
C	2.54190000	0.00010000	-0.02150000
C	3.16090000	1.22410000	-0.34400000
C	4.40430000	1.19850000	-0.97470000
H	4.89390000	2.13050000	-1.22760000
C	5.02520000	0.00030000	-1.28700000
H	5.99070000	0.00030000	-1.77770000
C	4.40450000	-1.19810000	-0.97470000
H	4.89420000	-2.13000000	-1.22750000
C	3.16110000	-1.22390000	-0.34390000
C	-3.16110000	1.22390000	-0.34400000
C	-2.54190000	-0.00010000	-0.02150000
H	2.68220000	2.16290000	-0.10760000
H	2.68250000	-2.16270000	-0.10730000

H -2.68250000 2.16280000 -0.10760000

H -2.68220000 -2.16300000 -0.10760000

1 2 2.0 3 1.0

2

3 11 2.0 12 1.0

4 5 1.0 6 2.0 28 1.0

5

6 7 1.0 8 1.0

7

8 9 1.0 10 2.0

9

10 29 1.0 33 1.0

11 17 1.0 29 1.0

12 13 2.0 19 1.0

13 14 1.0 15 1.0

14

15 16 1.0 17 2.0

16

17 18 1.0

18

19 20 2.0 27 1.0

20 21 1.0 30 1.0

21 22 1.0 23 2.0

22

23 24 1.0 25 1.0

24

25 26 1.0 27 2.0

26

27 31 1.0

28 29 2.0 32 1.0

29

30

31

32

33

Optimized Cartesian Coordinates for Model of $CNAr^{Ph2}$.

N	0.000000000	-1.183217000	-0.000017000
C	0.000028000	-2.366233000	0.000036000
C	-0.000001000	0.202119000	-0.000004000
C	-4.392401000	-0.847764000	-1.208705000
H	-4.867419000	-1.107341000	-2.156895000
C	-5.009698000	-1.181820000	0.000031000
H	-5.968739000	-1.703388000	0.000036000
C	-4.392158000	-0.848187000	1.208760000
H	-4.866986000	-1.108095000	2.156954000
C	-3.163112000	-0.183095000	1.209573000
C	-1.235903000	0.890335000	0.000012000
C	1.235900000	0.890336000	-0.000004000
C	1.209801000	2.290876000	0.000010000
H	2.158014000	2.831532000	0.000008000
C	-0.000002000	2.987973000	0.000022000
H	-0.000003000	4.079528000	0.000033000
C	-1.209805000	2.290875000	0.000023000
H	-2.158018000	2.831530000	0.000035000
C	2.536876000	0.156988000	-0.000020000
C	3.163115000	-0.183065000	-1.209581000
C	4.392161000	-0.848157000	-1.208777000
H	4.866994000	-1.108044000	-2.156974000
C	5.009696000	-1.181816000	-0.000052000
H	5.968737000	-1.703384000	-0.000064000
C	4.392393000	-0.847788000	1.208689000
H	4.867407000	-1.107386000	2.156874000

C	3.163348000	-0.182694000	1.209524000
C	-3.163356000	-0.182669000	-1.209532000
C	-2.536878000	0.156986000	0.000017000
H	2.680969000	0.074259000	-2.155107000
H	2.681381000	0.074920000	2.155064000
H	-2.681394000	0.074966000	-2.155068000
H	-2.680961000	0.074209000	2.155103000

Input file for model of [CNAr^{Ph2}]$_2$.

%chk=PhPh.chk

%nprocs=8

%mem=21GB

opt geom=connectivity bp86 def2tzvp int=superfinegrid

PhPh opt

0 1

C	3.18743813	7.09379403	10.27319610
C	5.03375584	7.54187781	11.76310543
C	3.72112675	6.85869317	11.46113140
C	3.86727570	7.92714762	9.24592700
H	3.43935886	8.02826752	8.29297865
C	4.97091376	8.59183374	9.57348905
C	1.86116895	6.57929252	9.84782549
C	5.62550577	8.32476907	10.86191005
H	6.52123403	8.79417935	11.08554294
C	6.71606662	6.49179277	13.21294246
C	5.69204211	7.35538333	13.05516337

C	0.77474759	7.20638140	10.30905571
C	5.19067262	8.19584101	14.18274668
C	1.75038051	5.42234850	8.89521903
C	-0.56412105	6.76023978	9.84558444
H	-1.41261355	7.24551229	10.19708082
C	0.53175171	5.03532070	8.49239887
H	0.41000590	4.23798551	7.84025524
C	7.34046712	6.38331012	14.56719454
H	8.11657365	5.70994092	14.73098298
C	-0.67592630	5.74365302	8.97851471
H	-1.60728735	5.44196039	8.63681573
C	5.78146384	8.09696764	15.37803441
H	5.47291062	8.67822655	16.18219504
C	6.89898150	7.14569540	15.58080603
H	7.32962011	7.07862268	16.51893419
C	7.36210005	11.12905365	7.95051408
C	5.50586708	10.66149914	6.47765877
C	6.79113454	11.35087040	6.74713074
C	6.69247300	10.28631375	8.98156046
H	7.12506250	10.18433792	9.92973755
C	5.58610460	9.61433983	8.65977847
C	8.68385245	11.65225783	8.36732334
C	4.92711702	9.87461621	7.37790326
H	4.03185738	9.39784105	7.15552309
C	3.80190345	11.70070744	5.03473278
C	4.83676265	10.84566819	5.18669596

C	9.76909489	11.03381119	7.89629041
C	5.33509468	10.01133785	4.05173680
C	8.78781021	12.80749081	9.31924087
C	11.10679260	11.49135432	8.35054585
H	11.95699330	11.01410953	7.99230064
C	10.00530719	13.20488637	9.71380459
H	10.12475474	14.00245498	10.36599689
C	3.16627858	11.80534039	3.68491353
H	2.38308675	12.47213284	3.52754306
C	11.21578690	12.50787706	9.21810961
H	12.14685080	12.81714197	9.55382536
C	4.73442333	10.10653490	2.86076169
H	5.04237732	9.52900539	2.05373899
C	3.60715831	11.04816252	2.66723592
H	3.16951204	11.11280725	1.73221727
N	3.13326901	5.90499827	12.43852429
C	2.72163995	5.17852315	13.22542286
N	7.36334668	12.31259859	5.76837842
C	7.80467906	13.05430619	5.01357723
H	6.13592677	9.32309681	4.20718910
H	3.45858959	12.29983813	5.84064605
H	7.05890452	5.88827195	12.41020934
H	4.39625753	8.89055894	14.02060662
H	0.86754504	8.03396716	10.95687184
H	2.61877118	4.90568234	8.55157491
H	7.91688454	13.31642974	9.66920666

H 9.67841635 10.20673916 7.24754238

1 3 2.0 4 1.0 7 1.0

2 3 1.0 8 2.0 11 1.0

3 53 1.0

4 5 1.0 6 2.0

5

6 8 1.0 32 1.0

7 12 2.0 14 1.0

8 9 1.0

9

10 11 2.0 19 1.0 59 1.0

11 13 1.0

12 15 1.0 61 1.0

13 23 2.0 60 1.0

14 17 2.0 62 1.0

15 16 1.0 21 2.0

16

17 18 1.0 21 1.0

18

19 20 1.0 25 2.0

20

21 22 1.0

22

23 24 1.0 25 1.0

24

25 26 1.0

26

27 29 2.0 30 1.0 33 1.0

28 29 1.0 34 2.0 37 1.0

29 55 1.0

30 31 1.0 32 2.0

31

32 34 1.0

33 38 2.0 40 1.0

34 35 1.0

35

36 37 2.0 45 1.0 58 1.0

37 39 1.0

38 41 1.0 64 1.0

39 49 2.0 57 1.0

40 43 2.0 63 1.0

41 42 1.0 47 2.0

42

43 44 1.0 47 1.0

44

45 46 1.0 51 2.0

46

47 48 1.0

48

49 50 1.0 51 1.0

50

51 52 1.0

52

53 54 3.0

54

55 56 3.0

56

57

58

59

60

61

62

63

64

Optimized Cartesian Coordinates for Model of [CNAr^{Ph2}]$_2$.

C	-2.871481000	1.173111000	0.327516000
C	-2.855346000	-1.181643000	-0.426237000
C	-3.558405000	-0.003055000	-0.068165000
C	-1.471163000	1.145506000	0.338396000
H	-0.943727000	2.036122000	0.684193000
C	-0.740930000	0.000556000	-0.018388000
C	-3.575335000	2.422876000	0.718660000
C	-1.455451000	-1.148320000	-0.392292000
H	-0.914546000	-2.052289000	-0.677491000
C	-3.142517000	-3.068292000	-2.046719000
C	-3.540193000	-2.428517000	-0.858473000
C	-4.579797000	2.426661000	1.702455000
C	-4.552894000	-3.019750000	-0.082654000
C	-3.204719000	3.646095000	0.130752000
C	-5.191756000	3.620303000	2.088486000
H	-5.965182000	3.604702000	2.858752000
C	-3.823352000	4.838560000	0.512104000
H	-3.530926000	5.776444000	0.035736000
C	-3.743380000	-4.262440000	-2.450438000
H	-3.429530000	-4.738103000	-3.381704000

C	-4.818131000	4.829510000	1.493964000
H	-5.302735000	5.760819000	1.793162000
C	-5.147039000	-4.217539000	-0.483436000
H	-5.927328000	-4.665212000	0.135024000
C	-4.746926000	-4.841892000	-1.668866000
H	-5.217432000	-5.775450000	-1.983187000
C	2.855339000	-1.181815000	0.426114000
C	2.871617000	1.172990000	-0.327519000
C	3.558455000	-0.003201000	0.068176000
C	1.455453000	-1.148431000	0.392100000
H	0.914507000	-2.052406000	0.677194000
C	0.741003000	0.000513000	0.018226000
C	3.540068000	-2.428751000	0.858358000
C	1.471288000	1.145415000	-0.338488000
H	0.943883000	2.036022000	-0.684351000
C	3.204848000	3.645982000	-0.130858000
C	3.575524000	2.422719000	-0.718606000
C	4.553094000	-3.019863000	0.082910000
C	4.580151000	2.426423000	-1.702273000
C	3.141837000	-3.068788000	2.046309000
C	5.147048000	-4.217749000	0.483726000
H	5.927600000	-4.665273000	-0.134509000
C	3.742488000	-4.263008000	2.450061000
H	3.428194000	-4.738873000	3.381075000
C	3.823545000	4.838425000	-0.512219000
H	3.531024000	5.776334000	-0.035962000
C	4.746390000	-4.842331000	1.668835000
H	5.216715000	-5.775960000	1.983207000
C	5.192193000	3.620017000	-2.088268000
H	5.965766000	3.604386000	-2.858386000
C	4.818486000	4.829288000	-1.493903000
H	5.303163000	5.760553000	-1.793127000
N	-4.937701000	0.023625000	-0.178450000
C	-6.115201000	0.053740000	-0.292917000
N	4.937739000	0.023547000	0.178699000
C	6.115215000	0.053783000	0.293370000
H	4.874109000	1.490362000	-2.179240000
H	2.439825000	3.655000000	0.648684000
H	-2.369677000	-2.610874000	-2.668387000
H	-4.867603000	-2.546604000	0.848544000
H	-4.873749000	1.490638000	2.179512000
H	-2.439792000	3.654978000	-0.648886000
H	2.368728000	-2.611450000	2.667699000
H	4.868277000	-2.546593000	-0.848068000

Input file for model of 1,4-[CNAr^{Ph2}]$_2$Ph.

%chk=PhPhPh.chk

%nprocs=8

%mem=21GB

opt geom=connectivity bp86 def2tzvp int=superfinegrid

PhPhPh optimization

0 1

C	2.45220000	5.54720000	11.50560000
C	4.24120000	6.00950000	13.06090000
C	3.05840000	5.32790000	12.76920000
C	3.05070000	6.39990000	10.61940000
H	2.64370000	6.53030000	9.77020000
C	4.22940000	7.08510000	10.90380000
C	4.78870000	8.09520000	9.97570000
C	5.90190000	10.22450000	9.63480000
H	6.31360000	10.99280000	10.01110000
C	1.08410000	5.00940000	11.12810000
C	4.79630000	6.85760000	12.15100000
H	5.59870000	7.31050000	12.37940000
C	5.94540000	4.96490000	14.58530000
C	4.89270000	5.86480000	14.44120000
C	5.42080000	9.22260000	10.46080000
H	5.53050000	9.31550000	11.39930000
C	-0.04820000	5.70380000	11.59310000
C	4.45520000	6.70290000	15.46410000
C	0.96960000	3.92750000	10.28020000

C	-1.29070000	5.25880000	11.19190000
H	-2.07220000	5.68180000	11.52470000
C	-0.31320000	3.55530000	9.87360000
H	-0.40760000	2.82380000	9.27410000
C	6.55360000	4.88840000	15.86530000
H	7.27260000	4.28710000	16.01550000
C	-1.40800000	4.18410000	10.29120000
H	-2.26350000	3.91020000	9.98350000
C	5.09790000	6.55460000	16.72040000
H	4.80560000	7.08570000	17.45270000
C	6.09030000	5.69830000	16.90460000
H	6.49690000	5.63380000	17.76030000
C	8.11640000	12.65240000	6.72830000
C	6.32740000	12.19010000	5.17290000
C	7.51020000	12.87170000	5.46470000
C	7.51780000	11.79970000	7.61450000
H	7.92490000	11.66930000	8.46370000
C	6.33920000	11.11450000	7.33000000
C	5.77980000	10.10440000	8.25810000
C	4.66670000	7.97510000	8.59910000
H	4.25490000	7.20680000	8.22280000
C	9.48440000	13.19020000	7.10570000
C	5.77230000	11.34200000	6.08280000
H	4.96980000	10.88910000	5.85440000
C	4.62320000	13.23470000	3.64860000
C	5.67590000	12.33480000	3.79260000

C	5.14780000	8.97700000	7.77310000
H	5.03810000	8.88410000	6.83460000
C	10.61680000	12.49580000	6.64080000
C	6.11340000	11.49670000	2.76970000
C	9.59900000	14.27210000	7.95360000
C	11.85930000	12.94080000	7.04190000
H	12.64080000	12.51780000	6.70910000
C	10.88180000	14.64430000	8.36020000
H	10.97620000	15.37580000	8.95980000
C	4.01490000	13.31120000	2.36860000
H	3.29600000	13.91250000	2.21830000
C	11.97660000	14.01550000	7.94270000
H	12.83210000	14.28940000	8.25040000
C	5.47070000	11.64500000	1.51340000
H	5.76300000	11.11390000	0.78120000
C	4.47830000	12.50130000	1.32920000
H	4.07170000	12.56580000	0.47360000
N	2.42860000	4.36380000	13.79170000
C	1.95280000	3.63550000	14.56410000
N	8.14000000	13.83580000	4.44230000
C	8.61580000	14.56410000	3.66990000
H	6.89244375	10.77943738	2.92307915
H	4.28849263	13.84025564	4.46479442
H	6.28016708	4.35933888	13.76913413
H	3.67615625	7.42016262	15.31072085
H	0.05168183	6.55142955	12.23842764

H 1.83360825 3.39220621 9.94575972

H 8.73501472 14.80742080 8.28805638

H 10.51693442 11.64809861 5.99556421

1 3 1.5 4 2.0 10 1.0

2 3 1.5 11 2.0 14 1.0

3 63 1.0

4 5 1.0 6 1.5

5

6 7 1.0 11 1.5

7 15 2.0 39 1.5

8 9 1.0 15 2.0 38 1.5

9

10 17 1.5 19 2.0

11 12 1.0

12

13 14 1.5 24 1.5 69 1.0

14 18 1.5

15 16 1.0

16

17 20 2.0 71 1.0

18 28 1.5 70 1.0

19 22 1.5 72 1.0

20 21 1.0 26 1.5

21

22 23 1.0 26 2.0

23

24 25 1.0 30 1.5

25

26 27 1.0

27

28 29 1.0 30 2.0

29

30 31 1.0

31

32 34 1.5 35 2.0 41 1.0

33 34 1.5 42 2.0 45 1.0

34 65 1.0

35 36 1.0 37 1.5

36

37 38 1.0 42 1.5

38 46 2.0

39 40 1.0 46 2.0

40

41 48 1.5 50 2.0

42 43 1.0

43

44 45 1.5 55 1.5 68 1.0

45 49 1.5

46 47 1.0

47

48 51 2.0 74 1.0

49 59 1.5 67 1.0

50 53 1.5 73 1.0

51 52 1.0 57 1.5

52

53 54 1.0 57 2.0

54

55 56 1.0 61 1.5

56

57 58 1.0

58

59 60 1.0 61 2.0

60

61 62 1.0

62

63 64 3.0

64

65 66 3.0

66

67

68

69

70

71

72

73

74

1 3 2.0 4 1.0 10 1.0

2 3 1.0 11 2.0 14 1.0

3 143 1.0

4 5 1.0 6 2.0

5

6 7 1.0 11 1.0

7 15 2.0 79 1.0

8 9 1.0 15 1.0 78 2.0

9

10 17 2.0 19 1.0

11 12 1.0

12

13 14 2.0 24 1.0 32 1.0

14 18 1.0

15 16 1.0

16

17 20 1.0 38 1.0

18 30 2.0 36 1.0

19 22 2.0 28 1.0

20 21 1.0 26 2.0

21

22 23 1.0 26 1.0

23

24 25 1.0 34 2.0

25

26 27 1.0

27

28 29 1.0 40 1.0 44 1.0

29

30 31 1.0 34 1.0

31

32 33 1.0 56 1.0 68 1.0

33

34 35 1.0

35

36 37 1.0 52 1.0 60 1.0

37

38 39 1.0 48 1.0 64 1.0

39

40 41 1.0 42 1.0 43 1.0

41

42

43

44 45 1.0 46 1.0 47 1.0

45

46

47

48 49 1.0 50 1.0 51 1.0

49

50

51

52 53 1.0 54 1.0 55 1.0

53

54

55

56 57 1.0 58 1.0 59 1.0

57

58

59

60 61 1.0 62 1.0 63 1.0

61

62

63

64 65 1.0 66 1.0 67 1.0

65

66

67

68 69 1.0 70 1.0 71 1.0

69

70

71

72 74 2.0 75 1.0 81 1.0

73 74 1.0 82 2.0 85 1.0

74 145 1.0

75 76 1.0 77 2.0

76

77 78 1.0 82 1.0

78 86 1.0

79 80 1.0 86 2.0

80

81 88 2.0 90 1.0

82 83 1.0

83

84 85 2.0 95 1.0 103 1.0

85 89 1.0

86 87 1.0

87

88 91 1.0 109 1.0

89 101 2.0 107 1.0

90 93 2.0 99 1.0

91 92 1.0 97 2.0

92

93 94 1.0 97 1.0

94

95 96 1.0 105 2.0

96

97 98 1.0

98

99 100 1.0 111 1.0 115 1.0

100

101 102 1.0 105 1.0

102

103 104 1.0 127 1.0 139 1.0

104

105 106 1.0

106

107 108 1.0 123 1.0 131 1.0

108

109 110 1.0 119 1.0 135 1.0

110

111 112 1.0 113 1.0 114 1.0

112

113

114

115 116 1.0 117 1.0 118 1.0

116

117

118

119 120 1.0 121 1.0 122 1.0

120

121

122

123 124 1.0 125 1.0 126 1.0

124

125

126

127 128 1.0 129 1.0 130 1.0

128

129

130

131 132 1.0 133 1.0 134 1.0

132

133

134

135 136 1.0 137 1.0 138 1.0

136

137

138

139 140 1.0 141 1.0 142 1.0

140

141

142

143 144 3.0

144

145 146 3.0

146

Optimized Cartesian Coordinates for Model of 1,4-[CNAr^{Ph2}]$_2$Ph.

C	5.031141000	1.236024000	0.028493000
C	5.030726000	-1.235950000	0.037622000
C	5.726576000	-0.000074000	0.043077000
C	3.630856000	1.204214000	0.026177000
H	3.096559000	2.154145000	-0.030812000
C	2.907064000	0.000657000	0.030541000
C	1.426036000	0.000083000	0.014107000
C	-0.689243000	-0.987477000	-0.695751000
H	-1.216259000	-1.746923000	-1.276837000
C	5.726982000	2.549878000	0.022304000
C	3.630654000	-1.202577000	0.032437000
H	3.095362000	-2.153676000	0.038254000
C	5.345156000	-3.521332000	1.010912000
C	5.724227000	-2.550902000	0.065361000

C	0.703236000	-0.987437000	-0.682378000
H	1.241528000	-1.746100000	-1.254064000
C	6.718976000	2.854711000	-0.926360000
C	6.726919000	-2.875055000	-0.865530000
C	5.361081000	3.538622000	0.953798000
C	7.323267000	4.112817000	-0.943739000
H	8.087036000	4.333391000	-1.691930000
C	5.971826000	4.794389000	0.940435000
H	5.682915000	5.544770000	1.679067000
C	5.954014000	-4.777973000	1.028353000
H	5.654809000	-5.513758000	1.777488000
C	6.954279000	5.086107000	-0.010037000
H	7.432775000	6.067243000	-0.021841000
C	7.329190000	-4.134244000	-0.851904000
H	8.101618000	-4.369902000	-1.586494000
C	6.947381000	-5.089119000	0.095502000
H	7.424381000	-6.070981000	0.108098000
C	-5.031153000	-1.236022000	-0.028477000
C	-5.030737000	1.235954000	-0.037610000
C	-5.726588000	0.000079000	-0.043061000
C	-3.630868000	-1.204209000	-0.026166000
H	-3.096569000	-2.154139000	0.030823000
C	-2.907075000	-0.000652000	-0.030529000
C	-1.426047000	-0.000078000	-0.014096000
C	0.689231000	0.987483000	0.695762000
H	1.216248000	1.746928000	1.276847000
C	-5.726982000	-2.549884000	-0.022293000
C	-3.630666000	1.202582000	-0.032425000
H	-3.095373000	2.153681000	-0.038246000
C	-5.345169000	3.521326000	-1.010922000
C	-5.724237000	2.550906000	-0.065361000
C	-0.703248000	0.987443000	0.682389000
H	-1.241540000	1.746105000	1.254075000
C	-6.718885000	-2.854784000	0.926445000
C	-6.726924000	2.875070000	0.865532000
C	-5.361141000	-3.538579000	-0.953864000
C	-7.323151000	-4.112903000	0.943815000
H	-8.086847000	-4.333528000	1.692065000
C	-5.971864000	-4.794356000	-0.940511000
H	-5.683004000	-5.544695000	-1.679206000
C	-5.954026000	4.777967000	-1.028374000
H	-5.654823000	5.513745000	-1.777518000
C	-6.954231000	-5.086138000	0.010031000
H	-7.432708000	-6.067283000	0.021827000
C	-7.329194000	4.134260000	0.851895000
H	-8.101618000	4.369927000	1.586486000
C	-6.947388000	5.089124000	-0.095523000
H	-7.424387000	6.070987000	-0.108127000
N	7.107268000	0.000529000	0.140074000
C	8.286076000	0.001342000	0.244134000
N	-7.107279000	-0.000513000	-0.140090000

C	-8.286084000	-0.001299000	-0.244185000
H	-7.027515000	2.141373000	1.614788000
H	-4.580604000	3.276770000	-1.751616000
H	4.580588000	-3.276784000	1.751604000
H	7.027512000	-2.141349000	-1.614777000
H	7.009056000	2.106447000	-1.665320000
H	4.605723000	3.308743000	1.708523000
H	-4.605851000	-3.308651000	-1.708643000
H	-7.008909000	-2.106568000	1.665475000

Input file for model of 1,4-[CNAr^{Ph2}]$_2$Ph$_2$.

%chk=PhPhPhPh.chk

%nprocs=8

%mem=21GB

opt geom=connectivity bp86 def2tzvp int=superfinegrid

PhPhPhPh optimization

0 1

C	0.16584300	-1.19752240	6.94059898
C	0.18902068	1.21293067	6.75016317
C	0.05729142	0.07308818	7.53916713
C	0.36507489	-1.30969658	5.62709183
H	0.46420467	-2.26717036	5.16245496
C	0.38672593	-0.16689033	4.87732256
C	0.06915924	-2.49703904	7.71976933
C	0.43851272	1.07548743	5.45494713
H	0.61415359	1.93398382	4.84293622

C	1.15695541	3.48270977	7.30619776
C	0.05662274	2.62184920	7.32835991
C	-1.12445536	-2.83165965	8.34998449
C	-1.15135392	3.06778933	7.87203114
C	1.13320909	-3.32736000	7.77117950
C	-1.24578029	-4.05698032	8.91164318
H	-2.19276187	-4.37737724	9.29588062
C	1.03895380	-4.52987311	8.46830274
H	1.89491540	-5.14876193	8.59221203
C	1.05030816	4.74454259	7.89042754
H	1.90822089	5.36987168	7.97912058
C	-0.14724555	-4.91010241	8.99190687
H	-0.23232584	-5.86160502	9.46189069
C	-1.26243767	4.38622397	8.32567054
H	-2.20897707	4.77073728	8.64322394
C	-0.18510388	5.19402105	8.36813139
H	-0.26925601	6.18077343	8.76377523
C	-0.19043183	1.19266228	-6.95279897
C	-0.14826709	-1.21663889	-6.74307440
C	-0.04617542	-0.08240603	-7.54058476
C	-0.42142959	1.29916924	-5.64443997
H	-0.59373605	2.25274537	-5.19121623
C	-0.38155621	0.16801151	-4.88067534

C	-0.08242129	2.48706552	-7.73491892
C	-0.35486767	-1.08249715	-5.44412857
H	-0.46216061	-1.94101097	-4.81629737
C	-1.13216225	-3.48633511	-7.26712130
C	-0.02629818	-2.62851745	-7.30947897
C	1.11102430	2.81587976	-8.36933241
C	1.17075023	-3.08308876	-7.86102309
C	-1.14296836	3.32294843	-7.78744397
C	1.23846556	4.03554891	-8.94509902
H	2.18181765	4.34956239	-9.33365198
C	-1.04236393	4.51837590	-8.49519350
H	-1.89820135	5.14015837	-8.61760831
C	-1.03612717	-4.75095683	-7.83943362
H	-1.90011031	-5.37615369	-7.91340355
C	0.13726545	4.88924163	-9.02549094
H	0.22657705	5.83783559	-9.50756382
C	1.27545551	-4.40523705	-8.30209346
H	2.21444758	-4.79557717	-8.62289337
C	0.18763856	-5.21176162	-8.32354298
H	0.27003533	-6.20002444	-8.70980051
N	-0.08759428	0.20975225	8.98814574
C	-0.20069972	0.31642828	10.11930067
N	0.08767089	-0.22592453	-8.98955151

C	0.19650861	-0.37982521	-10.11466392
H	2.01802034	-2.42970099	-7.91673107
H	-2.04790752	-3.16181388	-6.82305317
H	2.07817619	3.16721433	6.86891726
H	-2.00047845	2.41208175	7.91203031
H	-1.93933229	-2.14823613	8.35836452
H	2.05518743	-3.06440487	7.30016348
H	-2.06372238	3.06578254	-7.30956460
H	1.92819511	2.12935773	-8.37298017
C	-0.31094097	0.22563138	-3.40721567
C	-0.23477765	-1.01643472	-2.79742346
C	-0.29913119	1.40857602	-2.69225864
H	-0.21277356	-1.88958058	-3.40127083
H	-0.36968796	2.35451297	-3.19099277
C	-0.16594763	-1.07727478	-1.43598638
C	-0.17167990	1.36429392	-1.32127617
H	-0.14835987	-2.03216261	-0.93596075
H	-0.13633463	2.25950217	-0.73773567
C	-0.10199263	0.09431758	-0.73513093
C	0.31278333	-0.20977611	3.39665430
C	0.76451728	0.93555581	2.77331973
C	-0.22186145	-1.28356380	2.70488326
H	1.20798230	1.70458454	3.35203941

H	-0.54069020	-2.17602453	3.21117384
C	0.62920813	1.03922228	1.41082999
C	-0.36784968	-1.19654926	1.33673254
H	0.97445858	1.92001328	0.90348013
H	-0.79916639	-1.99584590	0.77033606
C	0.06154141	-0.01192754	0.73397455

1 3 1.5 4 2.0 7 1.0

2 3 1.5 8 2.0 11 1.0

3 53 1.0

4 5 1.0 6 1.5

5

6 8 1.5 75 1.0

7 12 1.5 14 2.0

8 9 1.0

9

10 11 1.5 19 1.5 59 1.0

11 13 1.5

12 15 2.0 61 1.0

13 23 1.5 60 1.0

14 17 1.5 62 1.0

15 16 1.0 21 1.5

16

17 18 1.0 21 2.0

18

19 20 1.0 25 1.5

20

21 22 1.0

22

23 24 1.0 25 2.0

24

25 26 1.0

26

27 29 1.5 30 2.0 33 1.0

28 29 1.5 34 2.0 37 1.0

29 55 1.0

30 31 1.0 32 1.5

31

32 34 1.5 65 1.0

33 38 1.5 40 2.0

34 35 1.0

35

36 37 1.5 45 1.5 58 1.0

37 39 1.5

38 41 2.0 64 1.0

39 49 1.5 57 1.0

40 43 1.5 63 1.0

41 42 1.0 47 1.5

42

43 44 1.0 47 2.0

44

45 46 1.0 51 1.5

46

47 48 1.0

48

49 50 1.0 51 2.0

50

51 52 1.0

52

53 54 3.0

54

55 56 3.0

56

57

58

59

60

61

62

63

64

65 66 1.5 67 1.5

66 68 1.0 70 1.5

67 69 1.0 71 1.5

68

69

70 72 1.0 74 1.5

71 73 1.0 74 1.5

72

73

74 84 1.0

75 76 1.5 77 1.5

76 78 1.0 80 1.5

77 79 1.0 81 1.5

78

79

80 82 1.0 84 1.5

81 83 1.0 84 1.5

82

83

84

Optimized Cartesian coordinates for 1,4-[CNAr^{Ph2}]$_2$Ph$_2$.

C	7.196934000	1.181960000	0.394455000
C	7.201210000	-1.174223000	-0.352292000
C	7.894977000	0.003072000	0.027682000
C	5.796917000	1.147440000	0.385534000
H	5.260187000	2.051797000	0.677464000
C	5.074739000	-0.002231000	0.027247000
C	7.888392000	2.430649000	0.811020000
C	5.800909000	-1.147213000	-0.339497000
H	5.267919000	-2.038285000	-0.675637000
C	7.538788000	-3.647144000	-0.157689000
C	7.898990000	-2.424452000	-0.753044000
C	8.886167000	3.021222000	0.015573000
C	8.887210000	-2.429684000	-1.753214000
C	7.512234000	3.073173000	2.004817000
C	9.486493000	4.220567000	0.402438000
H	10.255131000	4.667211000	-0.231226000
C	8.119049000	4.269042000	2.394522000
H	7.822084000	4.746494000	3.330467000
C	8.151302000	-4.840059000	-0.547507000
H	7.866769000	-5.777461000	-0.065348000
C	9.107562000	4.847670000	1.593381000
H	9.583028000	5.782335000	1.896863000
C	9.493344000	-3.623612000	-2.147511000
H	10.254136000	-3.608756000	-2.930316000
C	9.129973000	-4.832215000	-1.545425000
H	9.609916000	-5.763806000	-1.851274000
C	-7.201115000	-1.174243000	0.352267000
C	-7.197018000	1.181922000	-0.394508000
C	-7.894972000	0.002983000	-0.027739000
C	-5.800814000	-1.147131000	0.339406000
H	-5.267750000	-2.038132000	0.675621000
C	-5.074710000	-0.002097000	-0.027332000
C	-7.898787000	-2.424502000	0.753083000
C	-5.797004000	1.147524000	-0.385597000
H	-5.260377000	2.051903000	-0.677608000
C	-7.512436000	3.073287000	-2.004688000
C	-7.888618000	2.430557000	-0.811018000
C	-8.886739000	-2.429871000	1.753520000
C	-8.886618000	3.020819000	-0.015627000
C	-7.538715000	-3.647130000	0.157510000
C	-9.492772000	-3.623853000	2.147815000
H	-10.253366000	-3.609101000	2.930815000
C	-8.151111000	-4.840102000	0.547346000
H	-7.866676000	-5.777440000	0.065006000
C	-8.119417000	4.269103000	-2.394303000
H	-7.822429000	4.746739000	-3.330147000
C	-9.129550000	-4.832384000	1.545496000
H	-9.609405000	-5.764014000	1.851366000
C	-9.487098000	4.220115000	-0.402391000
H	-10.255904000	4.666529000	0.231233000
C	-9.108112000	4.847457000	-1.593195000

H	-9.583708000	5.782074000	-1.896619000
N	9.276187000	-0.022454000	0.114546000
C	10.455476000	-0.050786000	0.208634000
N	-9.276186000	-0.022595000	-0.114464000
C	-10.455485000	-0.050980000	-0.208430000
H	-9.184923000	2.545156000	0.919688000
H	-6.751552000	2.616506000	-2.641399000
H	6.786397000	-3.654922000	0.634059000
H	9.172857000	-1.494194000	-2.236297000
H	9.184434000	2.545757000	-0.919853000
H	6.751489000	2.616189000	2.641549000
H	-6.786503000	-3.654819000	-0.634410000
H	-9.172271000	-1.494441000	2.236788000
C	-3.593757000	-0.001043000	-0.018263000
C	-2.865422000	1.148236000	0.344415000
C	-2.861680000	-1.150412000	-0.372930000
H	-3.399431000	2.045629000	0.663510000
H	-3.392844000	-2.048306000	-0.695390000
C	-1.472867000	1.147706000	0.351912000
C	-1.469205000	-1.150124000	-0.366722000
H	-0.941696000	2.044795000	0.676509000
H	-0.934739000	-2.047381000	-0.685411000
C	-0.739938000	-0.001132000	-0.003844000
C	3.593809000	-0.001206000	0.018144000
C	2.861706000	-1.150526000	0.372871000
C	2.865554000	1.148082000	-0.344641000
H	3.392831000	-2.048456000	0.695303000
H	3.399644000	2.045443000	-0.663710000
C	1.469231000	-1.150184000	0.366627000
C	1.473002000	1.147618000	-0.352122000
H	0.934719000	-2.047425000	0.685276000
H	0.941876000	2.044738000	-0.676714000

Frontier molecular orbitals and energies for $CNAr^{Ph2}$, $[CNAr^{Ph2}]_2$, 1,4-$[CNAr^{Ph2}]_2Ph$, 1,4-$[CNAr^{Ph2}]_2Ph_2$.

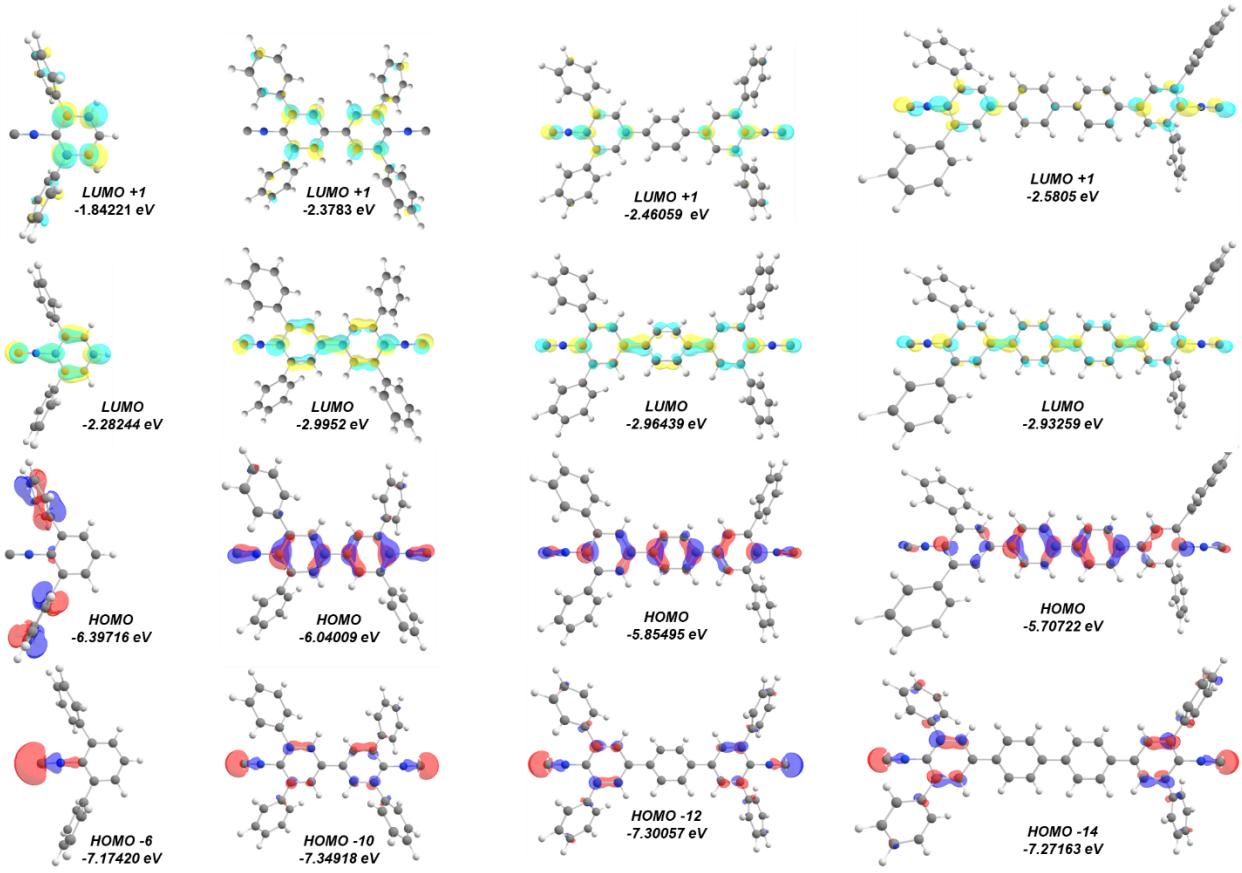

3.5 Details of crystallographic structure determinations

General Information. Single crystal X-ray structure determinations were carried out at low temperature on a Bruker P4, Platform or Kappa Diffractometer equipped with a Mo or Cu radiation source. Data were acquired with Bruker APEX II, Photon II or Dextris Eiger 1M detectors. All structures were solved via direct methods with SHELXS[51-52] and refined by full-matrix least-squares procedures using SHELXL[51-52] within the Olex2[53] software package. All H-atoms were refined using standard HFIX instruction. Crystallographic data collection and refinement information is listed in Table S3.1. The PLATON crystallographic tool[54] was used to account for overly disordered solvent using SQUEEZE routine,[55] and to identify twin laws in twinned crystalline habits using the TwinRotMat Routine.[56]

Information on Crystallographic Disorder and Twinning: The following molecules contain positionally disordered and/or pseudo-merohedrally twinned components. They are listed along with their respective disordered components.

[1,3,5-Tris(4-PhNCAr^{Dipp2})C$_6$H$_3$/1,3,5-Tris(4-PhNHCHOAr^{Dipp2})C$_6$H$_3$]:

Compositional disorder was observed in the formamide/isocyanide group, which was modeled using PART/FVAR commands then refined anisotropically. The crystallographically determined fraction of C1A and C1B/O1B is 63.7% C1A and the rest C1B/O1B.

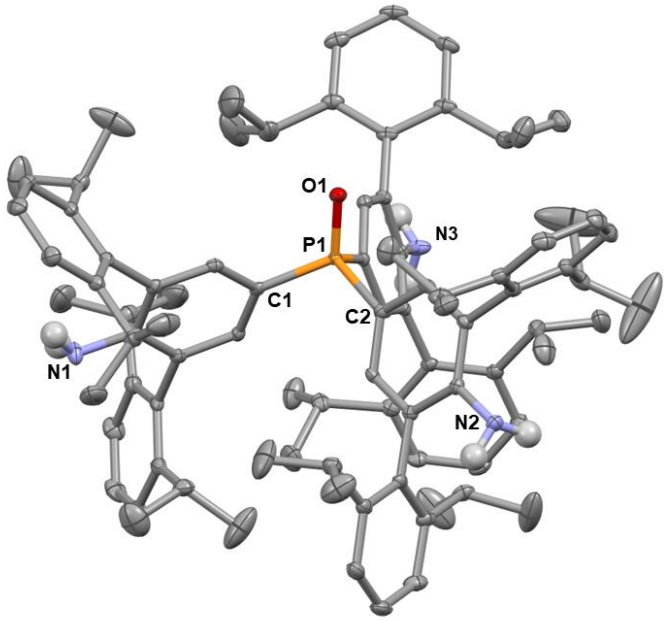

Figure 3.9 Molecular structure of $OP(^{Dipp2}ArNH_2)_3$. Hydrogen atoms, excluding NH_2 hydrogen atoms, omitted for clarity. Selected bond distances (Å) and angles (°): P-O = 1.486(2).

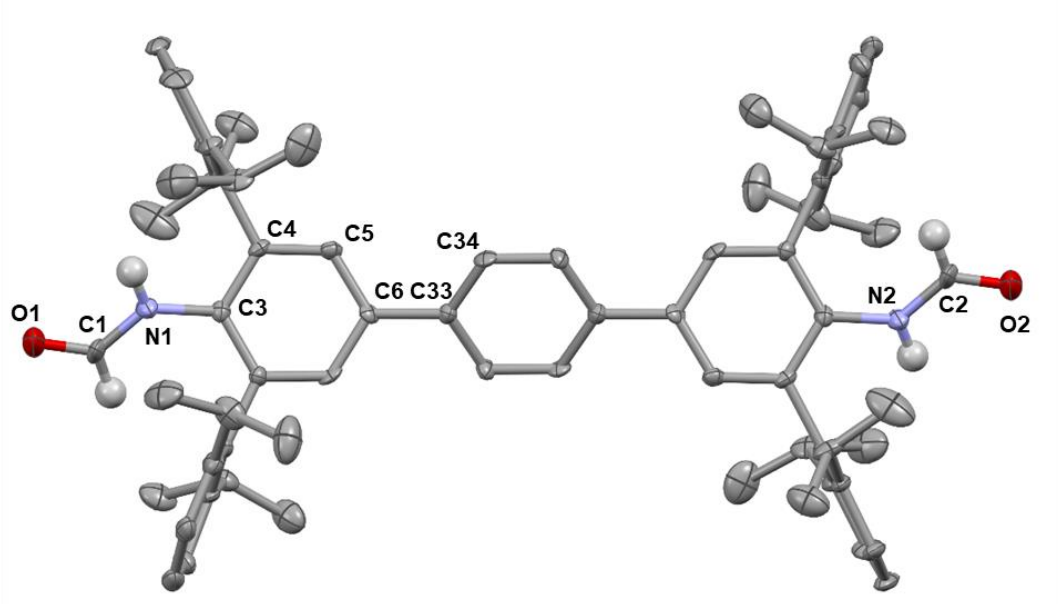

Figure 3.10 Molecular structure of 1,4-$(Ar^{Dipp2}NHCHO)_2(C_6H_4)$. Hydrogen atoms, excluding NHCHO hydrogens, are omitted for clarity. Selected bond distances (Å) and angles (°): C1-O1 = 1.203(10); N1-C1 = 1.322(12); C4-C3-N1-C1 = 39.209(0.183); C5-C6-C33-C34 = 30.412(0.176).

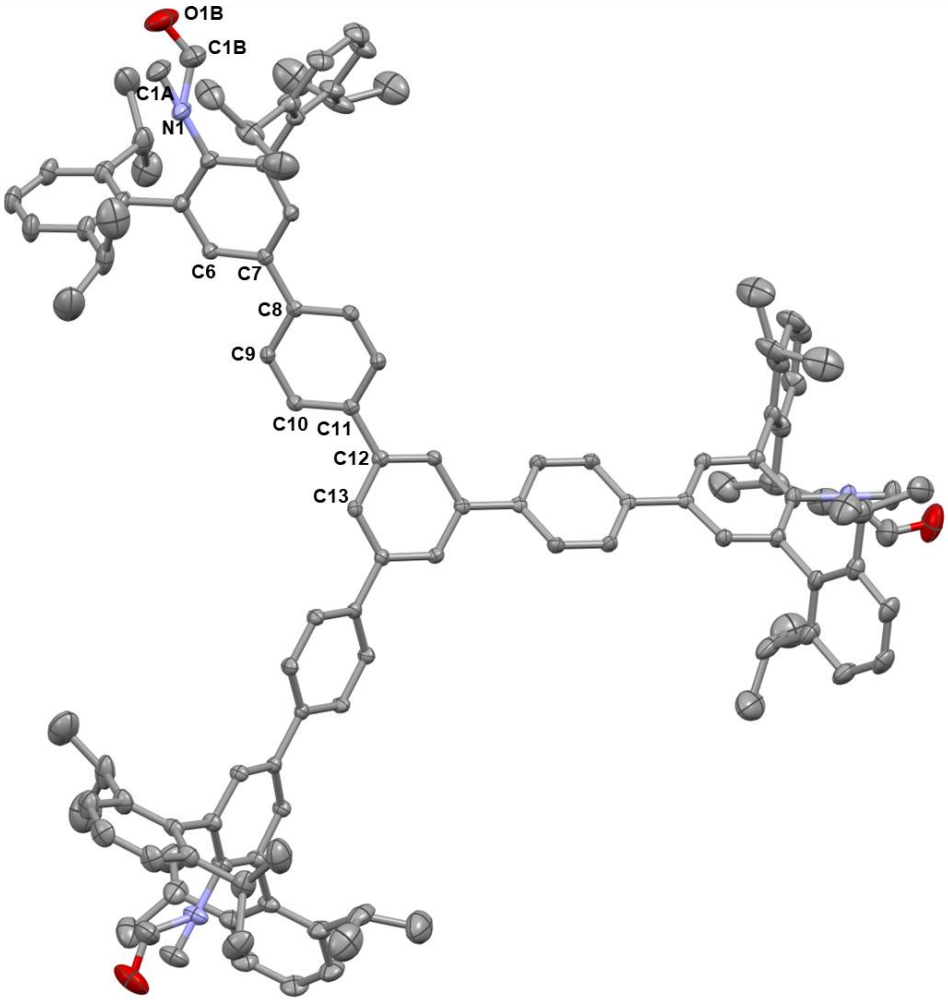

Figure 3.11 Molecular structure of [1,3,5-Tris(4-PhNCAr^{Dipp2})C_6H_3/1,3,5-Tris(4-PhNHCHOAr^{Dipp2})C_6H_3]. Hydrogen atoms and one co-crystalized molecule of C_6D_6 are omitted for clarity. Selected bond distances (Å) and angles (°): C1A-N1 = 1.157(7); C6-C7-C8-C9 = 6.694(0.043); C10-C11-C12-C13 = 32.427(0.189).

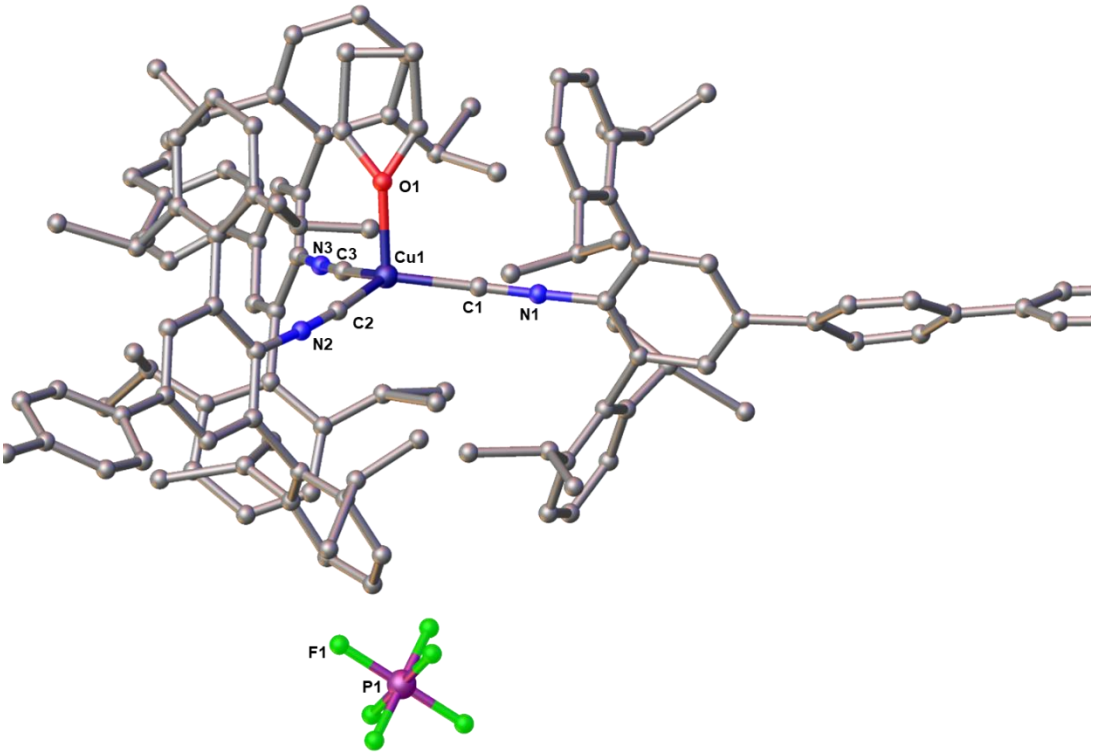

Figure 3.12 Structure of Cu^{ISO}CN-5. Hydrogen atoms are omitted for clarity. Selected bond distances (Å) and angles (°): Cu1-O1 = 1.96(3); Cu1-C1 = 1.88(2); N1-C1 = 1.22(2); C1-Cu1-C2 = 117.859.

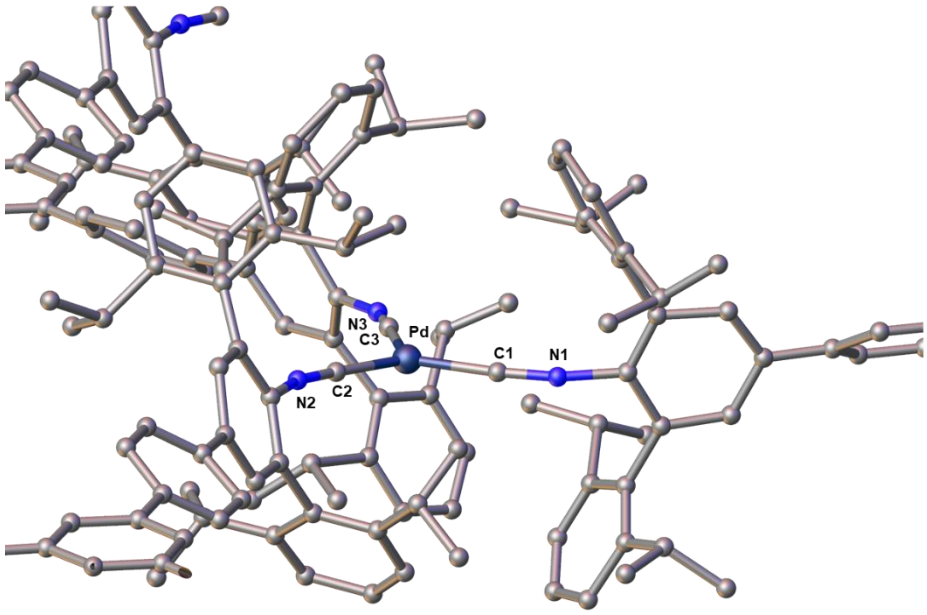

Figure 3.13 Structure of Pd^{ISO}CN-1. Hydrogen atoms and two co-crystallized toluene molecules are omitted for clarity. Selected bond distances (Å) and angles (°): Pd-C1 = 1.92(2); N1-C1 = 1.23(2); N2-C2 = 1.21(2); N3-C3 = 1.18(2); C1-Pd-C2 = 118.016; C2-Pd-C3 = 122.460; C3-Pd-C1 = 119.317.

Table 3.2 Crystallographic Data and Refinement Information

	$OP(^{Dipp2}ArNH_2)_3$	1,4-$(Ar^{Dipp2}NHCHO)_2(C_6H_4)$	[1,3,5-Tris(4-$PhNCAr^{Dipp2}$)C_6H_3/1,3,5-Tris(4-$PhNHCHOAr^{Dipp2}$)C_6H_3][C_6H_6]$_3$
Formula	$C_{90}H_{114}N_3PO$	$C_{68}H_{80}N_2O_2$	$C_{135}H_{144.26}N_3O_{1.09}$
Crystal System	Monoclinic	Monoclinic	Rhombohedral
Space Group	*P2₁/c*	*P2₁/n*	*R-3c*
a, Å	19.4848(14)	18.567(3)	22.4976(3)
b, Å	17.2984(10)	9.0998(15)	25.7018(3)
c, Å	24.1644(13)	19.911(3)	26.0938(6)
α, deg	90	90	90
β, deg	102.620(2)	113.658(4)	90
γ, deg	90	90	120
V, Å^3	7948.0(9)	3080.7 (8)	17069.3(5)
Z	4	2	6
Radiation (λ, Å)	Mo-Kα, 0.71073	Mo-Kα, 0.71073	Mo-Kα, 0.71073
ρ (calcd.), g/cm^3	1.074	1.032	1.066
μ (Mo Ka), mm^{-1}	0.081	0.061	0.061
Temp, K	100	100	100
θ max, deg	25.388	22.705	25.368
data/parameters	9576(883)	22998(1065)	2763(235)
R_1	0.0660	0.1885	0.0714
wR_2	0.2124	0.5494	0.2231
GOF	1.044	2.611	1.067

Table 3.3 Crystallographic Data and Refinement Information - Continued

	Cu^{ISO}CN-5	Pd^{ISO}CN-1
Formula	$C_{242}H_{164}Cu_2F_6N_6O_2P$	$C_{131}H_{120}N_3Pd$
Crystal System	Rhombohedral	Rhombohedral
Space Group	*R-3c*	*R-3c*
a, Å	24.8474(13)	24.5351(4)
b, Å	24.8474(13)	24.5351(4)
c, Å	36.005(3)	47.2026(15)
α, deg	90	90
β, deg	90	90
γ, deg	120	120
V, $Å^3$	19251(3)	24607.8(10)
Z	3	6
Radiation (λ, Å)	Cu-Kα, 1.54178	Cu-Kα, 1.54178
ρ (calcd.), g/cm^3	0.895	0.746
μ (Mo Ka), mm^{-1}	0.644	1.160
Temp, K	100	100
θ max, deg	42.636	44.529
data/parameters	2147 (177)	10228 (1129)
R_1	0.3646	0.1087
wR_2	0.7452	0.2882
GOF	3.987	1.156

3.6 Acknowledgments

Complexes discussed in chapter 3 are currently in preparation for publication by M. L. Neville, A. M. Grippo, A. L. Rheingold, J. S. Figueroa. The dissertation author is the primary author of this manuscript.

3.7 References

1. Yaghi, O. M.; O'Keeffe, M.; Ockwig, N. W.; Chae, H. K.; Eddaoudi, M.; Kim, J., *Nature* **2003,** *423* (6941), 705-714.

2. *Chemical Reviews* **2012,** *112* (2), 673-674.

3. Agnew, D. W.; Gembicky, M.; Moore, C. E.; Rheingold, A. L.; Figueroa, J. S., *Journal of the American Chemical Society* **2016,** *138* (46), 15138-15141.

4. Ding, M.; Cai, X.; Jiang, H.-L., *Chemical Science* **2019,** *10* (44), 10209-10230.

5. Pascanu, V.; González Miera, G.; Inge, A. K.; Martín-Matute, B., *Journal of the American Chemical Society* **2019,** *141* (18), 7223-7234.

6. Vermoortele, F.; Vandichel, M.; Van de Voorde, B.; Ameloot, R.; Waroquier, M.; Van Speybroeck, V.; De Vos, D. E., *Angew. Chem. Int. Ed.* **2012,** *51* (20), 4887-4890.

7. Hu, Z.; Zhao, D., *CrystEngComm* **2017,** *19* (29), 4066-4081.

8. Ji, P.; Drake, T.; Murakami, A.; Oliveres, P.; Skone, J. H.; Lin, W., *Journal of the American Chemical Society* **2018,** *140* (33), 10553-10561.

9. Bouhadir, G.; Bourissou, D., Ambiphilic Ligands. In *Ligand Design in Metal Chemistry*, 2016; pp 237-269.

10. Caballero, A.; Díaz-Requejo, M. M.; Fructos, M. R.; Urbano, J.; Pérez, P. J., Modern Applications of Trispyrazolylborate Ligands in Coinage Metal Catalysis. In *Ligand Design in Metal Chemistry*, 2016; pp 308-329.

11. de Bruin, B.; Gualco, P.; Paul, N. D., Redox Non-innocent Ligands. In *Ligand Design in Metal Chemistry*, 2016; pp 176-204.

12. Osten, K. M.; Aluthge, D. C.; Mehrkhodavandi, P., Ligand Design in Enantioselective Ring-opening Polymerization of Lactide. In *Ligand Design in Metal Chemistry*, 2016; pp 270-307.

13. Quigley, B. L.; Grubbs, R. H., Catalyst Structure and Cis–Trans Selectivity in Ruthenium-based Olefin Metathesis. In *Ligand Design in Metal Chemistry*, 2016; pp 15-45.

14. Stradiotto, M.; Lundgren, R. J., Application of Sterically Demanding Phosphine Ligands in Palladium-Catalyzed Cross-Coupling leading to C(sp 2)─E Bond Formation (E = NH2 , OH, and F). In *Ligand Design in Metal Chemistry*, 2016; pp 104-133.

15. Gonzalez, M. I.; Bloch, E. D.; Mason, J. A.; Teat, S. J.; Long, J. R., *Inorganic Chemistry* **2015,** *54* (6), 2995-3005.

16. Sikma, R. E.; Kunal, P.; Dunning, S. G.; Reynolds, J. E.; Lee, J. S.; Chang, J.-S.; Humphrey, S. M., *Journal of the American Chemical Society* **2018,** *140* (31), 9806-9809.

17. Dhakshinamoorthy, A.; Garcia, H., *Chemical Society Reviews* **2014,** *43* (16), 5750-5765.

18. Young, R. J.; Huxley, M. T.; Pardo, E.; Champness, N. R.; Sumby, C. J.; Doonan, C. J., *Chemical Science* **2020,** *11* (16), 4031-4050.

19. Jeoung, S.; Kim, S.; Kim, M.; Moon, H. R., *Coordination Chemistry Reviews* **2020,** *420*, 213377.

20. Kozuch, S.; Amatore, C.; Jutand, A.; Shaik, S., *Organomet. Chem.* **2005,** *24* (10), 2319-2330.

21. Fang, Z.; Bueken, B.; De Vos, D. E.; Fischer, R. A., *Angew. Chem. Int. Ed.* **2015,** *54* (25), 7234-7254.

22. Cao, Y.; Mi, X.; Li, X.; Wang, B., *Front Chem* **2021,** *9*, 673738-673738.

23. Xiang, W.; Zhang, Y.; Chen, Y.; Liu, C.-j.; Tu, X., *Journal of Materials Chemistry A* **2020,** *8* (41), 21526-21546.

24. Agnew, D. W.; DiMucci, I. M.; Arroyave, A.; Gembicky, M.; Moore, C. E.; MacMillan, S. N.; Rheingold, A. L.; Lancaster, K. M.; Figueroa, J. S., *Journal of the American Chemical Society* **2017,** *139* (48), 17257-17260.

25. Arroyave, A.; Gembicky, M.; Rheingold, A. L.; Figueroa, J. S., *Inorganic Chemistry* **2020,** *59* (17), 11868-11878.

26. Ditri, T.; Fox, B.; Moore, C.; Rheingold, A.; Figueroa, J., *Inorganic Chemistry* **2009,** *48* (17), 8362-8375.

27. Emerich, B. M.; Moore, C. E.; Fox, B. J.; Rheingold, A. L.; Figueroa, J. S., *Organomet. Chem.* **2011,** *30* (9), 2598-2608.

28. Power, P. P., *Inorganic Syntheses, Volume 37*. Wiley: 2018.

29. Marcoux, D.; Charette, A. B., *The Journal of Organic Chemistry* **2008,** *73* (2), 590-593.

30. Wang, Y.; Lai, C. W.; Kwong, F. Y.; Jia, W.; Chan, K. S., *Tetrahedron* **2004,** *60* (42), 9433-9439.

31. Salsi, F.; Neville, M.; Drance, M.; Hagenbach, A.; Chan, C.; Figueroa, J. S.; Abram, U., *Chem Commun* **2020,** *56* (51), 7009-7012.

32. Salsi, F.; Neville, M.; Drance, M.; Hagenbach, A.; Figueroa, J. S.; Abram, U., *Organomet. Chem.* **2021,** *40* (9), 1336-1343.

33. Devendar, P.; Qu, R.-Y.; Kang, W.-M.; He, B.; Yang, G.-F., *Journal of Agricultural and Food Chemistry* **2018,** *66* (34), 8914-8934.

34. Ruiz-Castillo, P.; Buchwald, S. L., *Chemical Reviews* **2016,** *116* (19), 12564-12649.

35. Casnati, A.; Voronov, A.; Ferrari, D. G.; Mancuso, R.; Gabriele, B.; Motti, E.; Della Ca', N., *Catalysts* **2020,** *10* (2), 176.

36. Lévay, K.; Tóth, K. D.; Kárpáti, T.; Hegedűs, L., *ACS Omega* **2020,** *5* (10), 5487-5497.

37. Sikma, R. E.; Cohen, S. M., *Angewandte Chemie* **2022,** *134* (11), e202115454.

38. Friesen, R. W.; Allouche, E. M. D., Tetrakis(triphenylphosphine)palladium(0). In *Encyclopedia of Reagents for Organic Synthesis*, pp 1-7.

39. Labios, L. A.; Millard, M. D.; Rheingold, A. L.; Figueroa, J. S., *Journal of the American Chemical Society* **2009,** *131* (32), 11318-11319.

40. Arnarego, W. L. F.; Chai, C. L. L., *Purification of Laboratory Chemicals*. 5th ed. ed.; Elsevier: 2003.

41. Pangborn, A. B.; Giardello, M. A.; Grubbs, R. H.; Rosen, R. K.; Timmers, F. J., *Organomet. Chem.* **1996,** *15* (5), 1518-1520.

42. Ditri, T. B.; Barnett, B. R.; Carpenter, A. E.; Mokhtarzadeh, C. C.; Agnew, D. W.; Figueroa, J. S., *Inorg. Synth.* **2018,** *37*, 109-115.

43. Fulmer, G. R.; Miller, A. J. M.; Sherden, N. H.; Gottlieb, H. E.; Nudelman, A.; Stoltz, B. M.; Bercaw, J. E.; Goldberg, K. I., *Organometallics* **2010,** *29* (9), 2176-2179.

44. Neese, F., *Wiley Interdisciplinary Reviews: Computational Molecular Science* **2011,** *2* (1), 73-78.

45. Frisch, M. J.; Trucks, G. W.; Schlegel, H. B.; Scuseria, G. E.; Robb, M. A.; Cheeseman, J. R.; Scalmani, G.; Barone, V.; Petersson, G. A.; Nakatsuji, H.; Li, X.; Caricato, M.; Marenich, A. V.; Bloino, J.; Janesko, B. G.; Gomperts, R.; Mennucci, B.; Hratchian, H. P.; Ortiz, J. V.; Izmaylov, A. F.; Sonnenberg, J. L.; Williams; Ding, F.; Lipparini, F.; Egidi, F.; Goings, J.; Peng, B.; Petrone, A.; Henderson, T.; Ranasinghe, D.; Zakrzewski, V. G.; Gao, J.; Rega, N.; Zheng, G.; Liang, W.; Hada, M.; Ehara, M.; Toyota, K.; Fukuda, R.; Hasegawa, J.; Ishida, M.; Nakajima, T.; Honda, Y.; Kitao, O.; Nakai, H.; Vreven, T.; Throssell, K.; Montgomery Jr., J. A.; Peralta, J. E.; Ogliaro, F.; Bearpark, M. J.; Heyd, J. J.; Brothers, E. N.; Kudin, K. N.; Staroverov, V. N.; Keith, T. A.; Kobayashi, R.; Normand, J.; Raghavachari, K.; Rendell, A. P.; Burant, J. C.; Iyengar, S. S.;

Tomasi, J.; Cossi, M.; Millam, J. M.; Klene, M.; Adamo, C.; Cammi, R.; Ochterski, J. W.; Martin, R. L.; Morokuma, K.; Farkas, O.; Foresman, J. B.; Fox, D. J. *Gaussian 16 Rev. C.01*, Wallingford, CT, 2016.

46. Becke, A. D., *Physical Review A* **1988,** *38* (6), 3098-3100.

47. Becke, A. D., *The Journal of Chemical Physics* **1986,** *84* (8), 4524-4529.

48. Weigend, F., *Physical Chemistry Chemical Physics* **2006,** *8* (9), 1057-1065.

49. Weigend, F.; Ahlrichs, R., *Physical Chemistry Chemical Physics* **2005,** *7* (18), 3297-3305.

50. D. A. Zhurko, G. A.; Zhurko, "ChemCraft 2014," can be found under

www.chemcraftprog.com, 2014.

51. Sheldrick, G. M., *Acta Crystallographica Section A Foundations of Crystallography* **2008,** *64* (Pt 1), 112-122.

52. Sheldrick, G., *Acta Crystallographica Section C* **2015,** *71* (1), 3-8.

53. Dolomanov, O. V.; Bourhis, L. J.; Gildea, R. J.; Howard, J. A. K.; Puschmann, H., *Journal of Applied Crystallography* **2009,** *42* (2), 339-341.

54. Spek, A., *Journal of Applied Crystallography* **2003,** *36* (1), 7-13.

55. Spek, A., *Acta Crystallographica Section C* **2015,** *71* (1), 9-18.

56. Ivlev, S. I.; Conrad, M.; Kraus, F., *Zeitschrift für Kristallographie - Crystalline Materials* **2019,** *234* (6), 415-418.

57. Other unsuccessful attempts to circumvent these synthetic challenges via non-Suzuki couplings (i.e. Ullman couplings to make ditopic *m*-terphenyliodides), aryl iodides, and pre-borylated linkers, are contained in the authors 6th Laboratory Notebook titled "Welcome to Ligand Land". Curious young students are encouraged to look there before embarking on their own journey to Ligand Land.